Epitranscriptomic Regulation in Synaptic Plasticity, Aging and Neurodegeneration

Dissertation

for the award of the degree

"Doctor rerum naturalium"

of the Georg-August-Universität Göttingen

within the doctoral program
Cellular and Molecular Physiology of the Brain
of the Georg-August University School of Science (GAUSS)

Submitted by

Ricardo Castro Hernández
From Mexico City, Mexico

Göttingen, 2022

Thesis Committee

1. **Prof. Dr. André Fischer**, Epigenetics and System Medicine in Neurodegenerative Diseases, German Center for Neurodegenerative Diseases, Göttingen

2. **Prof. Dr. Tiago Outeiro**, Department of Neurodegeneration and Restorative Research, University Medical Center, Göttingen

3. **Prof. Dr. Markus Zweckstetter**, Translational Structural Biology in Dementia, German Center for Neurodegenerative Diseases, Göttingen

Members of the Examination Board

First Referee: Prof. Dr. André Fischer, Epigenetics and System Medicine in Neurodegenerative Diseases, German Center for Neurodegenerative Diseases, Göttingen

Second Referee: Prof. Dr. Tiago Outeiro, Department of Neurodegeneration and Restorative Research, University Medical Center, Göttingen

Prof. Dr. Markus Zweckstetter, Translational Structural Biology in Dementia, German Center for Neurodegenerative Diseases, Göttingen

Prof. Dr. Thomas Dresbach, Department of Anatomy and Embryology, University Medical Center, Göttingen

Dr. Camin Dean, Synaptic Dysfunction in Neurodegeneration, German Center for Neurodegenerative Diseases, Berlin

Dr. Brett Carter, Synaptic Physiology and Plasticity, European Neuroscience Institute, Göttingen

Date of oral examination: 30 of March 2022

Declaration

I hereby declare that I have written the dissertation

  "Epitranscriptomic Regulation in Synaptic Plasticity, Aging and Neurodegeneration"

entirely by myself with no other aids or sources than quoted.

Ricardo Castro Hernández

Göttingen, 31.01.2022

To my son, Theo

Für meinen Lieblingsmensch, Janna

A mis padres

Table of contents

List of abbreviations

3' UTR	3' Untranslated region
5' UTR	5' Untranslated region
5XFAD	Tg(APPSwFlLon,PSEN1*M146L*L286V)6799Vas transgenic mice
ACC	Anterior cingulate cortex
AD	Alzheimer's disease
ADHD	Attention deficit/hyperactivity disorder
AMPA	α-amino-3-hydroxy-5-methyl-4-isoxazolepropionic acid
APP/PS1	Tg(APPswe,PSEN1dE9)85Dbo transgenic mice
Aβ	β-amyloid
CA	Cornu Ammonis
CC	Cingulate cortex
CDS	Coding sequence
CLIP	Cross-linking immunoprecipitation
CNS	Central nervous system
DG	Dentate gyrus
DIV	Days in vitro
EE	Environmental enrichment
FC	Fold change
FDR	False discovery rate
GABA	γ-aminobutyric acid
GO	Gene ontology
H3K36me3	Histone 3 lysine 36 trimethylation
IEG	Immediate early gene
IF	Immunofluorescence
IP	Immunoprecipitation
KD	Knock-down
KO	Knock-out
LLPS	Liquid-liquid phase separation
lncRNA	Long non-coding RNA
LPS	Local protein synthesis
LS	Limbic system
LTD	Long-term depression

LTP	Long-term potentiation
m^1A	N^1-methyladenosine
m5C	5-methylcitosine
m^6A	N^6-methyladenosine
m^6Am	N^6,2′-O-dimethyladenosine
meRIP	m^6A RNA immunoprecipitation
meRIP-Seq	m^6A RNA immunoprecipitation sequencing
meCLIP	m^6A cross-linking immunoprecipitation
miRNA	Micro RNA
mMC	m6A methyltransferase complex
mRNA	Messenger RNA
NGS	Next-generation sequencing
NFT	Neurofibrillary tangle
NMDA	N-methyl-D-aspartate
NSC	Neural stem cell
ON	Overnight
padj	Adjusted p value
PCC	Posterior cingulate cortex
PD	Parkinson's disease
PFC	Prefrontal cortex
piRNA	Piwi-associated RNA
PLA	Proximity ligation assay
ψ	Pseudouridine
PSD	Postsynaptic density
Puro-PLA	Puromycin proximity ligation assay
qPCR	Quantitative polymerase chain reaction
RBP	RNA-binding protein
RNA-Seq	Ribonucleic acid sequencing
RNPC	Ribonucleoprotein complex
rRNA	Ribosomal RNA
RT	Room temperature
siRNA	Small interference RNA
SRSF	Splicing regulation factors
tRNA	Transfer RNA
WB	Western blot

Summary

The regulation of synaptic transmission and plasticity is essential for correct brain function, especially for learning and memory, while the weakening of synaptic transmission and loss of plasticity are hallmarks of the decline of cognitive function during aging or disease. Genetic, epigenetic, and, more recently, epitranscriptomic factors are known to modulate synaptic function in a context and stimulus-dependent manner, and their disfunction is linked to the onset and progression of disease or aging-associated cognitive decline. Very recently, the role of the RNA modification N^6-methyladenosine (m^6A) in memory function and learning has been described, with a considerable contribution of its novel role in the regulation of synaptic function and plasticity.

With this in mind, my doctoral work aimed to evaluate the role that the m^6A epitranscriptome could be playing in the context of both impaired and enhanced cognition and synaptic function, a relationship that is still not well understood. To this end it was first necessary to establish a protocol for the processing of samples with very limited biological material (like that of patient brain samples) that would allow me to perform unbiased sequencing-based analyses of the m^6A state. Using this protocol to process and analyze samples from Alzheimer's disease (AD) patients, I was able to compare the changes in the m^6A epitranscriptome during neurodegeneration with those of a model of impaired cognition, the aged mouse brain. Then, by describing the changes in m^6A in a model of enhanced cognition, like environmental enrichment, I set to find common mechanisms regulated by m^6A function that could be related to cognitive function.

In this work I describe the epitranscriptome of several brain regions in both mouse and human samples, finding a remarkable conservation of the populations of methylated transcripts across species, and at the same time, strong tissue specificity. During aging, a widespread decrease in the methylation levels of mRNAs involved in synaptic function across brain regions was detected, an order of magnitude larger than the equivalent changes in gene expression. This work represents the first resource describing an unbiased approach for the analysis of differential methylation in AD. These brains displayed similar decreases in methylation of several of the same genes that saw a reduction of m^6A during aging in the mouse, particularly those genes involved in synaptic plasticity. Mechanistically, these changes in m^6A seem to have effects on the

local translation of proteins at the synapse, since one of these plasticity genes, the calcium/calmodulin-dependent protein kinase II (CaMKII), showed a strong decrease in the synthesis of its protein in synaptic compartments after the reduction of m^6A levels.

I also studied the epitranscriptome changes in a model where cognitive performance experiences an enhancement, rather than decline: environmental enrichment. Somewhat unexpectedly, based on the results of aging and AD, m^6A marks showed a decrease following ten weeks of enrichment in the CA1. These changes also targeted transcripts coding for synaptic proteins, although with more limited enrichment. Interestingly, despite decreased methylation, the protein levels of some of these transcripts were increased in synaptic compartments. The observed changes could be driven by an increased level of the m^6A reader FTO at the synapse, or through the involvement of another RNA modification, $N^6,2'$-O-dimethyladenosine (m^6Am). But more research focused on the role of m^6A readers at the synapse will be needed to determine the exact mechanism of action.

These results highlight the complexity and context-dependence of methylation marks and are a valuable addition to the growing evidence for the synaptic function of m^6A methylation. More importantly, they represent some of the first studies that have looked for a link between the epitranscriptome landscape and how it can affect the state of synaptic transmission during cognitive enhancement and decline,

Introduction

Introduction

RNA modifications: N^6-methyladenosine

The chemical modification of RNA nucleosides to modulate their cellular function is a well-known phenomenon within the biological regulatory networks (B. S. Zhao, Roundtree, and He 2017). By adding small chemical groups to existing nucleosides posttranscriptionally, cells can drastically modify the fate of RNAs carrying these marks and thus affect a myriad of cellular processes independently from genomic or transcriptomic changes (Lane 1998). Although most abundant in ribosomal RNA (rRNA) and transfer RNA (tRNA), chemical modifications can be found in all types of RNAs, including long non-coding RNAs (lncRNA), microRNAs (miRNAs), small interference RNAs (siRNAs), piwi-associated RNAs (piRNAs), as well as messenger RNA (mRNA) and viral RNAs (Grosjean 2015; Benne and Speijer 1998). To date, more than 150 distinct modifications are known across all species and cell types, but in spite of their high abundance their relevance as regulatory elements is only starting to be unraveled (Boccaletto et al. 2022).

RNA modifications can take multiple forms and alter RNA function in a variety of ways (Figure I1). For example, pseudouridine (ψ) – the first identified modification in RNA and the most abundant – is found in many species of non-coding RNAs and mRNA in eukaryotes (Charette and Gray 2000). It acts by stabilizing the structure and base pairing of labeled RNAs and, thus, enhancing ncRNA function and altering mRNA secondary structure and translation (Carlile et al. 2014). Another abundant modification, 5-methylcytosine (m^{5}C) – a well-known modification in epigenetics – can also be present in many types of RNAs . In mRNAs it can affect metabolism by altering molecular interactions, becoming recently a target of interest in cancer research (Squires et al. 2012; Xue, Zhao, and Li 2020). Other modifications, although first identified decades ago, still remain elusive in their molecular functions, such is the case of N^1-methyladenosine (m^{1}A; Dunn 1961). m^{1}A has long been known to modulate mainly tRNA structure, but it has only recently been identified in mRNAs as well (Dominissini et al. 2016). The function of m^{1}A beyond ncRNAs is thought to involve the regulation of secondary structures and binding of mRNAs during translation, although not much is known about the extent of its involvement in other regulatory processes.

Perhaps the most well-known RNA modification is also the most abundant modification in eukaryotic mRNA: N^6-methyladenosine (m^6A). Discovered – as were many other RNA modifications – many decades ago but initially largely ignored, the importance of m^6A in the regulation of mRNA fate and metabolism has brought it to the forefront of research in the last decade: from 12 publications mentioning m^6A in 2009, this number grew to 1509 in 2021 alone (Dubin and Taylor 1975; B. S. Zhao, Roundtree, and He 2017).

m^6A makes up 0.1–0.4% of the total adenosine in mammalian mRNA and is present
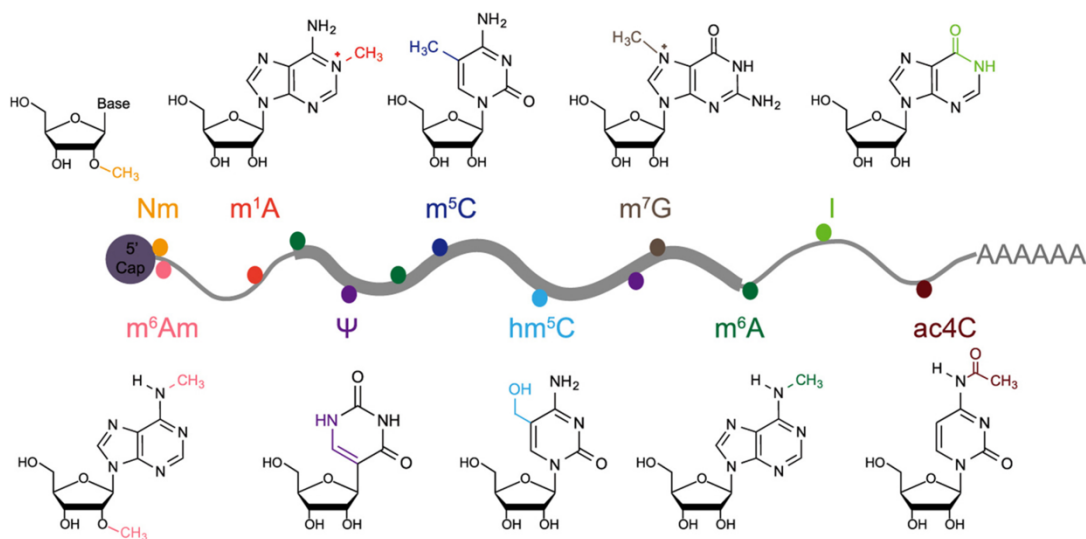
Figure I1. mRNA modifications. Common mRNA modifications and their locations along transcripts. Nm – 2'O-methylation, m^6Am – N^6,2'-O-dimethyladenosine, m^1A - N^1-methyladenosine, ψ – pseudouridine, m^5C – 5-methylcitosine, hm^5C – 5-hydroximethylcitosine, m^7G – 7-methylguanosine, m^6A – N^6-methyladenosine, I – inosine, N4-acetylcitidine. Modified from Song and Yi, 2020.

across multiple biological domains, from bacteria to eukaryotes and viruses (Meyer and Jaffrey 2014). Methylation marks are mostly added cotranscriptionally on targeted mRNAs at sites with the consensus motif sequence DRACH (where D=A,T or G, R=A or G, and H=A,T or C). These m^6A sites concentrate along the body of the labeled transcript, falling preferentially in the vicinity of stop codons, the 3' untranslated region (3' UTR) and on long exons (Dominissini et al. 2012; 2013). This location specificity gives m^6A sites a very particular distribution pattern along mRNA features that can be consistently replicated in practically all tissues and organisms that have been studied.

Existing marks can also be actively removed from labeled transcripts, a key property of m^{6}A that displays the dynamic nature of deposition and removal (Jia et al. 2011). In the same way that genetic information can be modulated through the modification of DNA or histone tails without altering its sequence, this novel regulatory layer controlling the fate of the transcriptome by adding, removing and binding marks on mRNA has been termed the epitranscriptome (Saletore et al. 2012). This has been key to the current interest in m^{6}A and brought about the inception of the field of epitranscriptomics.

The methylation machinery

m^{6}A writers

The addition of m^{6}A marks on the transcriptome is made possible by a group of proteins known as m^{6}A "writers". Within this group are the proteins methyltransferase-like 3 (METTL3, now named Methyltransferase 3, N^6-Adenosine- Methyltransferase Complex Catalytic Subunit) and methyltransferase-like 14 (METTL14, now named Methyltransferase 14, N^6-Adenosine-Methyltransferase Subunit) which form the catalytic core of the m^{6}A methyltransferase complex (mMC, J. Liu et al. 2014). These methyltransferases are sufficient to add m^{6}A marks on target transcripts with considerable specificity. From them, the main catalytic function is performed by METTL3 while METLL14 acts primarily binding to the mRNA and ensuring correct METTL3 positioning (Bokar et al. 1994; 1997). The catalytic core and the accessory, scaffolding and RNA-binding proteins (RBPs) associated with it are what is generally understood as the methyltransferase complex (Jianzhao Liu et al. 2014).

Another key member of the mMC is WT1 associated protein (WTAP), an adaptor protein that binds both METTL3 and METTL14 and is responsible for their recruitment to active methylation sites (Ping et al. 2014). WTAP is also responsible for part of the specificity of targeted mRNAs, being able to directly bind to transcripts in the vicinity of m^{6}A consensus sequences.

More recently, additional proteins have been identified as accessory proteins of the m^{6}A writer machinery and in certain literature they are considered components of the mMC (Moindrot et al. 2015; Schwartz et al. 2014). These are mainly other RBPs that are responsible for recruiting the core mMC to target mRNAs, conferring target specificity to the deposition of m^{6}A marks. One of such RBPs is the RNA binding motif protein 15

(RBM15). This protein was originally identified as a regulator of the hematopoietic lineage differentiation but it is now known to also regulate the deposition of m^6A marks in several types of RNA, being considered now a component of the mMC (Moindrot et al. 2015). RBM15 is key in the recruitment of the core mMC making possible the m^6A labeling of the ncRNA XIST, a key step in the silencing of chromosome X and thus, directly regulates dosage compensation in mammals (Patil et al. 2016). Evidence points to Rbm15 function as a binding protein of the mMC through its interaction with WTAP – directly or through its the bridging of zinc finger CCCH-type containing 13 (ZC3H13) – regulating the access of the methylation machinery to the vicinity of target transcripts (Knuckles et al. 2018, 3). This target specificity is likely made possible thanks to the ability of RBM15 to bind to chromatin-associated proteins like the SET domain bifurcated histone lysine methyltransferase 1 (SETDB1) or the SWI/SNF complex (Lee and Skalnik 2012, 15; Y. Xie et al. 2019).

ZC3H13 is itself also considered a key interactor of the methyltransferase complex, binding directly to WTAP and RBM15, and thus the core mMC (Knuckles et al. 2018, 3). ZC3H13 is key for the recruitment of the mMC to active transcription sites and to ensure its nuclear localization. Because of this, despite not being part of the core subunits or directly binding to them, Zc3h13 is a central component of the mMC and its absence results in a dramatic decrease in global m^6A, similar to the phenotype of Mettl3 removal (Wen et al. 2018).

Two other components of the mMC have been described in mammals: vir like m^6A methyltransferase associated (VIRMA) and Cbl Proto-Oncogene Like 1 (CBLL1, previously known as HAKAI). VIRMA acts as an additional recruiter of the mMC with a strong preference towards the stop codon and 3' UTR of mRNAs, and mediates the deposition of m^6A in those regions, as well as regulating 3' UTR length during processing (Yue et al. 2018). CBLL1 was originally identified as an E3 ubiquitin ligase, but the discovery of its ability to interact with the mMC has established it as another m^6A writer (Balacco and Soller 2019). CBLL1's precise function in mammals has remained elusive, but it was recently described to act as a stabilizer of the mMC. In the absence of CBLL1, mMC formation is impaired and therefore m^6A deposition is severely reduced (Bawankar et al. 2021).

m^{6}A Erasers

Like it is the case with many other RNA modifications, for decades it was thought of m^{6}A marks as stable, where following the methylation of a given adenosine nucleoside during transcription, the mRNA would retain this mark until being degraded. This model was changed in 2011 when the first m^{6}A demethylase, the FTO alpha-ketoglutarate dependent dioxygenase (FTO, previously known as fat mass and obesity associated) was described (Jia et al. 2011). This discovery transformed N^6-methyladenosine from just another of the many known RNA modifications into the most studied one in a very short span. The rekindled interest in m^{6}A has now developed into a research field of its own, "reborn" thanks to the rise of high throughput sequencing-based techniques and allowing us to revisit and rediscover a full level of biological regulation that remained forgotten for decades: *RNA epigenetics*, or the epitranscriptome (He 2010; Saletore et al. 2012).

FTO was originally described as a gene harboring multiple obesity and diabetes-associated polymorphisms, hence its original name (Frayling et al. 2007). Mice overexpressing this protein caused weight increases leading to obesity, whereas the complete removal of FTO caused a strong reduction in body weight accompanied by defects in dopaminergic neuron function (Hess et al. 2013; Gerken et al. 2007). Besides m^{6}A, FTO has now been shown to actively demethylate m^{6}Am and m^{1}A and is capable of binding to multiple RNA species, like mRNA snRNA and tRNA. FTO is mostly found in the nucleus, where it is often located at nuclear speckles, but it can also be found in the cytosol depending on the cellular context (Jia et al. 2011; Wei et al. 2018).

Another member of the nonheme Fe(II)- and α-KG-dependent dioxygenase ALKB family of proteins, the alkB homolog 5 (ALKBH5) is the only other known m^{6}A demethylase (Zheng et al. 2013). Although members of the same protein family, FTO and Alkbh5 share few structural similarities, functionally ALKBH5 is only able to demethylate m^{6}A (and not m^{6}Am or m^{1}A, like FTO) and they display limited overlap in expression, subcellular localization and target mRNAs (Zheng et al. 2013). Nevertheless, ALKBH5 has shown to be an important regulator of m^{6}A-dependent functions: mice lacking this protein show increased m^{6}A in a subset of transcripts which translates to altered splicing and increased degradation. Given the expression pattern of ALKBH5 and its

target genes, germ cells are especially vulnerable to its absence and *Alkbh5* knock-out (KO) mice are rendered infertile (Tang et al. 2018).

m^{6}A Readers

Methylation marks in mRNA can have multiple consequences for a labeled transcript – some of them even contradictory – depending on the cellular context, tissue, or in response to stimulus (Meyer and Jaffrey 2017). To be able to confer such a variety of possible outcomes to the same type of label, cells make use of multiple proteins that are able to recognize the presence of m^{6}A in RNAs and can alter the fate of the bound molecules. This process is not straightforward and a considerable effort has been put into disentangling the complexities of m^{6}A readers. The most direct way of m^{6}A reading depends on the direct detection of methylated adenosine in RNAs, a function that is mostly carried out by proteins of the YTH family (Liao, Sun, and Xu 2018). Other RBPs can detect the presence of m^{6}A marks through increased affinity of their target regions or by m^{6}A-induced changes in the secondary structure of RNA that expose otherwise unavailable binding sites (N. Liu et al. 2015; Arguello, DeLiberto, and Kleiner 2017).

The most widely studied type of m^{6}A readers are the members of the YTH family of RBPs, described as the first of the reader proteins (Fudong Li et al. 2014). Their name comes from the conserved YTH domain (YT521-B homology domain) shared by all members, and that makes them capable of binding directly to m^{6}A and modify the associated mRNA's cellular fate (Hartmann et al. 1999). In mammalian genomes, five YTH proteins have been identified as m^{6}A readers: YTHDF1. YTHDF2, YTHDF3, YTHDC1 and YTHDC2. Broadly, YTHDC1 is exclusively found in the nucleus where it regulates splicing, YTHDC2 has an RNA helicase activity and modulates RNA degradation, while YTHDF1–3 are cytoplasmic readers that regulate mRNA stability and translation (Liao, Sun, and Xu 2018; Scutenaire et al. 2018; Mao et al. 2019; Hsu et al. 2017).

Interaction studies have found dozens of additional potential m^{6}A reader proteins, with varying degrees of certainty about their actual binding ability and consequences for recognized transcripts (Arguello, DeLiberto, and Kleiner 2017). Members of two additional protein families contain multiple described m^{6}A readers, with various cellular functions: the heterogeneous nuclear ribonucleoprotein family (HnRNPC, HnRNPA2B1, and to a lesser extent hNRNPG) and the insulin-like growth factor 2 binding protein

(IGF2BP1, IGF2BP2 and IGF2BP3). hnRNPs are nuclear RBPs that act by binding to RNA secondary structures disrupted by m^{6}A and can alter splicing and processing of target precursor RNAs (Alarcón, et al. 2015; B. Wu et al. 2018), whereas IGF2BPs are primarily cytosolic proteins whose functions center around the regulation of mRNA stability and translation (Huilin Huang et al. 2018). Other reader proteins of relevance are the ELAV like RNA binding protein 1 (ELAVL1), the eukaryotic translation initiation factor 3 subunit A (EIF3A), the FMRP translational regulator 1 (FMR1) and METTL3 itself (Lin et al. 2016; Meyer et al. 2015; Dominissini et al. 2012).

The following section will delve deeper into the cellular consequences of m^{6}A labels and the specific reader proteins that mediate them (Figure I2), in addition to their known associations to the biology of healthy and disease organisms.
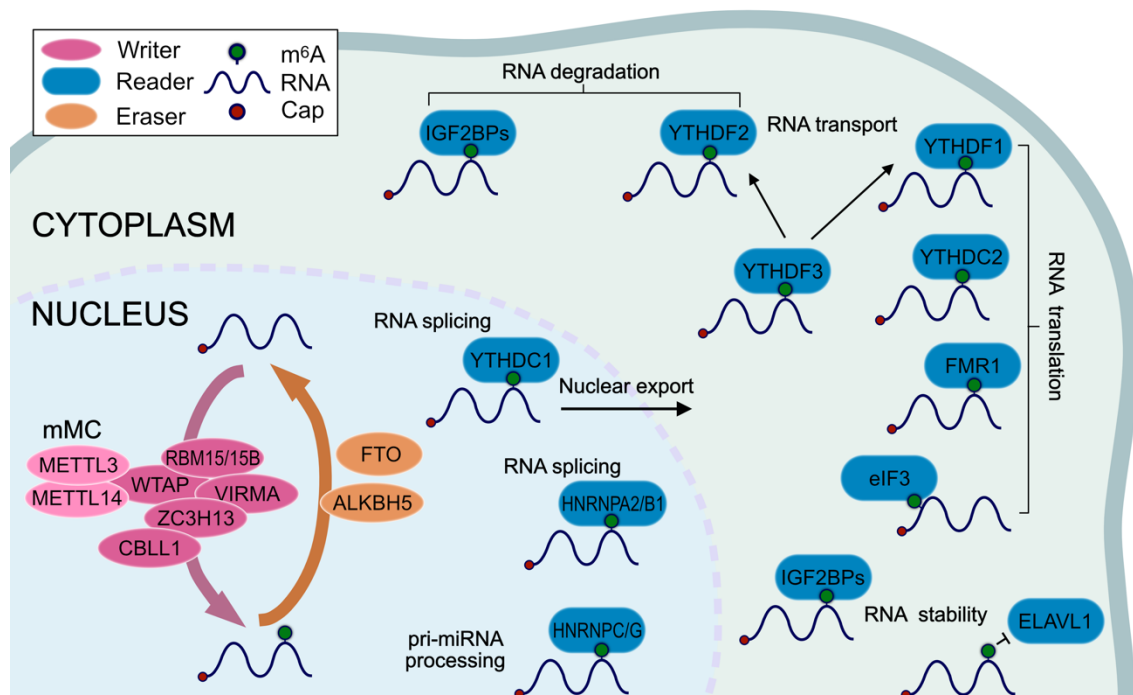
Figure I2. The m6A machinery and their role in RNA metabolism. Diagram showing the main members of the methylation machinery in the nucleus and cytoplasm. Highlighted are the principal downstream function for m^{6}A readers. Adapted and built upon from Zhang, 2020.

Roles of m^{6}A in RNA metabolism

Be it through the direct recruitment or repulsion of RBPs, or by altering RNA secondary structures to expose or hide RBP binding regions, the presence of m^{6}A marks on RNA

can have major consequences for its cellular fate. The regulation of mRNA splicing, nuclear export, transport, degradation, and translation are only some of the events that can be directly affected by the presence – or absence – of m^{6}A, in the majority of cases depending on the direct action of an m^{6}A reader (Y. Yang et al. 2018).

RNA processing

The processing of pre-mRNA through splicing to give rise to mature transcripts is a heavily regulated process, key for adequate cellular function. The involvement of m^{6}A in the regulation of splicing was hypothesized early on due to the location of methylation marks within intronic regions and close to splicing sites (Dominissini et al. 2012). The discovery of multiple splicing regulators that acted as m^{6}A readers supported this notion, however some debate still exists in the field whether splicing can actually be an m^{6}A-dependent mechanism (Ke et al. 2017; Adhikari et al. 2016).

Multiple pre-mRNA splicing regulation factors (SRSFs) were found to interact with methylated regions in a process mediated by the function of YTHDC1. The interaction of YTHDC1 with SRSF3 promotes exon inclusion and binds competitively to target sites with SRSF10 (Xiao et al. 2016; X. Zhao et al. 2014).

Another reader that has been implicated in the regulation of splicing is hnRNPA2B1. This nuclear factor is known to bind to mRNAs in an m^{6}A-dependent manner, and in its absence widespread alternative splicing events can be detected, similar to the splicing abnormalities that a global METTL3 reduction elicits (Alarcón, et al. 2015). Other members of the hnRNP family (particularly hnRNPC and hnRNPG) are also splicing regulators and have been identified as m^{6}A readers, but their specific functions as modulators of the processing of methylated mRNA are still not known (Dominissini et al. 2012; N. Liu et al. 2015; Edupuganti et al. 2017).

In addition to regulating mRNA splicing, hnRNPA2B1 was shown to directly affect the processing of primary miRNA precursors (pri-miRNAs) through its interaction with methylated adenosines in these molecules. By binding directly to the DGCR8 microprocessor complex subunit (DGCR8), it promotes the processing of methylated pri-miRNAs (Alarcón, et al. 2015).

mRNA stability

Shortly after the discovery of m^{6}A, it was reported that a negative correlation existed between the levels of m^{6}A and transcript half-life (Sommer, Lavi, and Darnell 1978). By now it is a well described phenomenon that m^{6}A can directly regulate the stability of labeled transcripts, although the specific mechanisms are varied and reader-dependent (X. Wang et al. 2014; Fu et al. 2014; Ke et al. 2017).

The cytoplasmic reader YTHDF2 has been widely described as a regulator of mRNA stability. YTHDF2 binding can promote degradation by directing m^{6}A-labeled mRNAs towards P-bodies (cellular sites of mRNA decay) or by recruiting the CCR4/NOT complex, responsible for mRNA degradation initiation (X. Wang et al. 2014).

The presence of m^{6}A can also promote degradation by impeding the binding of ELAVL1. This protein promotes mRNA stability and translation by interacting with miRNA binding sites in the 3' UTR of mRNA, thus preventing miRNA-driven degradation (Y. Wang et al. 2014; Simone and Keene 2013). In addition to this, the presence of m^{6}A marks in transcripts can promote their immediate degradation after transcription. Through the process known as co-transcriptional gene silencing, methylated transcripts can be targeted by DGCR8 for degradation, particularly in cellular stress conditions (Knuckles et al. 2017).

mRNA translation

In contrast to what its relationship to mRNA stability is, m^{6}A levels generally display a positive correlation to translational efficiency. Methylation at both the 3' UTR and 5' UTR has been shown to positively influence translation through multiple mechanisms (X. Wang et al. 2015; Meyer et al. 2015).

Two readers of the YTH family – YTHDF1 and YTHDF3 – are known to directly promote the translation of bound m^{6}A-labeled mRNAs. Both of these proteins bind to mRNA in the vicinity of the stop codon and their absence results in the strongly reduced translation of target mRNAs (X. Wang et al. 2015; Shi et al. 2017; Q. Li et al. 2017). Furthermore, YTHDF3 can interact with YTHDF1 and recruit it to bound transcripts, whereas YTHDF1 is able to directly associate with eIF3 and thus the translation machinery. m^{6}A marks located at the 5' UTR can also be directly bound by the eIF3,

promoting the cap-independent translation of stress-related transcripts (Meyer et al. 2015).

Another translational regulator that has been identified as an m^6A reader is FMR1. This protein is a well-known translational repressor that acts by blocking initiation and elongation, and is directly involved in the regulation of synaptic plasticity through local translation of synaptic transcripts (Laggerbauer et al. 2001; Sidorov, Auerbach, and Bear 2013). Mutations in FMR1 are known to cause several types of neuropsychiatric disorders including intellectual disability and autism (Bassell and Warren 2008). Not much is known about the downstream effects of m^6A-mediated FMR1 translational repression, but a model where competitive binding by YTHDF1 and FMR1 in a subset of mRNAs has been proposed (Edupuganti et al. 2017).

mRNA localization

The regulation of RNA transport to specific subcellular locations is a key process that can have consequences for the translation, storage or degradation of mRNAs. Little is known about the specific proteins responsible for the differential transport of methylated transcripts, but the phenomenon of m^6A-dependent localization of mRNAs is well documented (Madugalle et al. 2020).

Multiple studies have documented the observation that methylated transcripts are preferentially exported from the nucleus towards the cytoplasm, although the exact mechanism behind this m^6A function has remained elusive (Zheng et al. 2013). Several mechanisms have been proposed, ultimately involving the recruitment of the nuclear export factor 1 (NFX1) to promote the transport of m^6A-containing mRNAs outside of the nucleus (Arguello, DeLiberto, and Kleiner 2017; Edupuganti et al. 2017). A candidate for the responsible m^6A reader is YTHDC1, thanks to its interaction with SRFS3, a known regulator of nuclear export (Xiao et al. 2016).

Cytoplasmic ribonucleoprotein complexes (RNPCs) – like P-granules or stress granules – are membraneless organelles formed by liquid-liquid phase separation (LLPS) that concentrate groups of RNAs and proteins in specific locations to regulate the storage, degradation or synthesis of macromolecules. m^6A is known to promote the transport of labeled transcripts towards P-bodies in a YTHDF2-dependent manner, promoting their degradation (X. Wang et al. 2014; Ries et al. 2019). YTHDF3-bound, m^6A labeled

transcripts are also preferentially transported towards stress granules during oxidative stress (Anders et al. 2018). Furthermore, m^{6}A enhances the propensity of labeled mRNAs and associated readers (again YTHDF2) to undergo LLPS, a process key for RNC formation (Ries et al. 2019; S.-Y. Liu et al. 2020). These properties of methylated transcripts make m^{6}A an interesting candidate in the regulation of mRNA incorporation into other RNCs, like neuronal ribonucleoprotein particles, key regulators of mRNA availability in dendritic and axonal compartments (Formicola, Vijayakumar, and Besse 2019).

m^{6}A regulation in the central nervous system

The remarkable complexity of the mammalian central nervous system (CNS) is made possible thanks to the minute regulation of gene expression, beginning during early development, extending through maturity and senescence (A. Moccia and Martin 2018). Many regulatory mechanisms have to act in concert to achieve such fine-tuned spatiotemporal control during an organism's life. From genetic, to epigenetic factors, to signaling molecules and, more recently, epitranscriptomic regulators, the molecules involved in the establishment, maintenance and function of the CNS are still being described (Yen and Chen 2021).

The levels of m^{6}A are highest in the brain, and tissue-specific analyses of methylation in distinct brain regions paint a complex picture of epitranscriptome regulation across the mammalian CNS (Figure I3; Meyer et al. 2012; Jun'e Liu et al. 2020). N^6-methyladenosine plays major roles during CNS development, is crucial for its correct function and is likely involved in many of the pathological processes that involve CNS impairment (J. Yu, She, and Ji 2021; Chang et al. 2017).

During development

Already at the earliest developmental stages, m^{6}A regulation is involved in the maintenance of pluripotency and is necessary for the correct differentiation of early progenitors, through the regulation of the stability and translation of pluripotency-associated factors (Batista et al. 2014; Geula et al. 2015). This key function of m^{6}A is made evident by the early embryonic lethality of the constitutive KOs of both *Mettl3* and *Mettl14* (Geula et al. 2015).

At later stages, the development of the CNS is dependent on the formation of early neuronal precursors from neural stem cells (NSCs), which will further divide, differentiate and migrate to mature into functional neurons and – at later stages – glial cells (Paridaen and Huttner 2014). This process depends on a delicate balance between cellular proliferation, differentiation and migration. After the loss of m^{6}A by *Mettl3* or *Mettl14* depletion or after removal of YTHDF2, cortical NSCs show a dramatic delay in cell cycle progression due to altered mRNA translation and decay, resulting in decreased neuronal and glial differentiation and maturation in mice (Atlasi and Stunnenberg 2017; Weinberger et al. 2016; Frye et al. 2018). This relationship appears to have a physiological function in the regulation of the neurogenic potential of cortical neuronal progenitors. Certain similarities exist between these observations and studies performed on human-derived brain organoids, showing that m^{6}A-dependent regulation of neurogenesis might be a conserved mechanism across mammalian species (Yoon et al. 2017).

N^6-methyladenosine also plays a major role during the development of the cerebellum, a process that takes place postnatally. Alterations in m^{6}A-dependent regulation result in proliferation dysfunctions in progenitors and aberrant differentiation of granule cells, as well as impaired function of Purkinje cells (C.-X. Wang et al. 2018; Ma et al. 2018). Changes in mRNA stability, splicing and nuclear export were described as the mechanisms involved in this phenotype. Disruptions in m^{6}A function can also affect the differentiation of neural progenitors into non-neuronal lineages, like oligodendrocytes but the readers involved in this process are still not known (R. Wu et al. 2019).

In the adult CNS

From embryonic development and towards adulthood, m^{6}A levels in the CNS increase sharply, a change that highlights the importance of this mark for the function of the adult brain (Meyer et al. 2012). Looking at the subpopulations of methylated transcripts in the adult brain, it is clear that processes like neurogenesis, learning and memory as well as synaptic regulation could be targets for m^{6}A function in this context (Livneh et al. 2020). Evidence for this role of m^{6}A has been obtained from behavioral experiments in mice with altered epitranscriptomic regulation.

Two studies observed a direct relationship between the levels of the eraser FTO and hippocampal as well as cortical-dependent fear conditioning. Transient increases in FTO levels in the vicinity of synapses could be observed in response to fear conditioning and the deletion of this gene resulted in increased fear memory in mice. Interestingly, the removal of *Mettl3* also showed enhanced fear memory, although no mechanism has been put forward to reconcile these observations (Engel et al. 2018; Widagdo et al. 2016). Another study evaluated the effects of a mild decrease in methylation, conferred by the conditional KO of *Mettl14* in the striatum. These mice displayed alterations in striatum-mediated learning and deficient dopaminergic signaling (Koranda et al. 2018).
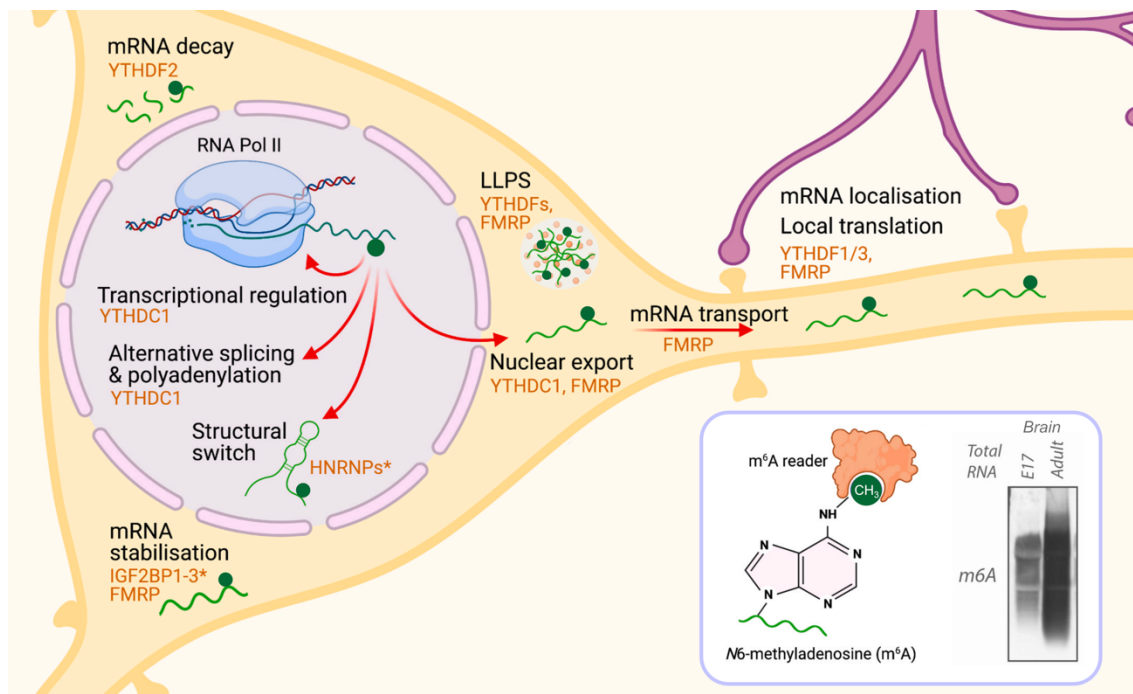
Figure I3. m6A regulation in neuronal function. The known roles of m6A in neuronal homeostasis and in response to stimulus. The responsible m6A readers are highlighted in orange. LLPS – liquid-liquid phase separation. Adapted from Widagdo 2018 and 2020.

Additionally, the m^6A reader YTHDF1 was shown to modulate the translation of activity-induced genes in response to neuronal activation during learning. In the absence of this reader, mice show impaired synaptic transmission and long-term potentiation, additionally, synaptic morphology defects can be observed in *in vitro* models (Shi et al. 2018).

The methylation of certain mRNAs was also shown to promote their transport to synaptic compartments, likely through the activity of YTHDF1 and 3. Among these mRNAs are several genes involved in the response to synaptic stimulus (many of them immediate early genes, IEGs), like APC. The depletion of *Ythdf1 in vitro* abolished the translation of several IEGs and hindered synaptic maturation and function, supporting the observations from the *Ythdf1* KO mouse (Merkurjev et al. 2018). This translation-dependent role of m^{6}A in synaptic regulation is further supported by another study that showed that hippocampal knock-down (KD) of *Mettl3* decreases the translational rate of IEGs in a way that emulates the phenotype of YTHDF1 removal (Z. Zhang et al. 2018). In contrast, *Mettl3* overexpression enhances long-term memory consolidation.

The recent research in this field has characterized well the importance of m^{6}A in the regulation of synaptic function and its consequences for learning and memory. Due to the nature of m^{6}A marks and the machinery that regulates them, disentangling the contributions of individual mechanisms to the overall effects of alterations in the m^{6}A machinery is challenging. The existing literature has not been able to make a distinction between the m^{6}A-dependent regulation of somatic translation and the possible modulation of translation at the synapse, but this possible role of m^{6}A has been put forward as a possibility in several studies (Widagdo and Anggono 2018; Leonetti et al. 2020). This idea is further supported by the presence of several members of the methylation machinery in dendritic and even synaptic compartments in cortical and hippocampal neurons, like METTL14 (and possibly also METTL3), FTO, as well as the readers YTHDF1–3 (Merkurjev et al. 2018; Gershoni-Emek et al. 2016). Additionally, studies show that the transcriptional repressor FMR1 is able to bind m^{6}A, although whether this interaction is direct is not yet clear (Edupuganti et al. 2017). FMR1's function as a major regulator of local translation at the synapse and its key role in CNS pathology might prove to be a missing piece in the puzzle of m^{6}A and translation in the CNS (Laggerbauer et al. 2001). Further evidence of local translation being affected by epitranscriptome changes comes from a study that showed the FTO-dependent regulation of axonal growth through modulation of local translation in dorsal ganglia neurons (J. Yu et al. 2018).

In cancer

A big contributor to the present popularity of epitranscriptome research is the extensive roles that m^{6}A and proteins of the methylation machinery have been shown to have in the regulation of oncogenic pathways in multiple types of cancer (Sun, Wu, and Ming 2019). In light of the myriad of molecular pathways that can be affected by epitranscriptomic regulation, including proliferation and migration, it is not surprising that m^{6}A would also act as a regulator in the progression of these diseases.

A few studies have focused on the relationship between methylation and cancer in the CNS. The presence of m^{6}A is associated with increased proliferation and tumorigenesis of glioblastoma stem cells as shown by the phenotypes of *Alkbh5*, *Mettl3* and *Mettl14* KDs (Q. Cui et al. 2017; Fuxi Li et al. 2019; S. Zhang et al. 2017). However, the exact nature of this relationship is still under debate, with conflicting reports of the molecular relationship between m^{6}A levels and tumorigenicity. In neuroblastoma, m^{6}A modifications were shown to inhibit the disease progression (Cheng et al. 2020).

Further functions of m^{6}A in multiple types of cancer have been widely researched and are thoroughly reviewed elsewhere (Sun, Wu, and Ming 2019), since this topic is beyond the scope of this work I will not delve further into this particular field of epitranscriptome research. It suffices to say that a lot of the knowledge that we have of m^{6}A function has been generated through the research of its function in cancer and, in this same vein, its relevance as an oncogenic regulator has made the members of the methylation machinery prime targets for the development of pharmacological therapies aiming to treat specific kinds of cancer (Moroz-Omori et al. 2021; G. Xie et al. 2021; Yankova et al. 2021).

In neurological disorders

In light of the significant role of m^{6}A in multiple aspects of CNS physiology, it is no surprise that disruptions in m^{6}A regulation have significant consequences for proper CNS function and ultimately can lead to pathologies (C. Yang et al. 2020; X. Jiang et al. 2021). Being a very active field of research, the precise m^{6}A mechanisms involved in disease onset are in many cases not yet clear.

Some evidence exists of a possible link between m^{6}A and psychiatric disorders, although these relationships are correlative they might point to a larger role of m^{6}A in

pathology. Certain allelic variants of *FTO* and *ALKBH5* showed significant association with major depression disorders and variants of *FTO* were also associated with attention deficit/hyperactivity disorder (ADHD; Du et al. 2015; Milaneschi et al. 2014; Choudhry et al. 2013). In addition, transcripts linked with mental disorders like autism and schizophrenia are known to be heavily regulated by m⁶A (Angelova et al. 2018).

In neurodegeneration

Neurodegenerative disorders are among the most prevalent diseases worldwide (Berson et al. 2018). An increasingly aging population added to the ineffectiveness of known treatments to control disease progression and address their symptoms, have made the search for novel pathways involved in neurodegeneration a crucial aim in current research. Synaptic dysfunction and the loss of plasticity, progressing into loss of cognitive function, are key hallmarks of various neurodegenerative diseases (Wilson et al. 2010). Given the known functions of m⁶A in synaptic transmission and memory, multiple groups have very recently studied the relationship between methylation and the etiology of neurodegeneration.

The existence of an FTO-dependent regulation of dopaminergic activity in the midbrain suggests a possible role of m⁶A during Parkinson's disease (PD) onset and progression (Hess et al. 2013). Indeed, decreased m⁶A was observed in an animal model of PD, caused by the overexpression of FTO (Chen et al. 2019). As a consequence of this change, dopaminergic neuron apoptosis was observed following glutamate ionotropic receptor NMDA type subunit 1-induced oxidative stress (GRIN1).

A few studies have been carried out to evaluate the role of m⁶A in Alzheimer's disease (AD). In the AD animal model APP/PS1, a global increase in m⁶A levels was detected along with the overexpression of METTL3 and decrease in FTO levels (M. Han et al. 2020). In contrast, another AD animal model (5XFAD) showed the opposite effect, with reduced METTL3 and increased FTO at both the mRNA and protein levels. In addition, many AD-related transcripts showed a significant reduction in m⁶A levels (Shafik et al. 2021). Post mortem samples from AD patients displayed reduced protein levels of METTL3, which would result in reduced m⁶A (He Huang et al. 2020). A study looking at postmortem AD patient samples showed a significant reduction in both m⁶A and METTL3 levels. These changes were caused by an oligomeric β-amyloid-dependent downregulation of *Mettl3* and had consequences for the level of certain synaptic

proteins associated with AD progression, causing synaptic loss and neuronal death (F. Zhao et al. 2021). In contrast to these results, another recent work showed a general trend towards the increase in global m^{6}A correlating with AD progression (Deng et al. 2021). Their observations also shed some light on the possible molecular mechanisms that could link m^{6}A dysfunction with AD and other tauopathies. In a model of tauopathy, methylated transcripts were increasingly recruited into stress granules through the binding of the reader hnRNPA2B1 and its interaction with oligomeric Tau, inhibiting the synthesis of neuronal function transcripts (Deng et al. 2021).

As evidenced by these studies, the nature of the relationship between m^{6}A and AD is not clear-cut, and some of the results published seem to contradict each other. Given the multiple roles of m^{6}A regulation in brain function, the use of different animal models and technical approaches, our ability to accurately model these interactions is currently limited. Further research will be needed in this field to unravel the complexities of the link between m^{6}A and AD, what are the consequences of this disease for the epitranscriptome and how alterations in the m^{6}A machinery can contribute to AD etiology. Of particular value will be the generation of large-scale sequencing data of the epitranscriptome in AD patients, which will allow us to gain insight into the molecular pathways most affected by AD-associated m^{6}A alterations.

Cellular and molecular basis of learning and memory

Huge steps have been taken in improving our understanding of learning and memory ever since at the end of the 19th century Ramón y Cajal put forward the idea that changes in the strength of the connections between his newly discovered neurons (which Charles Sherrington would later name synapses) could serve as the basis for memory (Cajal and Azoulay 1894; S. M. Foster 1895). This idea was further built on for decades until in 1948 Jerzy Konorski termed this concept synaptic plasticity, and only a year later Donald Hebb published his theory of synaptic adaptation during learning as the basis of memory formation (Konorski 1948; Hebb 1949). In the decades that have followed these seminal works, the importance of synaptic plasticity for learning and memory has been well established (Glanzman 2010; Mateos-Aparicio and Rodríguez-Moreno 2019). In spite of the big steps that have been taken in understanding the

mechanisms underlying the acquisition, storage and retrieval of certain types of memory, by and large, our knowledge of the molecular processes involved in learning and memory is still limited.

Learning and memory

The ability to sense stimuli and react to them is a key property of life, allowing organisms to interact with their environment and respond to it in a context-specific manner. But without the capacity to integrate the outcome of past experiences into a process of decision-making that will influence future interactions, organisms are limited to a life stimulus-response with little room for improvement. Such ability to incorporate past experiences to alter present and future behavior is what is understood as memory, and the process used by organisms to acquire and consolidate new memories is called learning (Okano, Hirano, and Balaban 2000). A life without memory formation might appear senseless and unimaginable to us humans, so it is no wonder that ever since the dawn of scientific research, the nature of memory formation and storage have puzzled humankind.

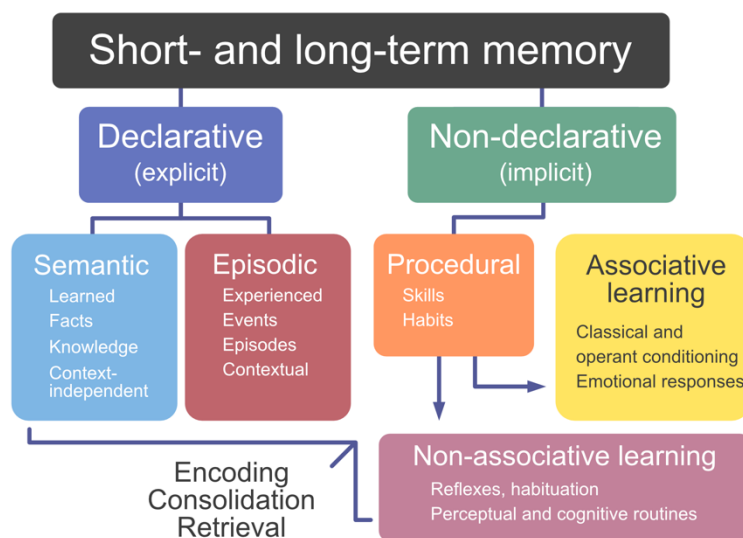**Figure I4. A simplified view of memory and learning.** Summary of the types of memory and learning associated with them. Adapted from Brem, 2013

Several types of learning have been defined and they describe the main strategies used by animals capable of learning to acquire memories, from nematodes to humans (Figure I4). Associative learning (often called conditioning) is the most commonly encountered

type of learning and it depends on the association between two stimuli or events, it can be further divided in operant and classical conditioning (Kandel, Dudai, and Mayford 2014). Operant conditioning is the type of associative learning that depends on the reinforcement (a reward or punishment) of a behavior to alter the frequency of said behavior. Whereas classical conditioning refers to the association between an existing response and a neutral stimulus, resulting in the ability of the neutral stimulus to elicit the original response. In contrast to the associative, non-associative learning does not depend on multiple stimuli and instead refers to the ability to change the intensity of response to a stimulus when this is repeated (Kandel, Dudai, and Mayford 2014). It can be called habituation (when repeated stimuli decrease the response) or sensitization (when the response intensifies).

The different types of memory can be defined by the type of functions they are most associated with: declarative (or explicit) memory concerns information, facts and events that are available and can be recalled consciously; this is in contrast to non-declarative (also procedural or implicit) memory that is not consciously available and relates to the storage of learned skills (Kandel, Dudai, and Mayford 2014). Studies made in the mid-20th century on amnesic patients due to the partial loss of certain brain regions showed that these types of memory reside in distinct locations in the brain and that significant connectivity exists among them (Scoville and Milner 1957). Although declarative and procedural memory are coded independently of each other they both rely heavily on the connectivity and function of the hippocampus (Bird and Burgess 2008).

Learning and memory in the limbic system

The limbic system (LS) occupies the medial cortical region of the frontal lobe, lying at the border between the brain hemispheres. This region of the brain contains multiple structures that are heavily involved in memory formation and storage, but also in other higher brain functions, including emotion, behavior and the reward system (Pessoa and Hof 2015). Many structures are considered part of the LS, but this being a term defined by anatomic location and not function, there is debate on which regions should be included and which not, or even whether the LS should be considered a single entity at all. Regardless, memory-associated regions of the LS include the amygdala, entorhinal cortex, nucleus accumbens, thalamus, hippocampus and cingulate cortex (Figure I5); Rolls 2015; Hornak et al. 2003). Despite the great importance of many of these

structures in brain connectivity, given the scope of my work, I will focus on the latter two regions: the hippocampus and the cingulate cortex.

The hippocampus is key for the formation and storage of declarative memory, for the recall of specific events in an organism's life (episodic memory) and to a lesser degree of facts, ideas and concepts (semantic memory), both subsets of the former (Kandel, Dudai, and Mayford 2014). This model stems from observations made in 1957 with the case study of a patient, referred to as H.M., who after a long history of epileptic seizures had a section of the medial temporal lobe (that included the hippocampus) surgically removed. After the intervention, H.M. suffered from complete retrograde amnesia affecting his declarative, but not procedural, memory (Scoville and Milner 1957). In the following decades, studies in non-human primates and other mammals have described the importance of the hippocampal circuitry in spatial learning, associative learning, and fear memory, placing the hippocampus and associated brain regions at the center of
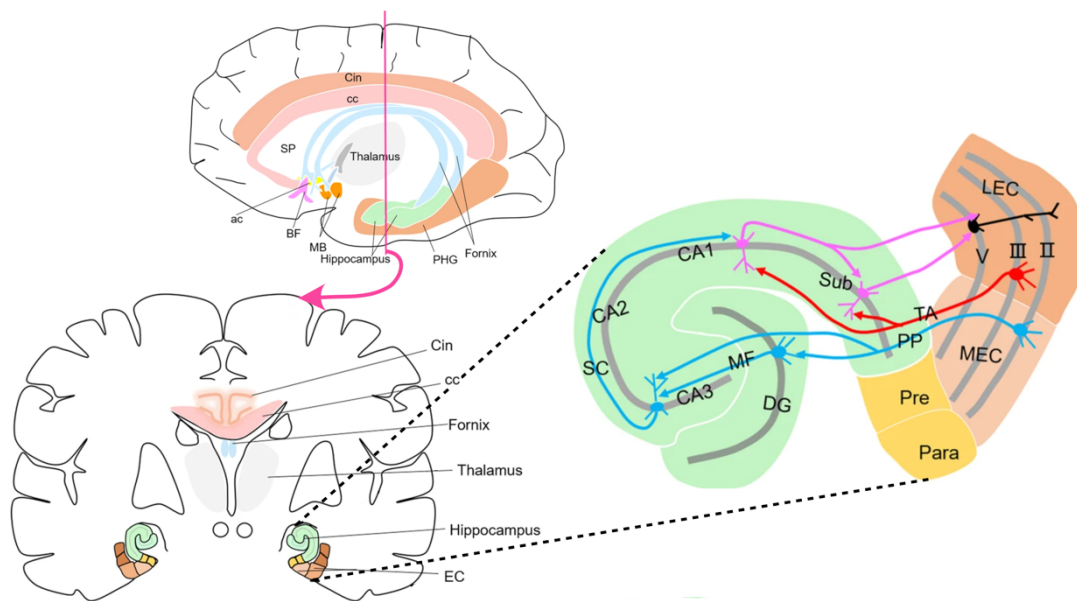

Figure I5. Structure and connectivity of the limbic system. Lateral and coronal view of the structures making the limbic system in the human brain. Inset shows the basic circuitry of the hippocampus. Input from the EC arrives to the DG through the PP. Granule cells innervate pyramidal neurons of the CA3 through the MF. SC of the CA3 project towards the CA1. ac - anterior commissure, ATN - anterior thalamic nuclei, BF - basal forebrain, cc - corpus callosum, Cin - cingulate gyrus, DG - dentate gyrus, EC - entorhinal cortex, LEC - lateral entorhinal cortex, MB - mammillary body, MEC - medial entorhinal cortex, MF - Mossy fibers, MTT - mammillothalamic tract, Para - parasubiculum, PHG - parahippocampal gyrus, PP - perforant path, Pre - presubiculum, Sub - subiculum, SC - Schaffer collateral, SP - septa pellucidum, TA - temporoammonic path. Modified from Yu - 2019.

multiple current models for memory formation, storage and retrieval (Bird and Burgess 2008; Bliss and Collingridge 1993).

Structurally, the hippocampus is composed of several distinct subregions, or subfields: the dentate gyrus (DG) and the cornu Ammonis (CA, sometimes referred to as hippocampus proper), further subdivided into CA1, CA2 and CA3 (Amaral and Witter 1989). The central circuitry of the hippocampus, involved in information processing and learning, depends on the transmission of signals from the perforant pathway of the entorhinal cortex into the DG, axonal mossy fibers of the DG project into the CA3, and in turn the Schaffer collateral axons originating in the CA3 can contact pyramidal neurons in the CA1, from where several brain regions are targeted (Bird and Burgess 2008; Arszovszki, Borhegyi, and Klausberger 2014). Hippocampal projections are known to target multiple brain areas, including the amygdala, prefrontal cortex, striatum, hypothalamus and cerebellum, making it a central component in the formation and retrieval of several types of memory (Saunders, Rosene, and Van Hoesen 1988; Z. Cui, Gerfen, and Young 3rd 2013; W. Yu and Krook-Magnuson 2015; Arszovszki, Borhegyi, and Klausberger 2014). It is also worth noting that the DG hosts the only known neurogenic niche in the adult human brain, a process that has been shown to be key in hippocampus-dependent memory formation (Lucassen et al. 2020).

Another LS structure, the cingulate cortex (CC), is a section of cerebral cortex located along the midline, above the corpus callosum, and it is better known due to its association with emotion (Rolls 2016). Structurally, the CC is commonly divided in two regions, the anterior cingulate cortex (ACC) and the posterior cingulate cortex (PCC) – some studies also refer to a midcingulate cortex (Rolls 2019). Unlike the hippocampus, the CC conservation across mammals is limited, although some functional and structural homology exists with the mouse ACC and PCC (Heukelum et al. 2020). The PCC has significant connectivity to the hippocampus and parahippocampal areas, playing a role in episodic memory (Leech and Sharp 2014). The ACC is more tightly connected to the amygdala and the orbitofrontal cortex, modulating the reward system and affecting emotion (Hornak et al. 2003). Given the distinct roles and signaling networks of its subregions, it has been proposed that the CC serves as a bridge between neocortical areas associated with reward systems and learning, and the hippocampal memory system (Rolls 2019).

Molecular organization of the synapse

The synapse is largely recognized as the unit of memory encoding. Hypothesized since the first time neurons could be observed up close more than a century ago, synapses have evolved in our understanding from largely static unidirectional communication points into a highly complex and dynamic hub for a myriad of signaling mechanisms on which memory relies (Cajal 1904; S. M. Foster 1895).

It is calculated that more than a hundred trillion synapses exist in the human CNS, connecting the more than one hundred billion neurons that comprise it (Pacitti, Privolizzi, and Bax 2019). In the broadest sense, synapses refer to the sites of communication existing between the terminal end of a neuron and another neuron (generally in a dendrite) and chemical synapses are the dominant type in the CNS (Choquet and Triller 2013).

Chemical synapses depend on the controlled release of a neurotransmitter from the terminal neuron (the presynaptic compartment) into the synaptic cleft and the subsequent binding of said neurotransmitter to specific receptors in the receiving neuron (postsynaptic compartment). Depending on the type of receptors present at the postsynapse (ionotropic or metabotropic), the neurotransmitter-mediated signaling can elicit a change in the membrane potential of the target cell to further propagate the signal, as well as initiate signaling cascades that will affect the way the postsynaptic neuron will respond to subsequent stimuli (Choquet and Triller 2013).

Glutamatergic synapses are the main excitatory synapses in the mammalian brain (whereas γ-aminobutyric acid [GABA]-ergic synapses are the main inhibitory ones), and the principal mediator of many higher brain functions, from sensory perception to emotion and cognition (Hassel and Dingledine 2012; Hackett and Ueda 2015). Glutamate is transported into neurons after crossing the blood-brain barrier and packaged into vesicles by multiple glutamate transporters (vesicle glutamate transporters, VGLUT1–3) and transported to the distal neuronal projections (Santos, Li, and Voglmaier 2009). At the presynapse, vesicle docking is mediated by a large group of vesicle- and membrane bound proteins that will anchor the vesicle in place, many of them corresponding to the SNARE protein complex (J. Han, Pluhackova, and Böckmann 2017). In response to a sudden transient depolarization of sufficient intensity (action potential), Ca^{2+} influx promotes the fusion of synaptic vesicles and subsequent

release of neurotransmitter into the synaptic cleft (Hackett and Ueda 2015). In the postsynapse, two main types of ionotropic (permeable to ion influx in response to activation) glutamate receptors exist, the NMDA (N-methyl-D-aspartate) and AMPA (α-amino-3-hydroxy-5-methyl-4-isoxazolepropionic acid) receptors (NMDARs and AMPARs; Bowie 2008). In addition to them, a group of metabotropic (G-protein coupled receptors that induce a signaling cascade in response to activation) receptors, mGluR1–8 can also be present (Pin and Duvoisin 1995; Ferraguti and Shigemoto 2006). It is through the complementary action of these receptors that signal transmission can be further propagated and modulated.
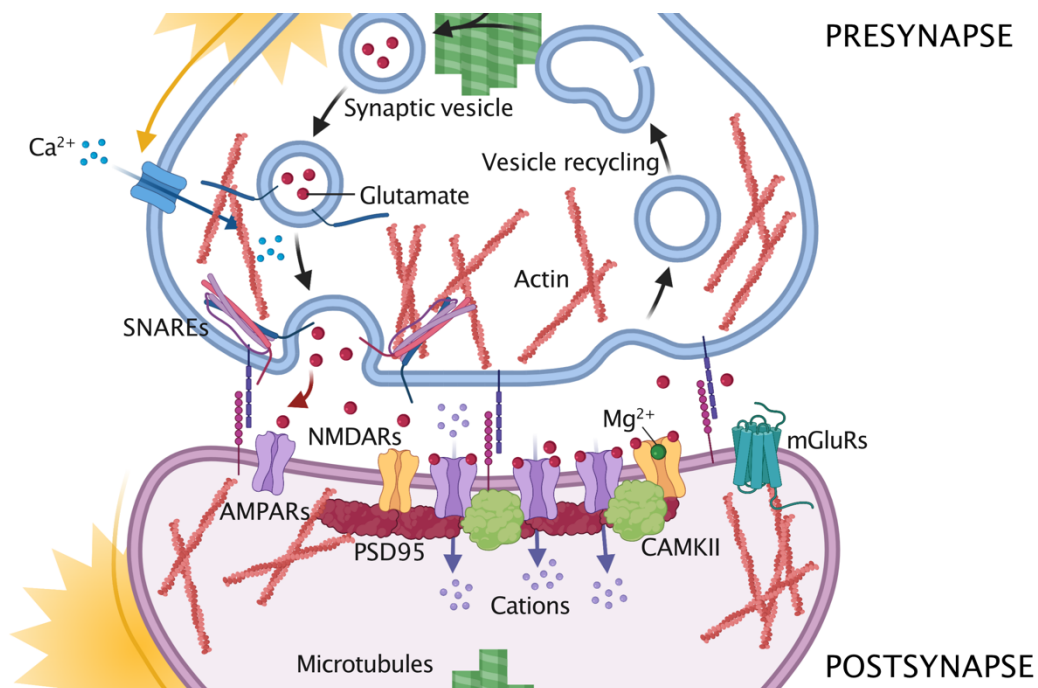

Figure I6. Molecular basis of glutamatergic synaptic transmission. Presynaptic depolarization elicits the activation of voltage-dependent Ca^{2+} channels, promoting the fusion and release of synaptic vesicles filled with glutamate. Postsynaptic glutamate receptors AMPARs, NMDARs (ionotropic), and mGluRs (metabotropic) mediate downstream mechanisms of signal propagation, from postsynaptic depolarization and action potential generation, to gene expression changes. CaMKII - calcium/calmodulin dependent protein kinase II, PSD95 – postsynaptic density protein 95

Every step of the process of synaptic transmission is a heavily regulated one, and the contribution of epigenetic factors, transcriptional regulation, translation, posttranscriptional and posttranslational modifications, as well as signaling molecules, among many others, can heavily influence synaptic function and hence learning and

memory (J. Jiang, Suppiramaniam, and Wooten 2006; Sheng and Kim 2011; Sultan and Day 2011).

Synaptic plasticity

Neural plasticity is understood as the ability of the brain to adapt to ever-changing stimuli and respond to them by altering brain structure, connectivity or function (Mateos-Aparicio and Rodríguez-Moreno 2019). At the synapse level, two mechanisms are considered the principal tools for the neural plasticity underlying learning and memory: long-term potentiation (LTP) and long-term depression (LTD; Figure I7; Malenka and Bear 2004).

Described in 1973 in the dentate gyrus of the hippocampus, LTP can occur in the glutamatergic postsynapses of multiple brain regions in the mammalian brain (Bliss and Lømo 1973; Bliss and Collingridge 1993). The most prominent form of LTP depends on the activation of the NMDA glutamate receptor in response to strong signaling and can last hours or longer. Experimentally, LPT can be induced by short (1 s) high-frequency stimulation (50–100 Hz) of presynaptic axons, for example in the Schaffer collaterals (Lüscher and Malenka 2012).

While both AMPARs and NMDARs are ionotropic ligand-activated receptors, the latter have the ability to also be activated by voltage changes in the postsynaptic membrane (Morris 2013). Indeed, under low intensity depolarization, NMDARs are blocked by extracellular Mg^{2+} limiting the cation influx through the channel pore. In response to strong depolarizations, the Mg^{2+} block is repelled and NDMARs allow the flow of cations through the membrane non-selectively, namely Na^+ and Ca^{2+} into and K^+ out of the cell. This sudden Ca^{2+} influx can induce multiple Ca^{2+}-dependent signaling cascades that can ultimately elicit lasting changes in the postsynaptic neurons, leading to synaptic potentiation (Lüscher and Malenka 2012). The main routes of Ca^{2+}-dependent LTP depend on the enhanced sensitivity of glutamate receptors, the increase in receptor number by exocytosis and long-term changes in the postsynaptic neuron due to the induction of transcription-dependent changes in gene expression (Choquet and Triller 2013). A major regulator of the transcriptional program during plasticity is the transcription factor CREB (cAMP response element-binding protein), responsible for the increased expression of genes associated with increased synaptic transmission and plasticity (Sakamoto, Karelina, and Obrietan 2011).

Many of the proteins involved in the induction and maintenance of LTP are protein kinases, chief among them is the calcium/calmodulin dependent protein kinase II (CaMKII), since without it LTP induction is not possible (Sacktor and Fenton 2018). Multiple isoforms of the CaMKII have been described in mammals (α, β, γ and δ), each with tissue and cell-specific expression patterns, but α, β, and to a lesser extent γ play key roles in LTP regulation (Zalcman, Federman, and Romano 2018). In response to strong Ca^{2+} influx at the postsynapse, CaMKII can phosphorylate itself increasing its sensitivity, translocate to the postsynaptic density (PSD) and bind to NMDARs. From there, CaMKII can directly affect the properties of AMPARs, as well as promote their trafficking and anchoring, effectively strengthening the potentiated synapse (Lisman, Schulman, and Cline 2002). Behavioral studies have shown that several types of memory are strongly impaired by the absence of CaMKII, cementing its role as a key regulator of LTP-mediated learning and memory (Sanhueza and Lisman 2013; Lisman, Schulman, and Cline 2002).
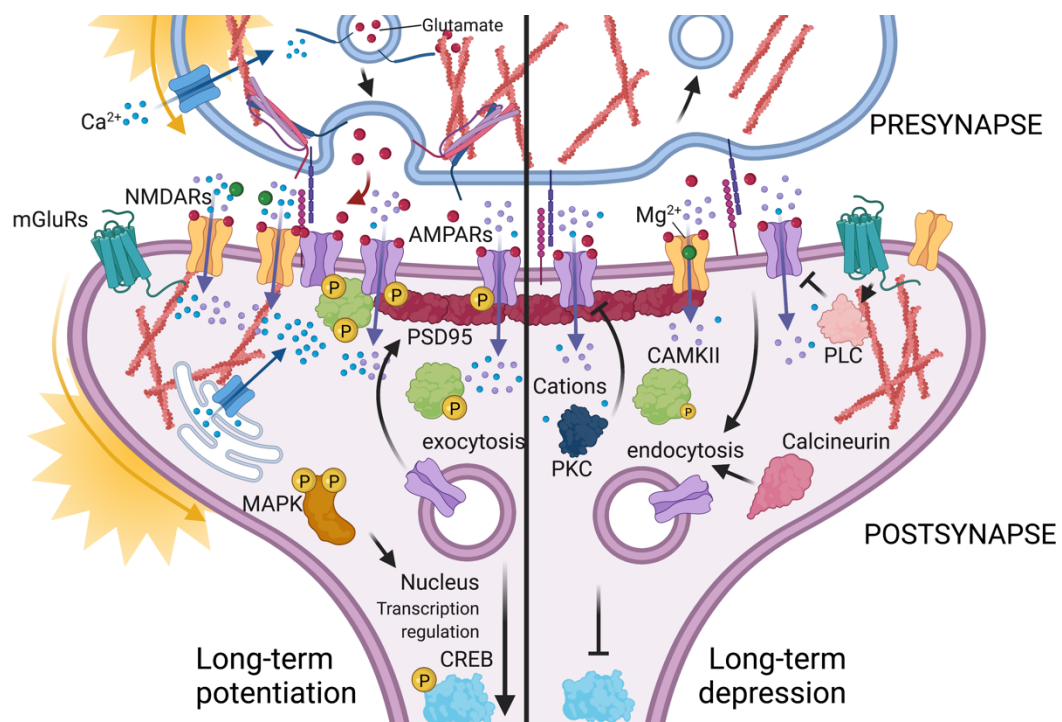
Figure I7. LTP and LTD in the postsynapse. The main mechanisms of plasticity, long-term potentiation (LTP, left) and long-term depression (LTD, right), highlighting the key molecules involved in the downstream increase or decrease of synaptic transmission in response to activation. PLC – phospholipase C, PKC – protein kinase C, MAPK – mitogen-activated protein kinase, CREB - cAMP response element-binding protein, CaMKII - calcium/calmodulin dependent protein kinase II, PSD95 – postsynaptic density protein 95.

In contrast to LTP, LTD refers to the dampening of postsynaptic signaling in response to stimulus. Surprisingly, LTD also depends on NMDAR activity but through a more modest activation and subsequent modest Ca^{2+} influx. Experimentally, LTD can be induced by longer (5–15 min) low-frequency stimulation (1–3 Hz) of presynaptic axons (Lüscher and Malenka 2012). Opposite to what is the case in LTP, downstream mechanisms of LTD depend on the activity of several phosphatases (like calcineurin and the protein phosphatase 2) that negatively affect AMPARs. In addition to this mechanism, the endocytosis and degradation of existing AMPARs is also a known mechanism of LTD (Collingridge et al. 2010).

The concerted action of LTP and LTD induction and maintenance in synapses allows for the kind of signal modulation that makes possible memory encoding in neuronal circuits (Abraham, Jones, and Glanzman 2019). Both processes are essential for learning and memory, but they do not paint the full picture of synaptic plasticity and its relationship with memory.

Local protein synthesis in the synapse

The size and large number of cellular contacts that the average excitatory neuron possesses makes it challenging to maintain and supply the large number of molecules that are needed at the most distal points of their projections for proper neuronal function (Ishizuka, Cowan, and Amaral 1995). Additionally, more than 2500 proteins are known to be located at the synapse (although not all of them are present at every synapse all of the time) with wildly varying copy numbers (Pielot et al. 2012). Synaptic plasticity involves the experience-dependent change in the number, size and strength of synapses. This process can affect one or several but not all synapses in a neuron, and therefore involves a significant compartmentalization of the synaptic environment to be able to regulate individual changes in plasticity (Govindarajan et al. 2011). To be able to achieve long-lasting plasticity changes, like the ones associated with memory formation, activity-dependent changes in RNA and protein synthesis are needed. But even the fastest cellular transport would take days to provide distal axons with newly synthesized proteins, making exclusively somatic responses to synaptic stimuli in a timely manner impossible (Maday et al. 2014).

To address these physiological constraints to the local regulation of plasticity within the timeframe needed to elicit the synaptic changes required for learning and memory

formation, neurons have evolved strategies to meet the local demand of proteins at synaptic sites, and synaptic local protein synthesis (LPS) is one of the main ones (Holt, Martin, and Schuman 2019). Recent works in this regard have described the presence of hundreds or thousands of mRNAs at the synapse, coding for many proteins crucial for synaptic function and plasticity, like CAMKIIα, MAP2 or PSD95 (Garner, Tucker, and Matus 1988; Burgin et al. 1990; R. Moccia et al. 2003). These transcripts are actively transported to distal regions of the neurons, and the 3' UTR and 5' UTR regions are important regulatory elements for their targeting, but little is known about the mechanisms that drive the selective transport toward synaptic compartments (Taliaferro et al. 2016; Turner-Bridger et al. 2018). In addition to these mRNAs, active ribosomes (mostly as monosomes and less often as polysomes) and translational regulators can be found in synaptic compartments (Hafner et al. 2019).

Functionally, LPS is required for certain types of circuit formation and plasticity. In the absence of LPS, BDNF-dependent potentiation is impaired and certain types of hippocampal LTP and LTD require de novo LPS (Huber, Kayser, and Bear 2000; Vickers, Dickson, and Wyllie 2005). In one of these studies, it was shown that even in the absence of the soma, LTP can be induced on isolated dendrites through the translation of mRNAs previously localized to the synapse (Vickers, Dickson, and Wyllie 2005). As mentioned previously, one of the most prominent mRNAs located in dendrites is the CaMKII isoform α (*Camk2a*). Newly synthesized CaMKIIα can be detected shortly after LTP in dendrites, and the removal of the 3' UTR region (key for synaptic localization) results in diminished LTP and a significant decrease in dendritic protein levels of CaMKIIα (Ouyang et al. 1999; Miller et al. 2002).

Due to the known function of m^6A in the partitioning of synaptically located mRNAs, the presence of some proteins of the m^6A machinery at the synapse, and the known role of m^6A in the regulation of mRNA stability and translation, this epitranscriptomic mark has become of great interest as a possible modulator of synaptic LPS (Merkurjev et al. 2018; Holt, Martin, and Schuman 2019).

Synaptic plasticity associated with cognition In aging

Aging is the process through which time gradually affects an organism to its detriment. It is generally an irreversible systemic process that alters the function and structure of an organism at the organ, tissue and cellular levels, at different rates (López-Otín et al. 2013). Due to its complexity, the CNS is especially vulnerable to aging, losing the ability to adequately interpret, react and adapt to changes in environmental cues (Figure I8). This is caused, at least partly, by a general decrease in the regenerative capacity of the CNS as well as a decline in cognitive functions (or cognitive decline), consequence of impaired synaptic maintenance and plasticity (Rando 2006; Mattson and Magnus 2006).
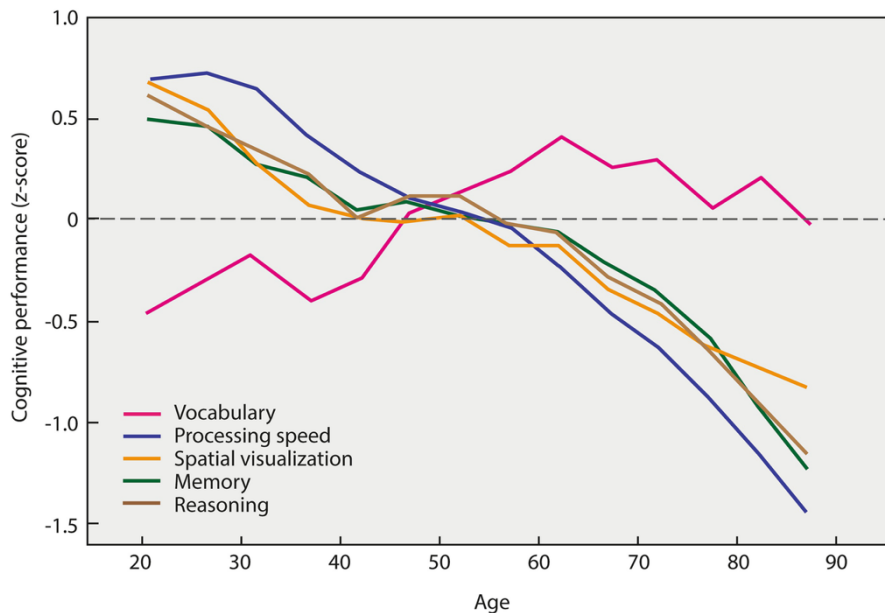

Figure I8. Cognitive aging. The effects of aging on cognitive functions. All categories of cognitive measurements (except for vocabulary abilities) display a consistent decline during aging, starting at around 50 years of age. Modified from Eikelboom, 2020.

Studies combining primate and non-primate mammalian models, as well as human imaging and post-mortem data have contributed to our understanding of the molecular and systemic consequences of aging in the CNS (Cuestas Torres and Cardenas 2020). At the cellular level, aging correlates with neuronal loss in certain brain regions associated with memory, like the hippocampus and prefrontal cortex (PFC) and not only that, dendritic branching and synapses suffer considerable decreases in their number

and strength, directly affecting memory function (Markham and Juraska 2002; Smith et al. 2004; Yassa, Muftuler, and Stark 2010). Aging is also known to affect synaptic plasticity by altering, among other mechanisms, Ca^{2+} homeostasis and thus hindering LTP (T. C. Foster and Norris 1997; Deupree, Bradley, and Turner 1993). Aged hippocampal synapses also display a clear decrease in the expression and density of NDMARs, further hindering plasticity and cognition (Magnusson 1998; Kumar 2015). Functionally, mice show significant impairment in cognitive abilities already at 15 months of age (equivalent to around a 53-year-old human) in multiple behavioral tests (Belblidia et al. 2018; Dutta and Sengupta 2016).

In the aged human and mouse brain, multiple studies have studied the effects of aging in gene expression, particularly at the transcriptome level (Ham and Lee 2020). Such analyses have shown significant, albeit mild, changes in the expression levels of synaptic plasticity and immune function genes in the hippocampus and PFC, even preceding the onset of symptoms of cognitive decline (Kang et al. 2011; Bae et al. 2018). Despite this, the magnitude of transcriptome changes is small (only 0.7% of expressed genes show expression changes during adulthood), highlighting the need of additional models that link the cognitive deficits and synaptic dysfunction observed during aging (Kang et al. 2011; Ham and Lee 2020).

In Alzheimer's disease

Alzheimer's disease (AD) is the most common neurodegenerative disease and the main cause of dementia, it is estimated to affect more than 44 million people worldwide. As the world's population has increased access to better healthcare and life expectancy increases, this figure is expected to triple by 2050, making AD and dementia one of the main public health challenges for the 21st century (Knopman et al. 2021).

Biologically, AD is characterized by the presence of extracellular β-amyloid (Aβ)-containing plaques and intracellular tau-containing neurofibrillary tangles (NFT) resulting in widespread neuronal death in the affected regions (Alzheimer 1907). AD progression generally begins in the medial temporal lobe, in the entorhinal cortex (Braak stages I-II) and spreads to other limbic regions (Braak stages III and IV), eventually ending in extensive neocortical neurodegeneration (Braak stages V and VI; Braak and Braak 1991). It generally presents with cognitive impairment affecting short term memory, speech and executive functions. Only a small fraction of AD cases have a genetic origin

(familial AD) and the vast majority of diagnoses correspond to "sporadic" AD (Tanzi 2012). Aging is a major risk factor in AD (and dementia in general) but many other environmental, genetic, and epigenetic factors have been associated with the etiology of AD. In spite of this, our understanding of the causes and early processes involved in disease onset are still limited.
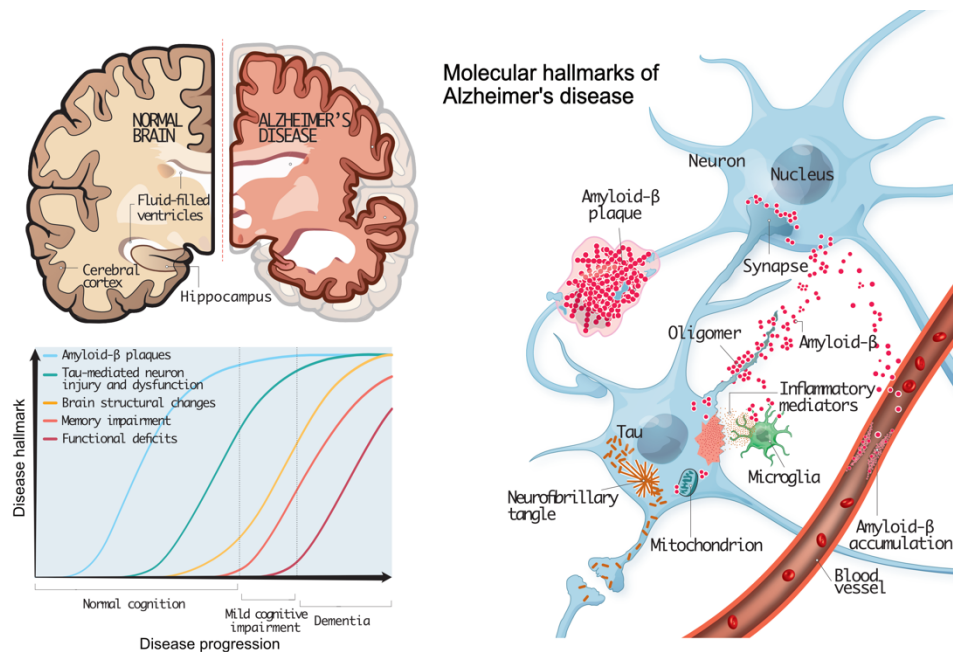

Figure I9. Hallmarks of Alzheimer's disease. Top left: Large-scale effects of advanced AD pathology on the brain. Bottom left – Different timepoints for the onset of classic AD hallmarks during disease progression. Right: Cellular and molecular hallmarks of AD, highlighting the importance of NFTs and Aβ in neuronal impairment and toxicity. Modified from Drew, 2018.

The hallmarks of AD, associated risk factors and mechanisms of neurodegeneration have all been studied extensively and cannot be covered appropriately in the extent of this text (Knopman et al. 2021). However, I will delve into the relationship between AD progression and synaptic dysregulation and collapse, a well-established central mechanism in the pathology of AD.

Synaptic loss is common in AD patients and it correlates most strongly with dementia and cognitive impairment. In contrast, no correlation exists between plaque accumulation and cognitive impairment but tangles do correlate with cognitive decline and synapse loss (Giannakopoulos et al. 2003; Arriagada et al. 1992). Furthermore, the

neurotoxicity caused by Aβ and Tau (mainly in their soluble oligomeric forms) has common effects on synaptic function and the resulting cognitive impairment (Spires-Jones and Hyman 2014). Aβ induces the loss of synaptic markers surrounding deposited plaques even preceding neuronal loss (Spires and Hyman 2005). Tau models also display increased synapse loss and aberrant localization of pathological Tau to synaptic compartments, further impairing synaptic transmission (Zhou et al. 2017; Arbel-Ornath et al. 2017).

At the synapse, Aβ is able to bind multiple key receptors (like NMDARs and mGluRs), sequestering them and impending their function, with consequences for LTP formation (Felice et al. 2007; Renner et al. 2010). Another major mechanism for synaptic loss and neurodegeneration is the Aβ-dependent increase in postsynaptic Ca^{2+} levels detected both *in vitro* and *in vivo* (Demuro et al. 2005; Kuchibhotla et al. 2008). This increased calcium influx interferes with postsynaptic LTP and LTD, and causes calcineurin activation that promotes the internalization of both NMDARs and AMPARs and can spread into the soma, causing neuronal death (Hsieh et al. 2006; H.-Y. Wu et al. 2012). Less is known about the role of Tau in promoting neuronal loss during AD, but disease associated variants of Tau can mislocalize to dendritic spines, where it can alter glutamate receptor trafficking to the postsynapse, thanks to its function as a microtubule-associated protein (Hoover et al. 2010).

In environmental enrichment

Memory and cognition are complex experience-dependent processes that benefit from a diverse environment, full of stimuli that will require an adaptive response from the brain. It is no surprise that in the type of captivity conditions common for research animals – where reduced space, unstimulating surroundings and lack of social interaction are the norm – behavioral and cognitive patterns develop abnormally and can suffer severe impairment (Kelley and Macías Garcia 2010). The benefits of exposure to an enriched environment have been observed at many levels in the organisms studied, particularly in the enhancement of synaptic plasticity and cognition (Hebb 1949; Fischer 2016). Environmental enrichment (EE) is understood as the exposure to changing and spacious surroundings, novel objects and stimuli, social interactions and the opportunity to exercise, in other words, an environment that more closely relates to the one an animal could experience in the wild (Newberry 1995). Although the effects of

EE are well described, some uncertainty exists about its consequences for synaptic function, partly due to the use of inconsistent EE exposure across studies but also due to the lack of cellular and molecular mechanisms that are known to mediate synaptic changes following EE (Eckert and Abraham 2013).

In rodents, EE has consistently shown to enhance hippocampus-dependent memory function and increased neurogenesis in the DG, even in protocols lacking exercise availability (Kempermann, Kuhn, and Gage 1997; Irvine and Abraham 2005; Eckert, Bilkey, and Abraham 2010). Furthermore, in animal models of AD, EE exposure significantly improves memory and reduces Aβ deposition in the hippocampus and cortex (Lazarov et al. 2005; Valero et al. 2011).
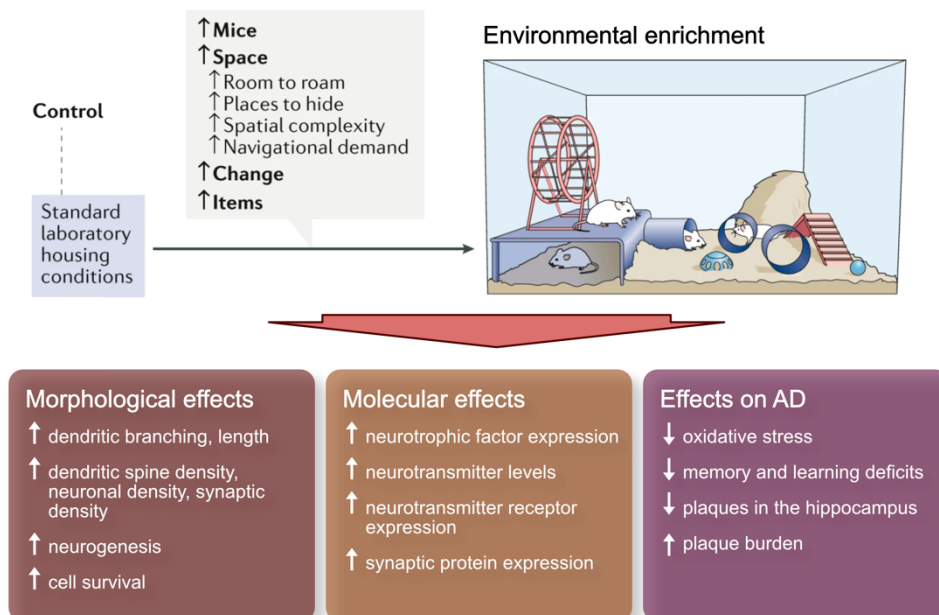
Figure I10. Effects of environmental enrichment. Top: Standard elements of EE protocols used in research. Bottom: Known effects of EE in cognitive function and in AD. Modified from Alwis and Rajan, 2014; Kemperman, 2019 and Akyuz and Eroglu, 2020.

EE exposure induces increases in excitatory synaptic transmission in the CA1 and DG, depending on the length and continuity of the exposure: short-lived (around 4 weeks), periodic (1–14 hours/day) show the biggest changes (Green and Greenough 1986; Malik and Chattarji 2012). In the CA1 enhanced LTP can be detected after EE, irrespective of the type of treatment (Duffy et al. 2001; Maggi et al. 2011). Interestingly, EE can also

potentially induce the reversal of existing LTP or LTD in the DG, when exposing mice after learning (Abraham et al. 2002; Abraham et al. 2006).

At the transcriptome level, EE induces mild changes in the expression of genes associated with synaptic signaling, plasticity, and extracellular matrix regulation, and the effects of EE with or without exercise are clearly distinct (Grégoire et al. 2018; Hüttenrauch, Salinas, and Wirths 2016). Moreover, EE is known to induce alterations in the epigenetic state of the hippocampus through changes on DNA marks, histone modifications and miRNAs, with consequences for neuronal function and plasticity (Irier et al. 2014; Kuzumaki et al. 2011). Some of them even showed the ability to be transmitted transgenerationally (Benito et al. 2018).

All in all, EE has been widely shown to generally improve cognitive function and memory, through the enhancement of hippocampal plasticity and synaptic transmission. Changes in gene expression and epigenetic factors can be detected following EE, giving us some insight into the molecules responsible for the effects of EE (Frick and Benoit 2010; Mora 2013). Despite this, little is known about the molecular mechanisms that regulate EE-dependent cognitive changes and exploring the effect of EE on other known regulators of synaptic function might take us a step closer to understanding them.

Chapter 1: Establishing a method for m^{6}A analysis from low input samples

Introduction

The presence of dynamic modifications within RNA molecules has given rise to a novel layer of post-transcriptional regulation of gene expression, the epitranscriptome (Saletore et al. 2012). The most abundant of these modifications, N^6-methyladenosine (m^6A), can modulate a broad range of molecular processes through modifications in mRNA metabolism in eukaryotes. In mammals, m^6A plays key roles in cellular regulation from early development, to adulthood and in pathology (Yue, Liu, and He 2015; Zhao, Roundtree, and He 2017). Furthermore, alterations in the expression or function of genes associated with m^6A (termed the m^6A methylation machinery) have been shown to contribute to the origin and progression of diseases, like multiple types of cancer and, more recently, neurodegenerative disorders (Angelova et al. 2018; Yang et al. 2020; Yu, She, and Ji 2021; Jiang et al. 2021). However, the vast majority of studies delving into the relationship between m^6A function and pathology have depended on the use of animal models or cell lines, due to the large amounts of material needed to perform reliable analyses of the epitranscriptome.

Traditionally, the study of m^6A marks in the transcriptome has been dependent on the immunoprecipitation (IP) of mRNA with antibodies detecting m^6A specifically, followed by next-generation sequencing (NGS; Dominissini et al. 2013). This approach, termed meRIP-Seq allows for the determination of the methylation level of a given transcript by analyzing the coverage of aligned reads on the transcriptome, a process that requires high quality libraries (Figure 1.1).

m^6A makes up for 0.1–0.4% of the total adenosines in mRNA (Meyer and Jaffrey 2014). In addition, like many RNA immunoprecipitations (RIPs), the IP of methylated mRNAs is highly inefficient, meaning that to be able to obtain high-quality libraries of sufficient complexity, a large amount of input RNA must be used, ranging from 100–300 μg of total RNA (Dominissini et al. 2012). This fact has made the study of the role of m^6A in pathology complicated, since the vast majority of patient samples can yield only single-digit μg amounts of RNA, drastically limiting the scope of these studies (Walker et al. 2016).
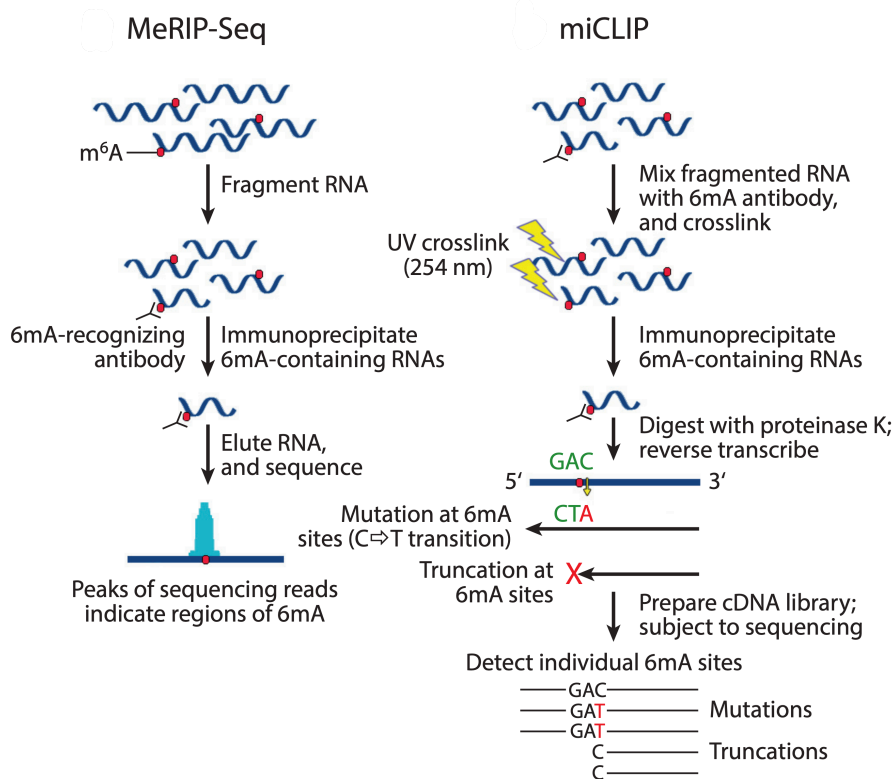
Figure 1.1. Methods to study the m6A epitranscriptome. Common methods for m6A analysis: meRIP-Seq (left) and miCLIP (right), showing the key steps in processing the RNAs, generating NGS libraries and analyzing them. Modified from Meyer et al. 2017.

Since the first described protocols for meRIP-Seq were described a decade ago, several improvements have been made in the efficiency of the protocols, allowing for higher quality data being produced with a fraction of the biological materials (Dominissini et al. 2012). Recently, taking advantage of considerable technological advances in the generation of NGS libraries from very low amounts of material, several protocols for low-input meRIP-seq have been published (Zeng et al. 2018; Weng et al. 2018; Dierks et al. 2021). Moreover, several novel technologies have shown promise in further improving our ability to analyze the epitranscriptome landscape in patient samples, reaching single-nucleotide resolution, with the aim of providing valuable information about the specific m^{6}A sites of relevance during pathological processes (Weng et al. 2018; Garcia-Campos et al. 2019; Parker et al. 2020; Wang et al. 2021).

Here I describe the steps taken to test, validate and optimize a protocol for low-input meRIP-seq to be used in patient samples, with the aim of studying changes in the m^{6}a epitranscriptome in the context of neurodegeneration. After several iterations of testing,

incorporating elements from several published protocols for low-input meRIP-Seq, I successfully produced a protocol that can reliably generate datasets of sufficient quality and depth for downstream bioinformatic analysis from a starting amount as low as 150 ng of rRNA-depleter RNA. This protocol has proven to be a valuable asset in the generation of both human and mouse datasets from different kinds of samples and has been used successfully in out laboratory and by collaborators.

Methods

Animals

All animal experiments were performed according to the protocols approved by the local ethics committee of the University Medical Center of the University Göttingen, Germany, the Lower Saxony State Office for Consumer Protection and Food Safety (LAVES) under animal protocol number 18.2857 and followed institutional, national, and international guidelines

RNA extraction

RNA was extracted from tissue using the NucleoSpin RNA/Protein Kit (Macherey-Nagel), according to the manufacturer's instructions. Tissue was dissociated with a handheld mechanized pistil on ice in an appropriate volume of lysis buffer.

RNA concentrations were determined by Nanodrop (Thermo) or Qubit with RNA HS Assay Kit (Thermo). For samples used for sequencing, RNA integrity was assayed by electropherogram in a Bioanalyzer using a total RNA Assay with a Pico/Nano Chip (Agilent). RNA samples were always kept on ice and stored at -80℃ when not in use to prevent degradation.

qPCR

cDNA was prepared using the Transcriptor cDNA first strand Synthesis Kit (Roche). The manufacturer's protocol for cDNA synthesis was followed, with a combination of random hexamers and Poly(dT) oligos. The full amount of IP and input (7%) RNA were used as input.

Synthesized cDNA was diluted 1:10 with nuclease-free water before being used for qPCR. Reactions were run in a Light Cycler 480 (Roche) in 96-well plates, using the Light Cycler 480 probes Master Mix. Each reaction was run in duplicate, in a volume of 20 µl and using 4 µl of cDNA per reaction. Primers used were custom designed, validated and used at a final concentration of 0.5 µM with the corresponding probe from the Universal Probe Library Mouse, when applicable. Reactions were run for a maximum of 55 cycles with a reference gene in every plate and quantified as expression relative to the reference. Two biological replicates were used in every case and statistical differences were determined by a t test, unless otherwise indicated.

Ingredient	Stock concentration	Final concentration	Volume in 20 µl (in µl)
Probe Master Mix	2X	1X	10
Primer Fwd	10 uM	0.5 uM	1
Primer Rev	10 uM	0.5 uM	1
UPL probe	10 uM	0.25 uM	0.5
PCR grade water			7.5

Table 1.1. qPCR pipetting scheme

Primer	Sequence	UPL probe
Kcnj3 Fw	gaacagttcgaggttgtcgtc	97
Kcnj3 Rv	tcgagcttgacaagtcattcc	
Dusp3 Fw	gagggtctacgtgggcaac	105
Dusp3 Rv	ctcggcagcattcaggac	
Gapdh Fw	gggttcctataaatacggactgc	52
Gapdh Rv	ccattttgtctacgggacga	

Table 1.2. qPCR primer sequences

Detailed low-input meRIP-Seq Protocol

A workflow for the whole process, from sample acquisition to analysis, and how it was applied to real-world samples can be found in the Appendix Figure 1.

Solutions

IP buffer

50 mM	Tris, pH 7.4
150 mM	NaCl
0.1 %	NP-40

Low Salt wash buffer

50 mM	Tris pH 7.4

50 mM	NaCl
1mM	EDTA
0.1%	NP-40
0.1%	SDS

High Salt wash buffer

50 mM Tris pH 7.4	
500 mM	NaCl
1mM	EDTA
0.1%	NP-40
0.1%	SDS

Elution buffer

1X	IP Buffer
6.7mM	m^6A

Other reagents

- · RNA fragmentation buffer (ThermoFisher; AM8740)
- · Protein A/G magnetic beads (Thermofisher; 88802)
- · m^6A Ab (Sysy; 202 003)
- · RiboMinus™ Eukaryote Kit v2 (Invitrogen; A15020)
- · RNA clean-up and concentrator from (ZymoResearch; R1016)
- · SUPERase In RNAse Inhibitor (ThermoFischer; AM2694)

Sample preparation

a. Split to S and L fractions (follow instructions from Zymo kit) and use only L fraction.

   This is to remove 5S rRNA which would otherwise get greatly enriched after 18S and 28S rRNA removal and make quantification difficult. In principle, it can be added later to include in the analysis.

b. Deplete 5 µg of total RNA (L fraction) with Invitrogen kit. Clean with Zymo kit, elute in 12 µl to obtain ~11 µl final volume. Check rRNA removal with Bioanalyzer Pico chip and concentration with Qubit.

c. Fragment at least 200 ng of depleted RNA to about 100-120 nt size – in 9 µl + 1µl Frag reagent for exactly 5 min at 70˚. Then add 1µl Stop solution and chill on ice.

   The lower limit I have tested and know works is ~160 ng right before IP, I would try to stay above 200 ng if possible

d. Purify RNA – Zymo kit. Elute in 22 µl. Check fragment size with Bioanalyzer (pico/small RNA chip), and concentration with Qubit.

From here on always use 2:1 vol of ethanol to sample + binding buffer mix (e.g. 50 µl sample + 100 µl binding buffer + 300 µl ethanol).

Day1

1. Save 5-10% from each sample as input – freeze

meRIP

Beads preparation

2. Use protein A/G beads, 30 µl per sample. Wash on magnetic stand twice with 500 µl of IP buffer.

3. Resuspend beads in 500 µl IP buffer and add 3 µl of m^{6}A antibody. Incubate ON at 4°C with rotation

Day2

4. Separate magnetic beads on magnetic stand and remove supernatant. Wash them twice with 500 µl IP buffer.

IP

5. Dilute RNA to 200 µl with IP buffer containing 5 µl SUPERaseIn.

6. Add diluted RNA to the Ab-bound beads and incubate with rotation at 4°C for 2h

Process IP samples

7. Wash beads twice with 900 µl IP buffer. Rotate at 4°C for 5 min for each wash.

8. Wash beads twice with 900 µl Low Salt wash buffer. Rotate at 4°C for 5 min for each wash.

9. Wash beads twice with 900 µl High Salt wash buffer. Rotate at 4°C for 5 min for each wash.

10. Wash beads twice with IP buffer 900 µl, rock at 4°C for 5 min

11. Add 100 µl Elution buffer and incubate for 1 hour at at 4°C shaking

12. Purify RNA with ZymoResearch kit. Elute in 9 µl of H$_2$O

Library Preparation

Perform the library prep (SMARTer Stranded Total RNA-seq v2 Pico Input). Follow protocol without fragmentation (option 2) and use 2-5 ng for inputs/all IPed samples.

Optional: Use only half of the cDNA for PCR amplification and keep the rest for qPCR confirmation of candidates.

When selecting indices, consider adding two i5 indices per lane (according to Illumina's recommendations for multiplexing) since, in my experience, using only one can lead to an increase of undetermined reads due to Ns in the corresponding index during demultiplexing.

For IP samples from ~200 ng starting material, 11-12 amplification samples give a good amount of DNA without many duplicates. For 2-4 ng of input, 9-10 cycles are enough. If necessary a half amplification qPCR can be performed after step 17 of section 4 of the protocol (after rRNA depletion from the library prep). See note.

After amplification and cleanup, resuspend DNA in 12 µl to increase concentration.

Ingredient	Volume in 10 µl (in µl)
SeqAmp CB PCR Buffer 2X	5
PCR2 Primers v2	0.4
SeqAmp DNA Polymerase	0.4
SYBR green (1:500)	0.2
DNA	1
Nuclease-free Water	3

Table 1.3. qPCR to check optimal amplification for SMARTer Pico input Mammalian Kit

Thermocycler program:

1 min	94°	
15 sec	98°	
15 sec	55°	30 cycles

30 sec   68°

Hold   4°

Take point of half amplification for each sample and average them by condition, then substract 2 or 3 cycles (round up or down depending on variation or type of samples) and use that as cycle number for final amplification. This number also roughly correlates to the Cp values if analyzed by absolute quant.

Bioinformatic analyses of meRIP-Seq

Raw reads were processed and demultiplexed using bcl2fastq 2.20.2 and low-quality reads were filtered out with Cutadapt 1.11.0 (Martin 2011). Filtered reads were mapped to the mouse (mm10) genome using the STAR aligner 2.5.2b (Dobin et al. 2013). The resulting bam files were sorted, indexed and the unmapped reads removed using SAMtools 1.9.0 (Li et al. 2009) Methylation sites were determined using MeTPeak 1.0.0 (Cui, et al. 2016) and differential methylation was assessed with Exomepeak 2.16.0 (Meng et al. 2013).

For visualization, bam files of both IP and input samples were collapsed for PCR duplicates using SAMtools and IP samples were normalized to their corresponding inputs and to their library size using deeptools 3.2.1 bamCompare (Ramírez et al. 2016). The resulting normalized tracks were visualized in the IGV Browser 2.9.2 (Robinson et al. 2011)

Additional bioinformatic packages and tools

Scripts and analysis pipelines were written in R 3.5.2 (Team 2013). Peak annotation was performed with Homer 4.10.4 (Heinz et al. 2010). Guitar plots were produced with the Guitar 1.20.1 (Cui, Wei, et al. 2016) R package. De novo motif analyses were performed with Homer's findMotifsGenome and the top enriched motif is displayed. Graphs, heatmaps and statistical analyses were performed on GraphPad Prism version 9.3.1 for Mac.

Results

Establishing a method for low-imput meRIP-Seq

Commonly used protocols for the high-throughput analysis of RNA modifications (in the case of m^{6}A, meRIP-Seq) require large amounts of RNA as a starting point, to obtain sufficient amounts of material with enough replicates to produce high-quality data (Dominissini et al. 2012). Recent advances in low-input and single cell library preparation have made it possible to perform these type of analyses from very low amounts of input material, allowing for the study of the epitranscriptome in scarce samples, like human brains. With this in mind, one or the first aims of my doctoral work was to test, optimize and establish a protocol for the processing, sequencing and analysis of low-input samples for meRIP-seq.

Taking advantage of recently published protocols, I adapted elements of them for my purposes and optimized the individual steps to strike the appropriate balance of efficiency and output quality (Zeng et al. 2018; Weng et al. 2018).

m^{6}A modifications are present not only on mRNA, but also in other more abundant RNA species. This is of special importance when planning a meRIP-Seq experiment, since mRNA makes up only 1–4% of all RNA in the cell and other RNA species could be co-immunoprecipitated and overwhelm the sequencing. A popular method to retain mRNA is polyA capture, but this has the downside of losing all non-polyadenylated RNAs, including some lncRNAs, pre-miRNAs and snRNAs, potentially discarding valuable information with them. With this in mind, it is more common to use rRNA depletion to remove this highly abundant RNA species (more than 80% of the total) instead. To this end, I performed rRNA depletion on two RNA samples obtained from the CA1 of two WT mice (10 µg each), using a commercially available kit that depends on RNAseH
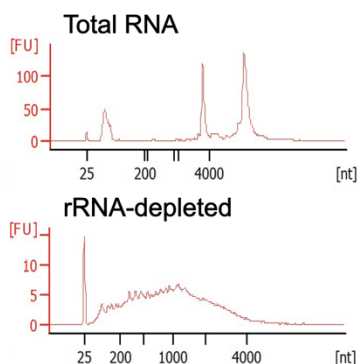

Figure 1.2. rRNA depletion. Electropherograms showing the fragment length profile of total RNA after extraction (top) and rRNA-depleted RNA (bottom). Ran on a Bioanalyzer RNA Nano Chip. FU – Fluorescence units, nt – nucleotide length

activity (NEBNext ribosomal RNA removal kit). The successful rRNA removal was confirmed by electropherogram and compared with the initial total RNA (Figure 1.2).

Some complications occurred, particularly with the reliability of the selected depletion method after repeated use and when scaling up reactions. Therefore, I decided to switch to another kit, this time based on the capture of rRNA in magnetic beads (RiboMinus Eukaryote Ribosomal Removal Kit, Invitrogen). For the definitive protocol, this was the selected option.

Next, I worked on optimizing another key step of the processing of samples for meRIP-seq, the fragmentation of mRNA. To be able to not only detect which RNAs contain m^6A, but also learn about the location of these marks within the transcript and thus gain insight into the target specificity of potential changes in the epitranscriptome, it is key to attain an adequate resolution. With this in mind, the fragmentation of the probed RNAs to smaller sizes is a key process, which allows us to enrich methylated sites and their immediate surroundings. Following sequencing, the coverage surrounding these enriched m^6A sites can be detected as peaks that can then be quantified. To reach the desired resolution during sequencing, an average fragment size between 60 and 80 nucleotides was desired.
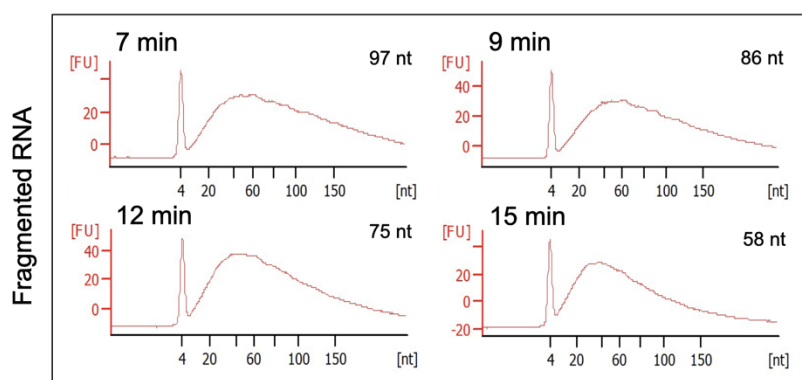

Figure 1.3. Establishing the appropriate fragmentation time. Electropherograms showing the fragment length profile of rRNA-depleted RNA, fragmented for different lengths of time. Fragmentation time is displayed on the left, the average fragment length is displayed on the right. Ran on a Bioanalyzer RNA Small RNA Chip. FU – Fluorescence units, nt – nucleotide length

I used a commercially available fragmentation kit (Fragmentation Reagents, Invitrogen) and different time points (5, 7, 9, 12 and 15 minutes) and concentrations (150 and 300 ng) to find the optimal length of treatment and test the effects of concentration in fragmentation times (Figure 1.3). Fragment sizes ranged from 111 nt at 5 minutes to 58 nt at 15 minutes, from these timepoints 9 minutes was selected as the optimal size.

Then it was only left to validate the m⁶A immunoprecipitation (IP), a key step in the selection of methylated transcripts for sequencing, using an input amount of 150 ng of rRNA-depleted RNA. The validation of this step was of the utmost importance, to confirm that even with very low input samples the necessary amount of RNA to construct a high-quality sequencing library could be immunoprecipitated. Based on the previously used protocol in the laboratory, as well as published ones, I used a tested m⁶A antibody bound to Protein A/G beads, followed by washes with high salt concentrations and a competitive elution using a highly concentrated m⁶A salt (see Methods for details).

To confirm the successful IP of m⁶A labeled transcripts, I prepared cDNA libraries from IP as well as input (7%) RNA. The cDNAs were probed by qPCR targeting known highly methylated transcripts. To further confirm the successful removal of a large part of the
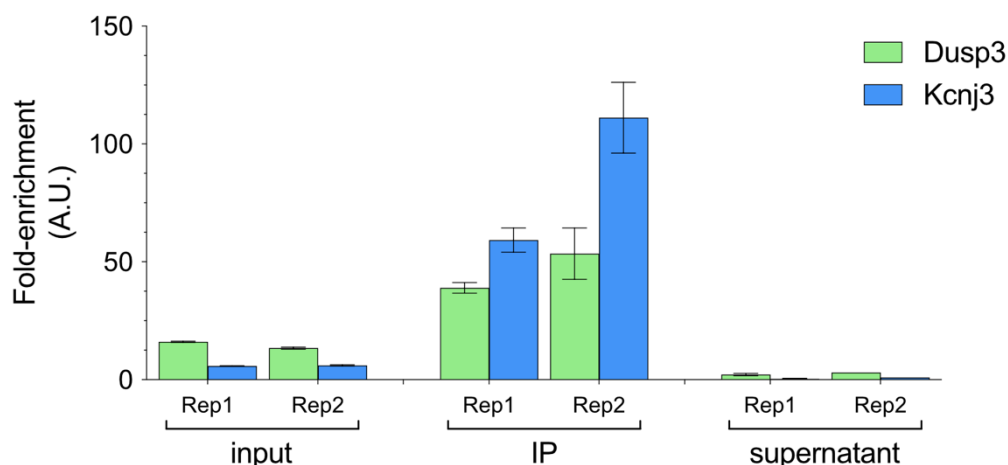

Figure 1.4. qPCR validation of meRIP. Levels of the corresponding transcripts shown as their enrichment with respect to the reference transcript Gapdh. Two biological replicates are displayed for each condition: 7% input, IP and supernatant. Each bar represents two technical replicates.

population of methylated transcripts, I also recovered the supernatant of the IP, purified the RNA and synthesized cDNA for parallel processing.

I focused on two highly expressed, highly methylated transcripts, *Kcnj3* and *Dusp3*. The IP samples displayed in both cases a very strong enrichment in their levels (20–50 fold) after immunoprecipitation (Figure 1.4). Additionally, supernatants were almost completely depleted of transcripts, confirming the high efficiency of the immunoprecipitation step as well as the high level of methylation in these transcripts.

These results show that the m^6A IP method used thus far successfully enriches the population of methylated RNAs and can be used as the basis for further optimization of the following steps for meRIP-Seq.

After the validation of individual key steps for the successful meRIP, I next processed the first batch of samples for sequencing, including cDNA synthesis and library preparation. Initially, IP and input RNAs were used for cDNA synthesis using a kit intended for the analysis of single cell RNA samples (SMARTseq V4, Takara), to take advantage of their technology used for very low-input samples. This kit used Polyd(T) oligos to synthesize cDNA from mRNA, but since our samples had been fragmented before the IP step, the additional end repair and polyadenylation of IP RNAs was necessary before processing. Sequencing libraries were prepared from these cDNAs with a compatible kit (Nextera XT DNA Library Prep Kit, Illumina). Then, samples were sequenced, mapped and analyzed for m^6A peak detection.

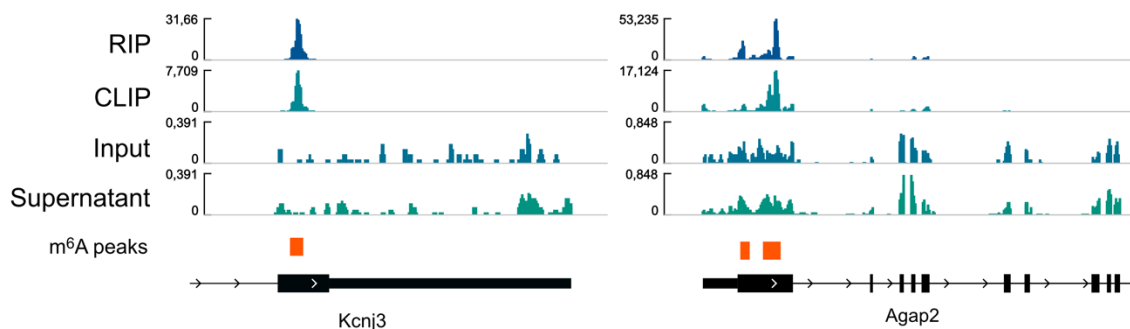**Figure 1.5. Coverage tracks from the first trial run**. Genome viewer tracks showing the coverage of IP samples (both RIP and CLIP), input samples and supernatants from one replicate from the first trial run. In red are detected m6A peaks. Scale displays raw read counts. Range is autoscaled for each track, except input and supernatant. Differences between distribution of m^6A in meRIP and meCLIP can be seen in Appendix Figure 2

RIP samples showed a very strong enrichment of reads located in peaks across the transcriptome, when compared with input samples. In contrast, the supernatant displayed a similar coverage pattern as the imput samples, but with a clear decrease in the read coverage in the region where IP samples showed their largest enrichment (Figure 4). Additionally, using the m^6A peak detection package MeTPeak, I could detect 1562 m^6A sites across the transcriptome (Figure 6). Moreover, de novo motif enrichment analysis showed that the most enriched sequence in the detected m^6A regions corresponded to the m^6A consensus motif sequence DRACH (where D = A, T or G, R = A or G, and H = A, T or C), confirming the successful enrichment and detection of methylated regions through meRIP-Seq.

These results showed that the novel protocol tested to work with very low inputs (150 ng) can successfully generate data that reflects the m^6A epitranscriptome in the samples, with sufficient quality for bioinformatic analysis. However, there were some important issues to resolve with the quality and depth of the data.

First, given the low amount of material, the sequencing depth was considerably low, particularly for IP samples. Samples averaged 1–7 million reads for IP, 4–11 million for inputs and 13–19 million for supernatants, which correlates to the amount of RNA used as input (Figure 1.6). Additionally, despite being able to detect more than 1500 m^6A

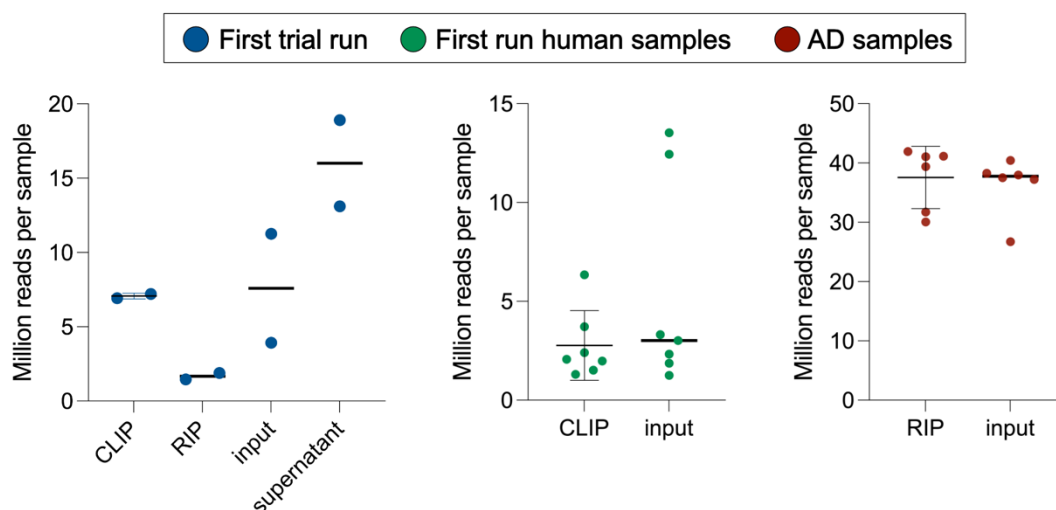**Figure 1.6. Comparison of sequencing depth**. Sequencing depth after sequencing from the first trial run (left), the first run with human samples (center) and the first run with human samples with the optimized meRIP protocol (right). Graphs show the total number of raw reads obtained from each sample after sequencing. Each dot represents a biological replicate, the line denotes the mean, error bars show SD.

peaks, other studies of this kind, even those using low input amounts, show close to 10,000 peaks detected in average per sample.

To address these issues, I decided to lower the fragmentation time to 5 minutes and therefore start with >100 nt fragments, to avoid carrying over during size selection the long primers used in library preparation. Additionally, fewer samples would be loaded per flowcell to increase the sequencing depth. Finally, when possible, the protocol would be performed with a starting amount of 300 ng, still well within the range obtainable from a single patient sample. Applying these modifications, I used this protocol to process the first set of real human samples, corresponding to the frontal cortex of healthy and frontotemporal dementia (FTD) patients.

Sequencing depth was slightly improved in these samples, where 1–6 million reads were produced for IP samples and 2–14 for inputs. However, unlike the previous run, the data obtained from these samples displayed very low percentages of mapped reads after being aligned to the reference genome, as well as decreased read quality. This was a result of an overabundance of adenosine sequences detected by the sequencer, brought upon by the likely over-polyadenylation of the samples during processing. Despite this, m^6A peak detection showed a slight increase in the number of methylated regions, with 2237 peaks detected.

While the polyadenylation of RNA fragments to be further processed had allowed for the use of very sensitive methods for library generation, the difficulty in controlling the length of PolyA tails (time of incubation, size of the fragment and concentration of the RNA being variables that can strongly affect them) produced a negative effect in the overall quality of the resulting data. In addition to this, the added handling of the samples for end repair and polyadenylation, significantly reduced the amount of leftover RNA with every additional step. For these reasons, I decided to adapt the current version of the protocol, using a different library preparation protocol that would circumvent the need to further process the RNA fragments after IP.

Several kit were tested, but the best results were obtained using the SMARTer Stranded Total RNA Kit v2 - Pico Input Mammalian (Takara). This kit uses random hexamers, instead of polyd(T) oligos to generate cDNA libraries, eliminating the need for additional steps following the IP. Furthermore, it includes all the steps for first strand cDNA synthesis, adaptor ligation and library amplification in the same kit, instead of requiring two different kits for this purpose, thus reducing the complexity and costs of this step.
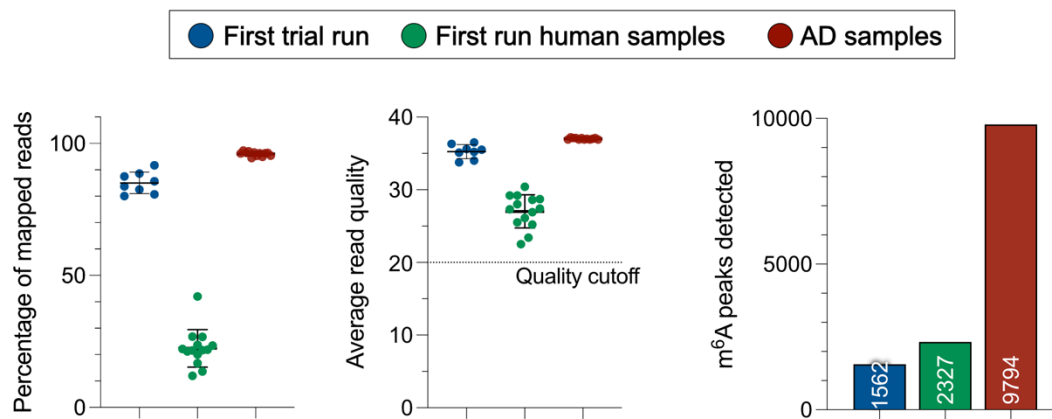
Figure 1.7. Comparisons of quality outcomes in the first trial run, the first run with human samples and the first run with human samples with the optimized meRIP protocol. The percentage of mapped reads (left), average read quality (center), and total number of detected peaks are shown. Line in center panel denotes the read quality cutoff. Numbers inside of the bars in the right panel show the total number of peaks. Dots represent biological replicates, line shows the mean value and error bars show SD.

The first set of real-world samples processed with this optimized protocol corresponded to brain samples from the cingulate gyrus of control and Alzheimer's disease (AD) patients. These samples displayed remarkable improvements in the amount and quality of data produced in all the metrics where the previous version lacked. Firstly, across the board sequencing depth and flowcell clustering was significantly improved, with samples ranging from 28–42 million reads per sample for both IP and input samples (Figure 1.7). More importantly, mapped reads increased significantly to more than 95% on average. In addition, the mean read quality was further increased to an average of 37 (with 20 being generally the accepted minimum quality value; Figure 1.7).

The m^6A peak detection analysis showed 9794 peaks in these samples, a stark increase from previous iterations and much closer to the standard number of peaks detected in other studies. The increased sequencing depth and corresponding increased coverage made it possible to more accurately measure the methylation state of a given region, allowing me to perform high-confidence differential methylation analyses with high statistical significance (Figure 1.8).
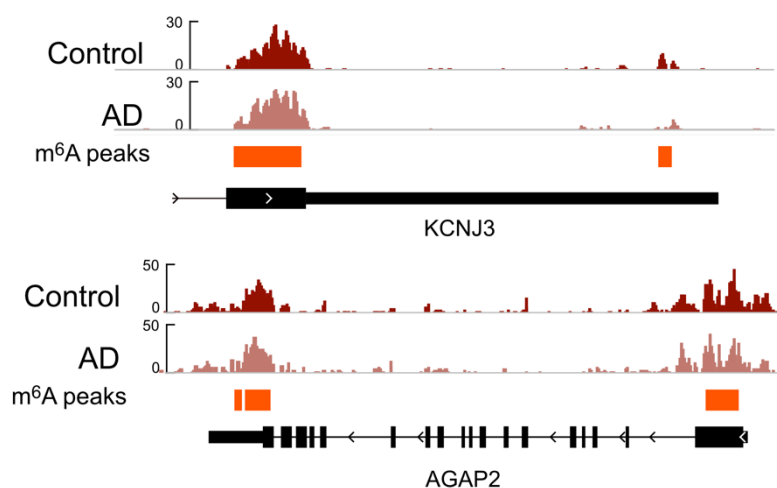
Figure 1.8. Coverage tracks from AD samples. Genome viewer tracks showing the coverage of AD and control samples processed with the optimized meRIP-Seq protocol. IP samples are normalized to their corresponding inputs and grouped. In orange are detected m6A peaks. Scale displays raw normalized read counts in CPM.

These results show that after testing and optimization, the current version of the low-input meRIP-seq protocol displays a robustness, throughput and quality output matching the current standard of meRIP-seq protocols in the field, irrespective of the initial amount needed. This has allowed me to successfully perform these type of analyses in multiple samples from both mouse and human with increased output, reproducibility while achieving reduced workloads and costs. Its use will provide other users in the laboratory to perform meRIP-seq analyses in a straightforward manner and without need for additional optimization.

References

Angelova, Margarita T., Dilyana G. Dimitrova, Nadja Dinges, Tina Lence, Lina Worpenberg, Clément Carré, and Jean-Yves Roignant. 2018. "The Emerging Field of Epitranscriptomics in Neurodevelopmental and Neuronal Disorders." Frontiers in Bioengineering and Biotechnology 6: 46. https://doi.org/10.3389/fbioe.2018.00046.

Dierks, David, Miguel Angel Garcia-Campos, Anna Uzonyi, Modi Safra, Sarit Edelheit, Alice Rossi, Theodora Sideri, et al. 2021. "Multiplexed Profiling Facilitates Robust M6A Quantification at Site, Gene and Sample Resolution." Nature Methods 18 (9): 1060–67. https://doi.org/10.1038/s41592-021-01242-z.

Dominissini, Dan, Sharon Moshitch-Moshkovitz, Mali Salmon-Divon, Ninette Amariglio, and Gideon Rechavi. 2013. "Transcriptome-Wide Mapping of N(6)-Methyladenosine by m(6)A-Seq Based on Immunocapturing and Massively Parallel Sequencing." Nature Protocols 8 (1): 176–89. https://doi.org/10.1038/nprot.2012.148.

Dominissini, Dan, Sharon Moshitch-Moshkovitz, Schraga Schwartz, Mali Salmon-Divon, Lior Ungar, Sivan Osenberg, Karen Cesarkas, et al. 2012. "Topology of the Human and Mouse M6A RNA Methylomes Revealed by M6A-Seq." Nature 485 (7397): 201–6. https://doi.org/10.1038/nature11112.

Garcia-Campos, Miguel Angel, Sarit Edelheit, Ursula Toth, Modi Safra, Ran Shachar, Sergey Viukov, Roni Winkler, et al. 2019. "Deciphering the 'M6A Code' via Antibody-Independent Quantitative Profiling." Cell 178 (3): 731-747.e16. https://doi.org/10.1016/j.cell.2019.06.013.

Jiang, Xiulin, Baiyang Liu, Zhi Nie, Lincan Duan, Qiuxia Xiong, Zhixian Jin, Cuiping Yang, and Yongbin Chen. 2021. "The Role of M6A Modification in the Biological Functions and Diseases." Signal Transduction and Targeted Therapy 6 (1): 74. https://doi.org/10.1038/s41392-020-00450-x.

Meyer, Kate D., and Samie R. Jaffrey. 2014. "The Dynamic Epitranscriptome: N6-Methyladenosine and Gene Expression Control." Nature Reviews. Molecular Cell Biology 15 (5): 313–26. https://doi.org/10.1038/nrm3785.

Parker, Matthew T, Katarzyna Knop, Anna V Sherwood, Nicholas J Schurch, Katarzyna Mackinnon, Peter D Gould, Anthony JW Hall, Geoffrey J Barton, and Gordon G Simpson. 2020. "Nanopore Direct RNA Sequencing Maps the Complexity of Arabidopsis MRNA Processing and M6A Modification." Edited by Yue Wan and Christian S Hardtke. ELife 9 (January): e49658. https://doi.org/10.7554/eLife.49658.

Saletore, Yogesh, Kate Meyer, Jonas Korlach, Igor D. Vilfan, Samie Jaffrey, and Christopher E. Mason. 2012. "The Birth of the Epitranscriptome: Deciphering the Function of RNA Modifications." Genome Biology 13 (10): 175. https://doi.org/10.1186/gb-2012-13-10-175.

Walker, Douglas G., Alexis M. Whetzel, Geidy Serrano, Lucia I. Sue, Lih-Fen Lue, and Thomas G. Beach. 2016. "Characterization of RNA Isolated from Eighteen Different Human Tissues: Results from a Rapid Human Autopsy Program." Cell and Tissue Banking 17 (3): 361–75. https://doi.org/10.1007/s10561-016-9555-8.

Wang, Yuru, Zijie Zhang, Caraline Sepich-Poore, Lisheng Zhang, Yu Xiao, and Chuan He. 2021. "LEAD-M6A-Seq for Locus-Specific Detection of N6-Methyladenosine and Quantification of Differential Methylation." Angewandte Chemie International Edition 60 (2): 873–80. https://doi.org/10.1002/anie.202007266.

Weng, Yi-Lan, Xu Wang, Ran An, Jessica Cassin, Caroline Vissers, Yuanyuan Liu, Yajing Liu, et al. 2018. "Epitranscriptomic M6A Regulation of Axon Regeneration in the Adult Mammalian Nervous System." Neuron 97 (2): 313-325.e6. https://doi.org/10.1016/j.neuron.2017.12.036.

Yang, Chuan, Yiyang Hu, Bo Zhou, Yulu Bao, Zhibin Li, Chunli Gong, Huan Yang, Sumin Wang, and Yufeng Xiao. 2020. "The Role of M6A Modification in Physiology and Disease." Cell Death & Disease 11 (11): 1–16. https://doi.org/10.1038/s41419-020-03143-z.

Yu, Jun, Yuanchu She, and Sheng-Jian Ji. 2021. "M6A Modification in Mammalian Nervous System Development, Functions, Disorders, and Injuries." Frontiers in Cell and Developmental Biology 9: 1343. https://doi.org/10.3389/fcell.2021.679662.

Yue, Yanan, Jianzhao Liu, and Chuan He. 2015. "RNA N6-Methyladenosine Methylation in Post-Transcriptional Gene Expression Regulation." Genes & Development 29 (13): 1343–55. https://doi.org/10.1101/gad.262766.115.

Zeng, Yong, Shiyan Wang, Shanshan Gao, Fraser Soares, Musadeqque Ahmed, Haiyang Guo, Miranda Wang, et al. 2018. "Refined RIP-Seq Protocol for Epitranscriptome Analysis with Low Input Materials." PLOS Biology 16 (9): e2006092. https://doi.org/10.1371/journal.pbio.2006092.

Zhao, Boxuan Simen, Ian A. Roundtree, and Chuan He. 2017. "Post-Transcriptional Gene Regulation by MRNA Modifications." Nature Reviews. Molecular Cell Biology 18 (1): 31–42. https://doi.org/10.1038/nrm.2016.132.

Chapter 2: The role of m^{6}A in aging and neurodegeneration

Conserved reduction of m^{6}A marks during aging and Alzheimer's disease affects the regulation of synaptic plasticity genes

Conserved reduction of m^{6}A marks during aging and Alzheimer's disease affects the regulation of synaptic plasticity genes

Ricardo Castro-Hernández[†1], Tea Berulava[†1], Maria Metelova[1], Robert Epple[1], Tonatiuh Peña Centeno[12], M Sadman Sakib[1], Susanne Burkhart[1], Gaurav Jain[1,2], Katherine E. Bohnsack[3], Markus T. Bohnsack[3], Andre Fischer[*1,4,5]

[1]Department for Epigenetics and Systems Medicine in Neurodegenerative Diseases, German Center for Neurodegenerative Diseases (DZNE), Göttingen, Germany

[2]Bioinformatics Unit, German Center for Neurodegenerative Diseases (DZNE), Göttingen, Germany

[3]Department of Molecular Biology, University Medical Center, Göttingen, Germany

[4]Department of Psychiatry and Psychotherapy, University Medical Center, Göttingen, Germany

[5]Cluster of Excellence "Multiscale Bioimaging: from Molecular Machines to Networks of Excitable Cells" (MBExC), University of Göttingen, Germany

† Co-authors

* Corresponding author

Abstract

The most abundant and widely studied of the mRNA modifications, N^6-methyladenosine (m^{6}A), plays diverse roles in the regulation of mRNA metabolism, and in the mammalian brain it is involved in memory function, synaptic transmission and plasticity. However, the mechanisms underlying this m6A-dependent regulation, as well as the role of m^{6}A in the context of impaired cognition, are still poorly understood. Here, we describe the mouse and human brain m^{6}A epitranscriptome in a tissue-specific manner, highlighting the conservation of m^{6}A marks across species. m6A levels undergo massive decreases across brain regions as a consequence of aging in the mouse brain. Similarly, Alzheimer's disease (AD) pathology in humans causes considerable decreases in methylation in a similar population of transcripts as the aged mouse brain. We observe that these common changes point towards the regulation of key synaptic plasticity genes, like the calcium/calmodulin-dependent kinase II (CaMKII), which undergoes reduced local translation at the synapse in response to reduced m^{6}A levels. Our results highlight the importance of m^{6}A-dependent regulation of brain function and its relationship with cognitive impairment.

Introduction

Decades after it was first described, the posttranscriptional modification and labeling of specific nucleotides in mRNA has become the target of intense research interest in recent years (Desrosiers, Friderici, and Rottman 1974). The most abundant of these marks, N^6-methyladenosine, has been at the forefront of research in multiple fields of biology due to its dynamic nature as well as the broad range of molecular consequences for m^6A -labeled transcripts, giving rise to the field of epitranscriptomics (Dominissini et al. 2012; Meyer et al. 2012; Fu et al. 2014).

The deposition of m^6A methylation marks on targeted mRNAs is made possible by the activity of a m^6A methylation complex formed by the methyltransferases (METTL) METTL3 and METTL14 with the adaptor protein WTAP (Jianzhao Liu et al. 2014; Ping et al. 2014; B. S. Zhao, Roundtree, and He 2017). m^6A sites can be found across the entire transcript but often concentrate close to the stop codon and in the 3'UTR, falling in the motif consensus sequence DRACH (where D= A,T or G, R= A or G, and H= A, T or C; Dominissini et al. 2012; Meyer et al. 2012; Linder et al. 2015). These methylation marks can in turn be removed by demethylases like Fat Mass and Obesity-Associated Protein (FTO) and Alpha-Ketoglutarate-Dependent Dioxygenase AlkB Homolog 5 (ALKBH5), making the regulation of m^6A levels a complex and highly dynamic process (Jia et al. 2011; Meyer and Jaffrey 2014; Rajecka, Skalicky, and Vanacova 2019). m^6A labeled transcripts are recognized by a wide array of reader proteins and thus m^6A RNA-methylation can affect a broad array of processes associated with mRNA metabolism, including nuclear export, transport, degradation and translation (Wang et al. 2015; B. S. Zhao, Roundtree, and He 2017; Huilin Huang et al. 2018; Yang et al. 2018).

These properties have brought the epitranscriptome forward as a key component of the intricate regulatory networks that rule complex physiological and pathological processes, ranging from development, to cancer, to the establishment, function and pathology of the nervous system (Yoon et al. 2017; Frye et al. 2018; Sun, Wu, and Ming 2019; Livneh et al. 2020; Yen and Chen 2021). While m^6A marks are widespread and highly dynamic they are highest in the adult mammalian brain, and in recent years research has focused on deciphering its role in the regulation of brain function (Meyer et al. 2012; Widagdo and Anggono 2018). Thus, m6A-dependent regulation in the adult brain has been linked to memory consolidation, learning and injury recovery (Chang et al. 2017; Weng et al. 2018; Zhang et al. 2018; Jiangtao Yu et al. 2020; Merkurjev et al.

2018; Shi et al. 2018) and although the current data varies, most studies suggest that decreased m^{6}A levels are associated with impaired learning, aberrant synapse formation and decreased cognitive function (Walters et al. 2017; Merkurjev et al. 2018; Shi et al. 2018; Zhang et al. 2018)

More recently multiple studies started to investigate m^{6}A levels in neurodegenerative diseases (Yen and Chen 2021; He Huang et al. 2020; Deng et al. 2021; Jiang et al. 2021; F. Zhao et al. 2021). While changes in m^{6}A levels have been observed, the magnitude, depth, directionality and functional consequences of these changes are still a matter of contention in the field (Han et al. 2020; He Huang et al. 2020; Du et al. 2021; Shafik et al. 2021; F. Zhao et al. 2021).

In this study we analyze the m^{6}A epitranscriptome across multiple regions of the adult mouse and human brain. We find a remarkable conservation of methylation marks between mouse and human related to transcripts that are linked to synapse function, while other processes such as gene expression control appear to be species-specific. Differential methylation analyses of cognitively impaired aged mice and human AD patients revealed a stark m^{6}A decrease within transcripts involved in synapse function in multiple brain subregions. The genes affected by m^{6}A changes converge on multiple synaptic plasticity-associated pathways in both aging and AD, among them CaMKII, a key regulator of synaptic signaling. Finally, we show that reducing m^{6}A levels within *Camk2* transcripts results in impaired synaptic synthesis of the corresponding protein, suggesting that loss of m^{6}A marks on transcripts associated with synaptic function and plasticity, is an early event in cognitive diseases which translates to decreased availability of the affected proteins in the postsynapse.

Methods

Animals

Ten male mice of 3 months of age (young) and ten male mice of 16 months of age (old) were purchased from Janvier Labs. Animals were housed in standard cages in a 12 hour light/ 12 hour dark cycle with food and water *ad libitum*. After a week of acclimation, the mice were sacrificed by cervical dislocation under anesthesia and their brains were immediately harvested.

All animal experiments were performed according to the protocols approved by the local ethics committee of the University Medical Center of the University Göttingen, Germany, the Lower Saxony State Office for Consumer Protection and Food Safety (LAVES) under animal protocol number 18.2857 and followed institutional, national, and international guidelines

Aged brain subregions dissection

The hippocampus of 10 young and 10 old mice was dissected into its corresponding subregions - CA1, CA3 and DG - using an 18G needle. The ACC was isolated with a scalpel. All dissections were performed on ice and the isolated tissue was flash-frozen in liquid nitrogen. Samples remained in -80℃ until right before RNA extraction.

Human AD tissue

A total of 12 post-mortem samples from the cingulate gyrus were obtained from the Netherlands Brain bank. The samples corresponded to 6 diagnosed AD patients (age 89.33 ±4.42 years, Braak and Braak stages IV, PMD 6:34 ±1:00) and 6 non-demented controls (age 86.33 ±3.25 years, Braak and Braak stages I-II, PMD 6:16 ±1:38), all individuals, except one AD patient were female. All experiments were approved by an ethics committee. To reduce variability in meRIP-seq analyses, two controls and one AD outlier samples were not considered.

RNA extraction

RNA used for sequencing was extracted from tissue using the NucleoSpin RNA/Protein Kit (Macherey-Nagel), according to the manufacturer's instructions.

For all other applications, cell or tissue samples were homogenized in an appropriate volume of TRI reagent (Sigma) using a Bead Ruptor Elite for 30 s with 0.5 mm ceramic

beads. RNA was isolated using the Direct-zol RNA miniprep kit or the Clean and concentrator -5 (Zymo Research) according to the manufacturer's instructions. RNA was eluted in nuclease-free water in a volume of 6–50 μl.

RNA concentrations were determined by Nanodrop (Thermo) or Qubit with RNA HS Assay Kit (Thermo). For samples used for sequencing, RNA integrity was assayed by electropherogram in a Bioanalyzer using a total RNA Assay with a Pico/Nano Chip (Agilent). RNA samples were always kept on ice and stored at -80℃ when not in use to prevent degradation.

meRIP

Mouse RNA samples were processed as previously described for meRIP-seq (Berulava et al. 2020). Briefly, isolated RNA was depleted from ribosomal RNA (rRNA) using the NEBNext ribosomal RNA removal kit (NEB), scaling up according to the initial amounts of RNA. The rRNA-depleted RNA from three or four mice was pooled together for each replicate, for a total of three replicates per condition and fragmented for 8 minutes at 70℃ to an average fragment size of ~80 nt using Fragmentation Reagents (Invitrogen). After each step, the RNA was cleaned using the Clean and Concentrator kit and eluted in an appropriate level of nuclease-free water. rRNA depletion, fragment size and RNA quality were controlled in the Bioanalyzer, using Pico, Nano or Small RNA chips as needed.

10 μg of anti- m^6A antibody (Synaptic Systems) or rabbit IgG control (Millipore) were added to 50 μl of Protein A/G beads (Thermo) and incubated in 500 μl of IP buffer (0.2 M Tris-HCl pH 7.5, 0.5 M NaCl, Igepal 2%) for 4 hours at 4℃ with constant rotation. 10 μg of fragmented RNA per replicate were used for the subsequent RIP, with 500 ng (5%) kept to serve as the input. The RNA was incubated with the antibody-beads conjugate, in 1 ml of IP buffer supplemented with 200 units SUPERase-in (Invitrogen) overnight (ON) at 4℃. Beads were washed 5 times with IP buffer and precipitated RNA was eluted with 6.7 mM m^6A in 200 μl IP buffer for 1 hour at 4℃ with agitation. Eluted RNA was cleaned before proceeding to library preparation.

Due to their low starting RNA concentration, human RNA samples were processed in a slightly different manner, based on a previously published protocol(Zeng et al. 2018). 5–10 μg of purified total RNA were depleted from rRNA using the RiboMinus Eukaryote Ribosomal Removal Kit (Invitrogen) and fragmented for 5 minutes at 70℃ to a fragment

size of 100–120 nt with Fragmentation Reagents. RNA was cleaned using the Clean and Concentrator Kit after every step and eluted in an appropriate volume of nuclease-free water. 500 ng of fragmented RNA were used for each IP, keeping 5% as input. 3 µg of anti- m^6A antibody was conjugated with 30 µl of Protein A/G beads for 2 hours at 4° C with rotation in 500 µl IP buffer. After washing the beads, RNA was added in 500 µl of IP buffer supplemented with 200 units SUPERase-in and incubated ON at 4℃ with rotation. Beads with immunoprecipitated (IP) RNA were washed 5 times with IP buffer and further washed with low-salt (50 mM Tris pH 7.4, 50 mM NaCl, 1mM EDTA, 1, 0.1% NP-40, 0.1% SDS) and high-salt (same as low-salt but with 500mM NaCl) buffers at 4℃ with rotation to remove nonspecific binding. RNA was eluted with 6.7 mM m^6A in 200 µl IP buffer for 1 hour at 4℃ with agitation. Eluted RNA was cleaned before proceeding to library preparation.

Library preparation and sequencing

Mice samples (including meRIP-seq, polysome sequencing and synaptosomal RNA-Seq) were prepared for sequencing using the TruSeq Stranded Total RNA Library Prep Kit (Illumina) according to the manufacturer's instructions. All of the RNA obtained from IP samples was used for library preparation, for input samples 300 ng was used. Libraries were amplified for a total of 13 cycles.

Human samples were prepared using the SMARTer Stranded Total RNA Kit v2 - Pico Input Mammalian (Takara) according to the manufacturer's instructions. Since samples were already fragmented, the fragmentation step was skipped. All of the RNA obtained from IP samples was used for library preparation, for input samples 2 ng were used. Libraries were amplified for 12 (input) or 16 (IP) cycles.

Prepared libraries were sequenced in a Hiseq 2000 System (Illumina) for 50 cycles in single-end reads.

Bioinformatic analysis of meRIP-Seq RNA-Seq

Raw reads were processed and demultiplexed using bcl2fastq 2.20.2 and low-quality reads were filtered out with Cutadapt 1.11.0 (Martin 2011). Filtered reads were mapped to the human (hg38) or mouse (mm10) genome using the STAR aligner 2.5.2b (Dobin et al. 2013). The resulting bam files were sorted, indexed and the unmapped reads removed using SAMtools 1.9.0 (H. Li et al. 2009) Methylation sites were determined using MeTPeak 1.0.0 (Cui, Meng, et al. 2016) and differential methylation was assessed

with exomePeak 2.16.0 (Meng et al. 2013), an adjusted p value (padj, also termed FDR [False Discovery Rate]) cutoff of 0.05 and fold-change (FC) cutoffs of 1.2 or 1.5 were used as indicated in the text. For mouse samples, only consistently significantly differentially methylated peaks were used, unless indicated; for human samples, significantly differentially methylated peaks were used.

For RNA-Seq analyses, read counts were obtained with subread featurecounts 1.5.1 (Y. Liao, Smyth, and Shi 2013) from the bam files of input samples. Differential gene expression was determined by DESeq2 3.5.12 (Love, Huber, and Anders 2014) using normalized read counts and correcting for covariates detected by RUVseq 1.16.1 (Risso et al. 2014). Cutoffs of padj $\leq$ 0.05, FC $\geq$ 1.2 and BaseMean $\geq$ 50 were applied to the results.

For visualization, bam files of both IP and input samples were collapsed for PCR duplicates using SAMtools and IP samples were normalized to their corresponding inputs and to their library size using deeptools bamCompare 3.2.1 (Ramírez et al. 2016). The resulting normalized tracks were visualized in the IGV Browser 2.9.2 (Robinson et al. 2011).

Gene ontology (GO) analyses

GO term enrichment analyses were performed using the App ClueGO v2.5.3 (Bindea et al. 2009) in Cytoscape v3.7.2 (Shannon et al. 2003), with GO Term Fusion enabled to collapse terms containing very similar gene lists. GO term tables for Biological process, Cellular component, Pathways and KEGG were produced and are labeled accordingly in the figures. Resulting enriched GO terms were visualized with a custom script using ggplot2 3.3.5 (Wickham 2009), displaying the adjusted p value for the GO term, the number of genes from the list that belong to said term and the percentage of the total genes in the GO term that are present in the list. Synaptic GO enrichment analyses were performed with SynGO 1.1 (syngoportal.org; Koopmans et al. 2019).

Additional bioinformatic packages and tools

Scripts and analysis pipelines were written in R 3.5.2 (Team 2013). Peak annotation was performed with Homer 4.10.4 (Heinz et al. 2010) and Annotatr 1.8.0 (Cavalcante and Sartor 2017). Guitar plots were produced with the Guitar 1.20.1 (Cui, et al. 2016) R package. Volcano plots were generated with plot.ly/orca 4.9.4.1 (Sievert 2019). Area-proportional Venn diagrams were produced with biovenn (www.biovenn.nl; Hulsen, de

Vlieg, and Alkema 2008) and multiple lists comparisons performed with Intervene/UpSet (asntech.shinyapps.io/intervene/; Khan and Mathelier 2017). Mouse/human homologs were determined by their annotation in NCBI's Homologene database using the Homologene (v1.4.68.19.3.27) R package. Odds ratios and p values to determine significance in overlapped datasets were calculated with the GeneOverlap R package 1.18.0 (Shen 2019). De novo motif analyses were performed with Homer's findMotifsGenome and motifs containing the DRACH consensus sequence out of the top 10 most significant are displayed. KEGG pathway enrichment was produced with KEGG Mapper (www.genome.jp/kegg/mapper; Kanehisa, Sato, and Kawashima 2021). Microscopy images were preprocessed with Fiji (Schindelin et al. 2012) and quantification was automated in Cell Profiler (cellprofiler.org; Jones et al. 2008; McQuin et al. 2018). Graphs, heatmaps and statistical analyses were performed on GraphPad Prism version 9.3.1 for Mac. Some custom figures were created with BioRender (biorender.com).

qPCR

cDNA synthesized from highly abundant samples was prepared using the Transcriptor cDNA first strand Synthesis Kit (Roche) using 100 ng-1 µg of total RNA or 5–20 ng of rRNA-depleted RNA as starting material. The manufacturer's protocol for cDNA synthesis was followed, with a combination of random hexamers and Poly(dT) oligos.

IP samples and low abundance samples were synthesized using the Maxima first strand cDNA synthesis Kit (Thermo), according to the manufacturer's instructions. 1–10 ng of rRNA-depleted RNA or the full amount of IP RNA were used as input.

Synthesized cDNA was diluted 1:5–1:10 with nuclease-free water before being used for qPCR. Reactions were run in a Light Cycler 480 (Roche) in 96- or 384-well plates, using the Light Cycler 480 SYBR Master Mix (Roche). Each reaction was run in duplicate, in a volume of 20 µl and using 4 µl of cDNA per reaction. Primers used were custom designed, validated and used at a final concentration of 0.5 µM. Reactions were run for a maximum of 45 cycles with a reference gene in every plate and quantified as expression relative to the reference (and input in the case of IPs). 3–6 biological replicates were used in every case and statistical differences were determined by a t test, unless otherwise indicated.

Primer sequences are available in Supplementary Table 1.1.

Hippocampal primary neuronal culture

Pregnant (embryonic day 15: E15) CD1 mice were purchased from Janvier Labs and sacrificed under anesthesia by cervical dislocation on day E17. The pups were dissected and their hippocampi were isolated and collected in ice-cold DPBS (pH 7.4, without Ca and Mg). The hippocampi of 8–14 pups were used to prepare the primary cultures using a mild dissociation protocol with papain to prevent cell death and increase neuronal yield. The Papain Dissociation System (Worthington Biochemical) was used according to the manufacturer's instructions with an incubation time of 45 minutes. The single-cell suspension was counted using a hemocytometer and cells were plated at a density of 30–40,000 cells/cm^2 in Neurobasal Plus Medium (Gibco) supplemented with 1X B27 Plus Supplement (Gibco), 1X PenStrep (Gibco) and 1X GlutaMAX (Gibco). Culture plates were kept at 37℃ and 100% humidity with 5% CO_2. Cells were supplemented with fresh medium after 5 days and half the medium was exchanged once a week after that.

siRNA/ LNA GAPmer transfection

Pre-designed control and Mettl3-targetting siRNAs were purchased from Origene, control and Mettl3-targeting LNA GAPmers were designed and purchased from Qiagen. 2 pmol of the corresponding control/Mettl3 siRNA/GAPmer were packaged into lipid nanoparticles (LNPs) specially formulated to deliver RNAi into primary mouse neurons using the Neuro9 siRNA Spark Kit (Precision Nanosystems). Cells were transfected with 0.3 µg/ml of siRNA/GAPmer supplemented with 1µg/ml ApoE4 on day *in vitro* (DIV) 7. A fluorescent control siRNA was used to confirm a transfection efficiency of more than 80%. Knockdown efficiency was initially validated by qPCR after 48 hours but sufficient decrease in METTL3 protein and m^{6}A levels were reached with the use of GAPmers after 6 days from transfection. Before fixation or RNA or protein extraction cells were washed with sterile DPBS to remove medium.

Western Blot

Cells or tissue were dissociated in an appropriate volume of RIPA buffer (140 mM NaCl, 1 mM EDTA, 0.1% sodium deoxycolate, 1% Triton X-100, 10 mM Tris pH 8, 1% SDS) supplemented with 1X cOmplete proteinase inhibitor (Roche). Protein concentration was quantified using the Pierce BCA Protein Assay Kit (Thermo) and 30 µg of protein were used per well of precast 4–15% polyacrylamide gels (Bio-Rad). Gels were run for

20 minutes at 90V followed by 50 minutes at 120V in Running buffer (25 mM Tris, 190 mM glycine, 0.1% SDS) and transferred into PVDF membranes (Bio-Rad) using the Trans-Blot Turbo Transfer System (Bio-Rad) in Auto mode.

Membranes were washed with PBST (1X PBS, 0.05% Tween-20) and blocked for 1 hour at room temperature (RT) in 5% BSA. Primary antibodies diluted in 5% BSA were incubated ON under shaking at 4℃. Fluorescent secondary antibodies (IRDye, LI-COR) were incubated for 2 hours at RT with shaking. Blots were imaged by fluorescence with an Odyssey DLx (LI-COR) and the resulting images were quantified with ImageStudio.

m^6A quantification

m^6A concentration was determined using a m^6A Methylation Assay Kit Fluorometric (Abcam). The starting material was 200 ng of rRNA-depleted RNA and the manufacturer's protocol was followed. All reactions were carried out in duplicate and a standard curve of m^6A /A was included to have quantitative results. Reactions were read in a FLUOstar Omega Multiplate reader (BMG) in fluorescence mode.

Immunofluorescence

Cells used for imaging were seeded on etched coverslips (2 hours in nitric acid, followed by 1 hour washing and 2 hours in 70% ethanol, kept on sterile water) coated with 0.5 mg/ml poly-D-lysine ON at 37℃. Cells were fixated for 10 minutes in fixating solution (4% paraformaldehyde, 4% sucrose in 1X PBS).

Coverslips were permeabilized using T-PBS (0.3% Triton-X100 in 1X PBS) for 30 minutes at RT followed by 1 hour in blocking solution (5% BSA in T-PBS). Primary antibodies were incubated ON at 4℃ with shaking and secondary antibodies for 2 hours at RT. All antibodies were diluted in T-PBS.

Antibodies used for Western blot, immunofluorescence and other applications, as well as the dilutions used are described in Supplementary Table 1.2.

Microscopy

Images were captured in a Leica dmi8 microscope fitted with a STEDycon STED/Confocal (Abberior). Immunofluorescence and Puro-PLA images were acquired in the confocal mode, with a 63X oil immersion objective and using identical acquisition settings for all images to be compared.

Puro-PLA

Puromycin-proximity ligation assay (Puro-PLA) was performed as previously described with minor alterations (tom Dieck et al. 2015). DIV 13 mouse primary hippocampal neurons were pretreated with 100 µg/ml cycloheximide for 30 minutes to arrest translational elongation. Cells were then treated with 3 µM puromycin for 10 minutes to label nascent polypeptide chains. This treatment time was chosen to balance labeling intensity and the propensity of labeled peptides to diffuse away from their synthesis sites (Enam et al. 2020; Hobson et al. 2020). Puromycin incorporation and cycloheximide pretreatment were validated by Western blot.

The PLA was performed using the Duolink Proximity Ligation Assay Kit Red (Merck) according to the manufacturer's instructions. Primary antibodies against puromycin and the protein of interest (targeting the N-terminal region) raised in different species were used for the PLA assay and incubated ON at 4℃. Counterstain antibodies (Map2 and SYP) were incubated ON at 4℃ along with the PLA primary antibodies, an additional incubation step was added after finishing the Puro-PLA protocol to add the secondary antibodies for the counterstains for 2 hours at RT before mounting.

For each condition and replicate, 7–13 neurons were captured by confocal imaging and analyzed using Cell Profiler to automate the analysis and remove biases. Background level PLA signal was adjusted to samples without puromycin treatment.

Polysome sequencing

Polysomes were prepared from the DG of five young and five old animals as described (Chassé et al. 2017). Briefly, tissue samples were lysed in Polysome buffer (50 mM Tris-HCl pH 7.4, 10 mM MgCl$_2$, 100 mM NaCl, 1% Triton-X-100, 1 mM DTT) supplemented with RNase inhibitors and 100 g/ml cycloheximide, using a MICCRA D-1 homogenizer. Cell debris was removed by centrifugation at 20,000 x g for 10 min at 4°C. The soluble whole cell extracts were separated on 10–50% sucrose density gradients (prepared in Polysome buffer with 100 g/ml cycloheximide) in an SW40Ti rotor by centrifugation for 3 h at 35,000 rpm. Fractions containing polysomes (determined by monitoring the absorbance of each fraction at 260 nm) were pooled and RNAs were extracted using phenol:chloroform:isoamyl alcohol (25:24:1), ethanol precipitated and resuspended in water.

Synaptosome isolation for sequencing

The hippocampi of 60 3-month and 60 16-month old mice were isolated to obtain the necessary amount of RNA for sequencing. Twenty bilateral hippocampi were pooled together, making up three independent samples that were processed to obtain high-quality synaptosomes, using an existing protocol (Boyken et al. 2013; Fischer von Mollard, Südhof, and Jahn 1991). In short, hippocampi were homogenized by 9 strokes at 900 rpm in 320 mM sucrose buffer and centrifuged at 4°C for 2 min at 5,000 rpm (SS-34 rotor). Supernatants were further centrifuged at 4°C for 12 min at 11,000 rpm. Pellets were loaded onto a Ficoll gradient (5–13% in 320 mM sucrose, 5 mM HEPES, pH 7.4) and centrifuged at 4°C for 35 min at 22,500 rpm (SW41Ti rotor). The interface between 13 and 9% Ficoll was washed by further centrifugation and then pelleted at 8700 rpm for 12 min in a SS-34 rotor. Resuspended synaptosomes were then centrifuged on a sucrose gradient (25–50% sucrose [w/v], 5 mM HEPES) for 3 h at 28,000 rpm (SW28Ti rotor). Finally, synaptosomes were fractionated via the Gilson Minipuls, and 21 fractions were collected and analyzed by dot blotting. For this, from each fraction, 2 µl of sample was pipetted onto a nitrocellulose membrane, and dried for 5 min. Blocking of nonspecific signal was done with 5% low-fat milk in TBST for 10 min. Antibodies against synaptobrevin and PSD95 were applied for 15 min at RT, then the membrane was washed three times for 3 min each in TBST with 5% milk. Secondary antibody was applied for 15 min at RT. The membrane was washed again three times with TBST without milk before being imaged. Only 5 fractions from each preparation showed a signal for synaptobrevin and PSD95, ensuring the presence of high-quality synaptosomes. These were then processed for total RNA sequencing

H3K36me3 chromatin immunoprecipitation (ChIP)

Cell type specific chromatin isolation and ChIP sequencing was performed as previously described (Michurina et al. 2022; Halder et al. 2016). 3–4 CA1 were pooled for each replicate and nuclei were FACS sorted by NeuN expression. 300ng of chromatin and 1 µg of H3K36me3 antibody (Abcam, ab9050) were used for each ChIP. Libraries were prepared with the NEBNext Ultra II DNA library preparation kit, 8 cycled of PCR amplifications were performed for both inputs and IP samples. Average fragment size of the libraries was 380bp.

Microfluidic chambers for synaptic RNAs

Custom made polydimethylsiloxane (PDMS) microfluidic chambers optimized for the harvesting of synaptic RNAs were produced as previously published (Epple et al. 2021). 70,000 cells were seeded on every side of the chamber and cultured for 7 days with daily medium exchange between the distinct compartments and replenishment to counteract evaporation. On DIV 7 the somas of cultured neurons on both the dendritic and axonal side of the chambers were treated with LNPs containing Control or Mettl3 KD LNA GAPmers. Cells were cultured for a further 6 days with constant medium replenishment before harvesting the synaptic RNAs. The synaptic compartment was excised using a purpose-built device and RNA was purified using the GenElute Total RNA Purification Kit (Sigma).

Results

The m^{6}A landscape in the adult mouse brain

Recent studies have implicated N^6-methyladenosine modifications in mRNA with learning and synaptic plasticity (Livneh et al. 2020; Widagdo and Anggono 2018; Bird and Burgess 2008). Our knowledge about the transcriptome-wide distribution of m^{6}A marks as well as the downstream molecular mechanisms involved in the regulation of neuronal plasticity is however still limited. Thus, we started our analysis by characterizing the landscape of m^{6}A modifications in the healthy adult brain. The brains of ten WT (C57BL/6J) three-month-old (young) mice were extracted and dissected to obtain hippocampal subregions: CA1, CA3 and dentate gyrus (DG); as well as the anterior cingulate cortex (ACC, Figure 2.1A). meRIP-seq was performed on the mRNAs extracted from these samples to determine the subregion-specific epitranscriptome landscape in young adult mice.

The analysis of methylated regions showed a large number of detected m^{6}A peaks in hippocampal brain subregions, with 18,270 peaks detected in the CA1, 20,415 in the CA3 and 16,686 in the DG (Suppl. Figure 1A). A remarkable number of transcripts were detected to be carrying this methylation mark, ranging from 40.27% of expressed genes in the DG to 42.81% and 44.38% in the CA1 and CA3, respectively (Figure 2.1B). On average, every methylated transcript had 2.4–2.7 methylated regions per transcript containing m^{6}A, depending on the hippocampal subregion (Suppl. Figure 1B). Motif enrichment analyses of the detected m^{6}A peaks showed a strong overrepresentation of the consensus m^{6}A motif DRACH, showing that the meRIP-Seq had successfully enriched for m^{6}A sites (Suppl. Figure 1C). The detected m^{6}A peaks follow a distribution along transcripts that corresponds with the well-described location of m^{6}A sites, with enrichment in the vicinity of the stop codon and 3'UTR, as well as internal exons (Figure 2.1B,C). The population of methylated transcripts exhibited a large similarity, with more than 60% of all transcripts with m^{6}A in all subregions being common across them. However, despite the large overlap, a subset of transcripts appeared to be methylated in a subregion-specific manner, ranging from 6.18% in CA1 to 12.21% of the total in CA3 (Figure 2.1D).

The 5,206 transcripts that are detected as being methylated in all hippocampal subregions showed a very significant enrichment for genes associated with

neurogenesis and neural development, RNA metabolism, as well as synapse assembly and function (Figure 2.1E), supporting the notion that m^{6}A acts as a crucial regulator of these processes in the adult brain. Subregion-specific transcripts showed an enrichment for more broad biological processes with no clear mechanism standing out (Suppl. Figure 1D,E,F).

To further understand how the epitranscriptomic landscape varies across brain subregions, we performed the meRIP-seq analysis on ACC samples obtained from the same young mice. The mouse ACC showed a considerable but reduced methylation level, compared to the hippocampus. In the ACC 11,816 m^{6}A peaks were detected, corresponding to 4,160 consistently methylated transcripts (2.83 peaks per transcript), which represented only 27.3% of the expressed genes, highlighting the remarkable tissue specificity of RNA methylation (Figure 2.1F, S1A,B).

Methylated transcripts in the ACC followed a similar distribution pattern along their sequence with enrichment in the CDS and 3'UTR (Figure 2.1F,G). Interestingly, the hippocampus and ACC shared a 61.29% of their methylated transcripts (Figure 2.1H). Commonly methylated transcripts across brain subregions showed a very strong enrichment in pathways associated with synaptic assembly, organization and signaling, as well as learning and memory, similar to what could be observed in ACC-specific mRNAs (Suppl. Figure 2A,B). In contrast, hippocampus-specific transcripts have functions in the regulation of gene expression and RNA metabolism (Suppl. Figure 2C).

Using SynGO (Koopmans et al. 2019), an experimentally annotated database for synaptic location and function gene ontology (GO), we could confirm that commonly methylated transcripts between hippocampus and ACC are highly enriched for synaptically located proteins, with the most significant enrichment in postsynaptic components associated with signaling and organization (Figure 2.1I). ACC-specific transcripts also display a very significant enrichment in presynaptic signaling regulation. In contrast, hippocampus-specific transcripts showed no significant synaptic enrichment (Suppl. Figure 2D).
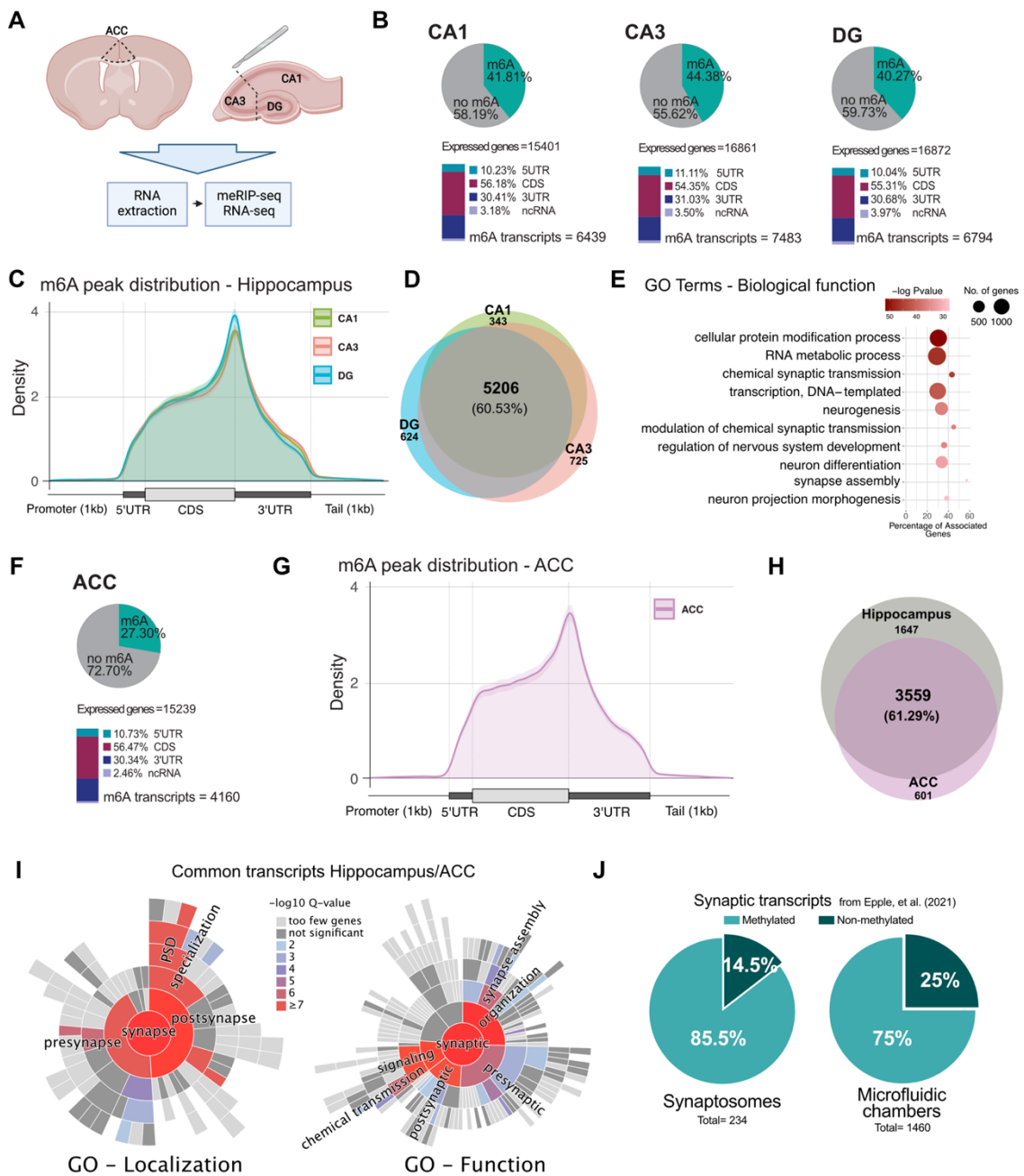
Figure 2.1. The m6A epitranscriptome in the adult mouse brain. A. Schematic for the dissection of brain subregions for meRIP and RNA-seq experiments. B. Distribution of methylation across the transcriptome in the hippocampal subregions. Percentage of m6A calculated against the corresponding expressed genes in inputs; annotated peak regions calculated from total m6A peaks. C. Guitar plot showing the distribution of m6A peaks along mRNA features in hippocampal subregions. D Overlap in methylated transcripts across hippocampal subregions. E. Enrichment of biological function Gene Ontology terms in commonly methylated hippocampal transcripts. (Continued in next page)

(Cont.) F. Distribution of methylation across the transcriptome in the ACC. G. Guitar plot showing the distribution of m6A peaks along mRNA features in the ACC. H. Overlap between methylated transcripts in the Hippocampus (common transcripts from D) and the ACC. I. Enrichment of synapse-specific GO terms in commonly methylated transcripts between the hippocampus and ACC. J. Percentage of methylated transcripts from an independent synaptic mRNA dataset obtained from the hippocampus (Epple, et al. 2021). ACC - anterior cingulate cortex, DG - dentate gyrus, 5UTR - 5' untranslated region, 3UTR - 3' untranslated region, CDS - coding sequence, ncRNA - non-coding RNA

These data suggest that m^{6}A transcripts might be specifically enriched at synapses which is in agreement with previous data that was able to detect m^{6}A mRNAs in synaptosomes (Merkurjev et al. 2018). To further explore this hypothesis, we made use of a recently published dataset containing a high-confidence hippocampal synaptic RNAome and compared it to our hippocampal epitranscriptome data. This synaptic RNA dataset was generated from purified synaptosomes from WT mice as well as primary neurons grown in microfluidic chambers to isolate their synaptic compartments, making it a robust resource of synaptically located RNAs (Epple et al. 2021; Suppl. Figure 2E,F). In both datasets, we observed a strong enrichment of methylated transcripts in synaptically located mRNAs with more than 70% of the synaptosome and 64% of the microfluid chamber transcriptome having at least one m^{6}A peak (Figure 2.1J).

These results go in accordance with previous reports describing the epitranscriptome as largely constant across brain regions, with comparatively small tissue-specific variations in methylated transcripts (Chang et al. 2017). Our data also provide further evidence of m^{6}A as a crucial regulator of synaptic organization and function in the adult brain.

The m^{6}A landscape in the adult human brain reveals a conserved enrichment of transcripts linked to synaptic function

Next, we decided to profile the m^{6}A distribution across transcripts of the human brain employing postmortem tissue of the anterior cingulate gyrus from 4 non-demented

individuals. In the human cingulate cortex (CC) we found that in 22.8% of all expressed transcripts (3625) at least one m^{6}A peak could be detected (Figure 2.2A). This corresponded to 11672 m^{6}A detected peaks, with an average of 3.17 peaks per methylated transcript (Suppl. Figure 3A). Similar to what is observed in mice, m^{6}A peaks fell predominantly along the CDS and 3' UTR with a marked peak in the vicinity of the stop codon (Figure 2.2A, B). The consensus motif sequence for m^{6}A marks DRACH, was consistently found enriched in the detected methylation peaks, confirming the specificity of the meRIP-seq method (Figure 2.2C). Human methylated transcripts belong to various molecular pathways, among them gene expression regulation, RNA metabolism, neural development and synaptic function (Suppl. Figure 3B).

To compare how conserved methylated transcripts were between homologous brain regions across species, in mouse and human we used the dataset previously generated for the mouse ACC and compared it with the human CC, both representing cortical brain regions. All transcripts with an assigned homolog in the corresponding species in NCBI's Homologene database were used in this comparison, which accounted for the vast majority of all m^{6}A transcripts (86% in mouse and 78% in human, Figure 2.2D). More than half (55%) of all methylated transcripts in human with an assigned homolog had their corresponding transcript in mouse methylated too; this accounted for 43% of methylated transcripts in the mouse ACC as well (Figure 2.2D).

Functionally, conserved transcripts were very strongly enriched for genes involved in CNS development, synaptic signaling and learning (Figure 2.2E). In addition, a synapse-specific GO analysis of conserved methylated transcripts shows a highly significant enrichment of synaptic location and function GO terms, particularly post-synaptic localization and functions related to synapse organization and signaling (Figure 2.2F).

Interestingly, not only the transcripts themselves were conserved in their methylation status, but also the location of methylation marks was in many cases conserved too. In the majority of them, annotated m^{6}A peaks fell within the same region of the corresponding homologous human/mouse transcript counterpart (Figure 2.2G, S3D).

In addition to these conserved methylated transcripts, both the human CC and the mouse ACC had a subset of transcripts uniquely methylated in a species-specific manner. In the case of the mouse ACC these transcripts corresponded to genes involved in neurogenesis, the regulation of signal transmission and synaptic function, albeit with considerably less significant enrichment as in conserved transcripts (Suppl.
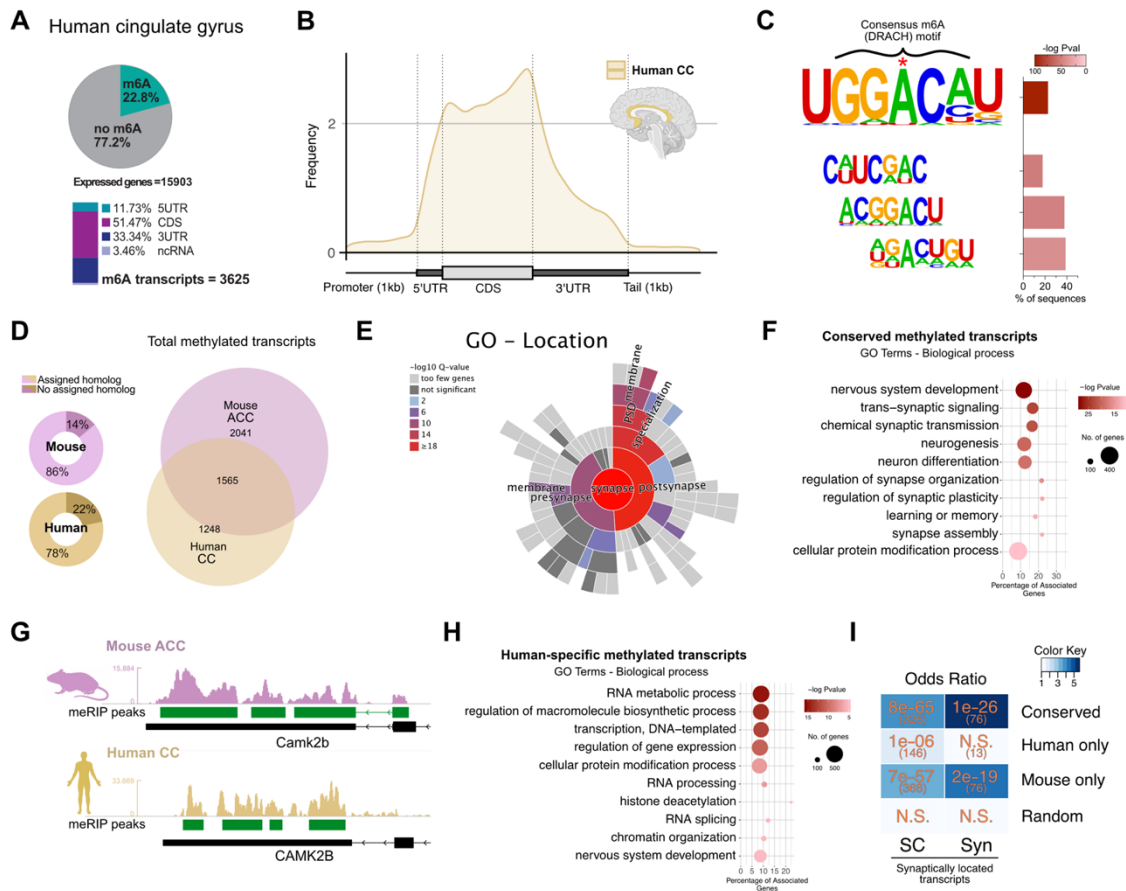
Figure 2.2. m6A marks are conserved between mouse and human. A. Percentage of methylated transcripts in the human CC, calculated against the background expression in the corresponding inputs; peak location by annotated region, percentages calculated from total m^{6}A peaks. B. Distribution of m^{6}A peaks along mRNA features in the human CC. C. Enriched motifs detected in the m^{6}A peaks, showing the consensus m^{6}A DRACH motif, where D = A, T or G, R = A or G, and H = A, T or C. D. Mouse/human genes with known homologs in human/mouse, respectively, used to compare methylated transcripts across species. Overlap of methylated transcripts in the adult mouse ACC with respect to the human CC, from those genes with an assigned homolog. E. Synapse-specific location GO term enrichment for conserved methylated transcripts. F. Enriched GO categories, Biological process for genes methylated only in the human CC. G. Representative coverage tracks showing conserved m^{6}A sites along the 3' end of homologous transcripts in the mouse ACC and human CC (Camk2b/CAMK2B). Tracks show coverage values for m^{6}A-RIP normalized for the corresponding inputs and library size. Scale in RPM. H. Enriched Gene Ontology categories, Biological process for genes methylated in both mouse ACC and human CC (conserved). I. Odds ratio showing the association between overlapping transcripts in conserved, human- and mouse-specific transcripts, compared to synaptically located RNAs, as published by Epple, et al. Color scale represents the numerical value of enrichment (odds ratio), numbers in orange correspond to the p value for the corresponding overlap, numbers in brackets show the size of the overlap. N.S.= not significant (p value ≥ 0.05). SC= RNAs detected in the synaptic compartments of microfluidic chambers; Syn= RNAs detected in synaptosomes. Random corresponds to 2000 randomly selected brain-expressed human genes. ACC - anterior cingulate cortex, CC - cingulate cortex

Figure 3D). Strikingly, transcripts uniquely methylated in the human CC showed a remarkable enrichment for genes associated with the regulation of gene expression, chromatin organization and RNA metabolism, furthermore, they showed no synaptic localization and were primarily located in the nucleus (Figure 2.2H, S3F). Supporting this functional specificity of conserved and non-conserved methylated transcripts, synaptically located mRNAs – both detected in synaptic compartments in microfluidic chambers and in synaptosomes – are consistently significantly overrepresented in the population of conserved and mouse-specific methylated transcripts. In contrast, human-specific methylated transcripts show low or no enrichment for synaptically located mRNAs, comparable to what could be expected by chance (Figure 2.2I).

These results indicate that the regulation of synaptic organization, function and plasticity through m^{6}A marks is a conserved mechanism in the adult mammalian cortex. Moreover, species-specific differences in the methylation status of certain transcripts show that m^{6}A marks are an evolutionarily dynamic regulatory mechanism, with certain populations of transcripts undergoing tissue- and species-specific labeling.

m^{6}A changes in models for cognitive decline and human AD patients

Our data supports the view that m^{6}A-mediated regulation of synaptic function and plasticity is a key mechanism in the maintenance of homeostasis in the adult mammalian brain. To further explore this, we decided to study the m^{6}A landscape during cognitive decline and chose age-associated memory impairment in mice as one model system. Previous studies have reported that age-associated memory impairment can be observed already in 16-month old mice, while at this stage only minor changes in neuronal gene expression are detected (M. Li et al. 2020; Ianov et al. 2017; Belblidia et al. 2018). We reasoned that the comparison of 3 vs. 16 months old mice would thus allow us to test if changes in m^{6}A RNA methylation may precede massive changes in gene expression, as it had been reported for example for heart failure, which similar to the brain represents a disease affecting an excitable and post-mitotic tissue (Berulava et al. 2020). To this end we collected the brain subregions (ACC, CA1, CA3, DG) from 3 (young) and 16 (old) months old mice and performed meRIP-seq analysis (Figure 2.3A). In line with previous observations, a differential expression analysis between old and

young samples in the aforementioned subregions revealed comparatively mild changes (FC > 1.2, FDR≤0.05), ranging from 40 differentially expressed genes (DEGs) in the DG to 155 in the ACC (Figure 2.3B). DEGs were not significantly enriched for specific GO categories and no specific pathway was considerably affected (Suppl. Figure 4A). In contrast to the transcriptome, the epitranscriptome of these same tissues showed remarkable changes, when m^{6}A levels in old mice were compared with the corresponding subregions in the young brain. Using the same cutoffs as for differential expression, a much larger number of genes showed differences in the methylation levels of at least one m^{6}A peak along their transcript, consistently across all replicates (Figure 2.3B). The DG showed the most widespread changes, with 1,971 transcripts differentially methylated, followed by the CA1 with 1,557, ACC with 1,373 and CA3 with 743.

A total of 1,698 peaks were detected as differentially methylated in the ACC, 2,136 in the CA1, 811 in the CA3, and 2,468 in the DG (Suppl. Figure 4B). In all subregions, differentially methylated transcripts averaged 1.24 peaks per transcript (Suppl. Figure 4C). At this level, sites of decreased m^{6}A (hypomethylated) greatly outnumbered those with increased m^{6}A (hypermethylated) across all brain subregions with the most striking changes occurring in the ACC and CA1 (Figure 2.3B). While the vast majority of differentially methylated transcripts (92–99%) showed consistent changes in methylation, in a few cases transcripts contained increased as well decreased m^{6}A peaks (mixed transcripts, Figure 2.3C). In all subregions, the bulk of differentially methylated transcripts showed consistent hypomethylation, with up to 94% of the total in the CA1 and 85% in the ACC belonging to this group. In contrast, only a small fraction of transcripts was consistently hypermethylated, with this population being most numerous in the CA3 and DG, with 21% and 22%, respectively (Figure 2.3C). Some variability was also observed in the magnitude of change across brain subregions, with the CA1 and ACC displaying a more dramatic reduction in m^{6}A, compared to the CA3 and DG (Suppl. Figure 5A).

The location of m^{6}A marks along the transcript has been associated with distinct fates for the labeled mRNAs. To determine whether aging-associated changes were favoring certain regions of labeled transcript, differentially methylated peaks were annotated according to their location. Like it is the case with the baseline methylated regions, differentially methylated peaks are enriched along the gene body, stop codon and 3'

UTR (Figure 2.1B, C, Figure 2.3D). Interestingly, the ACC shows a particular pattern for the location of hypomethylated peaks, with many of them falling within the 5' UTR and a slight enrichment in the vicinity of the stop codon, when compared to the other analyzed subregions (Figure 2.3D, S5E). Hypomethylated peaks in the DG displayed a stronger increase in their location surrounding the stop codon as well. Conversely, hypermethylated peaks showed a considerably larger variability in their location within mRNAs, in large part due to their smaller numbers (Suppl. Figure 5D-F).
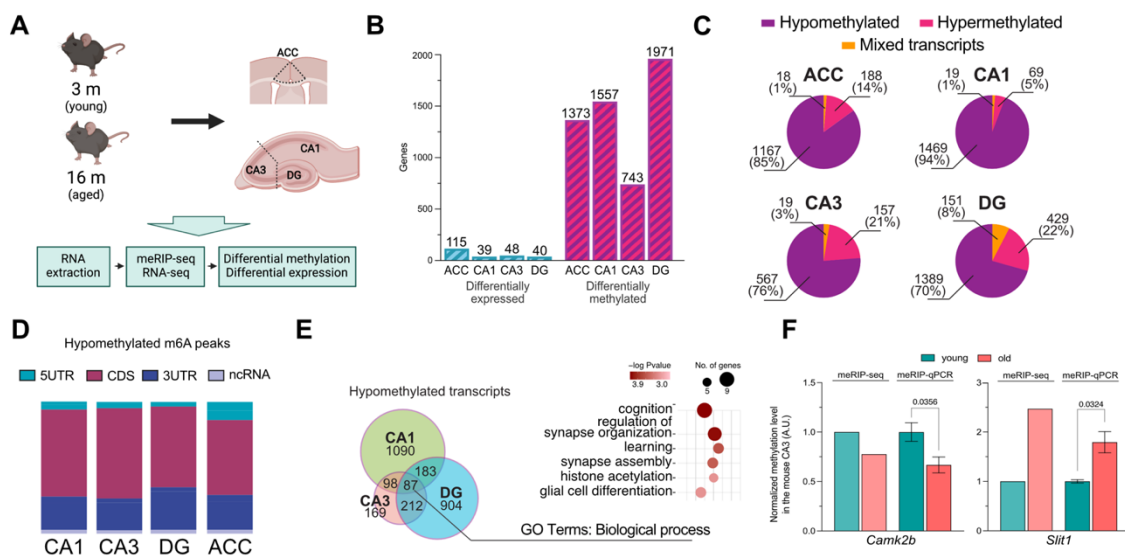

Figure 2.3. Tissue-specific changes in m6A occur during aging. A. Workflow for differential methylation analysis in aging. B. Number of differentially expressed and differentially methylated genes detected in the corresponding brain subregion, applying equal cutoffs for fold change and adjusted p value (FC > 1.2, padj ≤ 0.05). C. Proportion of methylated transcripts containing peaks with only reduced methylation levels in aging (hypomethylated), only increased methylation (hypermethylated) or a mixture of decreased and increased (mixed) peaks in all brain subregions. D. Annotated distribution of significantly hypomethylated peaks across transcripts for all brain subregions. E. Overlap of hypomethylated transcripts across hippocampal subregions, highlighting the unique transcripts as well as common transcripts in the hippocampus. GO terms biological process for the 87 common transcripts across the hippocampus. F. qPCR validation of two differentially methylated genes. The graph shows the FC in methylation in the probed region as detected by meRIP-Seq and meRIP-qPCR. Columns show the mean +/- SEM of 4 independent replicates per condition. Statistical significance was determined by Student's t test and the p value is displayed above the comparison. ACC. ACC - anterior cingulate cortex, DG - dentate gyrus, 5UTR - 5' untranslated region, 3UTR - 3' untranslated region, CDS - coding sequence, ncRNA - non-coding RNA

When comparing the hippocampus 87 mRNAs are detected as hypomethylated in all hippocampal subregions, whereas for shared hypermethylated transcripts the number is even lower with 2 (Figure 2.3E, S5C). Despite this limited commonality, the shared hypomethylated transcripts are highly enriched for pathways associated with cognition, learning and synaptic organization, showing that despite high tissue specificity, hypomethylation affects certain common pathways in the hippocampus (Figure 2.3E). Similarly, when comparing hypomethylated transcripts amongst hippocampal subregions and the ACC, only 33 of them could be detected in all tissues. The largest group of commonly hypomethylated transcripts is found in the ACC and CA1, where 387 of them are hypomethylated in both tissues (Figure 2.3E). Significantly differentially methylated regions could be visualized at the sequencing level and validated independently by meRIP-qPCR (Figure 2.3F).

Taken together, these data identify massive changes in m^6A levels in the aging brain at a time point when first memory impairment is observed and gene expression changes are comparatively moderate. The vast majority of the affected transcripts exhibit m^6A hypomethylation and represent genes localized at synapses and linked to synaptic plasticity.

The data hint towards a role of this mark in the development of age-associated cognitive decline, a role that would be in line with reported observations of the involvement of m^6A in learning and memory. Considering the commonality in m^6A transcripts in the brains of mice and humans (see Figure 2.2) we decided to study whether m^6A changes could be associated with cognitive impairment in humans. Thus, we analyzed the m^6A-epitranscriptome during Alzheimer's disease (AD), the most common cause of dementia in the elderly. Postmortem human cortex samples from AD patients were matched with corresponding non-demented controls (NDC) and analyzed by meRIP-seq. At the gene expression level, we detected a total of 185 genes as differentially expressed, with 100 of them being upregulated and 85 downregulated (FC > 1.2, FDR ≤ 0.05, Figure 2.4A, S6A). GO terms for upregulated genes show an enrichment of regulators of the Wnt signaling pathway, whereas downregulated genes not strongly associated with a given pathway. It is worth noting that no genes associated with the m^6A machinery were amongst those with significant expression changes in this dataset (Suppl. Figure 6A).

In stark contrast to the changes at the gene expression level, the differential methylation analysis of meRIP-seq shows massive changes in m^6A levels in AD. More than 2,500
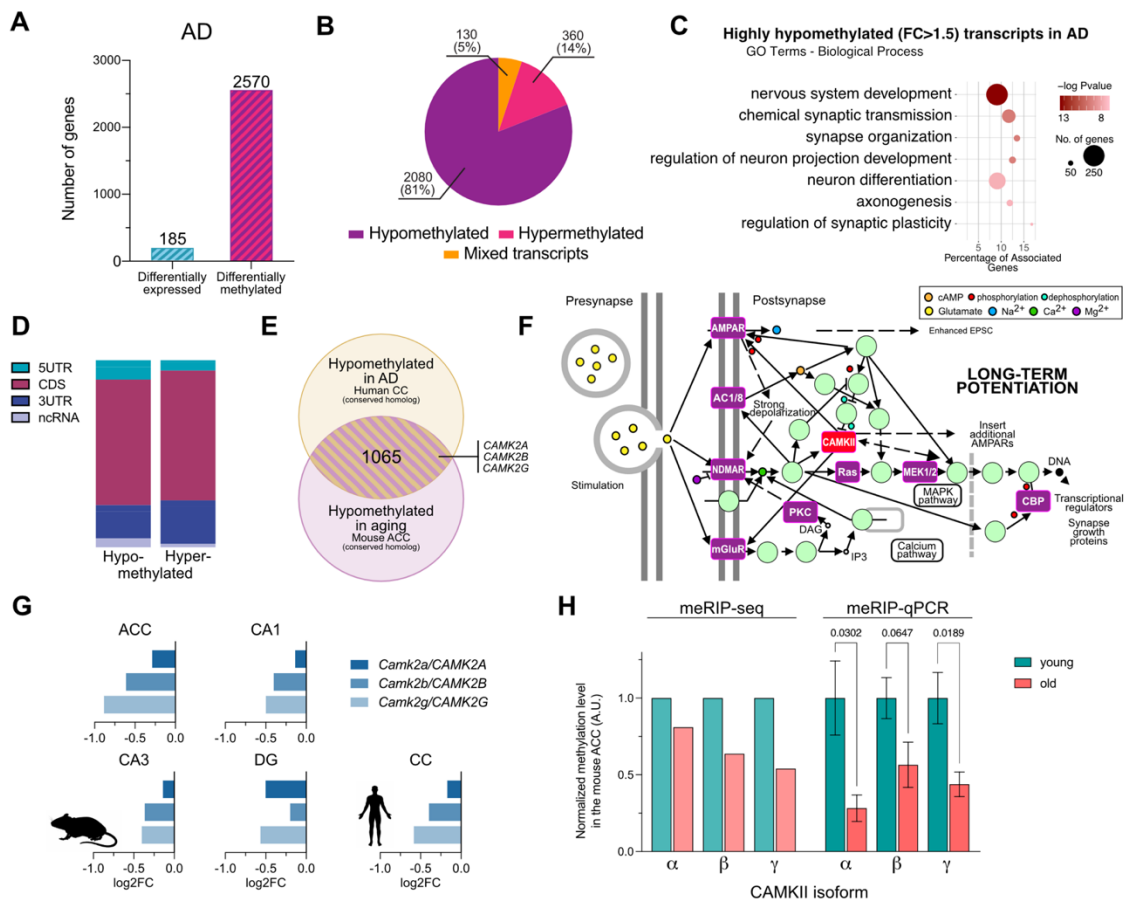
Figure 2.4. Epitranscriptome plasticity changes in neurodegeneration and aging. A. Comparison of differentially expressed and differentially methylated genes in AD vs Control samples applying equal cutoffs for fold change and adjusted p value (FC > 1.2, padj ≤ 0.05). B. Proportion of hypomethylated, hypermethylated and mixed transcripts in AD samples. C. Enriched GO categories Biological process for significant highly hypomethylated transcripts (FC > 1.5) in AD. D. Annotated distribution of differentially methylated peaks in AD along transcripts. E. Overlap of all detected significantly hypomethylated peaks in the aged mouse ACC and AD human CC, highlighted are CaMKII isoforms. F. KEGG pathway *Long-term potentiation* (hsa04720), highlighted in purple are pathway components that are commonly hypomethylated in aging and AD, in red is CaMKII. G. Changes in methylation in individual isoforms of CaMKII in the aged mouse brain and in the human CC in AD. Each bar represents the methylation site in the 3UTR of the corresponding transcript closest to the stop codon. H. qPCR validation of the hypomethylated region in the 3UTR of the displayed CaMKII isoforms. The graph shows the FC in methylation in the probed region as detected by meRIP-Seq and meRIP-qPCR. Bar shows the mean +/-SEM of 6/4 (young/old) independent replicates, p value is displayed above the comparison. Statistical significance was evaluated by Student's t test with Welch's correction for unequal variances. AD - Alzheimer's disease, ACC - anterior cingulate cortex, DG - dentate gyrus, 5UTR - 5' untranslated region, 3UTR - 3' untranslated region, CDS - coding sequence, ncRNA - non-coding RNA.

genes are detected as differentially methylated using the same FC and FDR cutoffs as the differential expression analysis (Figure 2.4A). These correspond to 3,288 differentially methylated peaks (2,568 hypo- and 424 hypermethylated) with an average of 1.26 m^{6}A peaks per differentially methylated transcript (Suppl. Figure 6B). Of them, the vast majority are exclusively hypomethylated transcripts (81%) with a smaller fraction (14%) showing only hypermethylation and the remaining 5% having both hypo- and hypermethylated regions (mixed transcripts, Figure 2.4B). Highly hypomethylated transcripts showed a very strong enrichment of genes associated with developmental processes, neuron projection and the regulation of synaptic transmission and plasticity, GO categories that also were highly affected by m^{6}A changes during aging in the mouse brain (Figure 2.4C). The location of these differentially methylated marks displayed a distribution favoring the CDS of the affected transcripts, with limited 3UTR location (Figure 2.4D. S6C).

These data are similar to the observed changes of m^{6}A levels in the aging mouse brain. In fact, there was a considerable overlap between the populations of hypomethylated transcripts in the aged mouse brain and the human AD brain and more than 1,000 hypomethylated m^{6}A transcripts were detected in both species (Figure 2.4E). Among these transcripts, the majority has well described roles in the regulation of synaptic function, learning and plasticity (Suppl. Figure 6D). Furthermore, there was a very significant overlap between these transcripts and RNAs previously described as synaptically located, as well as known synaptic methylated transcripts (Suppl. Figure 7A-C; Epple et al. 2021; Merkurjev et al. 2018). In this group, numerous components of pathways associated with the regulation of plasticity - like long-term potentiation (LTP) - and disease are highly overrepresented (Figure 2.4F, S6E). Many of the de-regulated transcripts observed in mice and humans are also known to be located to synapses. Within this subset we found the transcripts for multiple isoforms of one of the best described subfamilies of synaptic plasticity-associated proteins, the Calcium/calmodulin-dependent protein kinase type II (CaMKII): *Camk2a*, *Camk2b* and *Camk2g* (Figure 2.4E, F, S6F). CaMKII is central for memory formation and learning, with the α and β isoforms being essential for the establishment and maintenance of LTP (Zalcman, Federman, and Romano 2018). The corresponding transcripts were characterized by a consistent hypomethylation in the ageing mouse and human AD brain (Figure 2.4G) a finding that was confirmed by qPCR (Figure 2.4H).

Decreased m⁶A levels affect the local synthesis of the plasticity-related protein CaMKII

Next, we wanted to further elucidate the functional consequences of reduced m^{6}A methylation. The fact that we see comparatively few changes in gene expression while substantial m^{6}A-hypomethylation is observed in aged mice or AD brains, suggest that the m^{6}A changes detected in our experimental settings may not impact on transcript stability, a process that has been linked to m^{6}A RNA-methylation (Wang et al. 2014). In line with this hypothesis there was no strong correlation between m^{6}A changes and transcript levels in any of the analyzed tissues (Suppl. Figure 8A-E). This finding was further corroborated by our observation that levels of histone 3 tri-methylation at lysine 3 (H3K36me3), a repressive histone-mark that had been linked to changes in m^{6}A RNA-methylation (Huilin Huang et al. 2019), did not change when comparing hippocampal tissues samples from young and old mice via ChIP-sequencing (Fig.8F,G). m^{6}A labels on mRNA are also known to play a role in regulating the transport of certain synaptically-located transcripts, as well as on the somatic translation of plasticity-related genes (Merkurjev et al. 2018; Zhang et al. 2018; Shi et al. 2018). To determine whether these mechanisms could be acting downstream of the changes in m^{6}A levels during aging and AD we first isolated synaptosomal compartments from the hippocampi of young and old mice and performed RNA-seq on the resulting synaptic mRNA population (Suppl. Figure 9A). Similar to the analysis of bulk tissue (See Figure 2.4), we detected comparatively very few differentially expressed transcripts in synaptosomes when analyzing the data from 3 vs 16-month-old mice (3 transcripts up-regulated and none down-regulated). For these transcripts there was no correlation to their methylation status (Suppl. Figure 9B). In sum, these data suggest that aberrant transport of transcripts from the soma to the synapses may not be the major consequence of m^{6}A hypomethylation in our disease models. Another process linked to m^{6}A RNA-methylation is mRNA translation (Wang et al. 2015). Thus, we performed polysome sequencing on young and old hippocampal tissue samples. Differential binding analysis identified 83 genes to be differentially translated in during aging (Suppl. Figure 9C, D) but there was no significant overlap to the transcripts affected by differential m^{6}A methylation (Suppl. Figure 9E).

Since m^{6}A RNA-methylation has been associated with local protein synthesis (LPS), the analysis of bulk tissue via polysome-seq might not be sensitive enough to detect the respective changes. In fact, m^{6}A was shown to control axonal protein synthesis in neurons of the peripheral nervous system (Jun Yu et al. 2018; Zhang et al. 2018; Leonetti et al. 2020). Because synaptically localized transcripts were significantly over-represented amongst the hypomethylated mRNAs detected in aging mouse and human AD brains, we hypothesized that the observed changes in m^{6}A levels may affect synaptic protein synthesis. To address this hurdle, we opted to use a primary neuron model to evaluate the effect of reduced m^{6}A levels on LPS at the synapse, using well-described group of synaptically-located, locally-synthesized, plasticity-associated mRNAs/proteins: CaMKII.

To globally reduce m^{6}A levels, the methyltransferase *Mettl3* was knocked down (KD) on primary hippocampal mouse neurons. The KD of *Mettl3* has been reported to be challenging in primary neurons, due to increased cell death (Merkurjev et al. 2018). Indeed, when using siRNAs targeting *Mettl3*, considerable cell death could be observed and although Mettl3 mRNA and protein levels were considerably reduced, m^{6}A levels remained greatly unaffected after 4 days post-transfection (Suppl. Figure 10A,B). To improve on this, we decided to employ another technology, namely LNA GAPmers, at lower doses and for longer treatment periods. Primary neurons transfected with an LNA GAPmer targeting *Mettl3* packaged in lipid nanoparticles (LNPs) at day *in vitro* (DIV) 7 showed an almost complete reduction in the *Mettl3* mRNA level (> 95%) when measured 3 days later (Figure 2.5A). However, a further 3 days of culture were necessary to sufficiently decrease the METTL3 protein and m^{6}A levels (Figure 2.5B-D).

Since there are no suitable high-throughput methods to assay LPS, we decided to evaluate its rate and location by studying the synthesis of CaMKII via a puromycin-based proximity ligation assay (puro-PLA). Puro-PLA depends on the use of the antibiotic puromycin for the labeling of nascent protein chains and N-terminal primary antibodies to detect sites of translation through proximity ligation (Figure 2.5E, S10E; tom Dieck et al. 2015). A cycloheximide pretreatment was also applied to improve the spatial localization of sites of protein synthesis (Hobson et al. 2020). Puromycin labeling and translational arrest were confirmed in treated neurons (Suppl. Figure 10D).

We selected CaMKII as candidate since its mRNA is known to be located at synapses (Mayford et al. 1996; Epple et al. 2021), and moreover CaMKII transcripts were

consistently hypomethylated in aging mice and AD patients. DIV 13 primary neurons that had been treated at DIV 7 with either a Mettl3 KD or Control GAPmer, treated with
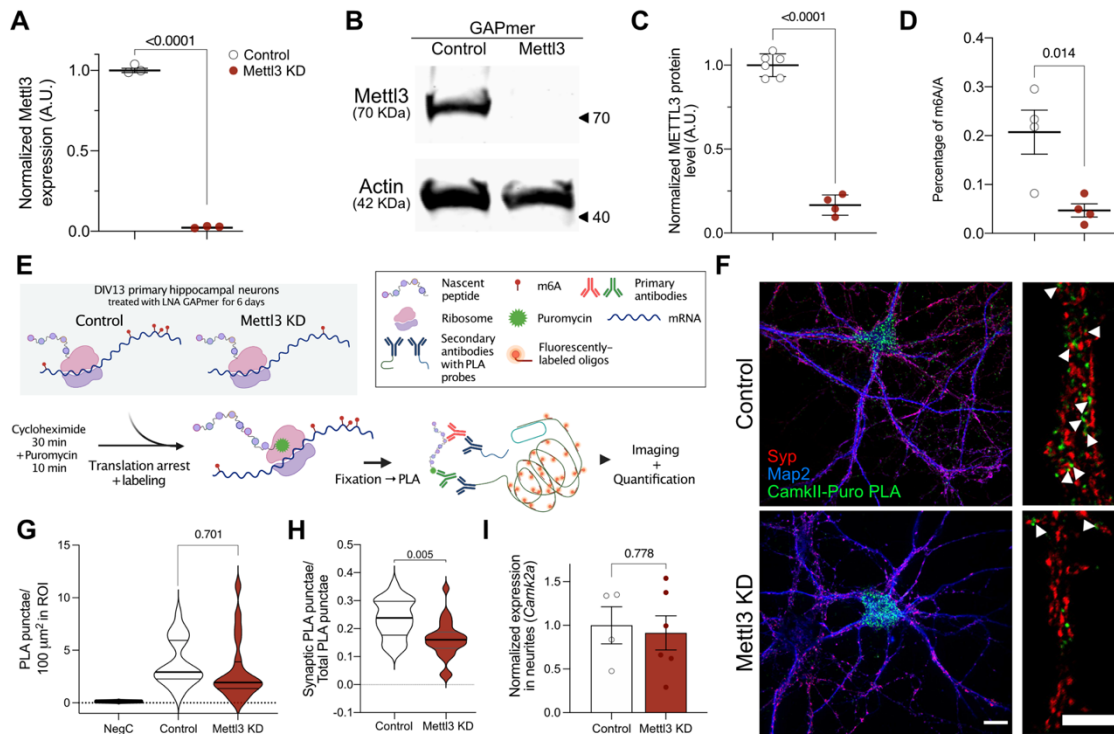

Figure 2.5. m6A changes influence the local protein synthesis of CaMKII. Validation of *in vitro* GAPmer-mediated knockdown of *Mettl3* at the A. transcript (qPCR), B.C. protein (Western blot), and D. m⁶A levels. Graphs in A, C and D display the mean +/- SEM of each condition. Each data point represents one independent replicate, statistical significance was determined by Student's t test. E. Schematic of the Puro-PLA labeling used to quantify the synthesis of CaMKII in primary neurons. F. Representative images of Control and Mettl3 KD primary hippocampal neurons displaying the localization of CaMKII-PLA punctae. CaMKII-PLA signal in green, Synaptophysin in red, Map2 in blue. Zoomed-in images show a large magnification image of a representative dendrite. Arrowheads show sites of CaMKII LPS in the close vicinity of synapses. G. Total number of detected PLA punctae in treated neurons. Negative control (NegC) was not treated with puromycin but was processed for PLA. H. Synaptically-located CaMKII-PLA punctae in control and Mettl3 KD-treated neurons. Graphs in G and H show the mean of 3 independent experiments, for each experiment 7-13 neurons were imaged and analyzed, individual data points were used to generate the violin plot. Quartiles are marked by gray lines. I. Normalized *Camk2a* mRNA levels in the synaptic compartments of treated and control primary cultures in microfluidic chambers. Dots in I represent individual independent replicate cultures. Statistical significance determined by Student's t test. For all panels, p values are displayed above the corresponding comparisons.

10 mins of puromycin and further processed for puro-PLA using an antibody that detects the N-terminal of CaMKII α, β and γ (Figure 2.5E,F). Puro-PLA-treated neurons were imaged by confocal microscope and the PLA punctae automatically detected and quantified, the synaptic marker Synaptophysin (SYP) was used to determine the synaptic localization of detected punctae (Figure 2.5F). Neurons with reduced levels of m^{6}A (Mettl3 KD) showed a reduction of PLA punctae in dendritic projections (Figure 2.5F, S11A). Quantitative analysis revealed that the total number of PLA punctae in the whole neuron was not significantly reduced (Figure 2.5H, S11B). The number of detected SYP+ synapses was also not significantly changed in response to decreased m^{6}A levels (Suppl. Figure 11C,D). However, when looking at the proportion of CaMKII-PLA punctae detected in vicinity to SYP+ synaptic compartments, the *Mettl3* KD-treated neurons showed significantly decreased numbers (Figure 2.5F,H).

To rule out the possibility of these differences being a consequence of decreased mRNA transport to synaptic compartments, we used a previously established culture system using custom-made microfluidic chambers to isolate synaptically located transcripts (Suppl. Figure 2E; Epple et al. 2021). Mettl3 KD treatment on the somas of the cultured neurons showed no significant effect on the amount of mRNA located in synaptic compartments for *Camk2a*, *Camk2b* and *Camk2g* (Figure 2.5I, S11E).

These results support the idea of a common downstream mechanism mediated by m^{6}A changes in aging and neurodegeneration that could have consequences for the regulation of synaptic function, plasticity and memory, through the regulation of the synaptic LPS of plasticity-related mRNAs.

Discussion

In this study, we aimed to further disentangle the role of m^{6}A function in the adult brain and analyzed the m^{6}A epitranscriptome in mice and humans. We found that 40–44% of the detected transcripts in the different hippocampal subregions in mice carried m^{6}A marks. These data are in line with recent studies in which different brain regions or bulk hippocampal tissue had been analyzed for m^{6}A RNA methylation (Engel et al. 2018; Jun'e Liu et al. 2020; Shafik et al. 2021). m^{6}A-labeled mRNAs in the adult hippocampus were strongly enriched for genes associated with the regulation of synaptic function and plasticity, mainly in postsynaptic compartments. This enrichment holds true for all hippocampal subregions, with a very considerable overlap between the populations of labeled transcripts in the CA1, CA3 and DG subregions.

We also compared the methylated transcripts between the ACC and the hippocampus, two more distantly related brain regions at the structural and functional level, and observed that 61% of the m^{6}A transcripts could be detected in both brain regions. These results go in accordance with previously published data that reported a considerable amount of tissue specificity in the populations of transcripts that are labeled by m^{6}A (Chang et al. 2017; Martinez De La Cruz et al. 2021; Jun'e Liu et al. 2020). While noticeable differences in the m^{6}A landscape were detected between brain subregions, the location of m^{6}A was mostly identical within all hippocampal regions and the ACC. The commonly m^{6}A methylated transcripts were mainly involved in synaptic signaling and structure, suggesting the general importance of certain m^{6}A-dependent regulatory networks in synaptic plasticity. Moreover, the m^{6}A transcripts commonly detected across brain regions exhibited a large over-representation of mRNAs that are localized to synapses, which is in line with data suggesting that m^{6}A transcripts are specifically enriched in synaptosomes (Merkurjev et al. 2018). The m^{6}A transcripts specific to the different hippocampal subregions were linked to more general cellular processes such as the negative regulation of protein complex assembly in the CA1 region, processes related to development and RNA processing in the DG and for example protein transport in the CA3 region. When comparing the m^{6}A landscape from the mouse anterior cingulate and human cingulate cortex, we observed that 56% of the methylated transcripts found in humans, were also detected in mice. This is remarkable, when considering that a similar degree of conservation is observed when the anterior cingulate cortex is compared to the hippocampus within the same species (61% in

mice). These data are in agreement with a previous study that found 62% overlap between m^{6}A transcripts of the mouse and human cerebellum (Jun'e Liu et al. 2020). The commonly methylated transcripts detected in the mouse and human cortex were linked to the regulation of synaptic function and plasticity and showed a strong overrepresentation of transcripts found at synapses. Interestingly, the m^{6}A transcripts specific to mice were enriched for GO-terms related to synaptic plasticity, while the methylated transcripts specific to the human cingulate cortex were also strongly enriched for GO-terms linked to RNA processing and gene expression control. These data may suggest that the orchestration of synaptic plasticity is an evolutionary conserved mechanism in mammals, while a role of m^{6}A RNA-methylation gained importance in the human brain. However, care has to be taken when comparing data from cortical regions in mice and humans.

To study the epitranscriptome in the context of cognitive dysfunction we employed aged mice and human AD patients. During aging, the onset of mild cognitive impairment represents a hallmark of the transition between normal aging and pathology (Belblidia et al. 2018; Wilson et al. 2010; Studart and Nitrini 2016) and previous data demonstrated that a significant memory impairment can first be detected when comparing mice at 3 vs. 16 months of age (Singhal et al. 2020; Belblidia et al. 2018). In addition to the fact that this animal model does not dependent on the expression of a transgene, previous studies showed that only minor changes in gene expression are observed in the hippocampus and cortex when comparing 3 to 16-month-old mice (Peleg et al. 2010), making these animals a suitable model to study changes in m^{6}A transcripts that do not affect RNA stability. We observed a massive hypomethylation across multiple transcripts in all investigated brain regions, while comparatively mild change in gene expression were observed. This is in agreement with data from other postmitotic tissues, namely the heart, where during the pathogenesis of heart failure massive changes in m^{6}A hypomethylation precede change in gene expression (Berulava et al. 2020). Amongst the different brain regions affected by aging, there was a noticeable tissue specificity, as many region-specific changes could be detected. These results show that different brain regions undergo distinct changes during aging, but the overall pathways affected by m^{6}A changes remain similar and were linked to GO-pathways such as cognition and synapse organization. These data suggest that loss of m^{6}A RNA-methylation is an early event in the aging brain that coincides with the onset of memory impairment. This view is supported by previous data showing that a KD of the m^{6}A

demethylase FTO in the prefrontal cortex of mice results in an improved consolidation of fear memories (Widagdo et al. 2016). Similarly, loss of the m^{6}A reader YTHDF1 which has been linked to enhanced translation, leads to impairment of hippocampal LTP and memory formation in mice (Shi et al. 2018). While we compared 3 vs 16 months-old mice, another recent study analyzed m^{6}A levels in the brains of 2 week, 1, 1.5, 6.5 and 13 months-old mice. The authors observe comparatively milder changes than in our study and the affected transcripts were mainly characterized by altered m^{6}A levels within the UTR that increased from 1.5 to 13 month of age (Shafik et al. 2021). Since animals at 13 months of age do not exhibit detectable memory impairment (Islam et al. 2021), these changes may represent compensatory mechanisms. In line with this interpretation, the affected pathways were linked for example to cellular stress signaling. The same study also analyzed m^{6}A levels in the brains of 6 months old 5xFAD mice, a mouse model for amyloid deposition as it is observed in AD (Shafik et al. 2021). Here, decreased m^{6}A levels were observed when comparing wild type to 5xFAD mice and the affected transcripts were linked to GO-terms such as synaptic transmission. On the basis of previous data showing that 5xFAD mice display memory impairment at 6 months of age (Kimura and Ohno 2009) these data are in agreement with our observations. Nevertheless, more research is needed to elucidate the dynamics of m^{6}A marks across the transcriptome of the aging and diseased brain.

Additional support for the hypothesis that cognitive decline is accompanied by m^{6}A hypomethylation of transcripts important for synaptic function stems from our analysis of postmortem human brain samples from AD patients. The AD brains showed significant changes in methylation, with the majority of transcripts being hypomethylated. When compared to the hypomethylated peaks in the aging mouse ACC, striking similarities could be found for the affected transcripts and in the corresponding pathways in both the aging mouse brain and the human AD brain. Among them, the regulation of synaptic plasticity, particularly long-term potentiation, as well as multiple neurodegeneration-associated pathways were strongly affected.

The finding that AD is associated with m^{6}A hypomethylation is in agreement with a recent study in which a strong decrease in the levels of the main m^{6}A methyltransferase METTL3 was observed in the hippocampus of AD patients at the mRNA and protein level (He Huang et al. 2020, 3). Reduced expression of m^{6}A writers could indeed be one mechanism to explain lower m^{6}A levels in AD. In line with this view, knock-down of

Mettl3 exacerbated Tau pathology in a Drosophila model for AD (Shafik et al. 2021). It should be mentioned that the role of RNA-methylation in neurodegenerative diseases may be more complex. For example, a recent study observed increased m^{6}A levels in a mouse model for Tau pathology and in the brains of human AD patients (Jiang et al. 2021). However, these data are based on a semi-quantitative analysis m^{6}A immunostaining within the soma, which is difficult to compare to sequencing-based approaches. Similarly, another recent study reported an increase of bulk m^{6}A and METTL3 levels, while FTO protein levels were decreased in the hippocampus and cortex of 9-month-old APP/PS1 mice (Han et al. 2020). The fact that the analysis of sequencing-based vs. bulk analysis of m^{6}A levels currently contradict, may indicate that there is an RNA-species which undergoes hypermethylation in neurodegenerative diseases, that is not captured by the current sequencing approaches but dominates the analysis of bulk m^{6}A levels. For example, recent evidence hints to an important role of N^{6}A-methylation of pre- and mature microRNAs (Alarcón et al. 2015; Erson-Bensan and Begik 2017) and it will be interesting to study microRNA methylation in brain diseases. Moreover, it will be important to study m^{6}A levels in neuronal subcompartments.

In fact, our data consistently show that m^{6}A hypo-methylation occurs often within synaptically located plasticity-associated transcripts, pointing to a role of this modification in the local translation of synaptic transcripts, a well-known phenomenon that ensures the supply of key proteins necessary for synaptic function and plasticity in response to stimuli (Kang and Schuman 1996; Richter 2001; Holt, Martin, and Schuman 2019) . The function of m^{6}A as a regulator of LPS has been shown in the axons of dorsal ganglia neurons (Jun Yu et al. 2018) and since then has been theorized in other contexts but so far, no direct experimental evidence has been put forward to prove this link.

Our results show that a reduction in m^{6}A caused by a decrease in *Mettl3* expression, akin to the reductions observed during aging and AD, significantly impact the rate of protein synthesis of the plasticity regulator CaMKII in or in the vicinity of synaptic compartments, away from the soma.

Considering that we found *CaMKII* transcripts to undergo m^{6}A hypomethylation in both aging and AD and that *CaMKII* was also among the list of transcripts that underwent hypomethylation in the cortex of 5xFAD mice (Shafik et al. 2021), suggest a m^{6}A-depedent mechanisms that orchestrates synaptic proteins synthesis and contributes to impaired synaptic plasticity when de-regulated.

Future research is needed to elucidate the precise mechanism by which m^{6}A levels control the synaptic translation of transcripts. In this context it is, however, noteworthy that the demethylase FTO was shown to locate at the synapse and that its levels decrease during learning (Walters et al. 2017). At the same time the m^{6}A reader YTHDF1 is also located in synaptic compartments and its protein levels significantly increase following fear conditioning in the hippocampus (Shi et al. 2018). Since YTHDF1 was shown to promote translation (Wang et al. 2015; Shi et al. 2018), although these data do not stem from synapses, this might be one mechanism by which reduced m^{6}A levels affect synaptic protein synthesis. Furthermore, the knockdowns of *Ythdf1* negatively affects spine formation, long-term potentiation, and learning in a hippocampus-dependent manner (Zhang et al. 2018, 3; Shi et al. 2018). More recently, the m^{6}A reader YTHDF3 as well as the eraser ALKBH5 have also been linked to the regulation of m^{6}A at the synapse, further increasing the possibilities for regulation in such compartments (Martinez De La Cruz et al. 2021). This is not to say that other proteins, could very well be involved in regulating synaptic mRNA translation directly or indirectly, via processes like degradation, transport or phase separation (Deng et al. 2021; Jiang et al. 2021; Merkurjev et al. 2018).

In conclusion, our data provide an important resource to the field and further elucidate the function of m^{6}A in regulating learning and memory in the healthy and diseases brain by showing that m^{6}A controls synaptic LPS and its relationship with decreased methylation of synaptic genes during aging and neurodegeneration.

Supplementary tables and figures

Antibody	Company	Catalog	Species	Dilution	Application
m6A	Synaptic Systems	202 003	Rabbit	1 µg/µl	meRIP
METTL3	Abclonal	A8370	Rabbit	1:1,000	WB
ACTIN	Novus	NB600-535	Mouse	1:5,000	WB
SYNAPTOPHYSIN	Synaptic Systems	101 004	Guinea pig	1:2,000	IF
MAP2	Biosensis	C-1382-50	Chicken	1:2,000	IF
Puromycin	Millipore	MABE343	Mouse	1:300, 1:10,000	PLA, WB
CaMKII	Abcam	ab52476	Rabbit	1:200	PLA
PSD95	Millipore	MABN68	Mouse	1:1,000	Dot blot
SYNAPTOBREVIN	Synaptic Systems	104 211	Mouse	1:1,000	Dot blot
Alexa 594 anti-chicken IgY	ThermoFischer	A-11042	Goat	1:400	IF
Alexa 488 anti-guinea pig IgG	ThermoFischer	A-11073	Goat	1:400	IF
IRDye 800CW anti-mouse	LI-COR	926-32210	Goat	1:5,000	WB, Dot blot
IRDye 680RD anti-rabbit	LI-COR	926-68070	Goat	1:5,000	WB, Dot blot

Supplementary table 2.1. Antibodies used and concentrations

| Primer	Fwd sequence	Rev sequence
Mettl3	GGACACGTGGAGCTCTATCC	GCCGCTTCTGGGTTCCTTA
Camk2a	ACGCATGCCTTTTTACAGCC	CCCAACCCATCCGACTCTTC
Camk2b	AGGGTGTTTGTCCACTCAGC	TATGGACCTGCATTGCCCAG
Camk2g	TGCTGACATTAGCCCCAGAAG	AGAGCTCTTTGAGACCCATAGC
Slit1	GGAGGAAGCTCACCTTCGAG	CCACCTCCTCAGCAAACGAA
Gapdh	GACACTGAGCAAGAGAGGC	GATGGAAATTGTGAGGGAGAT
18S	CTTAGAGGGACAAGTGGCG	ACGCTGAGCCAGTCAGTGTA

*Supplementary table 2.2. qPCR primers used and sequences*
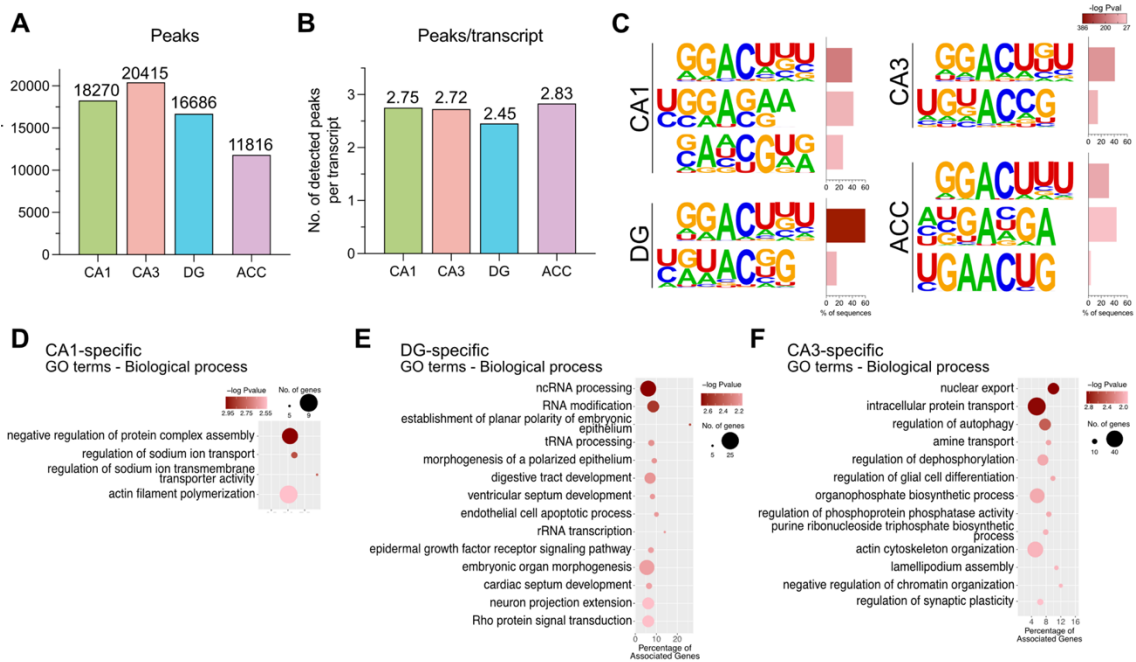
Supplementary Figure 2.1. Methylation in hippocampal subregions. A. Detected m^{6}A peaks in hippocampal subregions and the ACC in the adult mouse brain. B. Average number of m^{6}A peaks detected per methylated transcript. Exact values are displayed above the corresponding bar. C. Enriched motifs corresponding to the DRACH consensus sequence among the top overrepresented motifs in m^{6}A peaks. D-F. Enriched GO terms Biological process for CA1- (D), DG- (E) and CA3-specific (F) methylated transcripts.


Epple, et. al. 2021
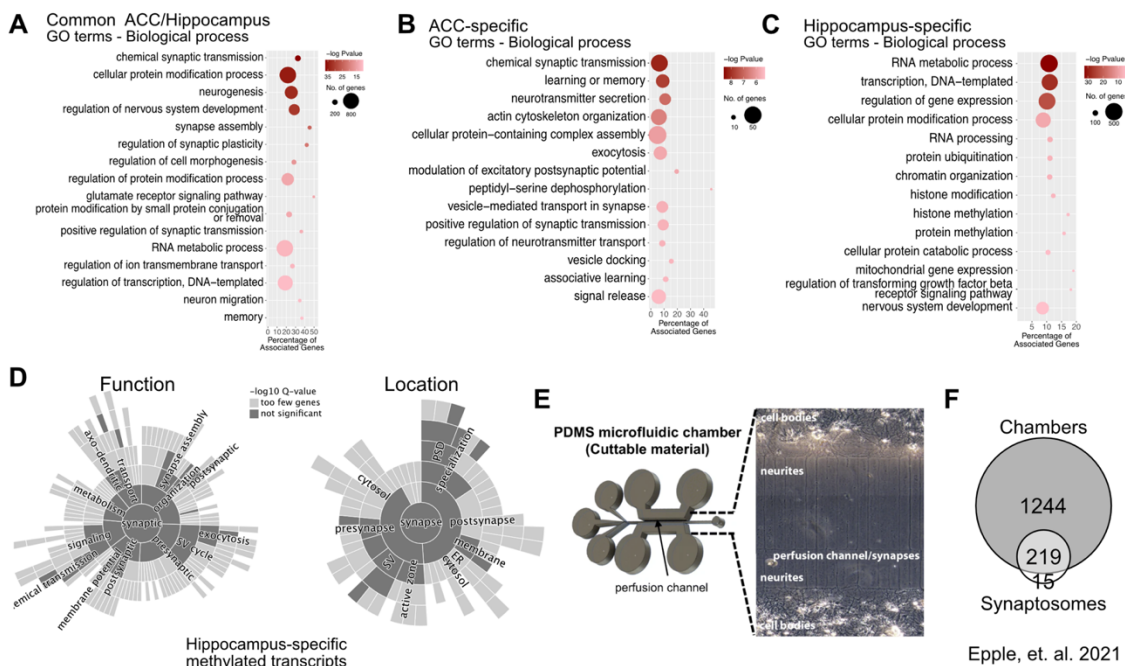
Supplementary Figure 2.2. Synaptic m6A in the hippocampus and ACC. A-C. Enriched GO terms biological process for methylated transcripts common between the hippocampus and the ACC (A), specific for the ACC (B) and specific for the hippocampus (C). D. Synaptic GO showing the lack of significant enrichment for synaptically annotated Function or Location GO terms in hippocampus-specific methylated transcripts. E. Diagram showing the microfluidic chambers used by Epple, et. al (2021) to isolate synaptically located RNAs. F. Summary of the synaptic transcriptome as described by Epple, et. al.
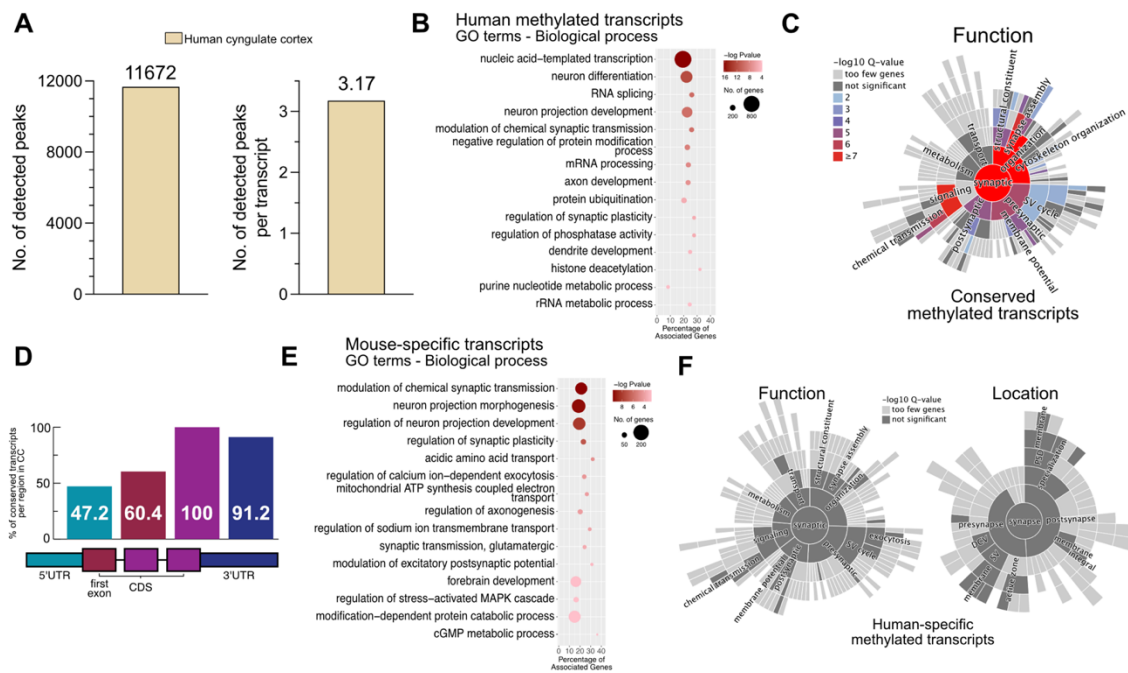

Supplementary Figure 2.3. Conserved epitranscriptome in human and mouse. A. Detected m^{6}A peaks in the human CC and the average number of peaks per methylated transcript. Exact number displayed above the corresponding bar. B. Enriched GO terms Biological process for all methylated transcripts in the human CC. C. Synaptic function annotated GO terms enriched in methylated transcripts conserved in mouse/human. D. Regional conservation of methylation sites in mouse/human. Bars show the percentage of peaks annotated for a given region in the human CC that have a corresponding peak annotated to the same region in the mouse homolog. Only broad regions were considered: 5' UTR, first exon, CDS and 3' UTR. E. Enriched GO terms Biological process for mouse specific methylated transcripts from the ACC. F. Synaptic GO terms for function and localization showing the lack of significant enrichment in these categories of human-specific methylated transcripts.
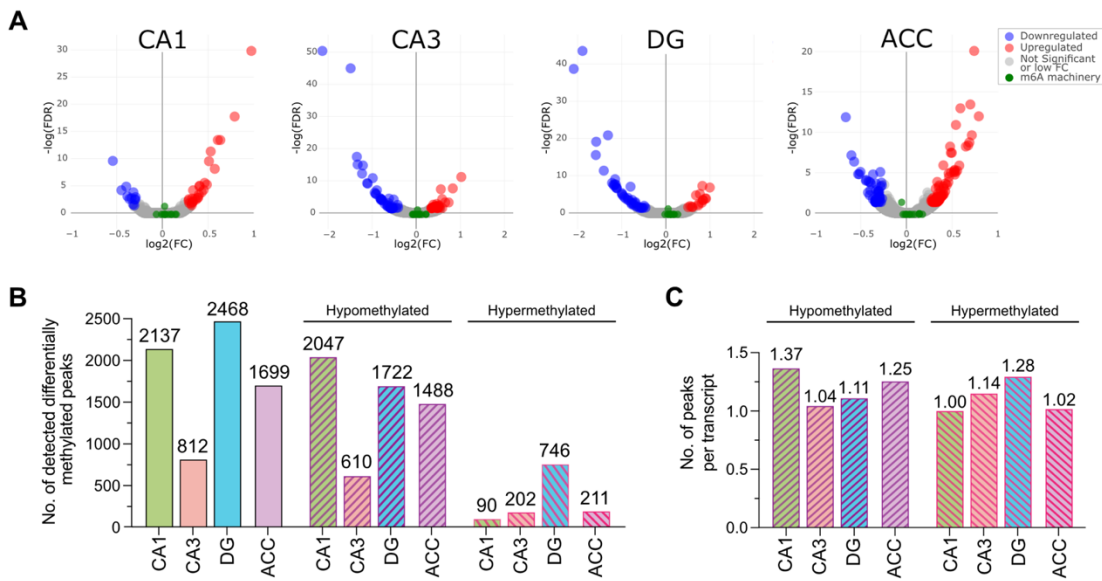
Supplementary Figure 2.4. Differential expression and methylation in aging. A. Volcano plots displaying the changes in gene expression across all brain subregions in aging. Cutoffs for significance are FC > 1.2 and FDR ≤ 0.05. Highlighted in green are the known m^6A writers, readers and erasers, showing that no m^6A associated protein is differentially expressed in the aged brain. B. Detected differentially methylated peaks (FC > 1.2, FDR ≤ 0.05) in all brain subregions and how many of them are hypo- and hypermethylated. C. Number of differentially methylated m^6A peaks per differentially methylated transcript. Numbers above the bars display the exact number of peaks.
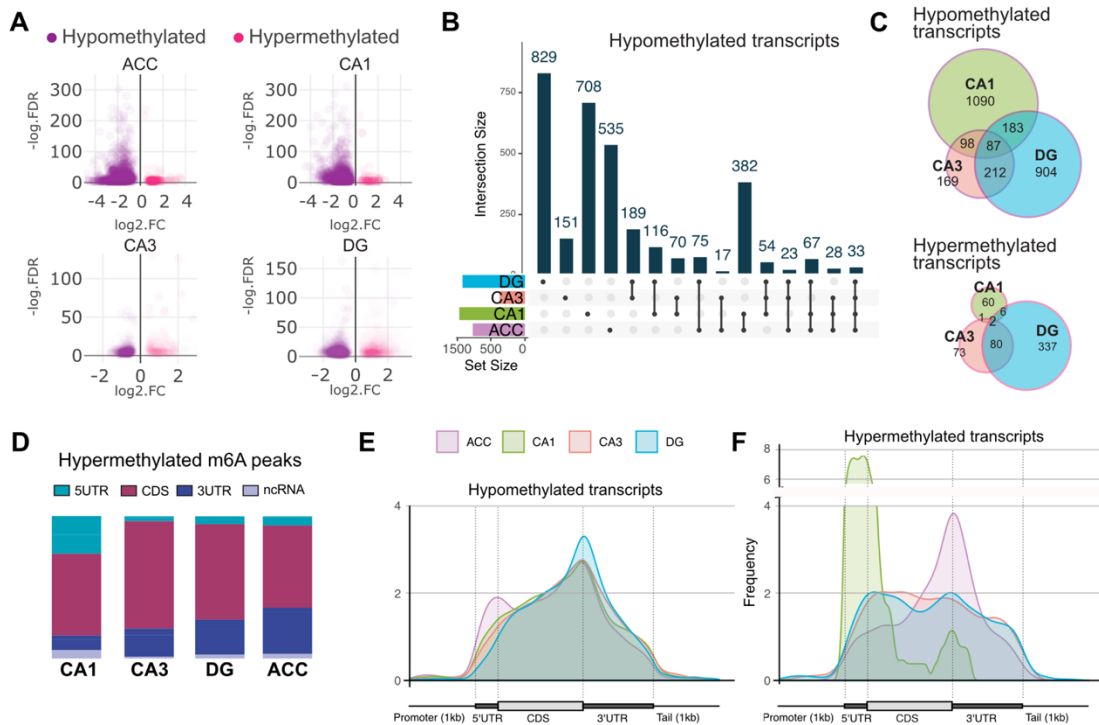
Supplementary Figure 2.5. Differential methylation in the aged hippocampus. A. Volcano plots showing the magnitude of changes in m^6A for every differentially methylated peak in all brain subregions. B. Intersect graph showing the overlap between hypomethylated transcripts across all brain subregions, as well as the region-specific hypomethylated transcripts. Dots and lines denote the displayed comparison and bars show the number of transcripts contained in the overlap. C. Overlap of hypomethylated and hypermethylated transcripts across hippocampal subregions only. D. Distribution of hypermethylated peaks along RNAs in all brain subregions. E, F. Guitar plots showing the frequency of hypomethylated (E) and hypermethylated (F) peaks along mRNA features in all brain subregions. ACC - anterior cingulate cortex, DG - dentate gyrus, 5UTR - 5' untranslated region, 3UTR - 3' untranslated region, CDS - coding sequence, ncRNA - non-coding RNA
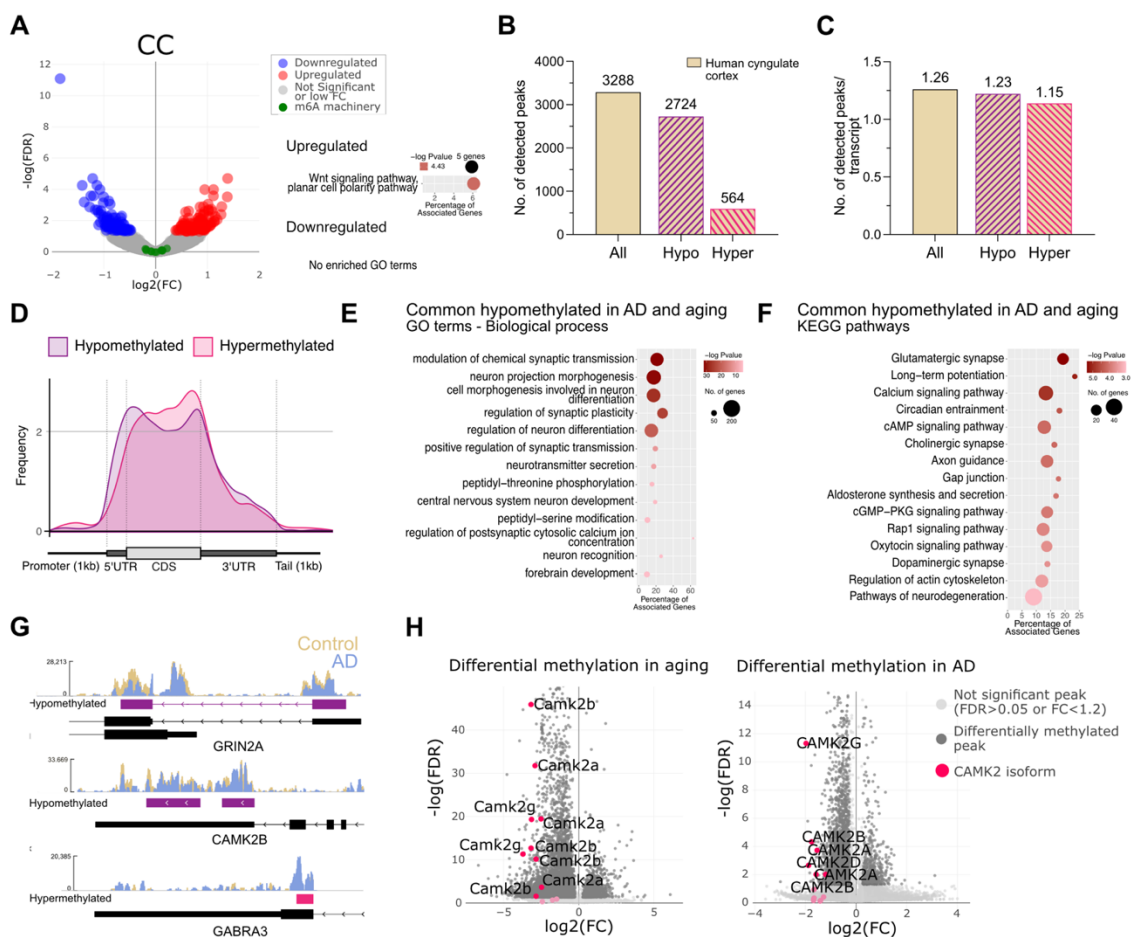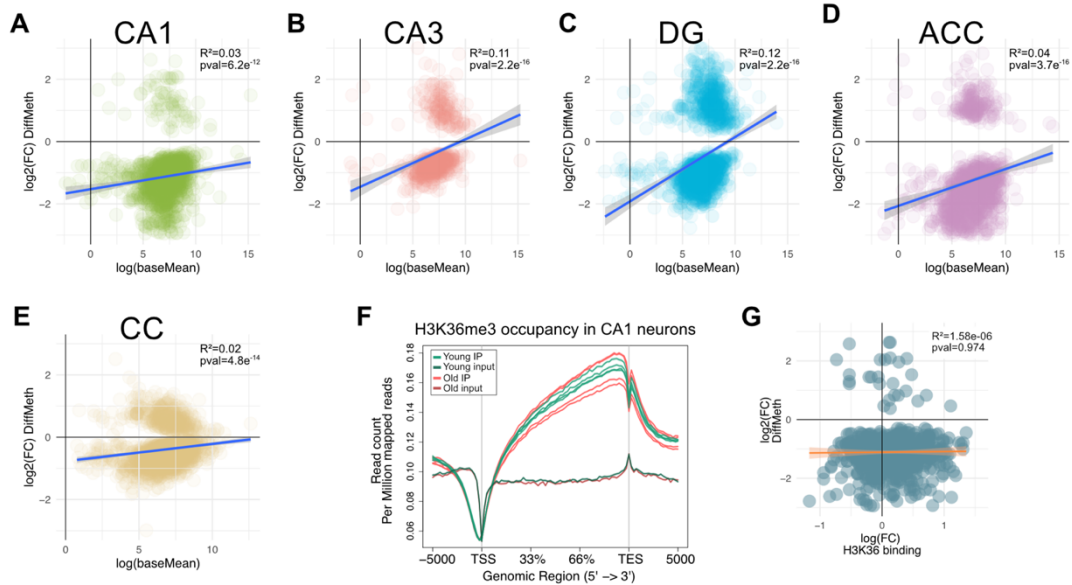

Supplementary Figure 2.6. Differential expression and methylation in AD. A. volcano plot displaying the changes in gene expression in the human CC in AD (FC > 1.2, FDR ≤ 0.05). Highlighted in green are the known m^6A writers, readers and erasers, showing their unaltered expression. Significantly enriched GO term Biological process for upregulated genes. Downregulated genes resulted in no enriched GO terms. B. Total number of differentially methylated m^6A peaks in AD compared (Continued in next page)

(Cont.) NDC samples, as well as hypo- and hypermethylated peaks. C. Average detected differentially methylated m⁶A peaks per differentially methylated transcript in AD. D. Guitar plot showing the distribution frequency of hypo- and hypermethylated peaks along mRNA features. E, F. Enriched GO terms Biological process (E) and enriched KEGG pathways (F) for commonly hypomethylated transcripts from all peaks in AD and the aged ACC in mouse (converted to their corresponding human homolog). G. Representative genome browser tracks of detected hypomethylated (*GRIN2A* and *CAMK2B,* in purple) and hypermethylated (*GABRA3*, in pink) regions in AD. H. Volcano plots showing the differentially methylated peaks in the aged ACC and in AD
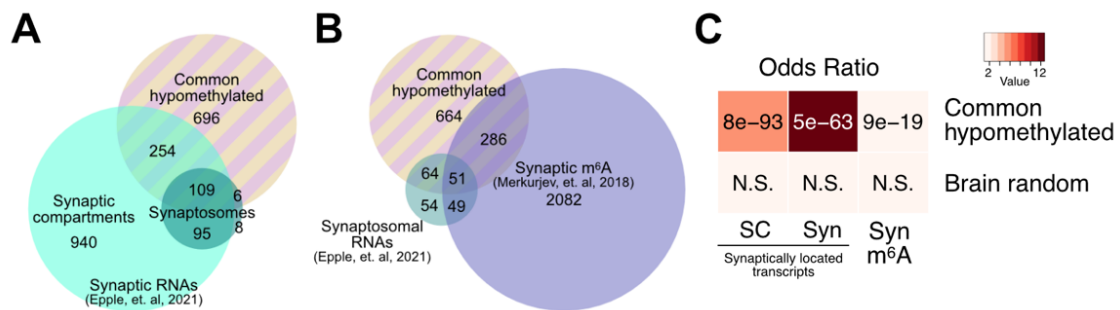
Supplementary Figure 2.7. Synaptic m6A in aging and AD. A. Overlap between commonly hypomethylated transcripts in the aged ACC and the AD CC and synaptically located RNAs, from Epple, et. al. 2021. B. Overlap between commonly hypomethylated transcripts, synaptosomal RNAs from Epple, et. al, 2021 as well as synaptic m⁶A transcripts from Merkurjev, et. al, 2018. C. Enrichment (odds ratio) and significance of the overlaps displayed in A and B. Color represents odds ratio of the comparison, p value is visible in the corresponding square. Brain random corresponds to a list of 2000 randomly selected brain-expressed transcripts, included as control. N.S.= not significant (p value ≥ 0.05). SC= RNAs detected in the synaptic compartments of microfluidic chambers; Syn= RNAs detected in synaptosomes, Syn m⁶A – synaptic m⁶A mRNAs.

Supplementary Figure 2.8. Correlation between methylation, expression and H3K36me3. Scatter plots showing the correlation between observed changes in methylation and expression levels of differentially methylated transcripts in the mouse A. CA1, B. CA3, C. DG, and D. ACC, as well as the E. human CC. F. Occupancy of H3K36me3 in FACS sorted CA1 neurons determined by ChIP. Curves show normalized reads mapped to the shown genomic regions in immunoprecipitated (IP) and input samples from young and old mice. G. Scatter plot displaying changes in H3K36me3 occupancy and m^6A changes in all differentially methylated transcripts in the aged CA1. In all scatter plots, line represents the best model fit for the data points, CI is also displayed. Reads in CPM. TSS = transcription start site, TES = transcription end site.
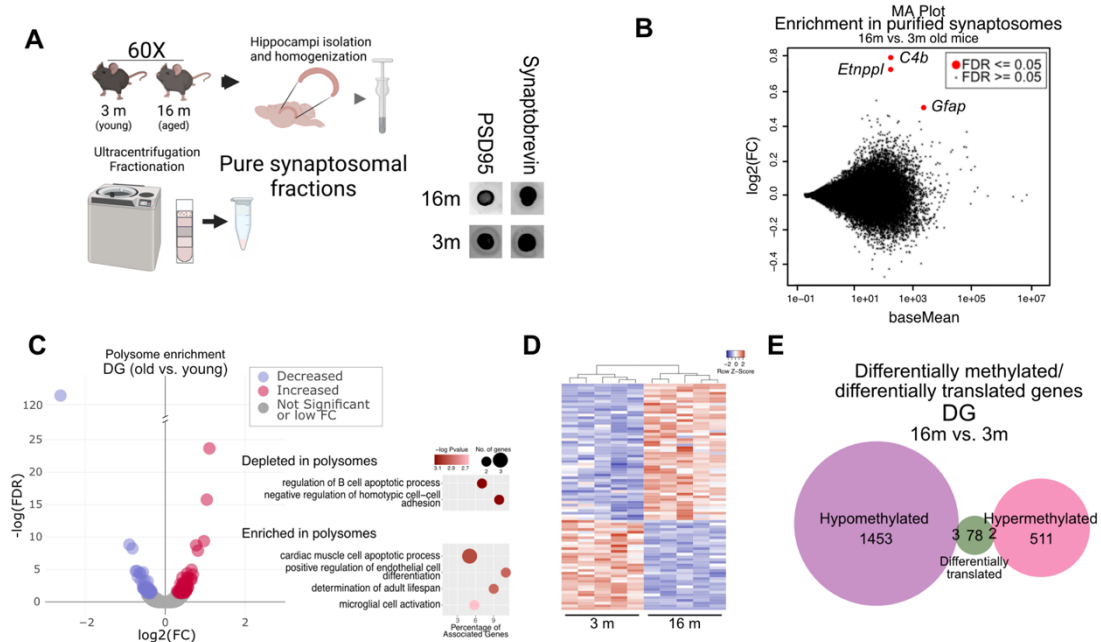
Supplementary Figure 2.9. Synaptosomal RNA and polysome sequencing in aging.
A. Diagram for synaptosomal fraction purification from young and old mice.
Synaptosome purity was confirmed by dot blot using the synaptic markers PSD95 and
synaptobrevin. B. MA Plot showing differential enrichment of RNAs in the old vs. young
hippocampus. Only three genes were significantly differentially located. C. Volcano plot
displaying the results of the differential translation analysis performed on polysomes
isolated from the DG of old and young mice. GO terms Biological process
overrepresented in mRNAs enriched and depleted in polysomal fractions in the aged DG
are shown. D. Heatmap displaying the differentially translated mRNAs across replicate
polysome samples. E. Venn diagram of differentially translated and differentially
methylated mRNAs in the aged DG showing little overlap between these populations.
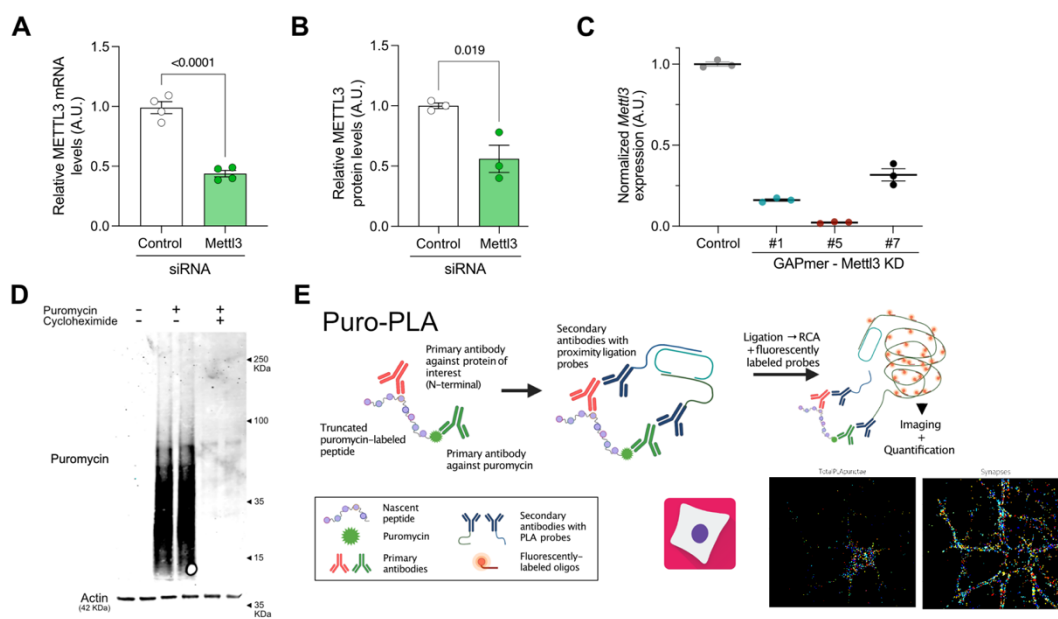
Supplementary Figure 2.10. *Mettl3* **KD and Puro-PLA validation.** A, B. *Mettl3* knock-
down using siRNAs. Decrease in Mettl3 at the mRNA (A) and protein (B) levels after 48
hours incubation. C. Validation of LNA GAPmer-dependent knock-down of Mettl3 in
primary neurons. Shown are the mRNA levels of Mettl3 after 48 hours treatment with
control or Mettl3-targeting GAPmers (1,5 and 7). GAPmer #5 was used moving forward.
Graphs in A-C display the mean +/- SEM of each condition. Each data point represents
one independent replicate, statistical significance was determined by Student's t test. D.
Validation of puromycin incorporation into nascent protein chains. Western blot using a
puromycin antibody showing the labeling of proteins and the function of the
cycloheximide pretreatment to cause translational arrest. E. Scheme of the Puro-PLA
process. Shown are representative images from the automated Puro-PLA and synapse
detection pipeline using Cell Profiler
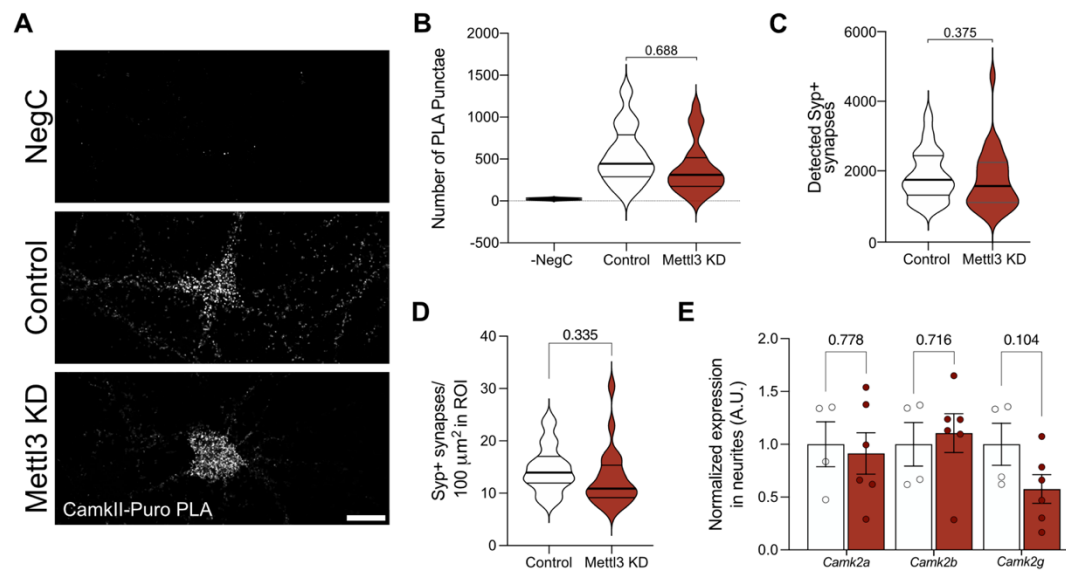
Supplementary Figure 2.11. CaMKII-PLA. A. Representative confocal images from untreated (without puromycin treatment, NegC), Control and Mettl3 KD CaMKII-Puro PLA punctae. B. Total number of detected CaMKII-Puro PLA punctae in Puromycin-, Control and Mettl3 KD neurons. C, D. Total number (C) and area normalized number (D) of synaptophysin+ (SYP+) synapses in Control and Mettl3 KD neurons. Graphs in B, C and D show the mean of 3 independent experiments, for each experiment 7-13 neurons were imaged and analyzed, individual data points were used to generate the violin plot. Quartiles are marked by gray lines. Statistical significance was determined by Student's t test on the mean values of each independent replicate. E. mRNA levels, determined by qPCR, of different CaMKII isoforms in the synaptic compartments of microfluidic chambers containing neurons treated with Control or Mettl3 GAPmers. Graphs display the mean +/- SEM of each condition. Each data point represents one independent replicate, statistical significance was determined by Student's t test

References

Alarcón, Claudio R., Hyeseung Lee, Hani Goodarzi, Nils Halberg, and Sohail F. Tavazoie. 2015. "N6-Methyladenosine Marks Primary MicroRNAs for Processing." *Nature* 519 (7544): 482–85. https://doi.org/10.1038/nature14281.

Belblidia, Hassina, Marianne Leger, Abdelouadoud Abdelmalek, Anne Quiedeville, Floriane Calocer, Michel Boulouard, Christelle Jozet-Alves, Thomas Freret, and Pascale Schumann-Bard. 2018. "Characterizing Age-Related Decline of Recognition Memory and Brain Activation Profile in Mice." *Experimental Gerontology* 106 (June): 222–31. https://doi.org/10.1016/j.exger.2018.03.006.

Berulava, Tea, Eric Buchholz, Vakhtang Elerdashvili, Tonatiuh Pena, Md Rezaul Islam, Dawid Lbik, Belal A. Mohamed, et al. 2020. "Changes in M6A RNA Methylation Contribute to Heart Failure Progression by Modulating Translation." *European Journal of Heart Failure* 22 (1): 54–66. https://doi.org/10.1002/ejhf.1672.

Bindea, Gabriela, Bernhard Mlecnik, Hubert Hackl, Pornpimol Charoentong, Marie Tosolini, Amos Kirilovsky, Wolf-Herman Fridman, Franck Pagès, Zlatko Trajanoski, and Jérôme Galon. 2009. "ClueGO: A Cytoscape Plug-in to Decipher Functionally Grouped Gene Ontology and Pathway Annotation Networks." *Bioinformatics* 25 (8): 1091–93. https://doi.org/10.1093/bioinformatics/btp101.

Bird, Chris M., and Neil Burgess. 2008. "The Hippocampus and Memory: Insights from Spatial Processing." *Nature Reviews Neuroscience* 9 (3): 182–94. https://doi.org/10.1038/nrn2335.

Boyken, Janina, Mads Grønborg, Dietmar Riedel, Henning Urlaub, Reinhard Jahn, and John Jia En Chua. 2013. "Molecular Profiling of Synaptic Vesicle Docking Sites Reveals Novel Proteins but Few Differences between Glutamatergic and GABAergic Synapses." *Neuron* 78 (2): 285–97. https://doi.org/10.1016/j.neuron.2013.02.027.

Cavalcante, Raymond G., and Maureen A. Sartor. 2017. "Annotatr: Genomic Regions in Context." *Bioinformatics (Oxford, England)* 33 (15): 2381–83. https://doi.org/10.1093/bioinformatics/btx183.

Chang, Mengqi, Hongyi Lv, Weilong Zhang, Chunhui Ma, Xue He, Shunli Zhao, Zhi-Wei Zhang, et al. 2017. "Region-Specific RNA M6A Methylation Represents a New Layer of Control in the Gene Regulatory Network in the Mouse Brain." *Open Biology* 7 (9): 170166. https://doi.org/10.1098/rsob.170166.

Chassé, Héloïse, Sandrine Boulben, Vlad Costache, Patrick Cormier, and Julia Morales. 2017. "Analysis of Translation Using Polysome Profiling." *Nucleic Acids Research* 45 (3): e15. https://doi.org/10.1093/nar/gkw907.

Cui, Xiaodong, Jia Meng, Shaowu Zhang, Yidong Chen, and Yufei Huang. 2016. "A Novel Algorithm for Calling MRNA M6A Peaks by Modeling Biological Variances in MeRIP-Seq Data." *Bioinformatics* 32 (12): i378–85. https://doi.org/10.1093/bioinformatics/btw281.

Cui, Xiaodong, Zhen Wei, Lin Zhang, Hui Liu, Lei Sun, Shao-Wu Zhang, Yufei Huang, and Jia Meng. 2016. "Guitar: An R/Bioconductor Package for Gene Annotation Guided Transcriptomic Analysis of RNA-Related Genomic Features." *BioMed Research International* 2016: 8367534. https://doi.org/10.1155/2016/8367534.

Deng, Yanyao, Hongwei Zhu, Le Xiao, Chao Liu, Ya-Lin Liu, and Wenzhe Gao. 2021. "Identification of the Function and Mechanism of M6A Reader IGF2BP2 in Alzheimer's Disease." *Aging* 13 (21): 24086–100. https://doi.org/10.18632/aging.203652.

Desrosiers, R., K. Friderici, and F. Rottman. 1974. "Identification of Methylated Nucleosides in Messenger RNA from Novikoff Hepatoma Cells." *Proceedings of the National Academy of Sciences of the United States of America* 71 (10): 3971–75. https://doi.org/10.1073/pnas.71.10.3971.

Dieck, Susanne tom, Lisa Kochen, Cyril Hanus, Maximilian Heumüller, Ina Bartnik, Belquis Nassim-Assir, Katrin Merk, et al. 2015. "Direct Visualization of Newly Synthesized Target Proteins in Situ." *Nature Methods* 12 (5): 411–14. https://doi.org/10.1038/nmeth.3319.

Dobin, Alexander, Carrie A. Davis, Felix Schlesinger, Jorg Drenkow, Chris Zaleski, Sonali Jha, Philippe Batut, Mark Chaisson, and Thomas R. Gingeras. 2013. "STAR: Ultrafast Universal RNA-Seq Aligner." *Bioinformatics (Oxford, England)* 29 (1): 15–21. https://doi.org/10.1093/bioinformatics/bts635.

Dominissini, Dan, Sharon Moshitch-Moshkovitz, Schraga Schwartz, Mali Salmon-Divon, Lior Ungar, Sivan Osenberg, Karen Cesarkas, et al. 2012. "Topology of the Human and Mouse M6A RNA Methylomes Revealed by M6A-Seq." *Nature* 485 (7397): 201–6. https://doi.org/10.1038/nature11112.

Du, Bingying, Yanbo Zhang, Meng Liang, Zengkan Du, Haibo Li, Cunxiu Fan, Hailing Zhang, Yan Jiang, and Xiaoying Bi. 2021. "N6-Methyladenosine (M6A) Modification and Its Clinical Relevance in Cognitive Dysfunctions." *Aging* 13 (16): 20716–37. https://doi.org/10.18632/aging.203457.

Enam, Syed Usman, Boris Zinshteyn, Daniel H. Goldman, Madeline Cassani, Nathan M. Livingston, Geraldine Seydoux, and Rachel Green. 2020. "Puromycin Reactivity Does Not Accurately Localize Translation at the Subcellular Level." *ELife* 9 (August): e60303. https://doi.org/10.7554/eLife.60303.

Engel, Mareen, Carola Eggert, Paul M. Kaplick, Matthias Eder, Simone Röh, Lisa Tietze, Christian Namendorf, et al. 2018. "The Role of M6A/m-RNA Methylation in Stress Response Regulation." *Neuron* 99 (2): 389-403.e9. https://doi.org/10.1016/j.neuron.2018.07.009.

Epple, Robert, Dennis Krüger, Tea Berulava, Gerrit Brehm, Momchil Ninov, Rezaul Islam, Sarah Köster, and Andre Fischer. 2021. "The Coding and Small Non-Coding Hippocampal Synaptic RNAome." *Molecular Neurobiology* 58 (6): 2940–53. https://doi.org/10.1007/s12035-021-02296-y.

Erson-Bensan, Ayse E., and Oguzhan Begik. 2017. "M6A Modification and Implications for MicroRNAs." *MicroRNA* 6 (2): 97–101. https://doi.org/10.2174/2211536606666170511102219.

Fischer von Mollard, G., T. C. Südhof, and R. Jahn. 1991. "A Small GTP-Binding Protein Dissociates from Synaptic Vesicles during Exocytosis." *Nature* 349 (6304): 79–81. https://doi.org/10.1038/349079a0.

Frye, Michaela, Bryan T. Harada, Mikaela Behm, and Chuan He. 2018. "RNA Modifications Modulate Gene Expression during Development." *Science (New York, N.Y.)* 361 (6409): 1346–49. https://doi.org/10.1126/science.aau1646.

Fu, Ye, Dan Dominissini, Gideon Rechavi, and Chuan He. 2014. "Gene Expression Regulation Mediated through Reversible M^{6}A RNA Methylation." *Nature Reviews. Genetics* 15 (5): 293–306. https://doi.org/10.1038/nrg3724.

Halder, Rashi, Magali Hennion, Ramon O. Vidal, Orr Shomroni, Raza-Ur Rahman, Ashish Rajput, Tonatiuh Pena Centeno, et al. 2016. "DNA Methylation Changes in Plasticity Genes Accompany the Formation and Maintenance of Memory." Nature Neuroscience 19 (1): 102–10. https://doi.org/10.1038/nn.4194.

Han, Min, Zhen Liu, Yingying Xu, Xiangtian Liu, Dewei Wang, Fan Li, Yun Wang, and Jianzhong Bi. 2020. "Abnormality of M6A MRNA Methylation Is Involved in Alzheimer's Disease." *Frontiers in Neuroscience* 14: 98. https://doi.org/10.3389/fnins.2020.00098.

Heinz, Sven, Christopher Benner, Nathanael Spann, Eric Bertolino, Yin C. Lin, Peter Laslo, Jason X. Cheng, Cornelis Murre, Harinder Singh, and Christopher K. Glass. 2010. "Simple Combinations of Lineage-Determining Transcription Factors Prime Cis-Regulatory Elements Required for Macrophage and B Cell Identities." *Molecular Cell* 38 (4): 576–89. https://doi.org/10.1016/j.molcel.2010.05.004.

Hobson, Benjamin D., Linghao Kong, Erik W. Hartwick, Ruben L. Gonzalez, and Peter A. Sims. 2020. "Elongation Inhibitors Do Not Prevent the Release of Puromycylated Nascent

Polypeptide Chains from Ribosomes." *ELife* 9 (August): e60048. https://doi.org/10.7554/eLife.60048.

Holt, Christine E., Kelsey C. Martin, and Erin M. Schuman. 2019. "Local Translation in Neurons: Visualization and Function." *Nature Structural & Molecular Biology* 26 (7): 557–66. https://doi.org/10.1038/s41594-019-0263-5.

Huang, He, Judith Camats-Perna, Rodrigo Medeiros, Victor Anggono, and Jocelyn Widagdo. 2020. "Altered Expression of the M6A Methyltransferase METTL3 in Alzheimer's Disease." *ENeuro* 7 (5): ENEURO.0125-20.2020. https://doi.org/10.1523/ENEURO.0125-20.2020.

Huang, Huilin, Hengyou Weng, Wenju Sun, Xi Qin, Hailing Shi, Huizhe Wu, Boxuan Simen Zhao, et al. 2018. "Recognition of RNA N6-Methyladenosine by IGF2BP Proteins Enhances MRNA Stability and Translation." *Nature Cell Biology* 20 (3): 285–95. https://doi.org/10.1038/s41556-018-0045-z.

Huang, Huilin, Hengyou Weng, Keren Zhou, Tong Wu, Boxuan Simen Zhao, Mingli Sun, Zhenhua Chen, et al. 2019. "Histone H3 Trimethylation at Lysine 36 Guides M6A RNA Modification Co-Transcriptionally." *Nature* 567 (7748): 414–19. https://doi.org/10.1038/s41586-019-1016-7.

Hulsen, Tim, Jacob de Vlieg, and Wynand Alkema. 2008. "BioVenn – a Web Application for the Comparison and Visualization of Biological Lists Using Area-Proportional Venn Diagrams." *BMC Genomics* 9 (1): 488. https://doi.org/10.1186/1471-2164-9-488.

Ianov, Lara, Matt De Both, Monica K. Chawla, Asha Rani, Andrew J. Kennedy, Ignazio Piras, Jeremy J. Day, et al. 2017. "Hippocampal Transcriptomic Profiles: Subfield Vulnerability to Age and Cognitive Impairment." *Frontiers in Aging Neuroscience* 9: 383. https://doi.org/10.3389/fnagi.2017.00383.

Islam, Md Rezaul, Lalit Kaurani, Tea Berulava, Urs Heilbronner, Monika Budde, Tonatiuh Pena Centeno, Vakthang Elerdashvili, et al. 2021. "A MicroRNA Signature That Correlates with Cognition and Is a Target against Cognitive Decline." *EMBO Molecular Medicine* 13 (11): e13659. https://doi.org/10.15252/emmm.202013659.

Jia, Guifang, Ye Fu, Xu Zhao, Qing Dai, Guanqun Zheng, Ying Yang, Chengqi Yi, et al. 2011. "N6-Methyladenosine in Nuclear RNA Is a Major Substrate of the Obesity-Associated FTO." *Nature Chemical Biology* 7 (12): 885–87. https://doi.org/10.1038/nchembio.687.

Jiang, Lulu, Weiwei Lin, Cheng Zhang, Peter E. A. Ash, Mamta Verma, Julian Kwan, Emily van Vliet, et al. 2021. "Interaction of Tau with HNRNPA2B1 and N6-Methyladenosine RNA Mediates the Progression of Tauopathy." *Molecular Cell* 81 (20): 4209-4227.e12. https://doi.org/10.1016/j.molcel.2021.07.038.

Jones, Thouis R., In Han Kang, Douglas B. Wheeler, Robert A. Lindquist, Adam Papallo, David M. Sabatini, Polina Golland, and Anne E. Carpenter. 2008. "CellProfiler Analyst: Data Exploration and Analysis Software for Complex Image-Based Screens." *BMC Bioinformatics* 9 (November): 482. https://doi.org/10.1186/1471-2105-9-482.

Kanehisa, Minoru, Yoko Sato, and Masayuki Kawashima. 2021. "KEGG Mapping Tools for Uncovering Hidden Features in Biological Data." *Protein Science: A Publication of the Protein Society*, August. https://doi.org/10.1002/pro.4172.

Kang, H., and E. M. Schuman. 1996. "A Requirement for Local Protein Synthesis in Neurotrophin-Induced Hippocampal Synaptic Plasticity." *Science (New York, N.Y.)* 273 (5280): 1402–6. https://doi.org/10.1126/science.273.5280.1402.

Khan, Aziz, and Anthony Mathelier. 2017. "Intervene: A Tool for Intersection and Visualization of Multiple Gene or Genomic Region Sets." *BMC Bioinformatics* 18 (1): 287. https://doi.org/10.1186/s12859-017-1708-7.

Kimura, Ryoichi, and Masuo Ohno. 2009. "Impairments in Remote Memory Stabilization Precede Hippocampal Synaptic and Cognitive Failures in 5XFAD Alzheimer Mouse Model." *Neurobiology of Disease* 33 (2): 229–35. https://doi.org/10.1016/j.nbd.2008.10.006.

Koopmans, Frank, Pim van Nierop, Maria Andres-Alonso, Andrea Byrnes, Tony Cijsouw, Marcelo P. Coba, L. Niels Cornelisse, et al. 2019. "SynGO: An Evidence-Based, Expert-Curated Knowledge Base for the Synapse." *Neuron* 103 (2): 217-234.e4. https://doi.org/10.1016/j.neuron.2019.05.002.

Leonetti, Amanda M., Ming Yin Chu, Fiona O. Ramnaraign, Samuel Holm, and Brandon J. Walters. 2020. "An Emerging Role of M6A in Memory: A Case for Translational Priming." *International Journal of Molecular Sciences* 21 (20): E7447. https://doi.org/10.3390/ijms21207447.

Li, Heng, Bob Handsaker, Alec Wysoker, Tim Fennell, Jue Ruan, Nils Homer, Gabor Marth, Goncalo Abecasis, Richard Durbin, and 1000 Genome Project Data Processing Subgroup. 2009. "The Sequence Alignment/Map Format and SAMtools." *Bioinformatics* 25 (16): 2078–79. https://doi.org/10.1093/bioinformatics/btp352.

Li, Mengqi, Songxue Su, Weihua Cai, Jing Cao, Xuerong Miao, Weidong Zang, Shichao Gao, et al. 2020. "Differentially Expressed Genes in the Brain of Aging Mice With Cognitive Alteration and Depression- and Anxiety-Like Behaviors." *Frontiers in Cell and Developmental Biology* 8: 814. https://doi.org/10.3389/fcell.2020.00814.

Liao, Shanhui, Hongbin Sun, and Chao Xu. 2018. "YTH Domain: A Family of N6-Methyladenosine (M6A) Readers." *Genomics, Proteomics & Bioinformatics* 16 (2): 99–107. https://doi.org/10.1016/j.gpb.2018.04.002.

Liao, Yang, Gordon K. Smyth, and Wei Shi. 2013. "The Subread Aligner: Fast, Accurate and Scalable Read Mapping by Seed-and-Vote." *Nucleic Acids Research* 41 (10): e108. https://doi.org/10.1093/nar/gkt214.

Linder, Bastian, Anya V. Grozhik, Anthony O. Olarerin-George, Cem Meydan, Christopher E. Mason, and Samie R. Jaffrey. 2015. "Single-Nucleotide-Resolution Mapping of M6A and M6Am throughout the Transcriptome." *Nature Methods* 12 (8): 767–72. https://doi.org/10.1038/nmeth.3453.

Liu, Jianzhao, Yanan Yue, Dali Han, Xiao Wang, Ye Fu, Liang Zhang, Guifang Jia, et al. 2014. "A METTL3-METTL14 Complex Mediates Mammalian Nuclear RNA N6-Adenosine Methylation." *Nature Chemical Biology* 10 (2): 93–95. https://doi.org/10.1038/nchembio.1432.

Liu, Jun'e, Kai Li, Jiabin Cai, Mingchang Zhang, Xiaoting Zhang, Xushen Xiong, Haowei Meng, et al. 2020. "Landscape and Regulation of M6A and M6Am Methylome across Human and Mouse Tissues." *Molecular Cell* 77 (2): 426-440.e6. https://doi.org/10.1016/j.molcel.2019.09.032.

Livneh, Ido, Sharon Moshitch-Moshkovitz, Ninette Amariglio, Gideon Rechavi, and Dan Dominissini. 2020. "The M6A Epitranscriptome: Transcriptome Plasticity in Brain Development and Function." *Nature Reviews. Neuroscience* 21 (1): 36–51. https://doi.org/10.1038/s41583-019-0244-z.

Love, Michael I., Wolfgang Huber, and Simon Anders. 2014. "Moderated Estimation of Fold Change and Dispersion for RNA-Seq Data with DESeq2." *Genome Biology* 15 (12): 550. https://doi.org/10.1186/s13059-014-0550-8.

Martin, Marcel. 2011. "Cutadapt Removes Adapter Sequences from High-Throughput Sequencing Reads." *EMBnet.Journal* 17 (1): 10–12. https://doi.org/10.14806/ej.17.1.200.

Martinez De La Cruz, Braulio, Robert Markus, Sunir Malla, Maria Isabel Haig, Chris Gell, Fei Sang, Eleanor Bellows, et al. 2021. "Modifying the M6A Brain Methylome by ALKBH5-Mediated Demethylation: A New Contender for Synaptic Tagging." *Molecular Psychiatry*, October, 1–13. https://doi.org/10.1038/s41380-021-01282-z.

Mayford, Mark, Danny Baranes, Katrina Podsypanina, and Eric R. Kandel. 1996. "The 3′-Untranslated Region of CaMKIIα Is a Cis-Acting Signal for the Localization and Translation of MRNA in Dendrites." *Proceedings of the National Academy of Sciences* 93 (23): 13250–55. https://doi.org/10.1073/pnas.93.23.13250.

McQuin, Claire, Allen Goodman, Vasiliy Chernyshev, Lee Kamentsky, Beth A. Cimini, Kyle W. Karhohs, Minh Doan, et al. 2018. "CellProfiler 3.0: Next-Generation Image Processing for Biology." *PLOS Biology* 16 (7): e2005970. https://doi.org/10.1371/journal.pbio.2005970.

Meng, Jia, Xiaodong Cui, Manjeet K. Rao, Yidong Chen, and Yufei Huang. 2013. "Exome-Based Analysis for RNA Epigenome Sequencing Data." *Bioinformatics* 29 (12): 1565–67. https://doi.org/10.1093/bioinformatics/btt171.

Merkurjev, Daria, Wan-Ting Hong, Kei Iida, Ikumi Oomoto, Belinda J. Goldie, Hitoshi Yamaguti, Takayuki Ohara, et al. 2018. "Synaptic N6-Methyladenosine (M6A) Epitranscriptome Reveals Functional Partitioning of Localized Transcripts." *Nature Neuroscience* 21 (7): 1004–14. https://doi.org/10.1038/s41593-018-0173-6.

Meyer, Kate D., and Samie R. Jaffrey. 2014. "The Dynamic Epitranscriptome: N6-Methyladenosine and Gene Expression Control." *Nature Reviews. Molecular Cell Biology* 15 (5): 313–26. https://doi.org/10.1038/nrm3785.

Meyer, Kate D., Yogesh Saletore, Paul Zumbo, Olivier Elemento, Christopher E. Mason, and Samie R. Jaffrey. 2012. "Comprehensive Analysis of MRNA Methylation Reveals Enrichment in 3' UTRs and near Stop Codons." *Cell* 149 (7): 1635–46. https://doi.org/10.1016/j.cell.2012.05.003.

Michurina, Alexandra, M. Sadman Sakib, Cemil Kerimoglu, Dennis Manfred Krüger, Lalit Kaurani, Md Rezaul Islam, Parth Devesh Joshi, et al. 2022. "Postnatal Expression of the Lysine Methyltransferase SETD1B Is Essential for Learning and the Regulation of Neuron-Enriched Genes." *The EMBO Journal* 41 (1): e106459. https://doi.org/10.15252/embj.2020106459.

Peleg, Shahaf, Farahnaz Sananbenesi, Athanasios Zovoilis, Susanne Burkhardt, Sanaz Bahari-Javan, Roberto Carlos Agis-Balboa, Perla Cota, et al. 2010. "Altered Histone Acetylation Is Associated with Age-Dependent Memory Impairment in Mice." *Science*, May. https://doi.org/10.1126/science.1186088.

Ping, Xiao-Li, Bao-Fa Sun, Lu Wang, Wen Xiao, Xin Yang, Wen-Jia Wang, Samir Adhikari, et al. 2014. "Mammalian WTAP Is a Regulatory Subunit of the RNA N6-Methyladenosine Methyltransferase." *Cell Research* 24 (2): 177–89. https://doi.org/10.1038/cr.2014.3.

Rajecka, Veronika, Tomas Skalicky, and Stepanka Vanacova. 2019. "The Role of RNA Adenosine Demethylases in the Control of Gene Expression." *Biochimica Et Biophysica Acta. Gene Regulatory Mechanisms* 1862 (3): 343–55. https://doi.org/10.1016/j.bbagrm.2018.12.001.

Ramírez, Fidel, Devon P Ryan, Björn Grüning, Vivek Bhardwaj, Fabian Kilpert, Andreas S Richter, Steffen Heyne, Friederike Dündar, and Thomas Manke. 2016. "DeepTools2: A next Generation Web Server for Deep-Sequencing Data Analysis." *Nucleic Acids Research* 44 (W1): W160–65. https://doi.org/10.1093/nar/gkw257.

Richter, Joel D. 2001. "Think Globally, Translate Locally: What Mitotic Spindles and Neuronal Synapses Have in Common." *Proceedings of the National Academy of Sciences* 98 (13): 7069–71. https://doi.org/10.1073/pnas.111146498.

Risso, Davide, John Ngai, Terence P. Speed, and Sandrine Dudoit. 2014. "Normalization of RNA-Seq Data Using Factor Analysis of Control Genes or Samples." *Nature Biotechnology* 32 (9): 896–902. https://doi.org/10.1038/nbt.2931.

Robinson, James T., Helga Thorvaldsdóttir, Wendy Winckler, Mitchell Guttman, Eric S. Lander, Gad Getz, and Jill P. Mesirov. 2011. "Integrative Genomics Viewer." *Nature Biotechnology* 29 (1): 24–26. https://doi.org/10.1038/nbt.1754.

Schindelin, Johannes, Ignacio Arganda-Carreras, Erwin Frise, Verena Kaynig, Mark Longair, Tobias Pietzsch, Stephan Preibisch, et al. 2012. "Fiji: An Open-Source Platform for Biological-Image Analysis." *Nature Methods* 9 (7): 676–82. https://doi.org/10.1038/nmeth.2019.

Shafik, Andrew M., Feiran Zhang, Zhenxing Guo, Qing Dai, Kinga Pajdzik, Yangping Li, Yunhee Kang, et al. 2021. "N6-Methyladenosine Dynamics in Neurodevelopment and Aging, and Its Potential Role in Alzheimer's Disease." *Genome Biology* 22 (1): 17. https://doi.org/10.1186/s13059-020-02249-z.

Shannon, Paul, Andrew Markiel, Owen Ozier, Nitin S. Baliga, Jonathan T. Wang, Daniel Ramage, Nada Amin, Benno Schwikowski, and Trey Ideker. 2003. "Cytoscape: A Software Environment for Integrated Models of Biomolecular Interaction Networks." *Genome Research* 13 (11): 2498–2504. https://doi.org/10.1101/gr.1239303.

Shen, Li. 2019. "GeneOverlap: An R Package to Test and Visualize Gene Overlaps," 10.

Shi, Hailing, Xuliang Zhang, Yi-Lan Weng, Zongyang Lu, Yajing Liu, Zhike Lu, Jianan Li, et al. 2018. "M6A Facilitates Hippocampus-Dependent Learning and Memory through YTHDF1." *Nature* 563 (7730): 249–53. https://doi.org/10.1038/s41586-018-0666-1.

Sievert, Carson. 2019. *Interactive Web-Based Data Visualization with R, Plotly, and Shiny.* https://plotly-r.com/.

Singhal, Gaurav, Julie Morgan, Magdalene C. Jawahar, Frances Corrigan, Emily J. Jaehne, Catherine Toben, James Breen, et al. 2020. "Effects of Aging on the Motor, Cognitive and Affective Behaviors, Neuroimmune Responses and Hippocampal Gene Expression." *Behavioural Brain Research* 383 (April): 112501. https://doi.org/10.1016/j.bbr.2020.112501.

Studart, Adalberto, and Ricardo Nitrini. 2016. "Subjective Cognitive Decline: The First Clinical Manifestation of Alzheimer's Disease?" *Dementia & Neuropsychologia* 10 (3): 170–77. https://doi.org/10.1590/S1980-5764-2016DN1003002.

Sun, Ting, Ruiyan Wu, and Liang Ming. 2019. "The Role of M6A RNA Methylation in Cancer." *Biomedicine & Pharmacotherapy = Biomedecine & Pharmacotherapie* 112 (April): 108613. https://doi.org/10.1016/j.biopha.2019.108613.

Team, R. Core. 2013. "R: A Language and Environment for Statistical Computing."

Walters, Brandon J., Valentina Mercaldo, Colleen J. Gillon, Matthew Yip, Rachael L. Neve, Frederick M. Boyce, Paul W. Frankland, and Sheena A. Josselyn. 2017. "The Role of The RNA Demethylase FTO (Fat Mass and Obesity-Associated) and MRNA Methylation in Hippocampal Memory Formation." *Neuropsychopharmacology: Official Publication of the American College of Neuropsychopharmacology* 42 (7): 1502–10. https://doi.org/10.1038/npp.2017.31.

Wang, Xiao, Zhike Lu, Adrian Gomez, Gary C. Hon, Yanan Yue, Dali Han, Ye Fu, et al. 2014. "N6-Methyladenosine-Dependent Regulation of Messenger RNA Stability." *Nature* 505 (7481): 117–20. https://doi.org/10.1038/nature12730.

Wang, Xiao, Boxuan Simen Zhao, Ian A. Roundtree, Zhike Lu, Dali Han, Honghui Ma, Xiaocheng Weng, Kai Chen, Hailing Shi, and Chuan He. 2015. "N6-Methyladenosine Modulates Messenger RNA Translation Efficiency." *Cell* 161 (6): 1388–99. https://doi.org/10.1016/j.cell.2015.05.014.

Weng, Yi-Lan, Xu Wang, Ran An, Jessica Cassin, Caroline Vissers, Yuanyuan Liu, Yajing Liu, et al. 2018. "Epitranscriptomic M6A Regulation of Axon Regeneration in the Adult Mammalian Nervous System." *Neuron* 97 (2): 313-325.e6. https://doi.org/10.1016/j.neuron.2017.12.036.

Wickham, Hadley. 2009. "Introduction." In *Ggplot2: Elegant Graphics for Data Analysis*, edited by Hadley Wickham, 1–7. Use R. New York, NY: Springer. https://doi.org/10.1007/978-0-387-98141-3_1.

Widagdo, Jocelyn, and Victor Anggono. 2018. "The M6A-Epitranscriptomic Signature in Neurobiology: From Neurodevelopment to Brain Plasticity." *Journal of Neurochemistry* 147 (2): 137–52. https://doi.org/10.1111/jnc.14481.

Widagdo, Jocelyn, Qiong-Yi Zhao, Marie-Jeanne Kempen, Men Chee Tan, Vikram S. Ratnu, Wei Wei, Laura Leighton, et al. 2016. "Experience-Dependent Accumulation of N6-Methyladenosine in the Prefrontal Cortex Is Associated with Memory Processes in

Mice." *The Journal of Neuroscience: The Official Journal of the Society for Neuroscience* 36 (25): 6771–77. https://doi.org/10.1523/JNEUROSCI.4053-15.2016.

Wilson, R.S., S.E. Leurgans, P.A. Boyle, J.A. Schneider, and D.A. Bennett. 2010. "Neurodegenerative Basis of Age-Related Cognitive Decline (e–Pub Ahead of Print)(CME)." *Neurology* 75 (12): 1070–78. https://doi.org/10.1212/WNL.0b013e3181f39adc.

Yang, Ying, Phillip J. Hsu, Yu-Sheng Chen, and Yun-Gui Yang. 2018. "Dynamic Transcriptomic M6A Decoration: Writers, Erasers, Readers and Functions in RNA Metabolism." *Cell Research* 28 (6): 616–24. https://doi.org/10.1038/s41422-018-0040-8.

Yen, Ya-Ping, and Jun-An Chen. 2021. "The M6A Epitranscriptome on Neural Development and Degeneration." *Journal of Biomedical Science* 28 (1): 40. https://doi.org/10.1186/s12929-021-00734-6.

Yoon, Ki-Jun, Francisca Rojas Ringeling, Caroline Vissers, Fadi Jacob, Michael Pokrass, Dennisse Jimenez-Cyrus, Yijing Su, et al. 2017. "Temporal Control of Mammalian Cortical Neurogenesis by M6A Methylation." *Cell* 171 (4): 877-889.e17. https://doi.org/10.1016/j.cell.2017.09.003.

Yu, Jiangtao, Yuxian Zhang, Haoli Ma, Rong Zeng, Ruining Liu, Pengcheng Wang, Xiaoqing Jin, and Yan Zhao. 2020. "Epitranscriptomic Profiling of N6-Methyladenosine-Related RNA Methylation in Rat Cerebral Cortex Following Traumatic Brain Injury." *Molecular Brain* 13 (1): 11. https://doi.org/10.1186/s13041-020-0554-0.

Yu, Jun, Mengxian Chen, Haijiao Huang, Junda Zhu, Huixue Song, Jian Zhu, Jaewon Park, and Sheng-Jian Ji. 2018. "Dynamic M6A Modification Regulates Local Translation of MRNA in Axons." *Nucleic Acids Research* 46 (3): 1412–23. https://doi.org/10.1093/nar/gkx1182.

Zalcman, Gisela, Noel Federman, and Arturo Romano. 2018. "CaMKII Isoforms in Learning and Memory: Localization and Function." *Frontiers in Molecular Neuroscience* 11 (December): 445. https://doi.org/10.3389/fnmol.2018.00445.

Zeng, Yong, Shiyan Wang, Shanshan Gao, Fraser Soares, Musadeqque Ahmed, Haiyang Guo, Miranda Wang, et al. 2018. "Refined RIP-Seq Protocol for Epitranscriptome Analysis with Low Input Materials." *PLOS Biology* 16 (9): e2006092. https://doi.org/10.1371/journal.pbio.2006092.

Zhang, Zeyu, Meng Wang, Dongfang Xie, Zenghui Huang, Lisha Zhang, Ying Yang, Dongxue Ma, et al. 2018. "METTL3-Mediated N6-Methyladenosine MRNA Modification Enhances Long-Term Memory Consolidation." *Cell Research* 28 (11): 1050–61. https://doi.org/10.1038/s41422-018-0092-9.

Zhao, Boxuan Simen, Ian A. Roundtree, and Chuan He. 2017. "Post-Transcriptional Gene Regulation by MRNA Modifications." *Nature Reviews. Molecular Cell Biology* 18 (1): 31–42. https://doi.org/10.1038/nrm.2016.132.

Zhao, Fanpeng, Ying Xu, Shichao Gao, Lixia Qin, Quillan Austria, Sandra L. Siedlak, Kinga Pajdzik, et al. 2021. "METTL3-Dependent RNA M6A Dysregulation Contributes to Neurodegeneration in Alzheimer's Disease through Aberrant Cell Cycle Events." *Molecular Neurodegeneration* 16 (1): 70. https://doi.org/10.1186/s13024-021-00484-x.

Zhao, Yanchun, Yuanfei Shi, Huafei Shen, and Wanzhuo Xie. 2020. "M6A-Binding Proteins: The Emerging Crucial Performers in Epigenetics." *Journal of Hematology & Oncology* 13 (1): 35. https://doi.org/10.1186/s13045-020-00872-8.

Chapter 3: Changes in m^{6}A in a model of enhanced cognition

Research article 2

Prepared for submission

Changes in the m^{6}A landscape following environmental enrichment regulate the availability of synaptic proteins

Changes in the m^{6}A landscape following environmental enrichment regulate the availability of synaptic proteins

Ricardo Castro-Hernández[1], Kristin Schneider[1], Tonatiuh Peña Centeno[12], Susanne Burkhart[1], Gaurav Jain[12], Andre Fischer*[134]

[1]Department for Epigenetics and Systems Medicine in Neurodegenerative Diseases, German Center for Neurodegenerative Diseases (DZNE), Göttingen, Germany

[2]Bioinformatics Unit, German Center for Neurodegenerative Diseases (DZNE), Göttingen, Germany

[3]Department of Psychiatry and Psychotherapy, University Medical Center, Göttingen, Germany

[4]Cluster of Excellence "Multiscale Bioimaging: from Molecular Machines to Networks of Excitable Cells" (MBExC), University of Göttingen, Germany

* Corresponding author

Abstract

The exposure to a complex, enriched environment has been long known to cause strong, long-lasting effects on the structure and function of the mammalian brain, enhancing cognitive performance and brain plasticity. Despite the well-established effects of environmental enrichment (EE) on cognition, little is known about the molecular mechanisms that mediate the enhanced synaptic transmission and plasticity observed following EE. Here, we show that EE exposure causes changes in the levels of N^6-methyladenosine (m^{6}A) in several mRNAs associated with synaptic function, with a large number of them displaying reduced m^{6}A. Some of these transcripts coding for proteins involved in synaptic transmission and plasticity show increased protein levels in synaptic compartments following EE, offering a possible mechanism for m^{6}A-mediated modulation. Our results add to the evidence of m^{6}A as a key regulator of cognition and plasticity, specifically in the context of enhanced cognition.

Introduction

Ever since the inception of the synaptic theory of memory formation and storage, early observations showed that the exposure to a complex and varied environment had remarkable effects on many learning and memory tasks, many of them depending on hippocampal function (Hebb 1949). Subsequent studies corroborated that exposure to a stimuli-rich environment can have strong effects on the structure and function of the brain, enhancing brain plasticity (Green and Greenough 1986; Duffy et al. 2001; Kempermann, Kuhn, and Gage 1997). Generally, models of increased environmental stimulus that enhance plasticity are termed environmental enrichment (EE) and consist of exposing animals to a setting with increased living space, colorful tunnels, toys, increased social interaction, and the ability to exercise in running wheels. EE exposure has also been shown to have powerful beneficial effects in cases of injury and disease, something that has also been observed in humans, with valuable implications for the treatment of neuropsychiatric and neurodegenerative diseases (Lazarov et al. 2005; Frick and Benoit 2010; Valero et al. 2011; Mora 2013).

In spite of all the evidence supporting the notion that EE neural plasticity, learning and memory functions, the mechanisms responsible for the onset of these changes are still poorly understood. The interpretation of these effects is further complicated by the existence of multiple different EE protocols that involve diverse kinds of stimuli and, more importantly, durations (Eckert and Abraham 2013). Despite this, it is a generally accepted notion that EE exposure improves learning by inducing changes in synaptic physiology that enhance synaptic transmission and can facilitate the induction and persistence of long-term potentiation (LTP) and long-term depression (LTD), two of the most important molecular processes mediating synaptic plasticity (Abraham et al. 2002; Irvine and Abraham 2005; Ohline and Abraham 2019).

In the hippocampus, previous studies have found that increased LTP in the CA1 can be observed after EE exposure, which manifests through enhanced performance in cognitive tests (Irvine and Abraham 2005). This cognitive enhancement can even be spread to subsequent generations through epigenetic mechanisms, showing that the effects of EE are broad and long-lasting (Arai and Feig 2011; Benito et al. 2018). Other studies have shown varying degrees of synaptic transmission enhancement, and some have even hinted at an LTP-inhibiting effect of enrichment. EE is also known to be able to reverse previously induced LTP and LTD, highlighting the complex nature of the

plasticity resulting from exposure to EE (Foster and Dumas 2001; Duffy et al. 2001; Artola et al. 2006; Eckert and Abraham 2013).

The molecular mechanisms underlying these changes in the brain are, however, still not well understood. Unbiased approaches to identify changes in gene expression after EE have identified small changes in the transcriptome or increased expression of certain synaptic function genes, but the effects on gene expression are generally not very strong (Hüttenrauch, Salinas, and Wirths 2016; Grégoire et al. 2018). Additionally, some epigenetic mechanisms have also been implicated in the regulation of EE-associated molecules, like the deposition of 5-hydroxymethylcytosine (5mC), changes in histone modifications or miRNA expression (Kuzumaki et al. 2011; Irier et al. 2014; Fischer 2016). This limited knowledge of the underlying processes regulating the enhanced plasticity observed after EE has made it imperative to further study the effects of enrichment on additional mechanisms involved in synaptic function.

One of such mechanisms is the regulation of gene expression through post-transcriptional RNA modifications. The most common and best understood of these modifications, m6A is a key regulator of RNA metabolism and it plays multiple roles in the function of the adult mammalian brain (Livneh et al. 2020). m6A is a common mark in mammalian mRNA and its deposition, removal and binding depends on a complex network of m6A writers, erasers and readers that will determine the specificity of these marks, as well as the ultimate cellular fate of labeled mRNAs (Meyer and Jaffrey 2017). The main writers are the methyltransferases METTL3 and METTL14, responsible for the addition of m6A to mRNAs cotranscriptionally (Balacco and Soller 2019). In contrast, labeled transcripts can be demethylated by the action of the erasers FTO and ALKBH5, making m6A a dynamic mark that can be added and removed in response to stimuli and depending on cellular context (Yang et al. 2018; W. Zhang, Qian, and Jia 2021). This property of methylation marks has given rise to the field of epitranscriptomics, referring to changes on the transcriptome that can affect gene expression without altering their sequence (Saletore et al. 2012).

The presence of methylation marks can have important consequences for the fate of labeled transcripts, from processing to transport and translation. m6A marks are known to regulate the transport of labeled mRNAs to specific cellular compartments, and in neurons methylation is known to promote the localization of a subset of synaptic mRNAs to dendrites and synaptic compartments (Yang et al. 2018; Merkurjev et al.

2018). In addition, m^{6}A marks are also known to promote the translation of labeled transcripts by distinct mechanisms, depending on the location of the methylation marks. Translational regulation is known to play a role during learning in the hippocampus and the absence of the m^{6}A reader YTHDF1 significantly impairs learning and cognitive function (Shi et al. 2018; Merkurjev et al. 2018). Additionally, other members of the methylation machinery, like METTL3 and FTO have been linked to the regulation of learning and memory formation and recall, making the epitranscriptome regulation of synaptic function an intriguing mechanism in the context of cognitive decline and enhancement (Z. Zhang et al. 2018; Walters et al. 2017). Epitranscriptome changes have also been associated with certain models for cognitive impairment and neuropsychiatric disorders, hinting at a direct association between m^{6}A dynamics and cognition in mammals (Choudhry et al. 2013; Jiang et al. 2021; Du et al. 2021; Shafik et al. 2021).

In this work, we set out to deepen our understanding of the molecular mechanisms underlying the changes in plasticity following environmental enrichment. To this end, we describe the effects of EE on the m^{6}A epitranscriptome in the mouse CA1, a key region for hippocampal-dependent learning that has been strongly linked to EE-induced synaptic plasticity. We show that transcripts undergoing changes in m^{6}A tended towards decreased methylation, localized preferentially at the 5' end of transcripts, and exhibited a tendency to regulate for synapse organization and function. This reduction of m^{6}A correlated with increased levels of protein in synaptic compartments for some transcripts, through a mechanism that might be regulated by the m^{6}A eraser FTO. Our results represent the first study that links EE exposure to changes in the epitranscriptome and their relevance for brain plasticity. More studies will be needed to better understand the mechanisms that mediate these epitranscriptomics changes and how they can be targeted to possibly potentiate the enhancing effect of EE in cognitive function.

Methods

Animals

All animal experiments were performed according to the protocols approved by the local ethics committee of the University Medical Center of the University Göttingen, Germany, the Lower Saxony State Office for Consumer Protection and Food Safety (LAVES) under animal protocol number 18.2857 and followed institutional, national, and international guidelines

Twenty male C57/B6J mice of 9 weeks of age were purchased from Janvier Labs. After a week of acclimation, the mice were randomly divided in two groups and housed in environmentally enriched or home cages. Animals were housed in these cages during the duration of the protocol, with regular cleaning but reduced human interaction, in a 12 hours light/ 12 hours dark cycle with food and water ad libitum.

Environmental enrichment

We performed EE on 10 mice as described previously (Benito et al. 2018), while 10 mice were used as control in home cages (HC) without novel objects and running wheels. For EE, mice of 10 weeks of age were kept in groups of 5 in large cages and provided with 8 toys per cage (colorful housing, tubes and different objects), as well as 2 running wheels. Two toys were exchanged and the rest were reorganized in the cage daily. Cages were changed weekly (for both EE and HC mice) and mice were kept in these conditions for a total of 10 weeks.

Dissections

Once the enrichment period was finished, the mice were sacrificed by cervical dislocation under anesthesia and their brains were isolated. The hippocampus was dissected into its corresponding subregions - CA1, CA3 and DG - using an 18G needle. All dissections were performed on ice and the isolated tissue was flash-frozen in liquid nitrogen. Samples remained in -80℃ until right before RNA extraction.

RNA extraction

RNA used for sequencing was extracted from tissue using the NucleoSpin RNA/Protein Kit (Macherey-Nagel), according to the manufacturer's instructions.

For all other applications, cell or tissue samples were homogenized in an appropriate volume of TRI reagent (Sigma) using a Bead Ruptor Elite for 30 s with 0.5 mm ceramic beads. RNA was isolated using the Direct-zol RNA miniprep kit or the Clean and concentrator -5 (Zymo Research) according to the manufacturer's instructions. RNA was eluted in nuclease-free water in a volume of 6–50 µl.

RNA concentrations were determined by Nanodrop (Thermo) or Qubit with RNA HS Assay Kit (Thermo). For samples used for sequencing, RNA integrity was assayed by electropherogram in a Bioanalyzer using a total RNA Assay with a Pico/Nano Chip (Agilent). RNA samples were always kept on ice and stored at -80℃ when not in use to prevent degradation.

meRIP

Samples for sequencing were processed using a protocol based on a previously published one with some modifications (Zeng et al. 2018). 5–10 µg of purified total RNA were depleted from rRNA using the RiboMinus Eukaryote Ribosomal Removal Kit (Invitrogen) and fragmented for 5 minutes at 70℃ to a fragment size of 100–120 nt with Fragmentation Reagents. RNA was cleaned using the Clean and Concentrator Kit after every step and eluted in an appropriate volume of nuclease-free water. To have enough material for the RIP, the fragmented RNA from two mice was pooled together for a total of 5 samples per condition. 300 ng of fragmented RNA were used for each IP, keeping 5% as input. 3 µg of anti-m^{6}A antibody was incubated with the RNA in 400 µl IP buffer (0.2 M Tris-HCl pH 7.5, 0.5 M NaCl, Igepal 2%) for 2 hours at 4° C with rotation. RNA-antibody mixes were then crosslinked twice with 0.15 J/cm2 of UV light (254 nm) in a UVP crosslinker (Analitik Jena). Antibody-RNA conjugates were incubated with 30 µl of Protein A/G beads overnight (ON) at 4℃ with rotation in 500 µl IP buffer supplemented with 200 units. Beads with immunoprecipitated RNA were washed 5 times with IP buffer and further washed with low-salt (50 mM Tris pH 7.4, 50 mM NaCl, 1mM EDTA, 1, 0.1% NP-40, 0.1% SDS) and high-salt (same as low-salt but with 500mM NaCl) buffers at 4℃ with rotation to remove nonspecific binding. RNA was eluted by incubating in 150 µl PKD buffer (Qiagen) with 10 µl of Proteinase K (Millipore) for 1 hour at 37℃ with agitation. Eluted RNA was cleaned before proceeding to library preparation.

Crosslinking was performed with the idea of analyzing m^{6}A CLIP sites (meCLIP) to determine specific sites of differential methylation (Weng et al. 2018). This analysis

produced unsatisfactory results that did not meet the necessary quality standards and therefore samples were treated as normal meRIP-Seq for analysis purposes (Appendix Figure 4). Samples used for qPCR were generated with the same protocol without crosslinking.

Library preparation and sequencing

meRIP-Seq were prepared using the SMARTer Stranded Total RNA Kit v2 - Pico Input Mammalian (Takara) according to the manufacturer's instructions. Since samples were already fragmented, the fragmentation step was skipped. All of the RNA obtained from IP samples was used for library preparation, for input samples 2 ng were used. Libraries were amplified for 12 (input) or 16 (IP) cycles.

RNA-Seq samples were prepared with the TruSeq Stranded mRNA Library Prep Kit (Illumina) according to the manufacturer's instructions. 50 ng of rRNA-depleted RNA from each of the inputs were used.

Prepared libraries were sequenced in a Hiseq 2000 System (Illumina) for 50 cycles in single-end reads.

Bioinformatic analyses of meRIP-Seq and RNA-Seq

Raw reads were processed and demultiplexed using bcl2fastq 2.20.2 and low-quality reads were filtered out with Cutadapt 1.11.0 (Martin 2011). Filtered reads were mapped to the mouse (mm10) genome using the STAR aligner 2.5.2b (Dobin et al. 2013). The resulting bam files were sorted, indexed and the unmapped reads removed using SAMtools 1.9.0 (Li et al. 2009) Methylation sites were determined using MeTPeak 1.0.0 (Cui, Meng, et al. 2016) and differential methylation was assessed with Exomepeak 2.16.0 (Meng et al. 2013). An FDR cutoff of 0.05 and fold-change (FC) cutoffs of 1.2 or 1.5 were used as indicated in the text. From the exomePeak output, significantly differentially methylated peaks were used.

For RNA-Seq analyses, read counts were obtained with subread 1.5.1 (Liao, Smyth, and Shi 2013) featurecounts from the bam files of input samples. Differential gene expression was determined by DESeq2 3.5.12 (Love, Huber, and Anders 2014) using normalized read counts and correcting for covariates detected by RUVseq 1.16.1 (Risso et al. 2014). Cutoffs of FDR ≤ 0.05, FC ≥ 1.2 and BaseMean ≥ 50 were applied to the results.

For visualization, bam files of both IP and input samples were collapsed for PCR duplicates using SAMtools and IP samples were normalized to their corresponding inputs and to their library size using deeptools 3.2.1 (Ramírez et al. 2016) bamCompare. The resulting normalized tracks were visualized in the IGV Browser 2.9.2 (Robinson et al. 2011)

Gene ontology (GO) analyses

GO term enrichment analyses were performed using the App ClueGO v2.5.3 (Bindea et al. 2009) in Cytoscape 3.7.2 (Shannon et al. 2003), with GO Term Fusion enabled to collapse terms containing very similar gene lists. GO term tables for Biological process, Cellular component, Pathways and KEGG were produced and are labeled accordingly in the figures. Resulting enriched GO terms were visualized with a custom script using ggplot2 3.3.5 (Wickham 2009), displaying the adjusted p value for the GO term, the number of genes from the list that belong to said term and the percentage of the total genes in the GO term that are present in the list. Synaptic GO enrichment analyses were performed with SynGO 1.1 (syngoportal.org/).

Additional bioinformatic packages and tools

Scripts and analysis pipelines were written in R 3.5.2 (Team 2013). Peak annotation was performed with Homer 4.10.4 (Heinz et al. 2010). Guitar plots were produced with the Guitar 1.20.1 (Cui, Wei, et al. 2016) R package. Volcano plots were generated with plot.ly/orca 4.9.4.1 (Sievert 2019). Area-proportional Venn diagrams were produced with biovenn (www.biovenn.nl; Hulsen, de Vlieg, and Alkema 2008). Odds ratios and p values to determine significance in overlapped datasets were calculated with the GeneOverlap R package 1.18.0 (Shen 2019). De novo motif analyses were performed with Homer's findMotifsGenome and the top enriched motif is displayed. Dot blot images were analyzed with ImageStudio (LI-COR) and Fiji (Schindelin et al. 2012). Graphs, heatmaps and statistical analyses were performed on GraphPad Prism version 9.3.1 for Mac. Some custom figures were created with BioRender (biorender.com).

qPCR

cDNA was prepared using the Transcriptor cDNA first strand Synthesis Kit (Roche) using 100 ng-1 µg of total RNA or 5–20 ng of rRNA-depleted RNA as starting material. The manufacturer's protocol for cDNA synthesis was followed, with a combination of

random hexamers and Poly(dT) oligos. For immunoprecipitated samples, the full amount of IP and input (5%) RNA were used as input.

Synthesized cDNA was diluted 1:5–1:10 with nuclease-free water before being used for qPCR. Reactions were run in a Light Cycler 480 (Roche) in 96- or 384-well plates, using the Light Cycler 480 probes Master Mix or SYBR Master Mix (Roche). Each reaction was run in duplicate, in a volume of 20 µl and using 4 µl of cDNA per reaction. Primers used were custom designed, validated and used at a final concentration of 0.5 µM with the corresponding probe from the Universal Probe Library Mouse, when applicable. Reactions were run for a maximum of 45 cycles with a reference gene in every plate and quantified as expression relative to the reference (and input in the case of IPs). 3–6 biological replicates were used in every case and statistical differences were determined by a t test, unless otherwise indicated.

Primer sequences are available in Supplementary Table 3.1.

m^6A quantification

m^6A concentration was determined using a m^6A Methylation Assay Kit Fluorometric (Abcam). The starting material was 200 ng of rRNA-depleted RNA and the manufacturer's protocol was followed. All reactions were carried out in duplicate and a standard curve of m^6A/A was included to have quantitative results. Reactions were read in a FLUOstar Omega Multiplate reader (BMG) in fluorescence mode.

Synaptosome isolation

The hippocampi of 10 HC and 10 EE mice were dissected. 5 bilateral hippocampi were pooled together making up two independent samples that were further processed to obtain high quality synaptosomes, using an existing protocol with some modifications (Carlin et al. 1980). In short, hippocampi were homogenized in 3 ml solution A (0.32 M sucrose, 1 mM HEPES pH 7.4, 1 mM $MgCl_2$, 0.5 mM $CaCl_2$) with a 5 ml glass-Teflon motorized Dounce homogenizer for 12 strokes at 900 rpm (homogenate corresponds to this fraction) and centrifuged at 1400 g for 10 min at 4° C. Supernatants were further centrifuged for 10 min at 13800 g at 4° C and the pellet was resuspended in 2 ml solution B (0.32 M sucrose, 1 mM HEPES pH 7.4) and loaded into a sucrose gradient (1.2 M, 1 M and 0.85 M in 1 mM HEPEs pH 7.4), then centrifuged for 2 hours at 82500 g at 4° C (SW41Ti rotor). The synaptosome fraction was collected from the interface between the

1 M and 1.2 M fractions with a long pipette tip and snap frozen in liquid nitrogen for later use.

Dot Blot

2 μl of synaptosomes was pipetted onto a nitrocellulose membrane, and dried for 5 min. Blocking of nonspecific signal was done with 5% low-fat milk in PBST for 10 min. Primary antibodies were applied for 15 min at room temperature (RT), then the membrane was washed three times for 3 min each in PBST with 5% milk. Secondary antibody was applied for 15 min at RT. The membrane was washed again three times with PBST without milk before being imaged. Blots were imaged by fluorescence with an Odyssey DLx (LI-COR) and the resulting images were quantified with ImageStudio.

Antibodies used and their dilutions are detailed in Table 3.2.

Results

The epitranscriptome of the CA1 in HC and EE mice

The process of memory formation and recall is very complex and many layers of regulation exist at a cellular and molecular level that allow the mammalian brain to fine-tune it in a context-dependent manner. Recently, the role of RNA modifications has taken a prominent role in this regard, particularly m^{6}A. Changes in this dynamic modification (known as the m^{6}A epitranscriptome) are known to be directly involved in certain kinds of learning, memory and synaptic function, and some evidence shows that it could also be involved in neurodegeneration. But to this date, nothing is known about the dynamic changes in the epitranscriptome in response to cognitive enhancement.

To address this question, we used environmental enrichment as a model of enhanced cognition. EE – the exposure to a complex environment with novel and varying stimuli, social interaction and the possibility to exercise – has been consistently shown to improve cognitive performance and increase brain plasticity.

Ten C57/B6J mice of ten weeks of age were subjected to ten weeks of environmental enrichment (EE), using a protocol previously shown to significantly increase cognition and plasticity (Figure 3.1A). The mice were housed in large cages, with 5 mice per cage, with continuous access to a running wheel, as well as a complex environment of novel objects, toys, and housing that were rearranged and changed daily. As control, another group of mice was housed in the same kind of cages (home-caged, HC) but deprived from all stimuli and with no access to a running wheel. Changes in the transcriptome and epitranscriptome in the hippocampal CA1 region as a consequence of EE exposure were analyzed by meRIP-Seq and RNA-Seq .

The meRIP-Seq analysis showed that a large number of m^{6}A peaks could be detected, 12,303 in the case of the HC samples and 11,429 in the EE (Figure 3.1B). Since each transcript can be methylated at multiple positions, individual methylated regions could be mapped to 4,756 and 4,596 mRNAs, respectively. This corresponded to 2.58 transcripts for the HC and 2.48 in the EE CA1 (Figure 3.1C). Methylated transcripts made up almost 40 percent of all expressed transcripts in both conditions, something

that matched previous observations of m⁶A levels in the brain and highlights the broad nature of methylation marks (Figure 3.1D).
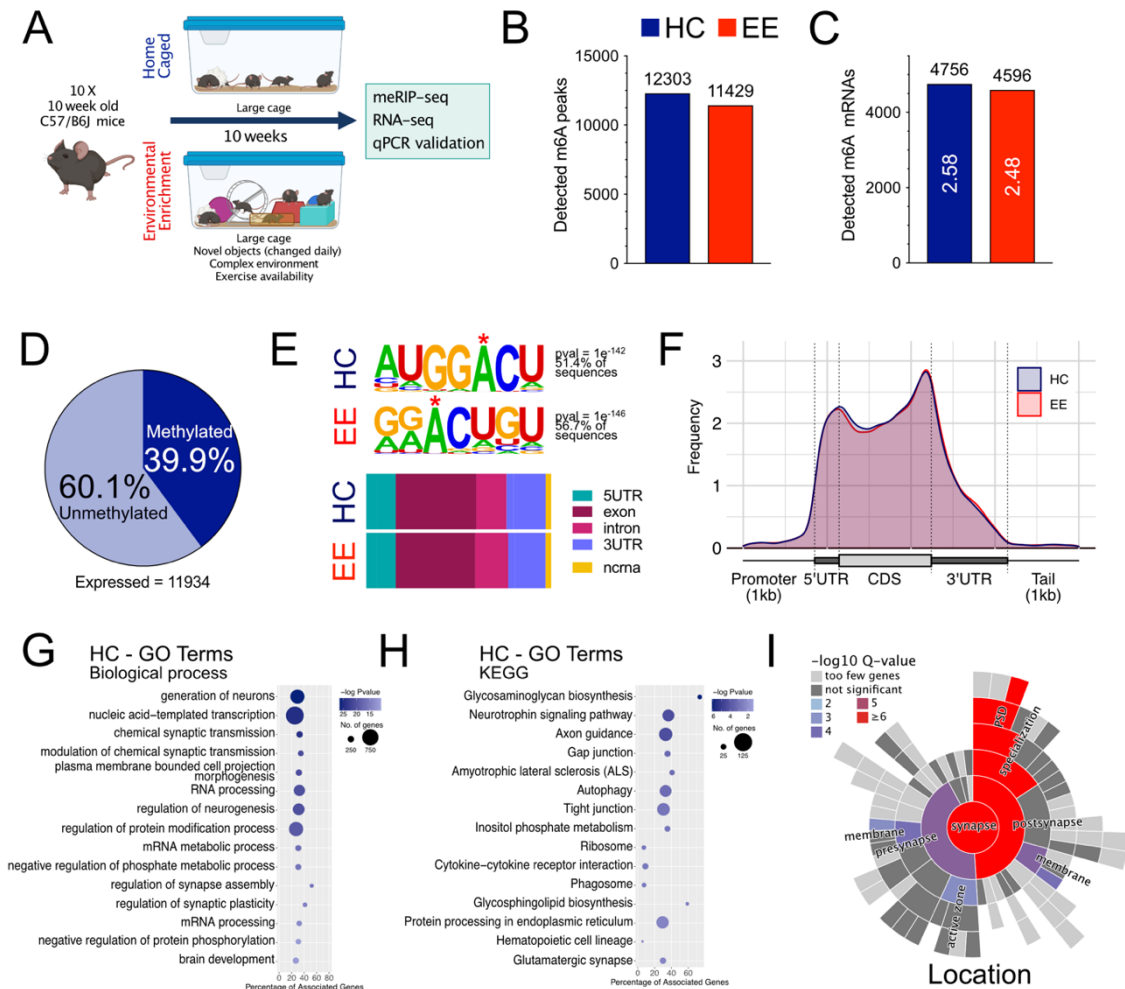

Figure 3.1. The epitranscriptome in HC and EE mice. A. Schematic of the EE protocol used and downstream applications. B. Total m⁶A peaks detected in HC and EE samples and C. number of methylated transcripts. Average number of peaks per transcripts is shown inside the corresponding column. D. Percentage of methylated mRNAs compared to all expressed genes in the CA1. E. Top enriched motif detected in the methylated regions in HC and EE samples. Methylated A is shown with a red *, p values and percentage of sequences are displayed. F. Annotated regions for detected m⁶A peaks. 5UTR - 5' untranslated region, 3'UTR - 3' untranslated region, CDS - coding sequence. F. Guitar plot showing the distribution density of m⁶A peaks along mRNA features. G. Enriched GO terms Biological process for methylated transcripts in HC samples. H. Enriched KEGG pathways in methylated transcripts in HC samples. I. Synaptic location GO enrichment analysis of methylated transcripts in HC samples.

De novo motif enrichment analysis showed that the most enriched motif in the methylated regions was the m⁶A consensus sequence DRACH (where D = A, T or G, R = A or G, and H = A, T or C), further validating the specificity of the meRIP-Seq. Interestingly, some differences could be detected in the nucleotide frequency at certain positions, hinting towards a possibly favored motif in methylated transcripts in EE (Figure 3.1E). In addition, methylated regions displayed a localization along the transcript very similar to the characteristic m⁶A distribution. m⁶A marks were enriched along the CDS with a marked peak in the vicinity of the stop codon and towards the 3' untranslated region (3' UTR). In both conditions, a smaller but clear peak could also be detected in the 5' untranslated region (5' UTR), something that can be observed in several datasets but is not as common as the 3' UTR peak (Figure 3.1 F,G).

A gene ontology (GO) pathway enrichment analysis showed that methylated transcripts in the HC samples were significantly enriched for genes related to brain development, the regulation of synaptic transmission, transcriptional regulation and RNA processing. Other works have previously described this property of methylated mRNAs in other brain regions as well as in the hippocampus, so it is not surprising that this also holds true in cells of the CA1. Furthermore, these genes largely belonged to general pathways associated with neurogenic processes and synaptic function, as evidenced by KEGG pathway enrichment. Given the overrepresentation of synapse-associated terms within methylated transcripts, we performed synapse-specific GO enrichment analysis using SynGO, a database of manually curated synaptic proteins (Koopmans et al. 2019). Methylated transcripts in the HC CA1 show a strong enrichment for synaptically located proteins, particularly postsynaptic and many of them membrane-bound (Figure 3.1H). According to their function, proteins involved in synapse assembly and synaptic signaling were mostly enriched. It is worth noting that, even though the genes detected as methylated in EE samples displayed an enrichment for synaptic function/location proteins too, it was less significant than the HC.

Epitranscriptome changes after 10 weeks of environmental enrichment

To determine what effect the 10-week enrichment protocol has on the epitranscriptome, a differential methylation analysis was performed. When using lax cutoffs (FDR ≤ 0.05,

FC ≥ 1.2), 1,028 peaks were detected as differentially methylated (Figure 3.2A). Of them, 441 showed an increase in methylation level (hypermethylated), while 587 decreased it (hypomethylated). Although the number of transcripts significantly differentially methylated was similar between hyper and hypomethylated, the magnitude of the changes was not. Hypomethylated mRNAs displayed more pronounced reductions in m^6A levels, whereas hypermethylation was mild (Figure 3.2B). When applying higher cutoffs for fold change in methylation (FDR ≤ 0.05, FC ≥ 1.5), the vast majority of the remaining peaks were hypomethylated – 314 against 40 hypermethylated (Figure 3.2A).

The differentially methylated peaks were located along 862 transcripts (FC ≥ 1.2), with an average of 1.19 peaks per transcript. The vast majority (95%) of all transcripts displayed consistent changes in methylation with only 43 containing both hyper and hypomethylated regions in the same mRNA (mixed transcript). With a FC ≥ 1.5 cutoff, 313 mRNAs were differentially methylated (1.12 peaks per transcript) and of them, only one was a mixed transcript (Figure 3.2C).

To assess whether methylation changes were driven by underlying changes in gene expression, we performed a differential expression analysis on the same samples. Using similar cutoffs as for differential methylation (FC ≥ 1.2), 270 genes could be detected as differentially expressed, with 183 being upregulated and 87 downregulated (Figure 3.2C). Changes in gene expression induced by EE were mild both in up- and downregulated genes, and when applying more stringent FC cutoffs (≥ 1.5) only two genes were not filtered out, both downregulated (Figure 3.2C,D). Surprisingly, the downregulated genes showed a mild but significant enrichment for genes involved in the regulation of synaptic transmission and neurotransmitter release, whereas upregulated genes showed no significant GO term enrichment (Figure 3.2E). Importantly, the genes with altered gene expression following EE did not overlap with differentially methylated mRNAs, regardless of the direction of change (Figure 3.2F).

These results show a considerable effect of EE on the methylation level of several mRNAs in the CA1, with a subset of transcripts more dramatically hypomethylated, in contrast with hypermethylated transcripts. Although small changes in gene expression could be detected, they do not drive the m^6A levels after EE.
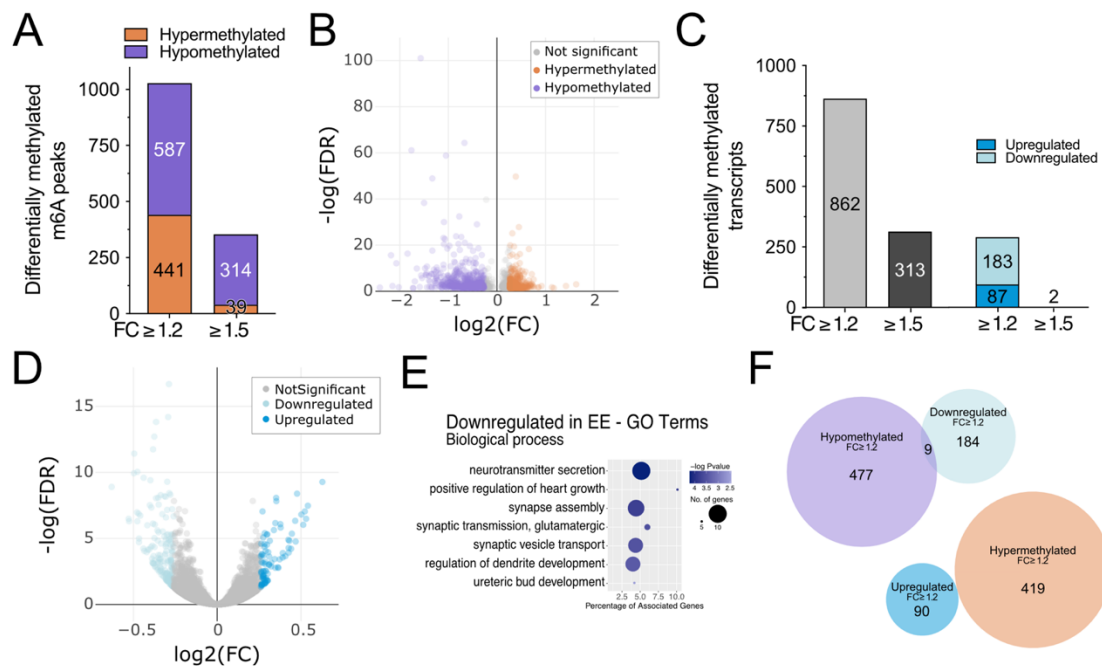
Figure 3.2. Changes in m⁶A and gene expression after EE. A. Differentially methylated peaks detected with FC cutoffs of ≥ 1.2 and ≥ 1.5. Hypo and hypermethylated peaks are stacked on top of each other. B. Volcano plot showing the magnitude and significance of changes in m⁶A for every significantly differentially methylated peak. FC cutoffs are set at ≥ 1.2 and FDR is ≤ 0.05. C. Number of differentially methylated and differentially expressed transcripts/genes, using FC cutoffs of ≥ 1.2 and ≥ 1.5. Differentially expressed genes are stacked. D. Volcano plot showing the magnitude and significance of differentially expressed genes. FC cutoffs are set at ≥ 1.2 and FDR is ≤ 0.05. E. Enriched GO terms Biological process for downregulated genes in EE. F. Overlap between gene expression and methylation changes. Upregulated and hypermethylated, as well as downregulated and hypomethylated are compared.

Differentially methylated transcripts (FC ≥ 1.2) were almost equally divided between exclusively hyper (376 or 43.6%) or hypomethylated (443 or 51.4%), while 43 were mixed transcripts (Suppl. Figure 3.1A). In this subset of mRNAs, hypomethylated regions fell preferentially on the CDS, while hypomethylated regions favored the 5' UTR in all transcripts and the 3' UTR in hypermethylated mRNAs (Suppl. Figure 3.1B,C). Functionally, both differentially hypo and hypermethylated transcripts were enriched for synaptic function genes. This enrichment was more highly significant in hypermethylated transcripts and involved presynaptic vesicle trafficking, synapse organization and trans-synaptic signaling (Suppl. Figure 3.1D).

Strong changes in m⁶A after EE target synaptic function

Hypomethylated mRNAs made up almost all the transcripts with highly changed m⁶A levels. With a FC cutoff of ≥ 1.5, 275 of them displayed exclusively reduced methylation sites, whereas 37 showed exclusively increased methylation; only one mixed transcript was part of this group (Figure 3.3A). Highly hypomethylated transcripts showed a significant enrichment for GO terms associated with a broad array of biological processes, including brain development, learning, cell signaling and transcriptional regulation, but no single main affected pathway. Highly hypermethylated mRNAs showed no significant enrichment for a particular GO term (Figure 3.3B). In contrast to the whole m⁶A epitranscriptome, highly hypomethylated transcripts were only mildly
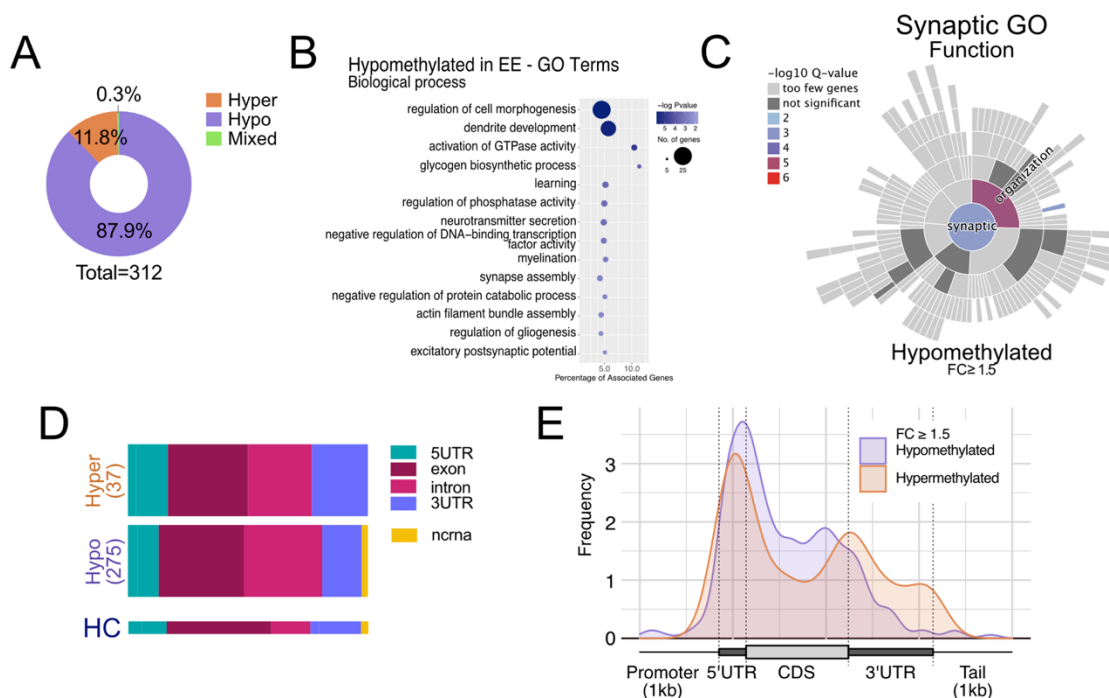

Figure 3.3. Highly hypomethylated transcripts regulate synaptic function. A. Percentage of highly hypomethylated mRNAs (FC ≥ 1.5) that are exclusively hypo-, hypermethylated, or mixed transcripts. B. Enriched GO terms Biological process for highly hypomethylated transcripts. C. Synaptic function GO enrichment analysis of highly hypomethylated transcripts. D. Annotated regions for highly hypomethylated peaks. 5UTR - 5' untranslated region, 3UTR - 3' untranslated region, CDS - coding sequence. E. Guitar plot showing the distribution density of highly hypo- and hypermethylated peaks along mRNA features.

enriched for synaptic location and function GO terms (Figure 3.3C). Enrichment was limited to synaptic organization and postsynaptic specialization, respectively (Suppl. Figure 3.1E). The hypomethylated regions in these transcripts were annotated preferentially to the CDS, in comparison to the baseline distribution of m^{6}A marks in all transcripts, while hypermethylated regions showed a small increase in the 5' UTR and 3' UTR (Figure 3.3D). This was made clear when looking at the distribution along the transcript body, where both hyper- and hypomethylated regions were highly enriched at the 5' UTR and the 5'end of the CDS (Figure 3.3E). This distribution pattern, distinct from the distribution pattern of m^{6}A across the transcriptome, may hint at region-dependent changes in m^{6}A deposition or removal in response to EE.

These results show that the changes in methylation after EE follow a complex pattern of distribution and magnitude, with different subsets of transcripts showing distinct changes in m^{6}A distribution and levels. Hypomethylated transcripts display the most dramatic changes after EE and although the regulation of synaptic function is enriched in this group, other cellular processes are affected by these mRNAs.

m^{6}A changes result in altered synaptic protein levels

To rule out that general alterations in the methylation machinery were responsible for the observed changes in m^{6}A following EE, we looked at the state of m^{6}A and associated proteins. The proportion of methylated adenosine in the mRNA of the CA1 in HC and EE samples was quantified. No changes were detected in the m^{6}A levels after EE, showing that the changes in methylation levels identified previously were not large enough to significantly affect global m^{6}A (Figure 3.4A). We also analyzed the expression levels of genes of the methylation machinery known to affect m^{6}A deposition or removal (writers and erasers): *Mettl3, Mettl14, Wtap, Alkbh5 and Fto*. None of these genes showed significant changes in gene expression in the sequencing data, and this was further confirmed by qPCR (Figure 3.4B).

The regulation of the synaptic location of methylated transcripts to control their availability at the synapse is a known role of m^{6}A modifications in mRNA. Therefore, we set to validate a possible consequence of m^{6}A changes in synaptic mRNAs in response to EE. Many of the hypomethylated transcripts are known to be located in synaptic
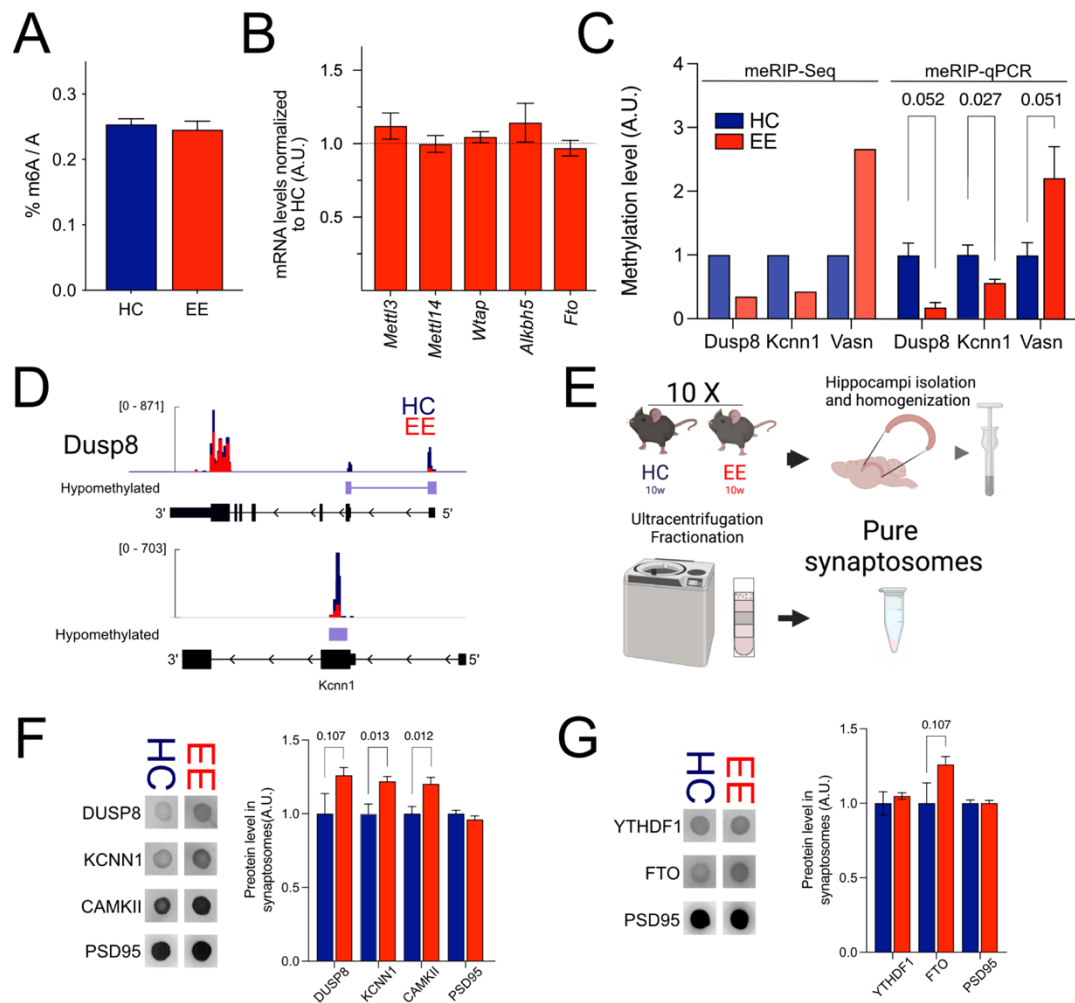
Figure 3.4. Changes in synaptic protein levels of methylated mRNAs in EE. A. Global m6A levels in mRNA from the CA1 of HC and EE mice. Graph shows the percentage of methylated A against total A. B. Expression level (mRNA) of members of the methylation machinery in EE compared to HC CA1. C. Validation of differential methylation sites by qPCR. The graph shows changes in m6A detected by meRIP-Seq and the equivalent experimental validation by qPCR. D. Tracks showing the read coverage at the probed methylation sites. Hypomethylated regions are marked in purple. Counts displayed are normalized IP/input for all replicates. Scale is in normalized read counts. E. Schematic of synaptosome purification. F. Dot blot for proteins coded by highly hypomethylated transcripts and G. m6A machinery proteins. PSD included as loading control. Graphs show the dot blot quantification. Graphs in B, C, F and G show the mean +SEM of expression/protein levels normalized to HC samples. Significance was determined by an unpaired t test. p values are displayed above the corresponding columns for significantly different comparisons.

compartments and many more code for synaptically located proteins (Supplementary Table 3.3). From these, we selected two highly hypomethylated transcripts, the dual specificity phosphatase 8 *Dusp8* and the potassium calcium-activated channel subfamily N member 1 *Kcnn1*, as well as a highly hypermethylated transcript (Vasorin, *Vasn*) for validation. For all these mRNAs, the changes in m^{6}A detected through meRIP-Seq could be confirmed by qPCR (Figure 3.4D).

To assess how EE could be affecting the synaptic availability of the proteins coded for in highly hypomethylated transcripts, we used synaptosomal preparations to measure the levels of our proteins of interest. Pure synaptosomes, including both pre and postsynaptic compartments, were isolated from the hippocampi of 10 mice that underwent EE and 10 HC control mice (Figure 3.4E). The presence and level of proteins of interest was determined by dot blot. Both DUSP8 and KCNN1 showed significant increases in their protein levels in synaptic compartments (Figure 3.4F). Interestingly, another protein that is highly abundant in the synapse and known to heavily regulate synaptic transmission and plasticity, CAMKII, was also significantly increased. CAMKII isoforms did not belong to the group of highly differentially methylated transcripts, but Camk2b displayed a hypermethylated region in the 5' UTR (1.2 FC).

To determine whether this decrease in methylation was a result of changes in the methylation machinery, we determined the protein levels of the m^{6}A eraser FTO. This demethylase has been previously shown to be located in synaptic compartments and has been directly linked with synaptic function during memory formation. In the hippocampal synaptosomes of EE mice, a small but significant increase in FTO levels could be detected (Figure 3.4G).

m^{6}A-dependent regulation of translation is dependent on the action of reader proteins, and YTHDF1 is widely considered the main reader involved in promoting the translation of methylated mRNAs. This reader has also been shown to be located in dendritic and in some synaptic compartments, so the possibility exists that it could mediate translation of methylated transcripts at the synapse. We detected no difference in the protein levels of YTHDF1 in synaptic compartments, though the protein could be detected (Figure 3.4G). No changes could be observed in the levels of the compared proteins in hippocampus crude homogenate fractions, meaning that no significant alterations in somatic protein levels were present either (Suppl. Figure 3.2).

These results show that no global changes occur in m^{6}A levels or in the m^{6}A machinery as a consequence of enrichment and therefore, the altered methylation in certain transcripts is specific. Furthermore, strongly hypomethylated transcripts display a significant increase in the levels of the proteins they code for in synaptic compartments.

Discussion

Our results show that the epitranscriptome of the CA1 in mice shows significant changes after being exposed to 10 weeks of environmental enrichment. In the control (HC) mice, the population of methylated transcripts was strongly enriched for genes involved in the regulation of synaptic function and plasticity, something that has been described previously for hippocampal tissue, as well as other brain regions in mice and humans (Chang et al. 2017; Widagdo and Anggono 2018). The distribution of peaks along transcripts in HC and EE mice showed the distinctive m⁶A pattern, with increased levels close to the stop codon and 3' UTR (Meyer et al. 2012). Interestingly, some additional enrichment could be observed in the 5' region of transcripts in both conditions, something that could be attributed to the use of a low-input meRIP protocol that is previously displayed this effect on peak detection (Zeng et al. 2018).

Our enrichment protocol involved the constant exposure of mice to EE, as they were housed in EE or HC conditions for its duration. This length of EE exposure has been previously shown to enhance LTP induction, measured by field EPSP in the CA1 (Duffy et al. 2001; Eckert and Abraham 2013). Long (>4 weeks) EE protocols have generally been observed to produce increased LTD and in some cases, no changes in both LTP and LTD could be detected in the CA1, evidencing the importance of using consistent EE paradigms when comparing their effects in plasticity (Artola et al. 2006; Eckert, Bilkey, and Abraham 2010). Regardless, it is widely accepted that changes in both LTP and LTD are necessary to achieve the enhanced synaptic plasticity needed in response to a complex enriched environment, even if synaptic transmission is not strongly affected (Irvine and Abraham 2005; Eckert, Bilkey, and Abraham 2010).

The epitranscriptome in the CA1 of EE mice shows a large number of transcripts undergoing m⁶A changes when compared to HC mice. These changes are equally distributed between those with increased (hypermethylated) and decreased (hypomethylated) m⁶A. Interestingly, when focusing only on mRNAs undergoing more dramatic changes in methylation, the vast majority of them displayed hypomethylation along the CDS with an enrichment towards the 5' end and 5' UTR. The enrichment of synaptically located proteins was still present in this subset of mRNAs, albeit less significant than for the whole population of methylated transcripts. Hypo- and hypermethylated mRNAs could be validated in transcripts undergoing large magnitude changes.

The analysis of synaptosomal fractions showed that the validated strongly hypomethylated transcripts *Dusp8* and *Kcnn1* displayed increased protein levels in synaptic compartments. The phosphatase DUSP8 is a regulator of the MAPK signaling cascade, which can directly regulate brain plasticity and modulate learning and memory (Ding et al. 2019). Additionally, lack of *Dusp8* causes decreased hippocampal volume and impaired memory performance (Baumann et al. 2019). Moreover, *Dusp8* mRNA is found in some synaptic mRNA datasets, and is known to translocate to synaptic compartments in response to stimulation *in vitro* (Cajigas et al. 2012; Epple et al. 2021). The potassium channel KCNN1 (formerly SK1) is a key regulator of LTP, by mediating afterhyperpolarization in response to synaptic activity (Autuori et al. 2019; Sourdet et al. 2003). Changes in the protein levels for these and other differentially methylated mRNAs (like *Camk2b*) could result in further modulation of synaptic plasticity after EE (Zalcman, Federman, and Romano 2018).

The pattern of methylation changes hints towards a specific mechanism regulating m^{6}A marks during and following EE. Our results show that FTO protein levels increase in synaptic compartments following EE, where it could directly affect the methylation state of synaptically located transcripts. The demethylase FTO is the main m^{6}A eraser and it has been shown to remove methylation marks in the 5' UTR of transcripts (Jia et al. 2011; Meyer et al. 2015). Furthermore, FTO was previously shown to be present in synaptic compartments and is known to regulate memory function (Walters et al. 2017).

Differentially methylated transcripts showed a preference towards localization in the CDS and towards the 5' end of transcripts. Both at the 3' UTR and 5' UTR, m^{6}A is known to enhance translation through distinct mechanisms (dependent on the readers YTHDF1 and eIF3), and m^{6}A levels generally positively correlate with translational rate (Wang et al. 2015; Meyer et al. 2015). Our observations show that hypomethylated transcripts decrease their protein levels in synaptic compartments but not overall. These apparently contradictory observations could be reconciled by the function of another proposed m^{6}A reader, FMR1. This transcriptional repressor is preferentially located at the synapse and is known to bind to m^{6}A sites in mRNAs, where it inhibits translation (Ascano et al. 2012; Bassell and Warren 2008). A model of FMR1 function in relation to m^{6}A proposes a competitive binding between YTHDF1 and FMR1 at m^{6}A sites, to determine the final translational rate of a methylated transcript (Edupuganti et al. 2017). However, FMR1

binding sites are not especially enriched at the 5'UTR and tend to follow the distinct distribution of m^6A (Ascano et al. 2012).

Another possible explanation for the observed effect on protein levels is the crosstalk between m^6A and $N^6,2'$-O-dimethyladenosine (m^6Am), another type of RNA modification that targets primarily the 5' end of transcripts and that has some cross-reactivity with m^6A antibodies (Linder et al. 2015; Liu et al. 2020). Given the difficulty of studying m^6Am independently of m^6A, our knowledge of this mark is still very limited. Despite this, some elements of the m^6Am machinery have been described, like the methyltransferase PCIF1, responsible for m^6Am deposition (Boulias et al. 2019). In addition, in mouse and humans m^6Am levels negatively correlate with protein levels in several tissues and cell lines, and several potential m^6Am readers have been identified, like ELAVL1, EIF3G and FUS (Liu et al. 2020; Sendinc et al. 2019). Furthermore, the m^6A reader FTO is also able to demethylate m^6Am in the 5' end of transcripts, and some theorize that m^6Am is its true molecular target (Wei et al. 2018; Mauer and Jaffrey 2018). Recent studies have made strides in developing tools to study m^6Am and m^6A independent from each other, further expanding our knowledge of m^6Am-dependent regulation (Sun et al. 2021; J. Jiang et al. 2021). Applying these approaches to samples from EE animals would address the contribution of m^6Am and m^6A to the epitranscriptomics effects described here.

Further studies will be needed to gain more knowledge about the relationship between EE and epitranscriptome changes, particularly in the search for the downstream molecular mechanisms that mediate m^6A changes. Our observations also highlight the need for further research in unraveling the role of m^6A-mediated regulation in the induction and maintenance of synaptic plasticity, and its relationship with cognitive function.

Supplementary tables and figures

Primer	Fwd sequence	Rev sequence	UPL probe
Dusp8	GGAAGGTGATGGACGCAAAGA	GAAGGACCGGCTGTCGATGA	NA
Kcnn1	ATGGTGAGGGACCACTAGGC	TACCCCTGGGTGGCTTACAT	NA
Vasn	GCACGGGCAACTTCTACAGC	GGCTCCAAAGGGGCTTTCAC	NA
Gapdh	GACACTGAGCAAGAGAGGC	GATGGAAATTGTGAGGGAGAT	NA
Mettl3	GAAACAGCTGGACTCGCTTC	GCTTCTGGGTTCCTTAAATCC	38
Mettl14	TTGGGAGAGATAGCACTATCAGG	GTAGTTACTGTTTGTAAGCGTTGGTC	100
Fto	TCTGTCTGCCATCCTGGTC	TGGTAAAGTCCGGACGACTC	12
Alkbh5	GTCGGAACCTGTGCTTTCTC	GCCGTATGCAGTGAGTGATTT	99
Wtap	ACATTCTTGTCATGCGGCTA	GCTTGAGGTACTGGATTTGAGTG	15
Gapdh	GGGTTCCTATAAATACGGACTGC	CCATTTTGTCTACGGGACGA	52

Supplementary table 3.1. qPCR primers used and sequences

| Antibody	Campany	Catalog	Species	Dilution	Application
m^{6}A	Synaptic Systems	202 003	Rabbit	1 ug/ul	meRIP
CaMKII	Abcam	ab52476	Rabbit	1:2,000	Dot blot
PSD95	Millipore	MABN68	Mouse	1:2,000	Dot blot
DUSP8	Abcam	ab184134	Rabbit	1:1,000	Dot blot
KCNN1	Thermo Scientific	PA5-77600	Rabbit	1:1,000	Dot blot
YTHDF1	Proteintech	17479-1-A	Rabbit	1:1,000	Dot blot
FTO	Abcam	ab92821	Mouse	1:1,000	Dot blot
IRDye 800CW anti-mouse	LI-COR	926-32210	Goat	1:5,000	Dot blot
IRDye 680RD anti-rabbit	LI-COR	926-68070	Goat	1:5,000	Dot blot

Supplementary table 3.2. qPCR primers used and sequences

Synaptic located protein	Synaptic located mRNA	Synaptic GO	log2(FC) in EE	Name	Description
	■		-2.07	Rtkn	rhotekin
■	■		-1.84	Ubqln4	ubiquilin 4
■	■		-1.76	Mfn2	mitofusin 2
■	■	■	-1.57	Ppp1r9b	protein phosphatase 1, regulatory subunit 9B
	■		-1.5	Dusp8	dual specificity phosphatase 8
	■		-1.48	Smpd3	sphingomyelin phosphodiesterase 3, neutral
	■		-1.44	Szrd1	SUZ RNA binding domain containing 1
	■		-1.35	Trank1	tetratricopeptide repeat and ankyrin repeat containing 1
	■		-1.33	Cep170b	centrosomal protein 170B
■			-1.26	Kcnn1	potassium intermediate/small conductance calcium-activated channel, subfamily N,
	■	■	-1.24	Znrf1	zinc and ring finger 1
	■		-1.24	Elfn2	leucine rich repeat and fibronectin type III, extracellular 2
	■		-1.24	Map3k11	mitogen-activated protein kinase kinase kinase 11
	■	■	-1.2	Pcdh8	protocadherin 8
	■		-1.16	Fam193b	family with sequence similarity 193, member B
	■		-1.16	Plxnb2	plexin B2
■		■	-1.15	Dvl1	dishevelled segment polarity protein 1
	■		-1.13	Rexo1	REX1, RNA exonuclease 1
	■		-1.1	Chpf	chondroitin polymerizing factor
	■		-1.1	Pkig	protein kinase inhibitor, gamma
■			-1.09	Agap2	ArfGAP with GTPase domain, ankyrin repeat and PH domain 2
	■		-1.07	Celsr2	cadherin, EGF LAG seven-pass G-type receptor 2
	■		-1.06	Ankrd11	ankyrin repeat domain 11
■			-1.05	Agap2	ArfGAP with GTPase domain, ankyrin repeat and PH domain 2
	■		-1	Rtn4rl1	reticulon 4 receptor-like 1
		■	-0.977	Adgrb1	adhesion G protein-coupled receptor B1
■	■		-0.96	Klc2	kinesin light chain 2
	■		-0.894	Reep2	receptor accessory protein 2
		■	-0.878	Adgrb1	adhesion G protein-coupled receptor B1
	■		-0.875	Kctd1	potassium channel tetramerisation domain containing 1
	■	■	-0.842	Adgrl1	adhesion G protein-coupled receptor L1
	■		-0.841	Gpr162	G protein-coupled receptor 162
	■		-0.836	Sstr4	somatostatin receptor 4
	■		-0.826	Col4a2	collagen, type IV, alpha 2
		■	-0.807	Bcl2l1	BCL2-like 1
	■		-0.804	Mical3	microtubule associated monooxygenase, calponin and LIM domain containing 3
		■	-0.792	Iqsec3	IQ motif and Sec7 domain 3
■	■		-0.756	Arid1b	AT rich interactive domain 1B (SWI-like)
■	■	■	-0.743	Map1a	microtubule-associated protein 1 A
		■	-0.735	Sparc	secreted acidic cysteine rich glycoprotein
	■		-0.705	Psme3	proteaseome (prosome, macropain) activator subunit 3 (PA28 gamma, Ki)
		■	-0.673	Zmynd8	zinc finger, MYND-type containing 8
■	■	■	-0.669	Dmtn	dematin actin binding protein
	■		-0.661	Col11a2	collagen, type XI, alpha 2
	■		-0.583	Otud7a	OTU domain containing 7A

Supplementary table 3.3. Strongly consistently hypomethylated transcripts and their synaptic location/function
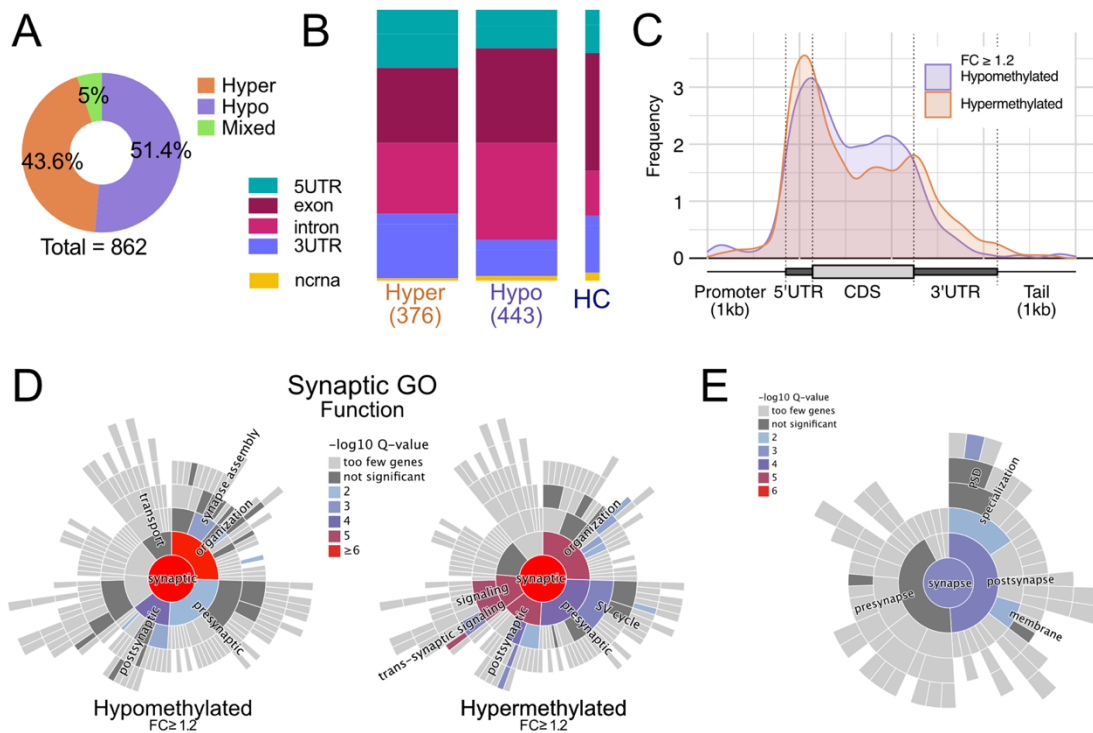
Supplementary Figure 3.1. Low FC changes in the CA1 after EE. A. Percentage of hypomethylated mRNAs (FC ≥ 1.2) that are exclusively hypo-, hypermethylated, or mixed transcripts. B. Annotated regions for highly hypomethylated peaks. 5UTR - 5' untranslated region, 3'UTR - 3' untranslated region, CDS - coding sequence. C. Guitar plot showing the distribution density of hypo- and hypermethylated peaks along mRNA features. D. Synaptic function GO enrichment analysis of hypomethylated and hypermethylated transcripts. E. Synaptic location GO enrichment of highly hypomethylated transcripts.
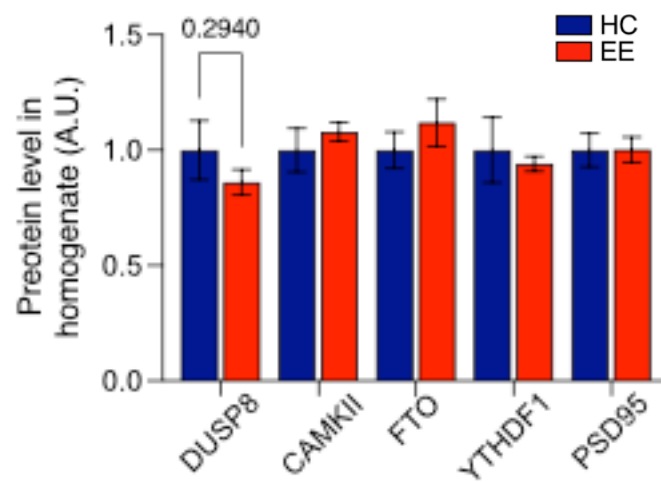
Supplementary figure 3.2. Protein levels in whole CA1 homogenate. Protein levels normalized to HC from proteins shown in Figure 3.4. Graphs display the main of two replicates, error bars show SD.

References

Abraham, Wickliffe C., Barbara Logan, Jeffrey M. Greenwood, and Michael Dragunow. 2002. "Induction and Experience-Dependent Consolidation of Stable Long-Term Potentiation Lasting Months in the Hippocampus." Journal of Neuroscience 22 (21): 9626–34. https://doi.org/10.1523/JNEUROSCI.22-21-09626.2002.

Arai, Junko A., and Larry A. Feig. 2011. "Long-Lasting and Transgenerational Effects of an Environmental Enrichment on Memory Formation." Brain Research Bulletin, Novel principles underlying memory formation, 85 (1): 30–35. https://doi.org/10.1016/j.brainresbull.2010.11.003.

Artola, Alain, Josefien C. von Frijtag, Patrick C. J. Fermont, Willem Hendrik Gispen, Loes H. Schrama, Amer Kamal, and Berry M. Spruijt. 2006. "Long-Lasting Modulation of the Induction of LTD and LTP in Rat Hippocampal CA1 by Behavioural Stress and Environmental Enrichment." The European Journal of Neuroscience 23 (1): 261–72. https://doi.org/10.1111/j.1460-9568.2005.04552.x.

Ascano, Manuel, Neelanjan Mukherjee, Pradeep Bandaru, Jason B. Miller, Jeff Nusbaum, David L. Corcoran, Christine Langlois, et al. 2012. "FMR1 Targets Distinct MRNA Sequence Elements to Regulate Protein Expression." Nature 492 (7429): 382–86. https://doi.org/10.1038/nature11737.

Autuori, Eleonora, Petra Sedlak, Li Xu, Margreet C. Ridder, Angelo Tedoldi, and Pankaj Sah. 2019. "RSK1 in Rat Neurons: A Controller of Membrane RSK2?" Frontiers in Neural Circuits 13. https://www.frontiersin.org/article/10.3389/fncir.2019.00021.

Balacco, Dario L., and Matthias Soller. 2019. "The M6A Writer: Rise of a Machine for Growing Tasks." Biochemistry 58 (5): 363–78. https://doi.org/10.1021/acs.biochem.8b01166.

Bassell, Gary J., and Stephen T. Warren. 2008. "Fragile X Syndrome: Loss of Local MRNA Regulation Alters Synaptic Development and Function." Neuron 60 (2): 201–14. https://doi.org/10.1016/j.neuron.2008.10.004.

Baumann, Peter, Sonja C. Schriever, Stephanie Kullmann, Annemarie Zimprich, Annette Feuchtinger, Oana Amarie, Andreas Peter, et al. 2019. "Dusp8 Affects Hippocampal Size and Behavior in Mice and Humans." Scientific Reports 9 (1): 19483. https://doi.org/10.1038/s41598-019-55527-7.

Benito, Eva, Cemil Kerimoglu, Binu Ramachandran, Tonatiuh Pena-Centeno, Gaurav Jain, Roman Manuel Stilling, Md Rezaul Islam, et al. 2018. "RNA-Dependent Intergenerational Inheritance of Enhanced Synaptic Plasticity after Environmental Enrichment." Cell Reports 23 (2): 546–54. https://doi.org/10.1016/j.celrep.2018.03.059.

Bindea, Gabriela, Bernhard Mlecnik, Hubert Hackl, Pornpimol Charoentong, Marie Tosolini, Amos Kirilovsky, Wolf-Herman Fridman, Franck Pagès, Zlatko Trajanoski, and Jérôme Galon. 2009. "ClueGO: A Cytoscape Plug-in to Decipher Functionally Grouped Gene Ontology and Pathway Annotation Networks." Bioinformatics 25 (8): 1091–93. https://doi.org/10.1093/bioinformatics/btp101.

Boulias, Konstantinos, Diana Toczydłowska-Socha, Ben R. Hawley, Noa Liberman, Ken Takashima, Sara Zaccara, Théo Guez, et al. 2019. "Identification of the M6Am Methyltransferase PCIF1 Reveals the Location and Functions of M6Am in the Transcriptome." Molecular Cell 75 (3): 631-643.e8. https://doi.org/10.1016/j.molcel.2019.06.006.

Cajigas, Iván J., Georgi Tushev, Tristan J. Will, Susanne tom Dieck, Nicole Fuerst, and Erin M. Schuman. 2012. "The Local Transcriptome in the Synaptic Neuropil Revealed by Deep Sequencing and High-Resolution Imaging." Neuron 74 (3): 453–66. https://doi.org/10.1016/j.neuron.2012.02.036.

Carlin, R K, D J Grab, R S Cohen, and P Siekevitz. 1980. "Isolation and Characterization of Postsynaptic Densities from Various Brain Regions: Enrichment of Different Types of

Postsynaptic Densities." Journal of Cell Biology 86 (3): 831–45. https://doi.org/10.1083/jcb.86.3.831.

Chang, Mengqi, Hongyi Lv, Weilong Zhang, Chunhui Ma, Xue He, Shunli Zhao, Zhi-Wei Zhang, et al. 2017. "Region-Specific RNA M6A Methylation Represents a New Layer of Control in the Gene Regulatory Network in the Mouse Brain." Open Biology 7 (9): 170166. https://doi.org/10.1098/rsob.170166.

Choudhry, Zia, Sarojini M. Sengupta, Natalie Grizenko, Geeta A. Thakur, Marie-Eve Fortier, Norbert Schmitz, and Ridha Joober. 2013. "Association between Obesity-Related Gene FTO and ADHD." Obesity (Silver Spring, Md.) 21 (12): E738-744. https://doi.org/10.1002/oby.20444.

Cui, Xiaodong, Jia Meng, Shaowu Zhang, Yidong Chen, and Yufei Huang. 2016. "A Novel Algorithm for Calling MRNA M6A Peaks by Modeling Biological Variances in MeRIP-Seq Data." Bioinformatics 32 (12): i378–85. https://doi.org/10.1093/bioinformatics/btw281.

Cui, Xiaodong, Zhen Wei, Lin Zhang, Hui Liu, Lei Sun, Shao-Wu Zhang, Yufei Huang, and Jia Meng. 2016. "Guitar: An R/Bioconductor Package for Gene Annotation Guided Transcriptomic Analysis of RNA-Related Genomic Features." BioMed Research International 2016: 8367534. https://doi.org/10.1155/2016/8367534.

Ding, Tao, Ya Zhou, Runying Long, Chao Chen, Juanjuan Zhao, Panpan Cui, Mengmeng Guo, Guiyou Liang, and Lin Xu. 2019. "DUSP8 Phosphatase: Structure, Functions, Expression Regulation and the Role in Human Diseases." Cell & Bioscience 9 (1): 70. https://doi.org/10.1186/s13578-019-0329-4.

Dobin, Alexander, Carrie A. Davis, Felix Schlesinger, Jorg Drenkow, Chris Zaleski, Sonali Jha, Philippe Batut, Mark Chaisson, and Thomas R. Gingeras. 2013. "STAR: Ultrafast Universal RNA-Seq Aligner." Bioinformatics (Oxford, England) 29 (1): 15–21. https://doi.org/10.1093/bioinformatics/bts635.

Du, Bingying, Yanbo Zhang, Meng Liang, Zengkan Du, Haibo Li, Cunxiu Fan, Hailing Zhang, Yan Jiang, and Xiaoying Bi. 2021. "N6-Methyladenosine (M6A) Modification and Its Clinical Relevance in Cognitive Dysfunctions." Aging 13 (16): 20716–37. https://doi.org/10.18632/aging.203457.

Duffy, Steven N., Kenneth J. Craddock, Ted Abel, and Peter V. Nguyen. 2001. "Environmental Enrichment Modifies the PKA-Dependence of Hippocampal LTP and Improves Hippocampus-Dependent Memory." Learning & Memory 8 (1): 26–34. https://doi.org/10.1101/lm.36301.

Eckert, Michael J., and Wickliffe C. Abraham. 2013. "Effects of Environmental Enrichment Exposure on Synaptic Transmission and Plasticity in the Hippocampus." Current Topics in Behavioral Neurosciences 15: 165–87. https://doi.org/10.1007/7854_2012_215.

Eckert, Michael J., David K. Bilkey, and Wickliffe C. Abraham. 2010. "Altered Plasticity in Hippocampal CA1, But Not Dentate Gyrus, Following Long-Term Environmental Enrichment." Journal of Neurophysiology 103 (6): 3320–29. https://doi.org/10.1152/jn.01037.2009.

Edupuganti, Raghu R., Simon Geiger, Rik G. H. Lindeboom, Hailing Shi, Phillip J. Hsu, Zhike Lu, Shuang-Yin Wang, et al. 2017. "N6-Methyladenosine (M6A) Recruits and Repels Proteins to Regulate MRNA Homeostasis." Nature Structural & Molecular Biology 24 (10): 870–78. https://doi.org/10.1038/nsmb.3462.

Epple, Robert, Dennis Krüger, Tea Berulava, Gerrit Brehm, Momchil Ninov, Rezaul Islam, Sarah Köster, and Andre Fischer. 2021. "The Coding and Small Non-Coding Hippocampal Synaptic RNAome." Molecular Neurobiology 58 (6): 2940–53. https://doi.org/10.1007/s12035-021-02296-y.

Fischer, Andre. 2016. "Environmental Enrichment as a Method to Improve Cognitive Function. What Can We Learn from Animal Models?" NeuroImage, Effects of Physical and Cognitive activity on brain structure and function, 131 (May): 42–47. https://doi.org/10.1016/j.neuroimage.2015.11.039.

Foster, T. C., and T. C. Dumas. 2001. "Mechanism for Increased Hippocampal Synaptic Strength Following Differential Experience." Journal of Neurophysiology 85 (4): 1377–83. https://doi.org/10.1152/jn.2001.85.4.1377.

Frick, Karyn M., and Jamie D. Benoit. 2010. "Use It or Lose It: Environmental Enrichment as a Means to Promote Successful Cognitive Aging." TheScientificWorldJOURNAL 10: 1129–41. https://doi.org/10.1100/tsw.2010.111.

Green, E. J., and W. T. Greenough. 1986. "Altered Synaptic Transmission in Dentate Gyrus of Rats Reared in Complex Environments: Evidence from Hippocampal Slices Maintained in Vitro." Journal of Neurophysiology 55 (4): 739–50. https://doi.org/10.1152/jn.1986.55.4.739.

Grégoire, Catherine-Alexandra, Stephanie Tobin, Brianna L. Goldenstein, Éric Samarut, Andréanne Leclerc, Anne Aumont, Pierre Drapeau, Stephanie Fulton, and Karl J. L. Fernandes. 2018. "RNA-Sequencing Reveals Unique Transcriptional Signatures of Running and Running-Independent Environmental Enrichment in the Adult Mouse Dentate Gyrus." Frontiers in Molecular Neuroscience 11. https://www.frontiersin.org/article/10.3389/fnmol.2018.00126.

Hebb, D. 1949. "The Organization of Behavior: A Neuropsychological Theory." In . https://doi.org/10.2307/1418888.

Heinz, Sven, Christopher Benner, Nathanael Spann, Eric Bertolino, Yin C. Lin, Peter Laslo, Jason X. Cheng, Cornelis Murre, Harinder Singh, and Christopher K. Glass. 2010. "Simple Combinations of Lineage-Determining Transcription Factors Prime Cis-Regulatory Elements Required for Macrophage and B Cell Identities." Molecular Cell 38 (4): 576–89. https://doi.org/10.1016/j.molcel.2010.05.004.

Hulsen, Tim, Jacob de Vlieg, and Wynand Alkema. 2008. "BioVenn – a Web Application for the Comparison and Visualization of Biological Lists Using Area-Proportional Venn Diagrams." BMC Genomics 9 (1): 488. https://doi.org/10.1186/1471-2164-9-488.

Hüttenrauch, Melanie, Gabriela Salinas, and Oliver Wirths. 2016. "Effects of Long-Term Environmental Enrichment on Anxiety, Memory, Hippocampal Plasticity and Overall Brain Gene Expression in C57BL6 Mice." Frontiers in Molecular Neuroscience 9. https://www.frontiersin.org/article/10.3389/fnmol.2016.00062.

Irier, Hasan, R. Craig Street, Ronak Dave, Li Lin, Catherine Cai, Timothy Hayden Davis, Bing Yao, Ying Cheng, and Peng Jin. 2014. "Environmental Enrichment Modulates 5-Hydroxymethylcytosine Dynamics in Hippocampus." Genomics, 5-hydroxymethylation, 104 (5): 376–82. https://doi.org/10.1016/j.ygeno.2014.08.019.

Irvine, Gemma I., and Wickliffe C. Abraham. 2005. "Enriched Environment Exposure Alters the Input-Output Dynamics of Synaptic Transmission in Area CA1 of Freely Moving Rats." Neuroscience Letters 391 (1): 32–37. https://doi.org/10.1016/j.neulet.2005.08.031.

Jia, Guifang, Ye Fu, Xu Zhao, Qing Dai, Guanqun Zheng, Ying Yang, Chengqi Yi, et al. 2011. "N6-Methyladenosine in Nuclear RNA Is a Major Substrate of the Obesity-Associated FTO." Nature Chemical Biology 7 (12): 885–87. https://doi.org/10.1038/nchembio.687.

Jiang, Jie, Bowen Song, Kunqi Chen, Zhiliang Lu, Rong Rong, Yu Zhong, and Jia Meng. 2021. "M6AmPred: Identifying RNA N6, 2′-O-Dimethyladenosine (M6Am) Sites Based on Sequence-Derived Information." Methods, February. https://doi.org/10.1016/j.ymeth.2021.01.007.

Jiang, Lulu, Weiwei Lin, Cheng Zhang, Peter E. A. Ash, Mamta Verma, Julian Kwan, Emily van Vliet, et al. 2021. "Interaction of Tau with HNRNPA2B1 and N6-Methyladenosine RNA Mediates the Progression of Tauopathy." Molecular Cell 81 (20): 4209-4227.e12. https://doi.org/10.1016/j.molcel.2021.07.038.

Kempermann, Gerd, H. Georg Kuhn, and Fred H. Gage. 1997. "More Hippocampal Neurons in Adult Mice Living in an Enriched Environment." Nature 386 (6624): 493–95. https://doi.org/10.1038/386493a0.

Kuzumaki, Naoko, Daigo Ikegami, Rie Tamura, Nana Hareyama, Satoshi Imai, Michiko Narita, Kazuhiro Torigoe, et al. 2011. "Hippocampal Epigenetic Modification at the Brain-Derived Neurotrophic Factor Gene Induced by an Enriched Environment." Hippocampus 21 (2): 127–32. https://doi.org/10.1002/hipo.20775.

Lazarov, Orly, John Robinson, Ya-Ping Tang, Ilana S. Hairston, Zeljka Korade-Mirnics, Virginia M. -Y. Lee, Louis B. Hersh, Robert M. Sapolsky, Karoly Mirnics, and Sangram S. Sisodia. 2005. "Environmental Enrichment Reduces Aβ Levels and Amyloid Deposition in Transgenic Mice." Cell 120 (5): 701–13. https://doi.org/10.1016/j.cell.2005.01.015.

Li, Heng, Bob Handsaker, Alec Wysoker, Tim Fennell, Jue Ruan, Nils Homer, Gabor Marth, Goncalo Abecasis, Richard Durbin, and 1000 Genome Project Data Processing Subgroup. 2009. "The Sequence Alignment/Map Format and SAMtools." Bioinformatics 25 (16): 2078–79. https://doi.org/10.1093/bioinformatics/btp352.

Liao, Yang, Gordon K. Smyth, and Wei Shi. 2013. "The Subread Aligner: Fast, Accurate and Scalable Read Mapping by Seed-and-Vote." Nucleic Acids Research 41 (10): e108. https://doi.org/10.1093/nar/gkt214.

Linder, Bastian, Anya V. Grozhik, Anthony O. Olarerin-George, Cem Meydan, Christopher E. Mason, and Samie R. Jaffrey. 2015. "Single-Nucleotide-Resolution Mapping of M6A and M6Am throughout the Transcriptome." Nature Methods 12 (8): 767–72. https://doi.org/10.1038/nmeth.3453.

Liu, Jun'e, Kai Li, Jiabin Cai, Mingchang Zhang, Xiaoting Zhang, Xushen Xiong, Haowei Meng, et al. 2020. "Landscape and Regulation of M6A and M6Am Methylome across Human and Mouse Tissues." Molecular Cell 77 (2): 426-440.e6. https://doi.org/10.1016/j.molcel.2019.09.032.

Livneh, Ido, Sharon Moshitch-Moshkovitz, Ninette Amariglio, Gideon Rechavi, and Dan Dominissini. 2020. "The M6A Epitranscriptome: Transcriptome Plasticity in Brain Development and Function." Nature Reviews. Neuroscience 21 (1): 36–51. https://doi.org/10.1038/s41583-019-0244-z.

Love, Michael I., Wolfgang Huber, and Simon Anders. 2014. "Moderated Estimation of Fold Change and Dispersion for RNA-Seq Data with DESeq2." Genome Biology 15 (12): 550. https://doi.org/10.1186/s13059-014-0550-8.

Martin, Marcel. 2011. "Cutadapt Removes Adapter Sequences from High-Throughput Sequencing Reads." EMBnet.Journal 17 (1): 10–12. https://doi.org/10.14806/ej.17.1.200.

Mauer, Jan, and Samie R. Jaffrey. 2018. "FTO, M6Am, and the Hypothesis of Reversible Epitranscriptomic MRNA Modifications." FEBS Letters 592 (12): 2012–22. https://doi.org/10.1002/1873-3468.13092.

Meng, Jia, Xiaodong Cui, Manjeet K. Rao, Yidong Chen, and Yufei Huang. 2013. "Exome-Based Analysis for RNA Epigenome Sequencing Data." Bioinformatics 29 (12): 1565–67. https://doi.org/10.1093/bioinformatics/btt171.

Merkurjev, Daria, Wan-Ting Hong, Kei Iida, Ikumi Oomoto, Belinda J. Goldie, Hitoshi Yamaguti, Takayuki Ohara, et al. 2018. "Synaptic N6-Methyladenosine (M6A) Epitranscriptome Reveals Functional Partitioning of Localized Transcripts." Nature Neuroscience 21 (7): 1004–14. https://doi.org/10.1038/s41593-018-0173-6.

Meyer, Kate D., and Samie R. Jaffrey. 2017. "Rethinking M6A Readers, Writers, and Erasers." Annual Review of Cell and Developmental Biology 33 (1): 319–42. https://doi.org/10.1146/annurev-cellbio-100616-060758.

Meyer, Kate D., Deepak P. Patil, Jun Zhou, Alexandra Zinoviev, Maxim A. Skabkin, Olivier Elemento, Tatyana V. Pestova, Shu-Bing Qian, and Samie R. Jaffrey. 2015. "5′ UTR M6A Promotes Cap-Independent Translation." Cell 163 (4): 999–1010. https://doi.org/10.1016/j.cell.2015.10.012.

Meyer, Kate D., Yogesh Saletore, Paul Zumbo, Olivier Elemento, Christopher E. Mason, and Samie R. Jaffrey. 2012. "Comprehensive Analysis of MRNA Methylation Reveals

Enrichment in 3' UTRs and near Stop Codons." Cell 149 (7): 1635–46. https://doi.org/10.1016/j.cell.2012.05.003.

Mora, Francisco. 2013. "Successful Brain Aging: Plasticity, Environmental Enrichment, and Lifestyle." Dialogues in Clinical Neuroscience 15 (1): 45–52.

Ohline, S. M., and W. C. Abraham. 2019. "Environmental Enrichment Effects on Synaptic and Cellular Physiology of Hippocampal Neurons." Neuropharmacology 145 (Pt A): 3–12. https://doi.org/10.1016/j.neuropharm.2018.04.007.

Ramírez, Fidel, Devon P Ryan, Björn Grüning, Vivek Bhardwaj, Fabian Kilpert, Andreas S Richter, Steffen Heyne, Friederike Dündar, and Thomas Manke. 2016. "DeepTools2: A next Generation Web Server for Deep-Sequencing Data Analysis." Nucleic Acids Research 44 (W1): W160–65. https://doi.org/10.1093/nar/gkw257.

Risso, Davide, John Ngai, Terence P. Speed, and Sandrine Dudoit. 2014. "Normalization of RNA-Seq Data Using Factor Analysis of Control Genes or Samples." Nature Biotechnology 32 (9): 896–902. https://doi.org/10.1038/nbt.2931.

Robinson, James T., Helga Thorvaldsdóttir, Wendy Winckler, Mitchell Guttman, Eric S. Lander, Gad Getz, and Jill P. Mesirov. 2011. "Integrative Genomics Viewer." Nature Biotechnology 29 (1): 24–26. https://doi.org/10.1038/nbt.1754.

Saletore, Yogesh, Kate Meyer, Jonas Korlach, Igor D. Vilfan, Samie Jaffrey, and Christopher E. Mason. 2012. "The Birth of the Epitranscriptome: Deciphering the Function of RNA Modifications." Genome Biology 13 (10): 175. https://doi.org/10.1186/gb-2012-13-10-175.

Schindelin, Johannes, Ignacio Arganda-Carreras, Erwin Frise, Verena Kaynig, Mark Longair, Tobias Pietzsch, Stephan Preibisch, et al. 2012. "Fiji: An Open-Source Platform for Biological-Image Analysis." Nature Methods 9 (7): 676–82. https://doi.org/10.1038/nmeth.2019.

Sendinc, Erdem, David Valle-Garcia, Abhinav Dhall, Hao Chen, Telmo Henriques, Jose Navarrete-Perea, Wanqiang Sheng, Steven P. Gygi, Karen Adelman, and Yang Shi. 2019. "PCIF1 Catalyzes M6Am MRNA Methylation to Regulate Gene Expression." Molecular Cell 75 (3): 620-630.e9. https://doi.org/10.1016/j.molcel.2019.05.030.

Shafik, Andrew M., Feiran Zhang, Zhenxing Guo, Qing Dai, Kinga Pajdzik, Yangping Li, Yunhee Kang, et al. 2021. "N6-Methyladenosine Dynamics in Neurodevelopment and Aging, and Its Potential Role in Alzheimer's Disease." Genome Biology 22 (1): 17. https://doi.org/10.1186/s13059-020-02249-z.

Shannon, Paul, Andrew Markiel, Owen Ozier, Nitin S. Baliga, Jonathan T. Wang, Daniel Ramage, Nada Amin, Benno Schwikowski, and Trey Ideker. 2003. "Cytoscape: A Software Environment for Integrated Models of Biomolecular Interaction Networks." Genome Research 13 (11): 2498–2504. https://doi.org/10.1101/gr.1239303.

Shen, Li. 2019. "GeneOverlap: An R Package to Test and Visualize Gene Overlaps," 10.

Shi, Hailing, Xuliang Zhang, Yi-Lan Weng, Zongyang Lu, Yajing Liu, Zhike Lu, Jianan Li, et al. 2018. "M6A Facilitates Hippocampus-Dependent Learning and Memory through YTHDF1." Nature 563 (7730): 249–53. https://doi.org/10.1038/s41586-018-0666-1.

Sievert, Carson. 2019. Interactive Web-Based Data Visualization with R, Plotly, and Shiny. https://plotly-r.com/.

Sourdet, Valérie, Michaël Russier, Gaël Daoudal, Norbert Ankri, and Dominique Debanne. 2003. "Long-Term Enhancement of Neuronal Excitability and Temporal Fidelity Mediated by Metabotropic Glutamate Receptor Subtype 5." The Journal of Neuroscience 23 (32): 10238–48. https://doi.org/10.1523/JNEUROSCI.23-32-10238.2003.

Sun, Hanxiao, Kai Li, Xiaoting Zhang, Jun'e Liu, Meiling Zhang, Haowei Meng, and Chengqi Yi. 2021. "M6Am-Seq Reveals the Dynamic M6Am Methylation in the Human Transcriptome." Nature Communications 12 (1): 4778. https://doi.org/10.1038/s41467-021-25105-5.

Team, R. Core. 2013. "R: A Language and Environment for Statistical Computing."

Valero, Jorge, Judit España, Arnaldo Parra-Damas, Elsa Martín, José Rodríguez-Álvarez, and Carlos A. Saura. 2011. "Short-Term Environmental Enrichment Rescues Adult Neurogenesis and Memory Deficits in APPSw,Ind Transgenic Mice." PLOS ONE 6 (2): e16832. https://doi.org/10.1371/journal.pone.0016832.

Walters, Brandon J., Valentina Mercaldo, Colleen J. Gillon, Matthew Yip, Rachael L. Neve, Frederick M. Boyce, Paul W. Frankland, and Sheena A. Josselyn. 2017. "The Role of The RNA Demethylase FTO (Fat Mass and Obesity-Associated) and MRNA Methylation in Hippocampal Memory Formation." Neuropsychopharmacology: Official Publication of the American College of Neuropsychopharmacology 42 (7): 1502–10. https://doi.org/10.1038/npp.2017.31.

Wang, Xiao, Boxuan Simen Zhao, Ian A. Roundtree, Zhike Lu, Dali Han, Honghui Ma, Xiaocheng Weng, Kai Chen, Hailing Shi, and Chuan He. 2015. "N6-Methyladenosine Modulates Messenger RNA Translation Efficiency." Cell 161 (6): 1388–99. https://doi.org/10.1016/j.cell.2015.05.014.

Wei, Jiangbo, Fange Liu, Zhike Lu, Qili Fei, Yuxi Ai, P. Cody He, Hailing Shi, et al. 2018. "Differential M6A, M6Am, and M1A Demethylation Mediated by FTO in the Cell Nucleus and Cytoplasm." Molecular Cell 71 (6): 973-985.e5. https://doi.org/10.1016/j.molcel.2018.08.011.

Weng, Yi-Lan, Xu Wang, Ran An, Jessica Cassin, Caroline Vissers, Yuanyuan Liu, Yajing Liu, et al. 2018. "Epitranscriptomic M6A Regulation of Axon Regeneration in the Adult Mammalian Nervous System." Neuron 97 (2): 313-325.e6. https://doi.org/10.1016/j.neuron.2017.12.036.

Wickham, Hadley. 2009. "Introduction." In Ggplot2: Elegant Graphics for Data Analysis, edited by Hadley Wickham, 1–7. Use R. New York, NY: Springer. https://doi.org/10.1007/978-0-387-98141-3_1.

Widagdo, Jocelyn, and Victor Anggono. 2018. "The M6A-Epitranscriptomic Signature in Neurobiology: From Neurodevelopment to Brain Plasticity." Journal of Neurochemistry 147 (2): 137–52. https://doi.org/10.1111/jnc.14481.

Yang, Ying, Phillip J. Hsu, Yu-Sheng Chen, and Yun-Gui Yang. 2018. "Dynamic Transcriptomic M6A Decoration: Writers, Erasers, Readers and Functions in RNA Metabolism." Cell Research 28 (6): 616–24. https://doi.org/10.1038/s41422-018-0040-8.

Zalcman, Gisela, Noel Federman, and Arturo Romano. 2018. "CaMKII Isoforms in Learning and Memory: Localization and Function." Frontiers in Molecular Neuroscience 11 (December): 445. https://doi.org/10.3389/fnmol.2018.00445.

Zeng, Yong, Shiyan Wang, Shanshan Gao, Fraser Soares, Musadeqque Ahmed, Haiyang Guo, Miranda Wang, et al. 2018. "Refined RIP-Seq Protocol for Epitranscriptome Analysis with Low Input Materials." PLOS Biology 16 (9): e2006092. https://doi.org/10.1371/journal.pbio.2006092.

Zhang, Wei, Yang Qian, and Guifang Jia. 2021. "The Detection and Functions of RNA Modification M6A Based on M6A Writers and Erasers." Journal of Biological Chemistry 297 (2). https://doi.org/10.1016/j.jbc.2021.100973.

Zhang, Zeyu, Meng Wang, Dongfang Xie, Zenghui Huang, Lisha Zhang, Ying Yang, Dongxue Ma, et al. 2018. "METTL3-Mediated N6-Methyladenosine MRNA Modification Enhances Long-Term Memory Consolidation." Cell Research 28 (11): 1050–61. https://doi.org/10.1038/s41422-018-0092-9.

Discussion

Discussion

Since the discovery of the dynamic nature of N[6]-methyladenosine just a decade ago, it has become abundantly clear that the m[6]A is a key RNA modification, controlling multiple mechanisms for the regulation of gene expression and cellular function in a wide variety of contexts (Jia et al. 2011; C. Yang et al. 2020). More recently, changes in m[6]A have been implicated in the process of memory formation, consolidation and recall, ushering in a rush to deepen our knowledge of the mechanisms laying up- and downstream from m[6]A function in the CNS (Livneh et al. 2020; Widagdo, Wong, and Anggono 2021). The relationship between the epitranscriptome and memory and cognition represents an intriguing avenue for research, particularly in the search for novel pathways that could allow us to target cognitive deficits associated with natural processes like aging, or pathologies like neurodegenerative diseases.

It is in this context that I set out to describe the epitranscriptome changes that occur in connection with age- and AD- associated cognitive impairment. This was done with the aim of finding possible commonalities in the epitranscriptome of both models and, therefore, shed some light on the molecular mechanisms involved in m[6]A-mediated changes in brain function. In addition, to better understand the intricacies of the link between m[6]A modifications and cognition, I also studied the changes that occurred in a model of enhanced cognition: environmental enrichment.

Establishing a novel protocol for the processing of low-input samples for meRIP-seq

There are several hurdles that in the past have hindered our ability to fully understand the complexities of m[6]A across species, tissues and cellular states. The first one was financial: large-scale, unbiased analyses of the epitranscriptome involve the generation of large amounts of data by next generation sequencing (meRIP-Seq), that could be prohibitively expensive for many groups to perform adequately (Sboner et al. 2011). With the advent of more affordable and efficient high-throughput sequencing and consumables, this is mostly a problem of the past and the production of high-quality datasets with sufficient biological insights is more achievable than ever. Another major obstacle in epitranscriptomic research is the large amounts of biologic material needed

to conduct an experiment. The most widely used protocols would call for very large RNA amounts, limiting much of the research to cell lines and large animal tissues (Dominissini et al. 2012; Meyer et al. 2012; Batista et al. 2014). Given the low availability and comparatively small yield of human samples – particularly brain tissue – unbiased approaches for epitranscriptomic analysis on this kind of samples were very limited. In recent years, some groups have published protocols that make it possible to perform meRIP-seq and similar experiments starting from very limited amounts of biological material, taking advantage of newer technologies for library synthesis (Zeng et al. 2018; Weng et al. 2018).

It was, therefore, the first aim during my doctorate to work on establishing and testing a working protocol for low input meRIP-Seq, that could allow me to address more complex questions regarding the role of m^6A in human pathology, from postmortem brain samples.

After multiple rounds of troubleshooting and validation, I was able to streamline a pipeline for the processing and analysis of samples for meRIP-Seq, starting from very low input amounts. With as little as 150 ng of rRNA-depleted RNA - equivalent to a starting amount of around 5 µg, instead of the more than 100 µg needed before - I was able to generate a high quality dataset, with comparative read coverage and depth to the previously used protocol (Berulava et al. 2020). From the resulting data, a similar amount of m^6A peaks could be detected as with the previous protocol, with a strong enrichment of the m^6A consensus motif and m^6A peaks following the characteristic distribution along mRNA features.

These results make this protocol equivalent with the previously used one and with other low-input protocols published, requiring only a fraction of the input amount and making it possible to adequately process human patient samples with sufficient replication (Zeng et al. 2018). Additionally, using this new protocol, it is possible to considerably reduce the time and cost needed for meRIP-seq experiments performed in mice, by drastically decreasing the number of individuals needed without compromising the quality of the resulting data. Besides the meRIP-seq performed on human AD and mouse EE samples presented in this work, this protocol has been successfully used in multiple other human and mice samples with satisfactory results.

The role of m^{6}A modifications in aging and neurodegeneration

The importance of mRNA modifications in the regulation of gene expression has moved to the forefront of research in the last few years and from these, the function of N^6-methyladenosine has become the most widely studied. Thanks to the broad consequences of m^{6}A on mRNA metabolism and function, its roles across biological processes are far-reaching and the total scope processes dependent on m^{6}A regulation, as well as the downstream mechanisms determining the outcomes for labeled transcripts are still not fully understood (Meyer and Jaffrey 2017; Y. Yang et al. 2018).

In the brain, m^{6}A function has been proven to be key for cognition, acting as a subtle modulator of mRNA and protein availability during memory formation, consolidation and recall (Walters et al. 2017; Engel et al. 2018; Koranda et al. 2018, 3; Z. Zhang et al. 2018, 3; Shi et al. 2018). Combined with the dynamic nature of this mark and the potential for pharmacological targeting of m^{6}A-associated components, this has made epitranscriptomic research a field of particular interest within molecular neuroscience (Yankova et al. 2021; Moroz-Omori et al. 2021). In light of the importance of m^{6}A-mediated regulation of proper CNS function, the second aim of my doctorate was to evaluate the epitranscriptomic landscape during processes involving impaired cognitive function: aging and neurodegeneration.

Using a dataset previously generated in the laboratory, I performed methylation analyses on young and old samples from different brain regions, to build on previous observations with a focus on the mechanistic aspect downstream of m^{6}A. The results show that m^{6}A-labeled mRNAs in the adult hippocampus are very strongly enriched for genes associated with the regulation of synaptic function and plasticity, mainly located in postsynaptic compartments. This enrichment holds true for all hippocampal subregions, with a very considerable overlap between the populations of labeled transcripts in the CA1, CA3 and DG. These results go in accordance with previously published works that have shown the strong enrichment of m^{6}A in synaptically located or synaptic function mRNA in different brain regions (Chang et al. 2017; Shi et al. 2018; Merkurjev et al. 2018).

The individual processing of the distinct hippocampal regions allowed us to observe the subtle differences in their epitranscriptome landscapes, and how differences in cellular

composition and function can affect m^{6}A targeting. Despite many works containing hippocampal data, this represents the first time that we are able to further dissect the contribution of the distinct subregions to the bulk hippocampal epitranscriptome.

This tissue and cell type specificity was further evidenced by the marked differences in methylated transcripts between the ACC and the hippocampus, two more distantly related brain regions at the structural and functional level. By looking at the overlap in methylated transcript populations between these regions, it became apparent that many of them were commonly methylated across all of them. These overlapping mRNAs showed once more a key involvement in the regulation of synaptic signaling, whereas tissue-specific methylation is associated with transcriptional regulation and RNA metabolism.

Although the methylated transcripts differ between brain subregions, the location of m^{6}A marks remained mostly identical with the ACC showing a small decrease in m^{6}A frequency near the stop codon and increased location towards the 5' UTR. These small differences in location might hint towards distinct downstream effects of m^{6}A on labeled transcripts. m^{6}A at the 5' UTR is known, for example, to promote translation of labeled transcripts through a cap-independent pathway (Meyer et al. 2015).

These results stress the importance of tissue and cell type specificity in m^{6}A regulation, made possible by the unique modulation of known multiple upstream and downstream elements of the m^{6}A machinery. This tissue specificity has been described for broad brain regions, like the cerebellum, cortex, hypothalamus and hippocampus, where the epitranscriptome displays high variability in the populations of methylated transcripts as well as the location of m^{6}A marks (Chang et al. 2017; Ma et al. 2018). They theorize specific methylated transcripts are involved in the regulation of tissue-specific transcriptional programs, particularly during development (Chang et al. 2017; Jun'e Liu et al. 2020). These results go in line with our observations, showing region-specific m^{6}A-dependent regulation of transcription and RNA metabolism. Furthermore, given that I can also observe considerable epitranscriptome specificity in hippocampal subregions, it would appear that the level of regulation for methylated populations is very high. In the future, it will be of great interest to further investigate the contribution of distinct cellular identities, cellular states, as well as the connectivity among them to the overall epitranscriptome in a given tissue.

Some studies have shown significant conservation of m^{6}A modifications between mouse and human in a variety of tissues, but the comparisons have thus far been broad in scope (Jun'e Liu et al. 2020; Shafik et al. 2021). Our results show that between the human CC and mouse ACC - two distinct but homologous brain regions (Heukelum et al. 2020) - a significant degree of conservation can be observed, not only in which transcripts were labeled by m^{6}A but also in the location of said methylation marks. The level of conservation that I observe between the ACC and CC is of similar magnitude to what previous studies reported in the cortex and cerebellum, showing that this degree of conservation could be more or less constant throughout the brain (Jun'e Liu et al. 2020).

Intriguingly, the regulation of synaptic function and plasticity is a key process that is strongly conserved across species. Moreover, these conserved transcripts show a very strong enrichment for synaptically located transcripts. Although the propensity of synaptically-located transcripts to be preferentially methylated is well known (Merkurjev et al. 2018), the degree of conservation of said modulation in humans is still not well understood. These findings shed more light on the importance of synaptic m^{6}A across species and can help make a case for translational studies seeking to target cognitive phenotypes therapeutically.

During aging, the onset of mild cognitive impairment represents a hallmark of the transition between normal aging and pathology and in mice, the first signs of impairment can be detected already by 16 months of age (Belblidia et al. 2018; Islam et al. 2021). I looked at the epitranscriptomic landscape of the previously described brain regions at this age and compared them to that of young mice to determine whether changes in m^{6}A corresponded to the onset of age-associated cognitive impairment. A general and dramatic decrease in methylation across multiple transcripts could be observed in all brain regions, with exclusively hypomethylated transcripts making up the bulk of the observed differential methylation. Unsurprisingly, the most affected pathways related to the regulation of synaptic plasticity and neural development. Tissue specificity was made more evident in the differential methylation analysis, as many region-specific changes could be detected and the overlap between hippocampal subregions and the ACC was limited. These results show that different brain regions undergo distinct changes during aging, but the overall pathways affected by m^{6}A changes remain similar.

Only one other group has sought out to see the relationship between aging and m^{6}A levels, as well as the conservation of m^{6}A marks in humans (Shafik et al. 2021). In their work, published during the final stages of this project, mild and non-significant changes in aging could be detected, hinting towards a discrete increase in methylation marks in mice at 12 months of age and aged humans. The differences between their observations and the results presented here could be due to the different ages of studied mice (12 months vs. 16 months) as well as the differences in tissues analyzed. Looking at the subregion specificity in the hippocampus, for example, it is possible that changes in the CA1, CA3 and DG could be confounded when looking at epitranscriptomic changes in the hippocampus as a whole.

The known involvement of m^{6}A in brain function and its emerging role as an important regulator of synaptic function, in addition to our results showing widespread changes in the epitranscriptome during aging, raise the question of whether m^{6}A could also be involved in neurodegenerative or psychiatric disorders (J. Yu, She, and Ji 2021). This role of m^{6}A has been hinted at in previous studies and some have found a direct relationship between the function of the m^{6}A machinery and brain pathology (Choudhry et al. 2013; Milaneschi et al. 2014; Angelova et al. 2018). Moreover, during the final stages of this research multiple works were published addressing the possible relationship between AD and gross m^{6}A changes (M. Han et al. 2020; He Huang et al. 2020; F. Zhao et al. 2021; Deng et al. 2021; Shafik et al. 2021). But to date, no publications have used unbiased sequencing-based approaches to show the changes that the epitranscriptome undergoes during AD. Given the difficulty to access patient brain samples and the limited material that can generally be obtained from them, performing meRIP-Seq analyses on them was in many cases not possible.

Making use of the newly established low-input meRIP-Seq protocol, I studied the epitranscriptomic changes in a small group of late-stage AD patients with the aim of finding the main processes targeted by AD onset. Of particular interest was to address whether common downstream effectors of m^{6}A changes exist in the cognitively impaired brain as a consequence of aging or neurodegeneration.

The AD brain showed significant changes in methylation, with the majority of them being hypomethylation. When compared to all the hypomethylated peaks in the aged ACC, striking similarities could be found in the pathways covered by the targeted transcripts in both aging and AD. Among them, the regulation of synaptic plasticity, particularly

long-term potentiation, as well as multiple neurodegeneration-associated pathways were strongly affected. The calcium/calmodulin-dependent protein kinase II (CaMKII) is one of such transcripts undergoing m^6A changes in both aging and AD. Given its pivotal role in the modulation of plasticity in response to activity, regulatory changes in multiple isoforms of this protein could have strong consequences for cognitive function (Lisman, Schulman, and Cline 2002; Zalcman, Federman, and Romano 2018).

As of the writing of this text, a few studies have very recently delved into the link between epitranscriptome changes and AD. One of them observed a strong decrease in the levels of the main m^6A methyltransferase METTL3 in the hippocampus of AD patients at the mRNA and protein level, which would likely translate to lower m^6A levels (He Huang et al. 2020). Studies undertaken in mouse models of AD make clear the complexity of m^6A regulation in AD lending support to some of my observations and contradicting others. APP/PS1 mice showed an increase in global m^6A levels accompanied by increased METTL3 expression and decreased FTO (M. Han et al. 2020). Interestingly, changes in m^6A at the transcript level were mixed. In contrast, 5XFAD mice showed the opposite results, with Mettl3 levels decreased and Fto increased at both the mRNA and protein levels (Zhao et al. 2021). In the case of these mice, AD-associated transcripts showed a significant decrease in m^6A levels (Shafik et al. 2021). Another recent study looked at global m^6A levels in the brains of AD patients and found a trend towards increased m^6A as the disease progresses, but no data was available that looked at m^6A levels at the transcript level, and their global m^6A data was based in fluorescence-based assays (Deng et al. 2021). Additionally, their data in an AD mouse model showed a significant decrease in m^6A levels of disease-associated transcripts, something that would go along the lines of our observations in AD patients.

Mechanistically, several options are possible for the downstream effects of reduced m^6A levels observed in aging and AD, due to the known roles of m^6A regulation in mRNA processing, transport, stability and translation (Y. Yang et al. 2018). Synaptosome sequencing showed no differential transport or stability in synaptic compartments of methylated transcripts in the aged mouse hippocampus, despite the role that m^6A plays in the partitioning of transcripts to these sites. Moreover, polysome sequencing showed mild changes in translation during aging but, once more, with no correlation with the observed methylation changes. It is known that, while somatic translation is polysome-dependent, local translation away from the neuronal soma occurs preferentially in

monosomes and not polysomes (Biever et al. 2020). Performing monosome isolation and sequencing could further clarify whether local translation is the mechanism responsible for defects in synaptic plasticity in aged mice *in vivo*.

The local translation of synaptic transcripts away from the neuronal soma is a well-known phenomenon that ensures the supply of key proteins necessary for synaptic function and plasticity in response to stimuli (Biever, Donlin-Asp, and Schuman 2019; Hafner et al. 2019). The function of m^6A as a regulator of LPS has been shown in the axons of dorsal root ganglia neurons (J. Yu et al. 2018) and since then has been theorized in other contexts but so far, this link has not been experimentally proven (Leonetti et al. 2020). Our results show that a reduction in m^6A caused by a decrease in *Mettl3* expression, akin to the reductions observed during aging and AD, significantly impact the rate of protein synthesis of the plasticity regulator CaMKII in or in the vicinity of synaptic compartments, away from the soma. This reduced synaptic synthesis is independent of global changes in CaMKII's translation rate or the localization of its mRNA to synaptic compartments, supporting the idea that it is local translation that is affected in this case.

These observations add a key piece to the puzzle of the mechanisms behind the local translational regulation of methylated transcripts at the synapse and in response to stimuli that has been put forward by previous studies (Widagdo and Anggono 2018; Leonetti et al. 2020; Widagdo, Wong, and Anggono 2021). For instance, the demethylase FTO was shown to locate at the synapse and its levels decrease during learning (Walters et al. 2017). The m^6A reader YTHDF1 is also located in synaptic compartments and its protein levels significantly increase following fear conditioning in the hippocampus (Shi et al. 2018). The knockdowns of *Mettl3* and *Ythdf1* are known to negatively affect spine formation, long-term potentiation, and learning in a hippocampus-dependent manner (Shi et al. 2018; Z. Zhang et al. 2018). Furthermore, during memory formation YTHDF1 and METTL3 are associated with changes in translation, albeit only observed in the soma. More recently, the m^6A reader YTHDF3 as well as de eraser ALKBH5 have also been linked to the regulation of m^6A at the synapse, further increasing the possibilities for regulation in such compartments (Martinez De La Cruz et al. 2021).

Our results support the idea of decreased methylation being associated with AD progression. Furthermore, the methylation changes within synaptically located

plasticity-associated transcripts offer a direct link to a possible downstream mechanism that could link AD phenotype with the epitranscriptome. Additional research will be needed to fully comprehend the complex regulatory network involving m^{6}A in neurodegeneration. Studies focusing on larger patient datasets to look at the epitranscriptome changes at different stages of AD progression will be key in improving our understanding of this relationship.

This data also adds to the known function of m^{6}A, its writers, readers, and erasers in regulating learning and memory, showing the importance of m^{6}A for synaptic LPS and its relationship with decreased methylation of synaptic genes during aging and neurodegeneration. The downstream mechanism is not yet known but one can speculate, based on their known function and localization, that synaptically located YTHDF1, YTHDF3, METLL3, ALKBH5 or FTO could be playing an important role, in an activity-dependent manner. This is not to say that other proteins, mainly readers, could very well be involved in regulating translation directly or indirectly, via processes like degradation, transport or phase separation (Ries et al. 2019; S.-Y. Liu et al. 2020). More research will be needed to further confirm our observations, particularly in an *in vivo* model, to broaden our knowledge of the depth and importance of LPS in the context of learning and memory in both mice and humans.

m^{6}A changes following environmental enrichment

My analyses show that m^{6}A undergoes significant decrease in both aging and AD, suggesting a link between m^{6}A functions and age- and AD-associated cognitive impairment. To deepen our knowledge of the relationship between m^{6}A modifications and cognitive function, I set out to analyze the effect that a model of enhanced cognition has on the m^{6}A epitranscriptome. By looking at both impaired as well as enhanced cognition, my aim was to find the commonly affected pathways and mechanisms in both of these conditions to be able to draw a more general model of the epitranscriptomic regulation of cognitive function.

I used an EE paradigm that previously showed a consistent enhancement of synaptic transmission (10 weeks continuous EE), with both complex environmental stimuli and access to exercise (Benito et al. 2018). This combination is generally considered to bolster the effects of either a complex environment or exercise individually (Grégoire et

al. 2018) and previous studies on similar cohorts showed limited changes at the gene expression and epigenetic levels (Hüttenrauch, Salinas, and Wirths 2016; T.-Y. Zhang et al. 2018; Ohline and Abraham 2019). Additionally, to date, no studies have been published that address the possible relationship between enhanced cognition following EE exposure and m^{6}A function. In the same vein as previous works and my own observations in aging and AD, I set out to explore whether epitranscriptome changes could be detected preceding larger changes in gene expression and function following EE.

The m^{6}A landscape in the CA1 of both control HC and EE mice draws multiple parallels to the hippocampal and CA1 epitranscriptome in young mice from chapter 1. The distribution of methylation marks, populations of methylated transcripts and the locations of m^{6}A peaks showed strong similarities. Interestingly, both HC and EE samples displayed a small enrichment of m^{6}A peaks at the 5' end of the CDS and the 5' UTR. This could be explained by the use of different protocols for meRIP-Seq and library preparations between these samples, which are known to better preserve read information at the 5' end (Jun'e Liu et al. 2020). Indeed, other datasets prepared with similar protocols show a small enrichment of reads in these positions (Zeng et al. 2018; Jun'e Liu et al. 2020). Another possibility is the known cross-reactivity of the used m^{6}A antibody with the related RNA methylation m^{6}Am, which could have been enhanced by the UV cross-linking that these samples underwent. m^{6}Am displays a characteristic distribution in mRNAs with a strong enrichment at the 5' UTR, close to the 5' Cap (Linder et al. 2015).

The results of the differential methylation analysis show that EE causes considerable changes in the methylation level of more than 850 transcripts. As in is the case during aging and AD, pathways associated with the regulation of synaptic transmission and plasticity were affected, albeit with a less significant enrichment. Surprisingly, the directionality of these changes was not the opposite of what is observed in aging and AD, and the most strongly affected transcripts overwhelmingly displayed hypomethylation. Moreover, these strongly hypomethylated transcripts displayed a particular distribution pattern with a strong enrichment at the 5' end of the CDS and the 5' UTR.

This decrease does not appear to stem from changes in the methylation machinery, given that the m^{6}A writers *Mettl3*, *Mettl14* and *Wtap*, as well as the erasers *Fto* and

Alkbh5 displayed no changes in expression. Additionally, no global decrease in m⁶A levels could be observed, showing that the hypomethylation observed in these transcripts was not due to a general decrease in m⁶A marks.

m⁶A is well known to modulate several cellular processes affecting RNA metabolism, from processing to transport, stability and translation (Meyer and Jaffrey 2017; Y. Yang et al. 2018). However, in the context of neuronal function and its relationship with learning and memory, m⁶A seems to function preferentially though the regulation of protein synthesis and, to a lesser degree, mRNA transport (Widagdo et al. 2016; Shi et al. 2018; Merkurjev et al. 2018; Engel et al. 2018). Once more taking advantage of the observations of methylation changes during aging and AD, I decided to first explore how this reduction in m⁶A following EE could affect protein levels. I used synaptosomal preparations to evaluate the protein levels of the highly hypomethylated transcripts Dusp8 and Kcnn1, both of which displayed significant increases.

DUSP8 is a phosphatase involved in the regulation of MAPK signaling, a key pathway involved in several cellular processes, including synaptic plasticity (Thomas and Huganir 2004; Ding et al. 2019). The absence of Dusp8 has strong consequences for brain function and structure, and mice lacking this protein display impaired memory performance and decreased brain size (Baumann et al. 2019). In addition to this, Dusp8 can be found in synaptic mRNA datasets and is known to localize to synaptic compartments preferentially in response to stimulation (Cajigas et al. 2012; Epple et al. 2021). The potassium channel KCNN1 is a synaptic protein, essential for the afterhyperpolarization of postsynaptic regions in response to stimulus. With other members of the SK family of channels, KCNN1 can control and prevent the induction of LTP, assisting in establishing the delicate balance of potentiation and depression needed to conserve synaptic plasticity (Ris et al. 2007; Autuori et al. 2019). The increase in these proteins as a consequence of decreased m⁶A levels in their transcripts following exposure to EE could be a result of the long-term maintenance of enhanced plasticity and depend on the continued synthesis of proteins in the vicinity of synaptic compartments.

In addition to hypomethylated transcripts, the m⁶A reader FTO also could be detected in synaptosomes where it displayed increased protein levels. FTO has been previously shown to locate at the synapse and it can directly affect the process of memory formation and consolidation, however the way it achieves it is still debated (Walters et

al. 2017). In contrast to FTO, the m^6A reader YTHDF1, the main reader involved in the regulation of translation, showed no change in its synaptic levels. This showed that not all methylation-related proteins undergo changes in synaptic localization following EE, although it is known that many of them do localize to synaptic compartments under basal conditions (Merkurjev et al. 2018; Shi et al. 2018). Nevertheless, the increase in FTO at the synapse could be a mechanism through which m^6A levels could be reduced in a subset of largely synaptically located transcripts. Exploring the changes in localization of other members of the methylation machinery to the synapse in response to EE could help us better understand how m^6A levels can be regulated in this context.

Generally, methylation levels correlate positively with the translation rate of a given transcript (X. Wang et al. 2015). In my observations of m^6A changes following EE, this seems to not be the case. The readers YTHDF1 and 3, as well as eIF3 can promote translation by binding at distinct regions of methylated mRNAs (the former two at the 3' UTR and CDS, the latter at the 5' UTR; X. Wang et al. 2015; Meyer et al. 2015). But there is another reader whose function represses translation, although its role in m^6A regulation is still not well understood: FMR1 (F. Zhang et al. 2018). This protein is a well-known translational repressor, linked with several neuropsychiatric disorders, that works by regulating the local protein synthesis (LPS) of several mRNAs at the synapse (Laggerbauer et al. 2001; Sidorov, Auerbach, and Bear 2013). FMR1 binds preferentially m^6A consensus sequences, with a preference for the 3' UTR and CDS, but also the 5' UTR inhibiting their translation (Ascano et al. 2012). It is thought that the competitive binding between FMR1 and YTHDF1 controls the translation rate of methylated transcripts, particularly in distal locations (Edupuganti et al. 2017). This possibility will need to be addressed in the future, to further understand how the changes in m^6A can translate to increased protein levels and enhanced plasticity.

It is worth noting, given the location of changes observed and the consequences for protein levels, that another mRNA modification could be responsible for the observed effects of EE. m^6Am is a closely related mark that is located almost exclusively at the 5' end of transcripts close to the 5'cap and UTR (Linder et al. 2015). It is a lot less abundant than m^6A, making up 0.02–0.04% of the total adenosines in mRNA, and a lot less is known about the machinery surrounding its function (Jun'e Liu et al. 2020). m^6Am marks are deposited by the writer PCIF1 and they can be removed by the activity of FTO, with some works theorizing that it is actually m^6Am and not m^6A that is the substrate of FTO

demethylation (Wei et al. 2018; Mauer and Jaffrey 2018; Sendinc et al. 2019; Boulias et al. 2019). The presence of m[6]Am marks can negatively regulate translation by inhibiting cap-dependent translation, so decreases in this mark could negatively affect protein levels (Sendinc et al. 2019). So far, no direct methods exist to study m[6]Am and they depend on the cross-reactivity of m[6]A antibodies and focusing on its 5' location. The development of novel techniques to overcome this limitations in the future could help us better understand the mechanisms at play during EE.

Although long EE protocols are known to enhance cognition and plasticity, shorter (< 4 weeks) or periodic (only for a limited period in any given day) protocols display stronger increases in synaptic transmission and plasticity (Eckert and Abraham 2013; Ohline and Abraham 2019). Given the length of EE exposure, in many cases the changes in plasticity undergo a long-term dampening that can mask some short-term changes in synaptic function (Eckert, Bilkey, and Abraham 2010; Eckert and Abraham 2013). Although a short (2 weeks) continuous exposure to EE did not display significant improvements in contextual or spatial learning (Appendix Figure 5), other studies have reported significant structural changes in the brain of these animals, including increased volume and gene expression changes, independent from classical transcriptional programs (T.-Y. Zhang et al. 2018; Vousden et al. 2018). Therefore, it would be of great interest to compare shorter, periodic EE protocols and analyze the hippocampal epitranscriptomic state of these mice to find commonalities and differences with the results obtained thus far.

Appendix

Appendix

Approved symbol	Approved name	Alias symbol	Previous name
ALKBH5	alkB homolog 5, RNA demethylase	FLJ20308	AlkB family member 5, RNA demethylase
APC	APC regulator of WNT signaling pathway	DP2	adenomatosis polyposis coli
BDNF	brain derived neurotrophic factor		neurotrophin
CAMK2A	calcium/calmodulin dependent protein kinase II alpha	CaMKIIα	calcium/calmodulin-dependent protein kinase (CaM kinase) II alpha
CAMK2B	calcium/calmodulin dependent protein kinase II beta	CaMKIIβ	calcium/calmodulin-dependent protein kinase (CaM kinase) II beta
CBLL1	Cbl proto-oncogene like 1	HAKAI	Cas-Br-M (murine) ecotropic retroviral transforming sequence-like 1
CCR4	C-C motif chemokine receptor 4	CC-CKR-4	chemokine (C-C motif) receptor 4
CNOT6	CCR4-NOT transcription complex subunit 6	CCR4	CCR4-NOT transcription complex, subunit 6
DGCR8	DGCR8 microprocessor complex subunit	DGCRK6	DiGeorge syndrome critical region gene 8
DLG4	discs large MAGUK scaffold protein 4	PSD95	
DUSP8	dual specificity phosphatase 8	HVH-5	chromosome 11 open reading frame 81
DUSP3	dual specificity phosphatase 3		
EIF3A	eukaryotic translation initiation factor 3 subunit A	eIF3-theta	eukaryotic translation initiation factor 3, subunit 10 theta0/170kDa
ELAVL1	ELAV like RNA binding protein 1	HuR	ELAV (embryonic lethal, abnormal vision, Drosophila)-like 1 (Hu antigen R)
FMR1	FMRP translational regulator 1	FMRP	fragile X mental retardation 1
FTO	FTO alpha-ketoglutarate dependent dioxygenase	KIAA1752	fat mass and obesity associated
GPRIN1	G protein regulated inducer of neurite outgrowth 1	GRIN1	
GRIN1	glutamate ionotropic receptor NMDA type subunit 1	GluN1	N-methyl-D-aspartate receptor subunit NR1
GRM1	glutamate metabotropic receptor 1	MGLUR1	protein phosphatase 1, regulatory subunit 85
HNRNPA2B1	heterogeneous nuclear ribonucleoprotein A2/B1		
HNRNPC	heterogeneous nuclear ribonucleoprotein C		heterogeneous nuclear ribonucleoprotein C (C1/C2)
IGF2BP1	insulin like growth factor 2 mRNA binding protein 1	IMP-1	insulin-like growth factor 2 mRNA binding protein 1
IGF2BP2	insulin like growth factor 2 mRNA binding protein 2	IMP-2	insulin-like growth factor 2 mRNA binding protein 2

IGF2BP3	insulin like growth factor 2 mRNA binding protein 3	IMP-3	insulin-like growth factor 2 mRNA binding protein 3
KCNJ3	potassium inwardly rectifying channel subfamily J member 3	GIRK1	G protein-activated inward rectifier potassium channel 1
KCNN1	potassium calcium-activated channel subfamily N member 1	hSK1	potassium intermediate/small conductance calcium-activated channel, subfamily N, member 1
MAP2	microtubule associated protein 2	MAP2A	
METTL14	methyltransferase 14, N6-adenosine-methyltransferase subunit	KIAA1627	methyltransferase like 14
METTL3	methyltransferase 3, N6-adenosine-methyltransferase complex catalytic subunit	Spo8	methyltransferase like 3
NFX1	nuclear transcription factor, X-box binding 1	NFX2	
PCIF1	phosphorylated CTD interacting factor 1	bA465L10.1	chromosome 20 open reading frame 67
RBM15	RNA binding motif protein 15	OTT	one twenty-two
SLC17A6	solute carrier family 17 member 6	VGLUT2	vesicular glutamate transporter 2
SLC17A7	solute carrier family 17 member 7	VGLUT1	vesicular glutamate transporter 1
SLC17A8	solute carrier family 17 member 8	VGLUT3	vesicular glutamate transporter 3
SRSF10	serine and arginine rich splicing factor 10	TASR1	FUS-interacting protein (serine-arginine rich) 2
SRSF3	serine and arginine rich splicing factor 3	SRp20	splicing factor, arginine/serine-rich 3
VASN	vasorin		slit-like 2 (Drosophila)
VIRMA	vir like m6A methyltransferase associated	DKFZP434I116	KIAA1429
WTAP	WT1 associated protein	KIAA0105	Wilms tumor 1 associated protein
XIST	X inactive specific transcript	NCRNA00001	X (inactive)-specific transcript
YTHDC1	YTH domain containing 1	YT521	
YTHDC2	YTH domain containing 2	FLJ2194	
YTHDF1	YTH N6-methyladenosine RNA binding protein 1	FLJ20391	YTH domain family 1
YTHDF2	YTH N6-methyladenosine RNA binding protein 2	HGRG8	YTH domain family 2
YTHDF3	YTH N6-methyladenosine RNA binding protein 3	FLJ31657	YTH domain family 3
ZC3H13	zinc finger CCCH-type containing 13	DKFZp434D1812	KIAA0853

Appendix table 1. Gene symbols, names and aliases mentioned throughout the text

ENSEMBL ID	Name	Description
ENSMUSG00000001911	Nfix	nuclear factor I/X
ENSMUSG00000002341	Ncan	neurocan
ENSMUSG00000004110	Cacna1e	calcium channel, voltage-dependent, R type, alpha 1E subunit
ENSMUSG00000008604	Ubqln4	ubiquilin 4
ENSMUSG00000013033	Adgrl1	adhesion G protein-coupled receptor L1
ENSMUSG00000015599	Ttbk1	tau tubulin kinase 1
ENSMUSG00000018547	Pip4k2b	phosphatidylinositol-5-phosphate 4-kinase, type II, beta
ENSMUSG00000020387	Jade2	jade family PHD finger 2
ENSMUSG00000022594	Lynx1	Ly6/neurotoxin 1
ENSMUSG00000023460	Rab12	RAB12, member RAS oncogene family
ENSMUSG00000024736	Tmem132a	transmembrane protein 132A
ENSMUSG00000024737	Slc15a3	solute carrier family 15, member 3
ENSMUSG00000031517	Gpm6a	glycoprotein m6a
ENSMUSG00000033960	Jcad	junctional cadherin 5 associated
ENSMUSG00000034912	Mdga2	MAM domain containing glycosylphosphatidylinositol anchor 2
ENSMUSG00000035226	Rims4	regulating synaptic membrane exocytosis 4
ENSMUSG00000037032	Apbb1	amyloid beta (A4) precursor protein-binding, family B, member 1
ENSMUSG00000037541	Shank2	SH3 and multiple ankyrin repeat domains 2
ENSMUSG00000038248	Sobp	sine oculis binding protein
ENSMUSG00000038429	Usp5	ubiquitin specific peptidase 5 (isopeptidase T)
ENSMUSG00000039477	Tnrc18	trinucleotide repeat containing 18
ENSMUSG00000040721	Zfhx2	zinc finger homeobox 2
ENSMUSG00000040761	Spen	spen family transcription repressor
ENSMUSG00000041037	Irgq	immunity-related GTPase family, Q
ENSMUSG00000041417	Pik3r1	phosphoinositide-3-kinase regulatory subunit 1
ENSMUSG00000042066	Tmcc2	transmembrane and coiled-coil domains 2
ENSMUSG00000045009	Prrt3	proline-rich transmembrane protein 3
ENSMUSG00000045374	Wdr81	WD repeat domain 81
ENSMUSG00000047013	Fbxo41	F-box protein 41
ENSMUSG00000059213	Ddn	dendrin
ENSMUSG00000068748	Ptprz1	protein tyrosine phosphatase, receptor type Z, polypeptide 1
ENSMUSG00000075478	Slitrk1	SLIT and NTRK-like family, member 1
ENSMUSG00000097767	Miat	myocardial infarction associated transcript (non-protein coding)

Appendix table 2. Transcripts commonly hypomethylated in the ACC and hippocampus of aged mice

ENSEMBL ID	Name	Description
ENSMUSG00000003360	Ddx23	DEAD box helicase 23
ENSMUSG00000009741	Ubp1	upstream binding protein 1
ENSMUSG00000010803	Gabra1	gamma-aminobutyric acid (GABA) A receptor, subunit alpha 1
ENSMUSG00000017639	Rab11fip4	RAB11 family interacting protein 4 (class II)
ENSMUSG00000019362	D8Ertd738e	DNA segment, Chr 8, ERATO Doi 738, expressed
ENSMUSG00000020152	Actr2	ARP2 actin-related protein 2
ENSMUSG00000020647	Ncoa1	nuclear receptor coactivator 1
ENSMUSG00000020705	Ddx42	DEAD box helicase 42
ENSMUSG00000020817	Rabep1	rabaptin, RAB GTPase binding effector protein 1
ENSMUSG00000020882	Cacnb1	calcium channel, voltage-dependent, beta 1 subunit
ENSMUSG00000020964	Sel1l	sel-1 suppressor of lin-12-like (C. elegans)
ENSMUSG00000024002	Brd4	bromodomain containing 4
ENSMUSG00000024109	Nrxn1	neurexin I
ENSMUSG00000024576	Csnk1a1	casein kinase 1, alpha 1
ENSMUSG00000025220	Oga	O-GlcNAcase
ENSMUSG00000025261	Huwe1	HECT, UBA and WWE domain containing 1
ENSMUSG00000028053	Ash1l	ASH1 like histone lysine methyltransferase
ENSMUSG00000028565	Nfia	nuclear factor I/A
ENSMUSG00000029245	Epha5	Eph receptor A5
ENSMUSG00000030213	Atf7ip	activating transcription factor 7 interacting protein
ENSMUSG00000030216	Wbp11	WW domain binding protein 11
ENSMUSG00000030397	Mark4	MAP/microtubule affinity regulating kinase 4
ENSMUSG00000030852	Tacc2	transforming, acidic coiled-coil containing protein 2
ENSMUSG00000034158	Lrrc58	leucine rich repeat containing 58
ENSMUSG00000034525	Ice1	interactor of little elongation complex ELL subunit 1
ENSMUSG00000034832	Tet3	tet methylcytosine dioxygenase 3
ENSMUSG00000034850	Tmem127	transmembrane protein 127
ENSMUSG00000035152	Ap2b1	adaptor-related protein complex 2, beta 1 subunit
ENSMUSG00000038143	Stox2	storkhead box 2
ENSMUSG00000038170	Pde4dip	phosphodiesterase 4D interacting protein (myomegalin)
ENSMUSG00000038495	Otud7b	OTU domain containing 7B
ENSMUSG00000038664	Herc1	HECT and RLD domain containing E3 ubiquitin protein ligase family member 1
ENSMUSG00000039952	Dag1	dystroglycan 1
ENSMUSG00000043909	Trp53bp1	transformation related protein 53 binding protein 1
ENSMUSG00000044708	Kcnj10	potassium inwardly-rectifying channel, subfamily J, member 10
ENSMUSG00000045515	Pou3f3	POU domain, class 3, transcription factor 3

ENSMUSG00000046876	Atxn1	ataxin 1
ENSMUSG00000047747	Rnf150	ring finger protein 150
ENSMUSG00000048874	Phf3	PHD finger protein 3
ENSMUSG00000051403	Ppp1r37	protein phosphatase 1, regulatory subunit 37
ENSMUSG00000055053	Nfic	nuclear factor I/C
ENSMUSG00000055430	Nap1l5	nucleosome assembly protein 1-like 5
ENSMUSG00000056342	Usp34	ubiquitin specific peptidase 34
ENSMUSG00000061578	Ksr2	kinase suppressor of ras 2
ENSMUSG00000066232	Ipo7	importin 7
ENSMUSG00000068267	Cenpb	centromere protein B
ENSMUSG00000068923	Syt11	synaptotagmin XI
ENSMUSG00000074505	Fat3	FAT atypical cadherin 3
ENSMUSG00000075318	Scn2a	sodium channel, voltage-gated, type II, alpha
ENSMUSG00000085438	Oip5os1	Opa interacting protein 5, opposite strand 1
ENSMUSG00000090061	Nwd2	NACHT and WD repeat domain containing 2
ENSMUSG00000094410	Zbed6	zinc finger, BED type containing 6
ENSMUSG00000098557	Kctd12	potassium channel tetramerisation domain containing 12
ENSMUSG00000102697	Pcdhac2	protocadherin alpha subfamily C, 2

Appendix table 3. Transcripts commonly hypomethylated exclusively in the hippocampus of aged mice
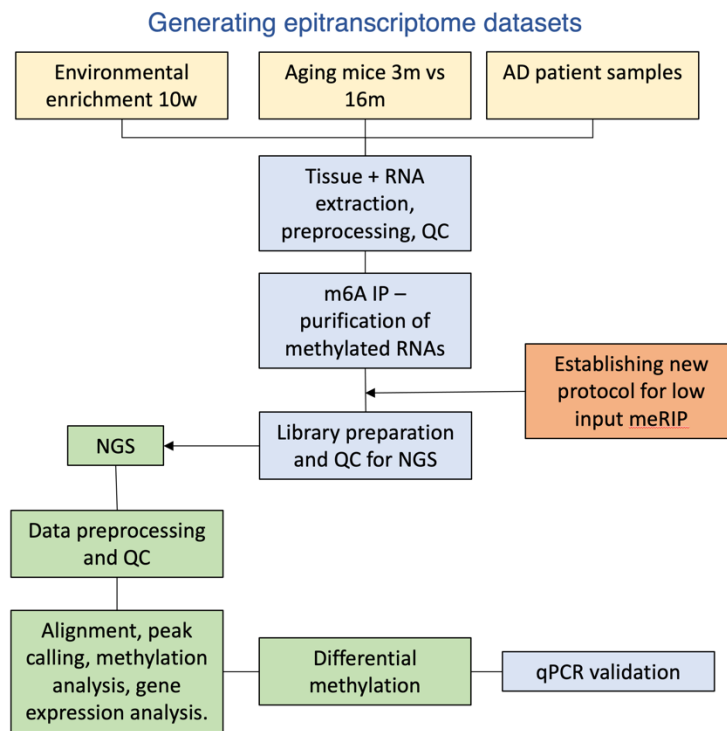
Appendix Figure 1. Workflow for the generation of epitranscriptome datasets. Details the steps taken from sample isolation, meRIP, sequencing to bioinformatic analyses. Blue denotes wet lab work, green is dry lab work. QC – quality control, NGS – next-generation sequencing.
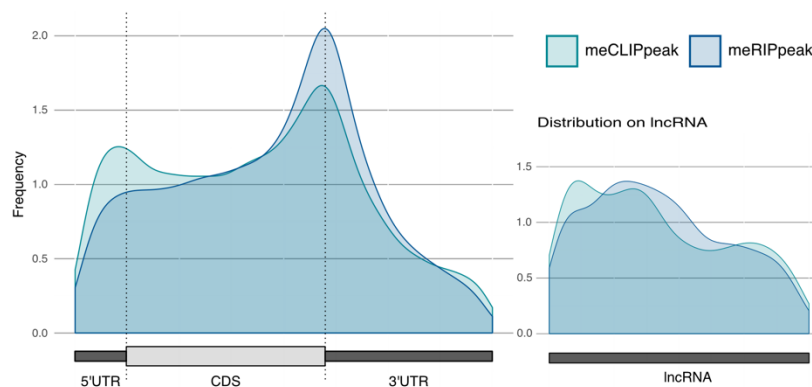
Appendix Figure 2. m6A distribution in meRIP and meCLIP. Distribution of m6A peaks along transcripts (left) and ncRNAs (right) in samples prepared for meRIP-seq or for meCLIP. 5' UTR – 5' untranslatd region, CDS – coding sequence, 3' UTR – 3' untranslated region
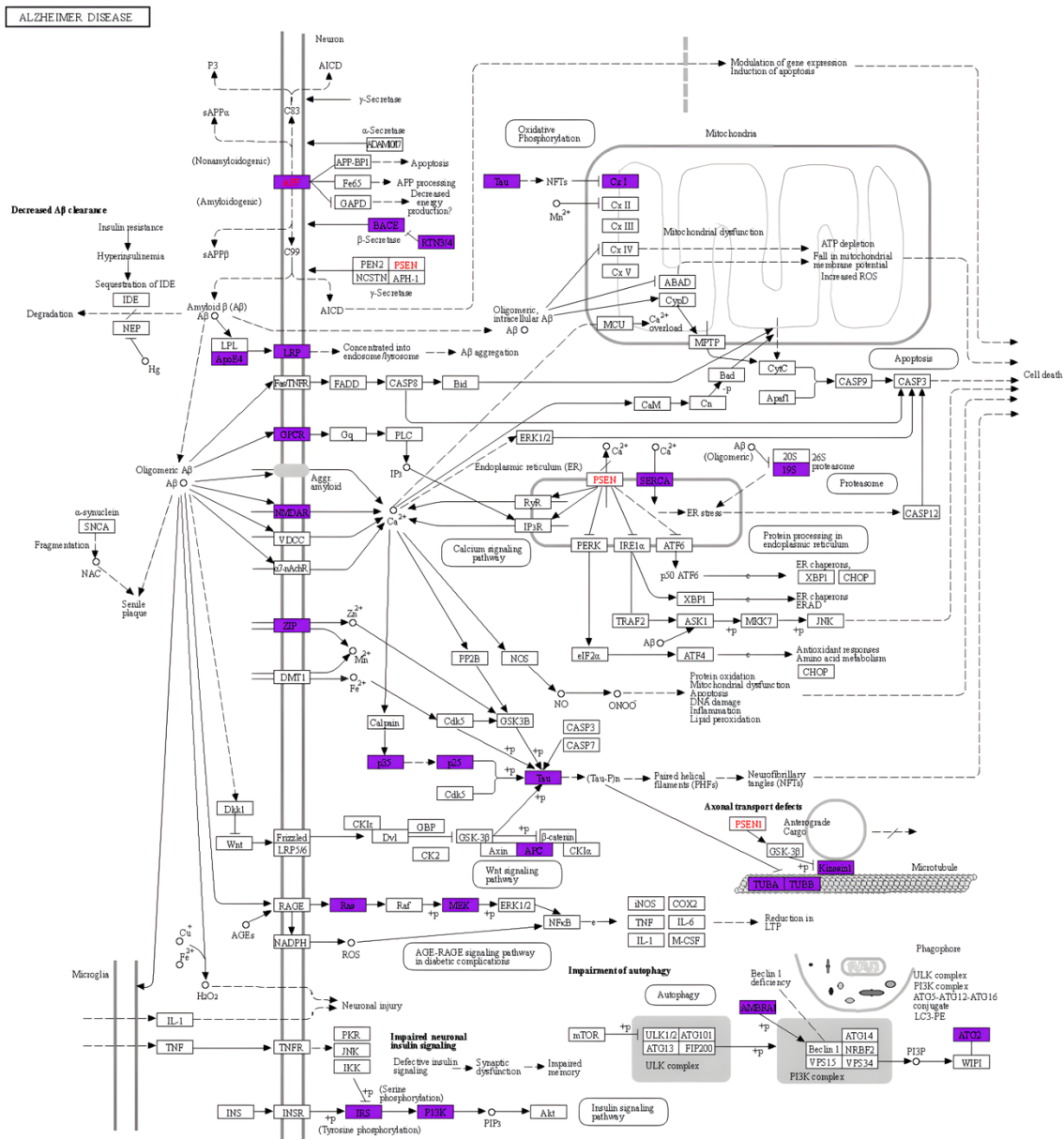
Appendix Figure 3. Pathways in AD. KEGG pathway Alzheimer's Disease (hsa05010), showing the major molecular patways involved in disease onset and progression. In red text are marked elements whose mutations are known to cause AD. In purple are highlighted elements of the pathways that are commonly hypomethylated in the aged ACC and the CC of AD patients.
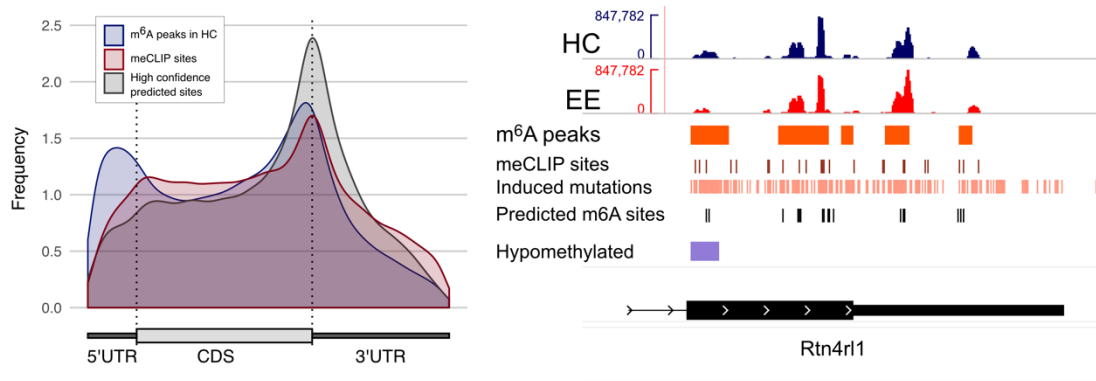
Appendix Figure 4. Approaches to determine m6A sites. Left: Guitar plot showing the distribution along transcripts of: m6A peaks (blue), detected meCLIP sites (red), and m^{6}A sites predicted by a deep learning algorithm (Deepm6A, black) in samples from HC mice. Right: Read coverage tracks showing the 3' region of Rtn4rl1. Little overlap is found between different methods to determine m^{6}A sites. Detected m^{6}A peaks are shown in orange, meCLIP sites, falling on DRACH motifs along the transcript are shown in red, while the total number of detected mutations is highlighted in pink, predicted m6A sites are shown in black, a hypomethylated region is in purple.
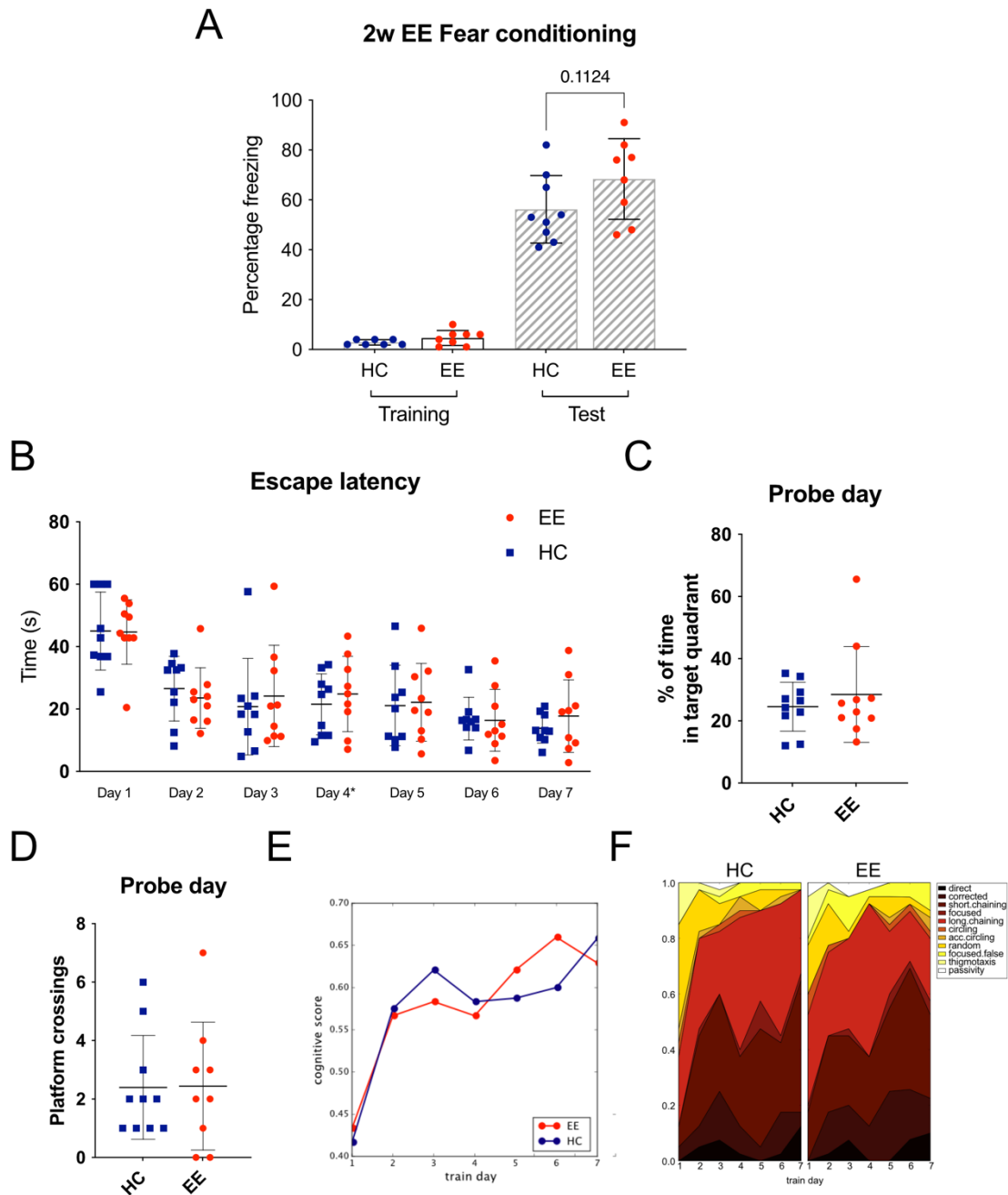
Appendix Figure 5. Behavioral tests in mice after 2 weeks EE. A. Effects on contextual memory, measured by fear conditioning. No significant difference is found between enriched mice when compared to controls on test day, following fear conditioning. B. Effects of EE on spatial learning measured by Morris Water Maze. Escape latency plotted during training days. C-F. No significant difference is found in spatial learning between EE and HC mice, measured by (C) percentage of time in target quadrant, (D) platform crossings, or (E, F) strategies used to find the platform, determined by machine learning.

References

References

Abraham, W. C., S. E. Mason-Parker, G. I. Irvine, B. Logan, and A. I. Gill. 2006. "Induction and Activity-Dependent Reversal of Persistent LTP and LTD in Lateral Perforant Path Synapses in Vivo." *Neurobiology of Learning and Memory* 86 (1): 82–90. https://doi.org/10.1016/j.nlm.2005.12.007.

Abraham, Wickliffe C., Owen D. Jones, and David L. Glanzman. 2019. "Is Plasticity of Synapses the Mechanism of Long-Term Memory Storage?" *Npj Science of Learning* 4 (1): 1–10. https://doi.org/10.1038/s41539-019-0048-y.

Abraham, Wickliffe C., Barbara Logan, Jeffrey M. Greenwood, and Michael Dragunow. 2002. "Induction and Experience-Dependent Consolidation of Stable Long-Term Potentiation Lasting Months in the Hippocampus." *Journal of Neuroscience* 22 (21): 9626–34. https://doi.org/10.1523/JNEUROSCI.22-21-09626.2002.

Adhikari, Samir, Wen Xiao, Yong-Liang Zhao, and Yun-Gui Yang. 2016. "M6A: Signaling for MRNA Splicing." *RNA Biology* 13 (9): 756–59. https://doi.org/10.1080/15476286.2016.1201628.

Akyuz, Enes, and Ece Eroglu. 2021. "Envisioning the Crosstalk between Environmental Enrichment and Epilepsy: A Novel Perspective." Epilepsy & Behavior 115 (February). https://doi.org/10.1016/j.yebeh.2020.107660.

Alarcón, Claudio R., Hani Goodarzi, Hyeseung Lee, Xuhang Liu, Saeed Tavazoie, and Sohail F. Tavazoie. 2015. "HNRNPA2B1 Is a Mediator of M6A-Dependent Nuclear RNA Processing Events." *Cell* 162 (6): 1299–1308. https://doi.org/10.1016/j.cell.2015.08.011.

Alarcón, Claudio R., Hyeseung Lee, Hani Goodarzi, Nils Halberg, and Sohail F. Tavazoie. 2015. "N6-Methyladenosine Marks Primary MicroRNAs for Processing." *Nature* 519 (7544): 482–85. https://doi.org/10.1038/nature14281.

Alwis, Dasuni S., and Ramesh Rajan. 2014. "Environmental Enrichment and the Sensory Brain: The Role of Enrichment in Remediating Brain Injury." Frontiers in Systems Neuroscience 8. https://www.frontiersin.org/article/10.3389/fnsys.2014.00156.Alzheimer, A. 1907. "Uber Eine Eigenartige Erkrankung Der Hirnrinde." *Zentralbl. Nervenh. Psych.* 18: 177–79.

Amaral, D. G., and M. P. Witter. 1989. "The Three-Dimensional Organization of the Hippocampal Formation: A Review of Anatomical Data." *Neuroscience* 31 (3): 571–91. https://doi.org/10.1016/0306-4522(89)90424-7.

Anders, Maximilian, Irina Chelysheva, Ingrid Goebel, Timo Trenkner, Jun Zhou, Yuanhui Mao, Silvia Verzini, Shu-Bing Qian, and Zoya Ignatova. 2018. "Dynamic M6A Methylation Facilitates MRNA Triaging to Stress Granules." *Life Science Alliance* 1 (4). https://doi.org/10.26508/lsa.201800113.

Angelova, Margarita T., Dilyana G. Dimitrova, Nadja Dinges, Tina Lence, Lina Worpenberg, Clément Carré, and Jean-Yves Roignant. 2018. "The Emerging Field of Epitranscriptomics in Neurodevelopmental and Neuronal Disorders." *Frontiers in Bioengineering and Biotechnology* 6: 46. https://doi.org/10.3389/fbioe.2018.00046.

Arbel-Ornath, Michal, Eloise Hudry, Josiah R. Boivin, Tadafumi Hashimoto, Shuko Takeda, Kishore V. Kuchibhotla, Steven Hou, et al. 2017. "Soluble Oligomeric Amyloid-β Induces Calcium Dyshomeostasis That Precedes Synapse Loss in the Living Mouse Brain." *Molecular Neurodegeneration* 12 (1): 27. https://doi.org/10.1186/s13024-017-0169-9.

Arguello, A. Emilia, Amanda N. DeLiberto, and Ralph E. Kleiner. 2017. "RNA Chemical Proteomics Reveals the N6-Methyladenosine (M6A)-Regulated Protein-RNA Interactome." *Journal of the American Chemical Society* 139 (48): 17249–52. https://doi.org/10.1021/jacs.7b09213.

Arriagada, Paulina V., John H. Growdon, E. Tessa Hedley-Whyte, and Bradley T. Hyman. 1992. "Neurofibrillary Tangles but Not Senile Plaques Parallel Duration and Severity of

Alzheimer's Disease." *Neurology* 42 (3): 631–631. https://doi.org/10.1212/WNL.42.3.631.

Arszovszki, Antónia, Zsolt Borhegyi, and Thomas Klausberger. 2014. "Three Axonal Projection Routes of Individual Pyramidal Cells in the Ventral CA1 Hippocampus." *Frontiers in Neuroanatomy* 8: 53. https://doi.org/10.3389/fnana.2014.00053.

Ascano, Manuel, Neelanjan Mukherjee, Pradeep Bandaru, Jason B. Miller, Jeff Nusbaum, David L. Corcoran, Christine Langlois, et al. 2012. "FMR1 Targets Distinct MRNA Sequence Elements to Regulate Protein Expression." *Nature* 492 (7429): 382–86. https://doi.org/10.1038/nature11737.

Atlasi, Yaser, and Hendrik G. Stunnenberg. 2017. "The Interplay of Epigenetic Marks during Stem Cell Differentiation and Development." *Nature Reviews. Genetics* 18 (11): 643–58. https://doi.org/10.1038/nrg.2017.57.

Autuori, Eleonora, Petra Sedlak, Li Xu, Margreet C. Ridder, Angelo Tedoldi, and Pankaj Sah. 2019. "RSK1 in Rat Neurons: A Controller of Membrane RSK2?" *Frontiers in Neural Circuits* 13. https://www.frontiersin.org/article/10.3389/fncir.2019.00021.

Bae, Sang-Hun, Han Wool Kim, SeoJeong Shin, Joopyung Kim, Yun-Hwa Jeong, and Jisook Moon. 2018. "Decipher Reliable Biomarkers of Brain Aging by Integrating Literature-Based Evidence with Interactome Data." *Experimental & Molecular Medicine* 50 (4): 1–15. https://doi.org/10.1038/s12276-018-0057-6.

Balacco, Dario L., and Matthias Soller. 2019. "The M6A Writer: Rise of a Machine for Growing Tasks." *Biochemistry* 58 (5): 363–78. https://doi.org/10.1021/acs.biochem.8b01166.

Bassell, Gary J., and Stephen T. Warren. 2008. "Fragile X Syndrome: Loss of Local MRNA Regulation Alters Synaptic Development and Function." *Neuron* 60 (2): 201–14. https://doi.org/10.1016/j.neuron.2008.10.004.

Batista, Pedro J., Benoit Molinie, Jinkai Wang, Kun Qu, Jiajing Zhang, Lingjie Li, Donna M. Bouley, et al. 2014. "M(6)A RNA Modification Controls Cell Fate Transition in Mammalian Embryonic Stem Cells." *Cell Stem Cell* 15 (6): 707–19. https://doi.org/10.1016/j.stem.2014.09.019.

Baumann, Peter, Sonja C. Schriever, Stephanie Kullmann, Annemarie Zimprich, Annette Feuchtinger, Oana Amarie, Andreas Peter, et al. 2019. "Dusp8 Affects Hippocampal Size and Behavior in Mice and Humans." *Scientific Reports* 9 (1): 19483. https://doi.org/10.1038/s41598-019-55527-7.

Bawankar, Praveen, Tina Lence, Chiara Paolantoni, Irmgard U. Haussmann, Migle Kazlauskiene, Dominik Jacob, Jan B. Heidelberger, et al. 2021. "Hakai Is Required for Stabilization of Core Components of the M6A MRNA Methylation Machinery." *Nature Communications* 12 (1): 3778. https://doi.org/10.1038/s41467-021-23892-5.

Belblidia, Hassina, Marianne Leger, Abdelouadoud Abdelmalek, Anne Quiedeville, Floriane Calocer, Michel Boulouard, Christelle Jozet-Alves, Thomas Freret, and Pascale Schumann-Bard. 2018. "Characterizing Age-Related Decline of Recognition Memory and Brain Activation Profile in Mice." *Experimental Gerontology* 106 (June): 222–31. https://doi.org/10.1016/j.exger.2018.03.006.

Benito, Eva, Cemil Kerimoglu, Binu Ramachandran, Tonatiuh Pena-Centeno, Gaurav Jain, Roman Manuel Stilling, Md Rezaul Islam, et al. 2018. "RNA-Dependent Intergenerational Inheritance of Enhanced Synaptic Plasticity after Environmental Enrichment." *Cell Reports* 23 (2): 546–54. https://doi.org/10.1016/j.celrep.2018.03.059.

Benne, Rob, and Dave Speijer. 1998. "RNA Editing Types and Characteristics." In *Modification and Editing of RNA*, 551–53. John Wiley & Sons, Ltd. https://doi.org/10.1128/9781555818296.app2.

Berson, Amit, Raffaella Nativio, Shelley L. Berger, and Nancy M. Bonini. 2018. "Epigenetic Regulation in Neurodegenerative Diseases." *Trends in Neurosciences* 41 (9): 587–98. https://doi.org/10.1016/j.tins.2018.05.005.

Berulava, Tea, Eric Buchholz, Vakhtang Elerdashvili, Tonatiuh Pena, Md Rezaul Islam, Dawid Lbik, Belal A. Mohamed, et al. 2020. "Changes in M6A RNA Methylation Contribute to Heart Failure Progression by Modulating Translation." *European Journal of Heart Failure* 22 (1): 54–66. https://doi.org/10.1002/ejhf.1672.

Biever, Anne, Paul G. Donlin-Asp, and Erin M. Schuman. 2019. "Local Translation in Neuronal Processes." *Current Opinion in Neurobiology* 57 (August): 141–48. https://doi.org/10.1016/j.conb.2019.02.008.

Biever, Anne, Caspar Glock, Georgi Tushev, Elena Ciirdaeva, Tamas Dalmay, Julian D. Langer, and Erin M. Schuman. 2020. "Monosomes Actively Translate Synaptic MRNAs in Neuronal Processes." *Science*, January. https://doi.org/10.1126/science.aay4991.

Bird, Chris M., and Neil Burgess. 2008. "The Hippocampus and Memory: Insights from Spatial Processing." *Nature Reviews Neuroscience* 9 (3): 182–94. https://doi.org/10.1038/nrn2335.

Bliss, T. V. P., and G. L. Collingridge. 1993. "A Synaptic Model of Memory: Long-Term Potentiation in the Hippocampus." *Nature* 361 (6407): 31–39. https://doi.org/10.1038/361031a0.

Bliss, T. V. P., and T. Lømo. 1973. "Long-Lasting Potentiation of Synaptic Transmission in the Dentate Area of the Anaesthetized Rabbit Following Stimulation of the Perforant Path." *The Journal of Physiology* 232 (2): 331–56. https://doi.org/10.1113/jphysiol.1973.sp010273.

Boccaletto, Pietro, Filip Stefaniak, Angana Ray, Andrea Cappannini, Sunandan Mukherjee, Elżbieta Purta, Małgorzata Kurkowska, et al. 2022. "MODOMICS: A Database of RNA Modification Pathways. 2021 Update." *Nucleic Acids Research* 50 (D1): D231–35. https://doi.org/10.1093/nar/gkab1083.

Bokar, J. A., M. E. Rath-Shambaugh, R. Ludwiczak, P. Narayan, and F. Rottman. 1994. "Characterization and Partial Purification of MRNA N6-Adenosine Methyltransferase from HeLa Cell Nuclei. Internal MRNA Methylation Requires a Multisubunit Complex." *The Journal of Biological Chemistry* 269 (26): 17697–704.

Bokar, J. A., M. E. Shambaugh, D. Polayes, A. G. Matera, and F. M. Rottman. 1997. "Purification and CDNA Cloning of the AdoMet-Binding Subunit of the Human MRNA (N6-Adenosine)-Methyltransferase." *RNA (New York, N.Y.)* 3 (11): 1233–47.

Boulias, Konstantinos, Diana Toczydłowska-Socha, Ben R. Hawley, Noa Liberman, Ken Takashima, Sara Zaccara, Théo Guez, et al. 2019. "Identification of the M6Am Methyltransferase PCIF1 Reveals the Location and Functions of M6Am in the Transcriptome." *Molecular Cell* 75 (3): 631-643.e8. https://doi.org/10.1016/j.molcel.2019.06.006.

Bowie, Derek. 2008. "Ionotropic Glutamate Receptors & CNS Disorders." *CNS & Neurological Disorders - Drug Targets- CNS & Neurological Disorders)* 7 (2): 129–43.

Braak, H., and E. Braak. 1991. "Neuropathological Stageing of Alzheimer-Related Changes." *Acta Neuropathologica* 82 (4): 239–59. https://doi.org/10.1007/BF00308809.

Brem, Anna-Katharine, Kathy Ran and Alvaro Pascual-Leone. 2013. "Learning and Memory." Handbook of Clinical Neurology 116: 693–737. https://doi.org/10.1016/B978-0-444-53497-2.00055-3.

Burgin, K. E., M. N. Waxham, S. Rickling, S. A. Westgate, W. C. Mobley, and P. T. Kelly. 1990. "In Situ Hybridization Histochemistry of Ca2+/Calmodulin-Dependent Protein Kinase in Developing Rat Brain." *The Journal of Neuroscience: The Official Journal of the Society for Neuroscience* 10 (6): 1788–98.

Cajal, Santiago Ramón y. 1904. "Textura Del Sistema Nervioso Del Hombre y de Los Vertebrados, 1899–1904." In *Textura Del Sistema Nervioso Del Hombre y de Los Vertebrados, 1899–1904*, 216–19. Princeton University Press. https://doi.org/10.1515/9780691183978-016.

Cajal, Santiago Ramón y, and L. Azoulay. 1894. *Les nouvelles idées sur la structure du système nerveux chez l'homme et chez les vertébrés*. C. Reinwald.

Cajigas, Iván J., Georgi Tushev, Tristan J. Will, Susanne tom Dieck, Nicole Fuerst, and Erin M. Schuman. 2012. "The Local Transcriptome in the Synaptic Neuropil Revealed by Deep Sequencing and High-Resolution Imaging." *Neuron* 74 (3): 453–66. https://doi.org/10.1016/j.neuron.2012.02.036.

Carlile, Thomas M., Maria F. Rojas-Duran, Boris Zinshteyn, Hakyung Shin, Kristen M. Bartoli, and Wendy V. Gilbert. 2014. "Pseudouridine Profiling Reveals Regulated MRNA Pseudouridylation in Yeast and Human Cells." *Nature* 515 (7525): 143–46. https://doi.org/10.1038/nature13802.

Chang, Mengqi, Hongyi Lv, Weilong Zhang, Chunhui Ma, Xue He, Shunli Zhao, Zhi-Wei Zhang, et al. 2017. "Region-Specific RNA M6A Methylation Represents a New Layer of Control in the Gene Regulatory Network in the Mouse Brain." *Open Biology* 7 (9): 170166. https://doi.org/10.1098/rsob.170166.

Charette, Michael, and Michael W. Gray. 2000. "Pseudouridine in RNA: What, Where, How, and Why." *IUBMB Life* 49 (5): 341–51. https://doi.org/10.1080/152165400410182.

Chen, Xuechai, Chunyu Yu, Minjun Guo, Xiaotong Zheng, Sakhawat Ali, Hua Huang, Lihua Zhang, et al. 2019. "Down-Regulation of M6A MRNA Methylation Is Involved in Dopaminergic Neuronal Death." *ACS Chemical Neuroscience* 10 (5): 2355–63. https://doi.org/10.1021/acschemneuro.8b00657.

Cheng, Junmei, Lingling Xu, Liqiang Deng, Lan Xue, Qingmei Meng, Furong Wei, and Jinghua Wang. 2020. "RNA N6-Methyladenosine Modification Is Required for MiR-98/MYCN Axis-Mediated Inhibition of Neuroblastoma Progression." *Scientific Reports* 10 (1): 13624. https://doi.org/10.1038/s41598-020-64682-1.

Choquet, Daniel, and Antoine Triller. 2013. "The Dynamic Synapse." *Neuron* 80 (3): 691–703. https://doi.org/10.1016/j.neuron.2013.10.013.

Choudhry, Zia, Sarojini M. Sengupta, Natalie Grizenko, Geeta A. Thakur, Marie-Eve Fortier, Norbert Schmitz, and Ridha Joober. 2013. "Association between Obesity-Related Gene FTO and ADHD." *Obesity (Silver Spring, Md.)* 21 (12): E738-744. https://doi.org/10.1002/oby.20444.

Collingridge, Graham L., Stephane Peineau, John G. Howland, and Yu Tian Wang. 2010. "Long-Term Depression in the CNS." *Nature Reviews Neuroscience* 11 (7): 459–73. https://doi.org/10.1038/nrn2867.

Cuestas Torres, Diana Marcela, and Fernando P. Cardenas. 2020. "Synaptic Plasticity in Alzheimer's Disease and Healthy Aging." *Reviews in the Neurosciences* 31 (3): 245–68. https://doi.org/10.1515/revneuro-2019-0058.

Cui, Qi, Hailing Shi, Peng Ye, Li Li, Qiuhao Qu, Guoqiang Sun, Guihua Sun, et al. 2017. "M6A RNA Methylation Regulates the Self-Renewal and Tumorigenesis of Glioblastoma Stem Cells." *Cell Reports* 18 (11): 2622–34. https://doi.org/10.1016/j.celrep.2017.02.059.

Cui, Zhenzhong, Charles R. Gerfen, and W. Scott Young 3rd. 2013. "Hypothalamic and Other Connections with Dorsal CA2 Area of the Mouse Hippocampus." *Journal of Comparative Neurology* 521 (8): 1844–66. https://doi.org/10.1002/cne.23263.

Demuro, Angelo, Erene Mina, Rakez Kayed, Saskia C. Milton, Ian Parker, and Charles G. Glabe. 2005. "Calcium Dysregulation and Membrane Disruption as a Ubiquitous Neurotoxic Mechanism of Soluble Amyloid Oligomers *." *Journal of Biological Chemistry* 280 (17): 17294–300. https://doi.org/10.1074/jbc.M500997200.

Deng, Yanyao, Hongwei Zhu, Le Xiao, Chao Liu, Ya-Lin Liu, and Wenzhe Gao. 2021. "Identification of the Function and Mechanism of M6A Reader IGF2BP2 in Alzheimer's Disease." *Aging* 13 (21): 24086–100. https://doi.org/10.18632/aging.203652.

Deupree, David L., Jennifer Bradley, and Dennis A. Turner. 1993. "Age-Related Alterations in Potentiation in the CA1 Region in F344 Rats." *Neurobiology of Aging* 14 (3): 249–58. https://doi.org/10.1016/0197-4580(93)90009-Z.

Ding, Tao, Ya Zhou, Runying Long, Chao Chen, Juanjuan Zhao, Panpan Cui, Mengmeng Guo, Guiyou Liang, and Lin Xu. 2019. "DUSP8 Phosphatase: Structure, Functions, Expression Regulation and the Role in Human Diseases." *Cell & Bioscience* 9 (1): 70. https://doi.org/10.1186/s13578-019-0329-4.

Dominissini, Dan, Sharon Moshitch-Moshkovitz, Mali Salmon-Divon, Ninette Amariglio, and Gideon Rechavi. 2013. "Transcriptome-Wide Mapping of N(6)-Methyladenosine by m(6)A-Seq Based on Immunocapturing and Massively Parallel Sequencing." *Nature Protocols* 8 (1): 176–89. https://doi.org/10.1038/nprot.2012.148.

Dominissini, Dan, Sharon Moshitch-Moshkovitz, Schraga Schwartz, Mali Salmon-Divon, Lior Ungar, Sivan Osenberg, Karen Cesarkas, et al. 2012. "Topology of the Human and Mouse M6A RNA Methylomes Revealed by M6A-Seq." *Nature* 485 (7397): 201–6. https://doi.org/10.1038/nature11112.

Dominissini, Dan, Sigrid Nachtergaele, Sharon Moshitch-Moshkovitz, Eyal Peer, Nitzan Kol, Moshe Shay Ben-Haim, Qing Dai, et al. 2016. "The Dynamic N(1)-Methyladenosine Methylome in Eukaryotic Messenger RNA." *Nature* 530 (7591): 441–46. https://doi.org/10.1038/nature16998.

Drew, Liam. 2018. "An Age-Old Story of Dementia." Nature 559 (7715): S2–3. https://doi.org/10.1038/d41586-018-05718-5.

Du, Tingfu, Shuquan Rao, Lin Wu, Ning Ye, Zeyue Liu, Huiling Hu, Jianbo Xiu, Yan Shen, and Qi Xu. 2015. "An Association Study of the M6A Genes with Major Depressive Disorder in Chinese Han Population." *Journal of Affective Disorders* 183 (September): 279–86. https://doi.org/10.1016/j.jad.2015.05.025.

Dubin, D T, and R H Taylor. 1975. "The Methylation State of Poly A-Containing Messenger RNA from Cultured Hamster Cells." *Nucleic Acids Research* 2 (10): 1653–68.

Duffy, Steven N., Kenneth J. Craddock, Ted Abel, and Peter V. Nguyen. 2001. "Environmental Enrichment Modifies the PKA-Dependence of Hippocampal LTP and Improves Hippocampus-Dependent Memory." *Learning & Memory* 8 (1): 26–34. https://doi.org/10.1101/lm.36301.

Dunn, D. B. 1961. "The Occurrence of 1-Methyladenine in Ribonucleic Acid." *Biochimica Et Biophysica Acta* 46 (January): 198–200. https://doi.org/10.1016/0006-3002(61)90668-0.

Dutta, Sulagna, and Pallav Sengupta. 2016. "Men and Mice: Relating Their Ages." *Life Sciences* 152 (May): 244–48. https://doi.org/10.1016/j.lfs.2015.10.025.

Eckert, Michael J., and Wickliffe C. Abraham. 2013. "Effects of Environmental Enrichment Exposure on Synaptic Transmission and Plasticity in the Hippocampus." *Current Topics in Behavioral Neurosciences* 15: 165–87. https://doi.org/10.1007/7854_2012_215.

Eckert, Michael J., David K. Bilkey, and Wickliffe C. Abraham. 2010. "Altered Plasticity in Hippocampal CA1, But Not Dentate Gyrus, Following Long-Term Environmental Enrichment." *Journal of Neurophysiology* 103 (6): 3320–29. https://doi.org/10.1152/jn.01037.2009.

Edupuganti, Raghu R., Simon Geiger, Rik G. H. Lindeboom, Hailing Shi, Phillip J. Hsu, Zhike Lu, Shuang-Yin Wang, et al. 2017. "N6-Methyladenosine (M6A) Recruits and Repels Proteins to Regulate MRNA Homeostasis." *Nature Structural & Molecular Biology* 24 (10): 870–78. https://doi.org/10.1038/nsmb.3462.

Eikelboom, Willem S., Dirk Bertens, and Roy P. C. Kessels. 2020. "Cognitive Rehabilitation in Normal Aging and Individuals with Subjective Cognitive Decline." In Cognitive Rehabilitation and Neuroimaging: Examining the Evidence from Brain to Behavior, edited by John DeLuca, Nancy D. Chiaravalloti, and Erica Weber, 37–67. Cham: Springer International Publishing. https://doi.org/10.1007/978-3-030-48382-1_3.

Engel, Mareen, Carola Eggert, Paul M. Kaplick, Matthias Eder, Simone Röh, Lisa Tietze, Christian Namendorf, et al. 2018. "The Role of M6A/m-RNA Methylation in Stress Response Regulation." *Neuron* 99 (2): 389-403.e9. https://doi.org/10.1016/j.neuron.2018.07.009.

Epple, Robert, Dennis Krüger, Tea Berulava, Gerrit Brehm, Momchil Ninov, Rezaul Islam, Sarah Köster, and Andre Fischer. 2021. "The Coding and Small Non-Coding Hippocampal Synaptic RNAome." *Molecular Neurobiology* 58 (6): 2940–53. https://doi.org/10.1007/s12035-021-02296-y.

Felice, Fernanda G. De, Pauline T. Velasco, Mary P. Lambert, Kirsten Viola, Sara J. Fernandez, Sergio T. Ferreira, and William L. Klein. 2007. "Aβ Oligomers Induce Neuronal Oxidative Stress through an N-Methyl-D-Aspartate Receptor-Dependent Mechanism That Is Blocked by the Alzheimer Drug Memantine *." *Journal of Biological Chemistry* 282 (15): 11590–601. https://doi.org/10.1074/jbc.M607483200.

Ferraguti, Francesco, and Ryuichi Shigemoto. 2006. "Metabotropic Glutamate Receptors." *Cell and Tissue Research* 326 (2): 483–504. https://doi.org/10.1007/s00441-006-0266-5.

Fischer, Andre. 2016. "Environmental Enrichment as a Method to Improve Cognitive Function. What Can We Learn from Animal Models?" *NeuroImage*, Effects of Physical and Cognitive activity on brain structure and function, 131 (May): 42–47. https://doi.org/10.1016/j.neuroimage.2015.11.039.

Formicola, Nadia, Jeshlee Vijayakumar, and Florence Besse. 2019. "Neuronal Ribonucleoprotein Granules: Dynamic Sensors of Localized Signals." *Traffic (Copenhagen, Denmark)* 20 (9): 639–49. https://doi.org/10.1111/tra.12672.

Foster, Sir Michael. 1895. *A Text-Book of Physiology*. Lea Bros & Company.

Foster, Thomas C., and Christopher M. Norris. 1997. "Age-Associated Changes in Ca2+-Dependent Processes: Relation to Hippocampal Synaptic Plasticity." *Hippocampus* 7 (6): 602–12. https://doi.org/10.1002/(SICI)1098-1063(1997)7:6<602::AID-HIPO3>3.0.CO;2-G.

Frayling, Timothy M., Nicholas J. Timpson, Michael N. Weedon, Eleftheria Zeggini, Rachel M. Freathy, Cecilia M. Lindgren, John R. B. Perry, et al. 2007. "A Common Variant in the FTO Gene Is Associated with Body Mass Index and Predisposes to Childhood and Adult Obesity." *Science*, May. https://doi.org/10.1126/science.1141634.

Frick, Karyn M., and Jamie D. Benoit. 2010. "Use It or Lose It: Environmental Enrichment as a Means to Promote Successful Cognitive Aging." *TheScientificWorldJOURNAL* 10: 1129–41. https://doi.org/10.1100/tsw.2010.111.

Frye, Michaela, Bryan T. Harada, Mikaela Behm, and Chuan He. 2018. "RNA Modifications Modulate Gene Expression during Development." *Science (New York, N.Y.)* 361 (6409): 1346–49. https://doi.org/10.1126/science.aau1646.

Fu, Ye, Dan Dominissini, Gideon Rechavi, and Chuan He. 2014. "Gene Expression Regulation Mediated through Reversible M^{6}A RNA Methylation." *Nature Reviews. Genetics* 15 (5): 293–306. https://doi.org/10.1038/nrg3724.

Garner, C. C., R. P. Tucker, and A. Matus. 1988. "Selective Localization of Messenger RNA for Cytoskeletal Protein MAP2 in Dendrites." *Nature* 336 (6200): 674–77. https://doi.org/10.1038/336674a0.

Gerken, Thomas, Christophe A. Girard, Yi-Chun Loraine Tung, Celia J. Webby, Vladimir Saudek, Kirsty S. Hewitson, Giles S. H. Yeo, et al. 2007. "The Obesity-Associated FTO Gene Encodes a 2-Oxoglutarate-Dependent Nucleic Acid Demethylase." *Science*, November. https://doi.org/10.1126/science.1151710.

Gershoni-Emek, Noga, Arnon Mazza, Michael Chein, Tal Gradus-Pery, Xin Xiang, Ka Wan Li, Roded Sharan, and Eran Perlson. 2016. "Proteomic Analysis of Dynein-Interacting Proteins in Amyotrophic Lateral Sclerosis Synaptosomes Reveals Alterations in the RNA-Binding Protein Staufen1." *Molecular & Cellular Proteomics: MCP* 15 (2): 506–22. https://doi.org/10.1074/mcp.M115.049965.

Geula, Shay, Sharon Moshitch-Moshkovitz, Dan Dominissini, Abed AlFatah Mansour, Nitzan Kol, Mali Salmon-Divon, Vera Hershkovitz, et al. 2015. "Stem Cells. M6A MRNA Methylation Facilitates Resolution of Naïve Pluripotency toward Differentiation." *Science (New York, N.Y.)* 347 (6225): 1002–6. https://doi.org/10.1126/science.1261417.

Giannakopoulos, P., F. R. Herrmann, T. Bussière, C. Bouras, E. Kövari, D. P. Perl, J. H. Morrison, G. Gold, and P. R. Hof. 2003. "Tangle and Neuron Numbers, but Not Amyloid Load, Predict Cognitive Status in Alzheimer's Disease." *Neurology* 60 (9): 1495–1500. https://doi.org/10.1212/01.WNL.0000063311.58879.01.

Glanzman, David L. 2010. "Common Mechanisms of Synaptic Plasticity in Vertebrates and Invertebrates." *Current Biology: CB* 20 (1): R31-36. https://doi.org/10.1016/j.cub.2009.10.023.

Govindarajan, Arvind, Inbal Israely, Shu-Ying Huang, and Susumu Tonegawa. 2011. "The Dendritic Branch Is the Preferred Integrative Unit for Protein Synthesis-Dependent LTP." *Neuron* 69 (1): 132–46. https://doi.org/10.1016/j.neuron.2010.12.008.

Green, E. J., and W. T. Greenough. 1986. "Altered Synaptic Transmission in Dentate Gyrus of Rats Reared in Complex Environments: Evidence from Hippocampal Slices Maintained in Vitro." *Journal of Neurophysiology* 55 (4): 739–50. https://doi.org/10.1152/jn.1986.55.4.739.

Grégoire, Catherine-Alexandra, Stephanie Tobin, Brianna L. Goldenstein, Éric Samarut, Andréanne Leclerc, Anne Aumont, Pierre Drapeau, Stephanie Fulton, and Karl J. L. Fernandes. 2018. "RNA-Sequencing Reveals Unique Transcriptional Signatures of Running and Running-Independent Environmental Enrichment in the Adult Mouse Dentate Gyrus." *Frontiers in Molecular Neuroscience* 11. https://www.frontiersin.org/article/10.3389/fnmol.2018.00126.

Grosjean, Henri. 2015. "RNA Modification: The Golden Period 1995–2015." *RNA* 21 (4): 625–26. https://doi.org/10.1261/rna.049866.115.

Hackett, John T., and Tetsufumi Ueda. 2015. "Glutamate Release." *Neurochemical Research* 40 (12): 2443–60. https://doi.org/10.1007/s11064-015-1622-1.

Hafner, Anne-Sophie, Paul G. Donlin-Asp, Beulah Leitch, Etienne Herzog, and Erin M. Schuman. 2019. "Local Protein Synthesis Is a Ubiquitous Feature of Neuronal Pre- and Postsynaptic Compartments." *Science (New York, N.Y.)* 364 (6441): eaau3644. https://doi.org/10.1126/science.aau3644.

Ham, Seokjin, and Seung-Jae V. Lee. 2020. "Advances in Transcriptome Analysis of Human Brain Aging." *Experimental & Molecular Medicine* 52 (11): 1787–97. https://doi.org/10.1038/s12276-020-00522-6.

Han, Jing, Kristyna Pluhackova, and Rainer A. Böckmann. 2017. "The Multifaceted Role of SNARE Proteins in Membrane Fusion." *Frontiers in Physiology* 8: 5. https://doi.org/10.3389/fphys.2017.00005.

Han, Min, Zhen Liu, Yingying Xu, Xiangtian Liu, Dewei Wang, Fan Li, Yun Wang, and Jianzhong Bi. 2020. "Abnormality of M6A MRNA Methylation Is Involved in Alzheimer's Disease." *Frontiers in Neuroscience* 14: 98. https://doi.org/10.3389/fnins.2020.00098.

Hartmann, A. M., O. Nayler, F. W. Schwaiger, A. Obermeier, and S. Stamm. 1999. "The Interaction and Colocalization of Sam68 with the Splicing-Associated Factor YT521-B in Nuclear Dots Is Regulated by the Src Family Kinase P59(Fyn)." *Molecular Biology of the Cell* 10 (11): 3909–26. https://doi.org/10.1091/mbc.10.11.3909.

Hassel, Bjørnar, and Raymond Dingledine. 2012. "Chapter 17 - Glutamate and Glutamate Receptors." In *Basic Neurochemistry (Eighth Edition)*, edited by Scott T. Brady, George J. Siegel, R. Wayne Albers, and Donald L. Price, 342–66. New York: Academic Press. https://doi.org/10.1016/B978-0-12-374947-5.00017-1.

He, Chuan. 2010. "Grand Challenge Commentary: RNA Epigenetics?" *Nature Chemical Biology* 6 (12): 863–65. https://doi.org/10.1038/nchembio.482.

Hebb, D. 1949. "The Organization of Behavior: A Neuropsychological Theory." In . https://doi.org/10.2307/1418888.

Hess, Martin E., Simon Hess, Kate D. Meyer, Linda A. W. Verhagen, Linda Koch, Hella S. Brönneke, Marcelo O. Dietrich, et al. 2013. "The Fat Mass and Obesity Associated Gene

(Fto) Regulates Activity of the Dopaminergic Midbrain Circuitry." *Nature Neuroscience* 16 (8): 1042–48. https://doi.org/10.1038/nn.3449.

Heukelum, Sabrina van, Rogier B. Mars, Martin Guthrie, Jan K. Buitelaar, Christian F. Beckmann, Paul H. E. Tiesinga, Brent A. Vogt, Jeffrey C. Glennon, and Martha N. Havenith. 2020. "Where Is Cingulate Cortex? A Cross-Species View." *Trends in Neurosciences* 43 (5): 285–99. https://doi.org/10.1016/j.tins.2020.03.007.

Holt, Christine E., Kelsey C. Martin, and Erin M. Schuman. 2019. "Local Translation in Neurons: Visualization and Function." *Nature Structural & Molecular Biology* 26 (7): 557–66. https://doi.org/10.1038/s41594-019-0263-5.

Hoover, Brian R., Miranda N. Reed, Jianjun Su, Rachel D. Penrod, Linda A. Kotilinek, Marianne K. Grant, Rose Pitstick, et al. 2010. "Tau Mislocalization to Dendritic Spines Mediates Synaptic Dysfunction Independently of Neurodegeneration." *Neuron* 68 (6): 1067–81. https://doi.org/10.1016/j.neuron.2010.11.030.

Hornak, J., J. Bramham, E. T. Rolls, R. G. Morris, J. O'Doherty, P. R. Bullock, and C. E. Polkey. 2003. "Changes in Emotion after Circumscribed Surgical Lesions of the Orbitofrontal and Cingulate Cortices." *Brain: A Journal of Neurology* 126 (Pt 7): 1691–1712. https://doi.org/10.1093/brain/awg168.

Hsieh, Helen, Jannic Boehm, Chihiro Sato, Takeshi Iwatsubo, Taisuke Tomita, Sangram Sisodia, and Roberto Malinow. 2006. "AMPAR Removal Underlies Aβ-Induced Synaptic Depression and Dendritic Spine Loss." *Neuron* 52 (5): 831–43. https://doi.org/10.1016/j.neuron.2006.10.035.

Hsu, Phillip J., Yunfei Zhu, Honghui Ma, Yueshuai Guo, Xiaodan Shi, Yuanyuan Liu, Meijie Qi, et al. 2017. "Ythdc2 Is an N6-Methyladenosine Binding Protein That Regulates Mammalian Spermatogenesis." *Cell Research* 27 (9): 1115–27. https://doi.org/10.1038/cr.2017.99.

Huang, He, Judith Camats-Perna, Rodrigo Medeiros, Victor Anggono, and Jocelyn Widagdo. 2020. "Altered Expression of the M6A Methyltransferase METTL3 in Alzheimer's Disease." *ENeuro* 7 (5): ENEURO.0125-20.2020. https://doi.org/10.1523/ENEURO.0125-20.2020.

Huang, Huilin, Hengyou Weng, Wenju Sun, Xi Qin, Hailing Shi, Huizhe Wu, Boxuan Simen Zhao, et al. 2018. "Recognition of RNA N6-Methyladenosine by IGF2BP Proteins Enhances MRNA Stability and Translation." *Nature Cell Biology* 20 (3): 285–95. https://doi.org/10.1038/s41556-018-0045-z.

Huber, K. M., M. S. Kayser, and M. F. Bear. 2000. "Role for Rapid Dendritic Protein Synthesis in Hippocampal MGluR-Dependent Long-Term Depression." *Science (New York, N.Y.)* 288 (5469): 1254–57. https://doi.org/10.1126/science.288.5469.1254.

Hüttenrauch, Melanie, Gabriela Salinas, and Oliver Wirths. 2016. "Effects of Long-Term Environmental Enrichment on Anxiety, Memory, Hippocampal Plasticity and Overall Brain Gene Expression in C57BL6 Mice." *Frontiers in Molecular Neuroscience* 9. https://www.frontiersin.org/article/10.3389/fnmol.2016.00062.

Irier, Hasan, R. Craig Street, Ronak Dave, Li Lin, Catherine Cai, Timothy Hayden Davis, Bing Yao, Ying Cheng, and Peng Jin. 2014. "Environmental Enrichment Modulates 5-Hydroxymethylcytosine Dynamics in Hippocampus." *Genomics*, 5-hydroxymethylation, 104 (5): 376–82. https://doi.org/10.1016/j.ygeno.2014.08.019.

Irvine, Gemma I., and Wickliffe C. Abraham. 2005. "Enriched Environment Exposure Alters the Input-Output Dynamics of Synaptic Transmission in Area CA1 of Freely Moving Rats." *Neuroscience Letters* 391 (1): 32–37. https://doi.org/10.1016/j.neulet.2005.08.031.

Ishizuka, N., W. M. Cowan, and D. G. Amaral. 1995. "A Quantitative Analysis of the Dendritic Organization of Pyramidal Cells in the Rat Hippocampus." *The Journal of Comparative Neurology* 362 (1): 17–45. https://doi.org/10.1002/cne.903620103.

Islam, Md Rezaul, Lalit Kaurani, Tea Berulava, Urs Heilbronner, Monika Budde, Tonatiuh Pena Centeno, Vakthang Elerdashvili, et al. 2021. "A MicroRNA Signature That Correlates with

Cognition and Is a Target against Cognitive Decline." *EMBO Molecular Medicine* 13 (11): e13659. https://doi.org/10.15252/emmm.202013659.

Jia, Guifang, Ye Fu, Xu Zhao, Qing Dai, Guanqun Zheng, Ying Yang, Chengqi Yi, et al. 2011. "N6-Methyladenosine in Nuclear RNA Is a Major Substrate of the Obesity-Associated FTO." *Nature Chemical Biology* 7 (12): 885–87. https://doi.org/10.1038/nchembio.687.

Jiang, Jianxiong, Vishnu Suppiramaniam, and Marie W. Wooten. 2006. "Posttranslational Modifications and Receptor-Associated Proteins in AMPA Receptor Trafficking and Synaptic Plasticity." *Neuro-Signals* 15 (5): 266–82. https://doi.org/10.1159/000105517.

Jiang, Xiulin, Baiyang Liu, Zhi Nie, Lincan Duan, Qiuxia Xiong, Zhixian Jin, Cuiping Yang, and Yongbin Chen. 2021. "The Role of M6A Modification in the Biological Functions and Diseases." *Signal Transduction and Targeted Therapy* 6 (1): 74. https://doi.org/10.1038/s41392-020-00450-x.

Kandel, Eric R., Yadin Dudai, and Mark R. Mayford. 2014. "The Molecular and Systems Biology of Memory." *Cell* 157 (1): 163–86. https://doi.org/10.1016/j.cell.2014.03.001.

Kang, Hyo Jung, Yuka Imamura Kawasawa, Feng Cheng, Ying Zhu, Xuming Xu, Mingfeng Li, André M. M. Sousa, et al. 2011. "Spatio-Temporal Transcriptome of the Human Brain." *Nature* 478 (7370): 483–89. https://doi.org/10.1038/nature10523.

Ke, Shengdong, Amy Pandya-Jones, Yuhki Saito, John J. Fak, Cathrine Broberg Vågbø, Shay Geula, Jacob H. Hanna, Douglas L. Black, James E. Darnell, and Robert B. Darnell. 2017. "M6A MRNA Modifications Are Deposited in Nascent Pre-MRNA and Are Not Required for Splicing but Do Specify Cytoplasmic Turnover." *Genes & Development* 31 (10): 990–1006. https://doi.org/10.1101/gad.301036.117.

Kelley, J. L., and C. Macías Garcia. 2010. "Ontogenetic Effects of Captive Breeding." In *Encyclopedia of Animal Behavior*, edited by Michael D. Breed and Janice Moore, 589–95. Oxford: Academic Press. https://doi.org/10.1016/B978-0-08-045337-8.00290-4.

Kempermann, Gerd, H. Georg Kuhn, and Fred H. Gage. 1997. "More Hippocampal Neurons in Adult Mice Living in an Enriched Environment." *Nature* 386 (6624): 493–95. https://doi.org/10.1038/386493a0.

Kempermann, Gerd. 2019. "Environmental Enrichment, New Neurons and the Neurobiology of Individuality." Nature Reviews Neuroscience 20 (4): 235–45. https://doi.org/10.1038/s41583-019-0120-x.

Knopman, David S., Helene Amieva, Ronald C. Petersen, Gäel Chételat, David M. Holtzman, Bradley T. Hyman, Ralph A. Nixon, and David T. Jones. 2021. "Alzheimer Disease." *Nature Reviews Disease Primers* 7 (1): 1–21. https://doi.org/10.1038/s41572-021-00269-y.

Knuckles, Philip, Sarah H. Carl, Michael Musheev, Christof Niehrs, Alice Wenger, and Marc Bühler. 2017. "RNA Fate Determination through Cotranscriptional Adenosine Methylation and Microprocessor Binding." *Nature Structural & Molecular Biology* 24 (7): 561–69. https://doi.org/10.1038/nsmb.3419.

Knuckles, Philip, Tina Lence, Irmgard U. Haussmann, Dominik Jacob, Nastasja Kreim, Sarah H. Carl, Irene Masiello, et al. 2018. "Zc3h13/Flacc Is Required for Adenosine Methylation by Bridging the MRNA-Binding Factor Rbm15/Spenito to the M6A Machinery Component Wtap/Fl(2)d." *Genes & Development* 32 (5–6): 415–29. https://doi.org/10.1101/gad.309146.117.

Konorski, J. 1948. "Conditioned Reflexes and Neuron Organization." *Conditioned Reflexes and Neuron Organization.* https://www.cabdirect.org/cabdirect/abstract/19512202723.

Koranda, Jessica L., Lou Dore, Hailing Shi, Meera J. Patel, Lee O. Vaasjo, Meghana N. Rao, Kai Chen, et al. 2018. "Mettl14 Is Essential for Epitranscriptomic Regulation of Striatal Function and Learning." *Neuron* 99 (2): 283-292.e5. https://doi.org/10.1016/j.neuron.2018.06.007.

Kuchibhotla, Kishore V., Samuel T. Goldman, Carli R. Lattarulo, Hai-Yan Wu, Bradley T. Hyman, and Brian J. Bacskai. 2008. "Aβ Plaques Lead to Aberrant Regulation of Calcium

Homeostasis In Vivo Resulting in Structural and Functional Disruption of Neuronal Networks." *Neuron* 59 (2): 214–25. https://doi.org/10.1016/j.neuron.2008.06.008.

Kumar, Ashok. 2015. "NMDA Receptor Function During Senescence: Implication on Cognitive Performance." *Frontiers in Neuroscience* 9. https://www.frontiersin.org/article/10.3389/fnins.2015.00473.

Kuzumaki, Naoko, Daigo Ikegami, Rie Tamura, Nana Hareyama, Satoshi Imai, Michiko Narita, Kazuhiro Torigoe, et al. 2011. "Hippocampal Epigenetic Modification at the Brain-Derived Neurotrophic Factor Gene Induced by an Enriched Environment." *Hippocampus* 21 (2): 127–32. https://doi.org/10.1002/hipo.20775.

Laggerbauer, Bernhard, Dirk Ostareck, Eva-Maria Keidel, Antje Ostareck-Lederer, and Utz Fischer. 2001. "Evidence That Fragile X Mental Retardation Protein Is a Negative Regulator of Translation." *Human Molecular Genetics* 10 (4): 329–38. https://doi.org/10.1093/hmg/10.4.329.

Lane, Byron G. 1998. "Historical Perspectives on RNA Nucleoside Modifications." In *Modification and Editing of RNA*, 1–20. John Wiley & Sons, Ltd. https://doi.org/10.1128/9781555818296.ch1.

Lazarov, Orly, John Robinson, Ya-Ping Tang, Ilana S. Hairston, Zeljka Korade-Mirnics, Virginia M. -Y. Lee, Louis B. Hersh, Robert M. Sapolsky, Karoly Mirnics, and Sangram S. Sisodia. 2005. "Environmental Enrichment Reduces Aβ Levels and Amyloid Deposition in Transgenic Mice." *Cell* 120 (5): 701–13. https://doi.org/10.1016/j.cell.2005.01.015.

Lee, Jeong-Heon, and David G. Skalnik. 2012. "Rbm15-Mkl1 Interacts with the Setd1b Histone H3-Lys4 Methyltransferase via a SPOC Domain That Is Required for Cytokine-Independent Proliferation." *PloS One* 7 (8): e42965. https://doi.org/10.1371/journal.pone.0042965.

Leech, Robert, and David J. Sharp. 2014. "The Role of the Posterior Cingulate Cortex in Cognition and Disease." *Brain* 137 (1): 12–32. https://doi.org/10.1093/brain/awt162.

Leonetti, Amanda M., Ming Yin Chu, Fiona O. Ramnaraign, Samuel Holm, and Brandon J. Walters. 2020. "An Emerging Role of M6A in Memory: A Case for Translational Priming." *International Journal of Molecular Sciences* 21 (20): E7447. https://doi.org/10.3390/ijms21207447.

Li, Fudong, Debiao Zhao, Jihui Wu, and Yunyu Shi. 2014. "Structure of the YTH Domain of Human YTHDF2 in Complex with an M6A Mononucleotide Reveals an Aromatic Cage for M6A Recognition." *Cell Research* 24 (12): 1490–92. https://doi.org/10.1038/cr.2014.153.

Li, Fuxi, Yang Yi, Yanyan Miao, Wenyong Long, Teng Long, Siyun Chen, Weisheng Cheng, et al. 2019. "N6-Methyladenosine Modulates Nonsense-Mediated MRNA Decay in Human Glioblastoma." *Cancer Research* 79 (22): 5785–98. https://doi.org/10.1158/0008-5472.CAN-18-2868.

Li, Qiu, Xiu Li, Hao Tang, Bin Jiang, Yali Dou, Myriam Gorospe, and Wengong Wang. 2017. "NSUN2-Mediated M5C Methylation and METTL3/METTL14-Mediated M6A Methylation Cooperatively Enhance P21 Translation." *Journal of Cellular Biochemistry* 118 (9): 2587–98. https://doi.org/10.1002/jcb.25957.

Liao, Shanhui, Hongbin Sun, and Chao Xu. 2018. "YTH Domain: A Family of N6-Methyladenosine (M6A) Readers." *Genomics, Proteomics & Bioinformatics* 16 (2): 99–107. https://doi.org/10.1016/j.gpb.2018.04.002.

Lin, Shuibin, Junho Choe, Peng Du, Robinson Triboulet, and Richard I. Gregory. 2016. "The m(6)A Methyltransferase METTL3 Promotes Translation in Human Cancer Cells." *Molecular Cell* 62 (3): 335–45. https://doi.org/10.1016/j.molcel.2016.03.021.

Linder, Bastian, Anya V. Grozhik, Anthony O. Olarerin-George, Cem Meydan, Christopher E. Mason, and Samie R. Jaffrey. 2015. "Single-Nucleotide-Resolution Mapping of M6A and M6Am throughout the Transcriptome." *Nature Methods* 12 (8): 767–72. https://doi.org/10.1038/nmeth.3453.

Lisman, John, Howard Schulman, and Hollis Cline. 2002. "The Molecular Basis of CaMKII Function in Synaptic and Behavioural Memory." *Nature Reviews Neuroscience* 3 (3): 175–90. https://doi.org/10.1038/nrn753.

Liu, Jianzhao, Yanan Yue, Dali Han, Xiao Wang, Ye Fu, Liang Zhang, Guifang Jia, et al. 2014. "A METTL3-METTL14 Complex Mediates Mammalian Nuclear RNA N6-Adenosine Methylation." *Nature Chemical Biology* 10 (2): 93–95. https://doi.org/10.1038/nchembio.1432.

Liu, Jun'e, Kai Li, Jiabin Cai, Mingchang Zhang, Xiaoting Zhang, Xushen Xiong, Haowei Meng, et al. 2020. "Landscape and Regulation of M6A and M6Am Methylome across Human and Mouse Tissues." *Molecular Cell* 77 (2): 426-440.e6. https://doi.org/10.1016/j.molcel.2019.09.032.

Liu, Nian, Qing Dai, Guanqun Zheng, Chuan He, Marc Parisien, and Tao Pan. 2015. "N(6)-Methyladenosine-Dependent RNA Structural Switches Regulate RNA-Protein Interactions." *Nature* 518 (7540): 560–64. https://doi.org/10.1038/nature14234.

Liu, Si-Yu, Yi Feng, Jun-Jie Wu, Ming-Li Zou, Zi-Li Sun, Xia Li, and Feng-Lai Yuan. 2020. "M6A Facilitates YTHDF-Independent Phase Separation." *Journal of Cellular and Molecular Medicine* 24 (2): 2070–72. https://doi.org/10.1111/jcmm.14847.

Livneh, Ido, Sharon Moshitch-Moshkovitz, Ninette Amariglio, Gideon Rechavi, and Dan Dominissini. 2020. "The M6A Epitranscriptome: Transcriptome Plasticity in Brain Development and Function." *Nature Reviews. Neuroscience* 21 (1): 36–51. https://doi.org/10.1038/s41583-019-0244-z.

López-Otín, Carlos, Maria A. Blasco, Linda Partridge, Manuel Serrano, and Guido Kroemer. 2013. "The Hallmarks of Aging." *Cell* 153 (6): 1194–1217. https://doi.org/10.1016/j.cell.2013.05.039.

Lucassen, Paul J., Carlos P. Fitzsimons, Evgenia Salta, and Mirjana Maletic-Savatic. 2020. "Adult Neurogenesis, Human after All (Again): Classic, Optimized, and Future Approaches." *Behavioural Brain Research* 381 (March): 112458. https://doi.org/10.1016/j.bbr.2019.112458.

Lüscher, Christian, and Robert C. Malenka. 2012. "NMDA Receptor-Dependent Long-Term Potentiation and Long-Term Depression (LTP/LTD)." *Cold Spring Harbor Perspectives in Biology* 4 (6): a005710. https://doi.org/10.1101/cshperspect.a005710.

Ma, Chunhui, Mengqi Chang, Hongyi Lv, Zhi-Wei Zhang, Weilong Zhang, Xue He, Gaolang Wu, et al. 2018. "RNA M6A Methylation Participates in Regulation of Postnatal Development of the Mouse Cerebellum." *Genome Biology* 19 (1): 68. https://doi.org/10.1186/s13059-018-1435-z.

Maday, Sandra, Alison E. Twelvetrees, Armen J. Moughamian, and Erika L. F. Holzbaur. 2014. "Axonal Transport: Cargo-Specific Mechanisms of Motility and Regulation." *Neuron* 84 (2): 292–309. https://doi.org/10.1016/j.neuron.2014.10.019.

Madugalle, Sachithrani U., Kate Meyer, Dan Ohtan Wang, and Timothy W. Bredy. 2020. "RNA N6-Methyladenosine and the Regulation of RNA Localization and Function in the Brain." *Trends in Neurosciences* 43 (12): 1011–23. https://doi.org/10.1016/j.tins.2020.09.005.

Maggi, Laura, Maria Scianni, Igor Branchi, Ivana D'Andrea, Clotilde Lauro, and Cristina Limatola. 2011. "CX3CR1 Deficiency Alters Hippocampal-Dependent Plasticity Phenomena Blunting the Effects of Enriched Environment." *Frontiers in Cellular Neuroscience* 5. https://www.frontiersin.org/article/10.3389/fncel.2011.00022.

Magnusson, Kathy R. 1998. "Aging of Glutamate Receptors: Correlations between Binding and Spatial Memory Performance in Mice." *Mechanisms of Ageing and Development* 104 (3): 227–48. https://doi.org/10.1016/S0047-6374(98)00076-1.

Malenka, Robert C., and Mark F. Bear. 2004. "LTP and LTD: An Embarrassment of Riches." *Neuron* 44 (1): 5–21. https://doi.org/10.1016/j.neuron.2004.09.012.

Malik, Ruchi, and Sumantra Chattarji. 2012. "Enhanced Intrinsic Excitability and EPSP-Spike Coupling Accompany Enriched Environment-Induced Facilitation of LTP in Hippocampal

CA1 Pyramidal Neurons." *Journal of Neurophysiology* 107 (5): 1366–78. https://doi.org/10.1152/jn.01009.2011.

Mao, Yuanhui, Leiming Dong, Xiao-Min Liu, Jiayin Guo, Honghui Ma, Bin Shen, and Shu-Bing Qian. 2019. "M6A in MRNA Coding Regions Promotes Translation via the RNA Helicase-Containing YTHDC2." *Nature Communications* 10 (1): 5332. https://doi.org/10.1038/s41467-019-13317-9.

Markham, Julie A, and Janice M Juraska. 2002. "Aging and Sex Influence the Anatomy of the Rat Anterior Cingulate Cortex." *Neurobiology of Aging* 23 (4): 579–88. https://doi.org/10.1016/S0197-4580(02)00004-0.

Martinez De La Cruz, Braulio, Robert Markus, Sunir Malla, Maria Isabel Haig, Chris Gell, Fei Sang, Eleanor Bellows, et al. 2021. "Modifying the M6A Brain Methylome by ALKBH5-Mediated Demethylation: A New Contender for Synaptic Tagging." *Molecular Psychiatry*, October, 1–13. https://doi.org/10.1038/s41380-021-01282-z.

Mateos-Aparicio, Pedro, and Antonio Rodríguez-Moreno. 2019. "The Impact of Studying Brain Plasticity." *Frontiers in Cellular Neuroscience* 13: 66. https://doi.org/10.3389/fncel.2019.00066.

Mattson, Mark P., and Tim Magnus. 2006. "Ageing and Neuronal Vulnerability." *Nature Reviews Neuroscience* 7 (4): 278–94. https://doi.org/10.1038/nrn1886.

Mauer, Jan, and Samie R. Jaffrey. 2018. "FTO, M6Am, and the Hypothesis of Reversible Epitranscriptomic MRNA Modifications." *FEBS Letters* 592 (12): 2012–22. https://doi.org/10.1002/1873-3468.13092.

Merkurjev, Daria, Wan-Ting Hong, Kei Iida, Ikumi Oomoto, Belinda J. Goldie, Hitoshi Yamaguti, Takayuki Ohara, et al. 2018. "Synaptic N6-Methyladenosine (M6A) Epitranscriptome Reveals Functional Partitioning of Localized Transcripts." *Nature Neuroscience* 21 (7): 1004–14. https://doi.org/10.1038/s41593-018-0173-6.

Meyer, Kate D., and Samie R. Jaffrey. 2014. "The Dynamic Epitranscriptome: N6-Methyladenosine and Gene Expression Control." *Nature Reviews. Molecular Cell Biology* 15 (5): 313–26. https://doi.org/10.1038/nrm3785.

Meyer, Kate D., and Samie R. Jaffrey. 2017. "Rethinking M6A Readers, Writers, and Erasers." *Annual Review of Cell and Developmental Biology* 33 (1): 319–42. https://doi.org/10.1146/annurev-cellbio-100616-060758.

Meyer, Kate D., Deepak P. Patil, Jun Zhou, Alexandra Zinoviev, Maxim A. Skabkin, Olivier Elemento, Tatyana V. Pestova, Shu-Bing Qian, and Samie R. Jaffrey. 2015. "5′ UTR M6A Promotes Cap-Independent Translation." *Cell* 163 (4): 999–1010. https://doi.org/10.1016/j.cell.2015.10.012.

Meyer, Kate D., Yogesh Saletore, Paul Zumbo, Olivier Elemento, Christopher E. Mason, and Samie R. Jaffrey. 2012. "Comprehensive Analysis of MRNA Methylation Reveals Enrichment in 3' UTRs and near Stop Codons." *Cell* 149 (7): 1635–46. https://doi.org/10.1016/j.cell.2012.05.003.

Milaneschi, Y., F. Lamers, H. Mbarek, J.-J. Hottenga, D. I. Boomsma, and B. W. J. H. Penninx. 2014. "The Effect of FTO Rs9939609 on Major Depression Differs across MDD Subtypes." *Molecular Psychiatry* 19 (9): 960–62. https://doi.org/10.1038/mp.2014.4.

Miller, Stephan, Masahiro Yasuda, Jennifer K. Coats, Ying Jones, Maryann E. Martone, and Mark Mayford. 2002. "Disruption of Dendritic Translation of CaMKIIalpha Impairs Stabilization of Synaptic Plasticity and Memory Consolidation." *Neuron* 36 (3): 507–19. https://doi.org/10.1016/s0896-6273(02)00978-9.

Moccia, Amanda, and Donna M. Martin. 2018. "Nervous System Development and Disease: A Focus on Trithorax Related Proteins and Chromatin Remodelers." *Molecular and Cellular Neuroscience*, Chromatin in nervous system development and disease, 87 (March): 46–54. https://doi.org/10.1016/j.mcn.2017.11.016.

Moccia, Robert, Dillon Chen, Vlasta Lyles, Estreya Kapuya, Yaping E, Sergey Kalachikov, Christian M. T. Spahn, et al. 2003. "An Unbiased CDNA Library Prepared from Isolated

Aplysia Sensory Neuron Processes Is Enriched for Cytoskeletal and Translational MRNAs." *The Journal of Neuroscience: The Official Journal of the Society for Neuroscience* 23 (28): 9409–17.

Moindrot, Benoit, Andrea Cerase, Heather Coker, Osamu Masui, Anne Grijzenhout, Greta Pintacuda, Lothar Schermelleh, Tatyana B. Nesterova, and Neil Brockdorff. 2015. "A Pooled ShRNA Screen Identifies Rbm15, Spen, and Wtap as Factors Required for Xist RNA-Mediated Silencing." *Cell Reports* 12 (4): 562–72. https://doi.org/10.1016/j.celrep.2015.06.053.

Mora, Francisco. 2013. "Successful Brain Aging: Plasticity, Environmental Enrichment, and Lifestyle." *Dialogues in Clinical Neuroscience* 15 (1): 45–52.

Moroz-Omori, Elena V., Danzhi Huang, Rajiv Kumar Bedi, Sherry J. Cheriyamkunnel, Elena Bochenkova, Aymeric Dolbois, Maciej D. Rzeczkowski, Yaozong Li, Lars Wiedmer, and Amedeo Caflisch. 2021. "METTL3 Inhibitors for Epitranscriptomic Modulation of Cellular Processes." *ChemMedChem* 16 (19): 3035–43. https://doi.org/10.1002/cmdc.202100291.

Morris, Richard G. M. 2013. "NMDA Receptors and Memory Encoding." *Neuropharmacology*, Glutamate Receptor-Dependent Synaptic Plasticity, 74 (November): 32–40. https://doi.org/10.1016/j.neuropharm.2013.04.014.

Newberry, Ruth C. 1995. "Environmental Enrichment: Increasing the Biological Relevance of Captive Environments." *Applied Animal Behaviour Science*, International Society for Applied Ethology 1995, 44 (2): 229–43. https://doi.org/10.1016/0168-1591(95)00616-Z.

Ohline, S. M., and W. C. Abraham. 2019. "Environmental Enrichment Effects on Synaptic and Cellular Physiology of Hippocampal Neurons." *Neuropharmacology* 145 (Pt A): 3–12. https://doi.org/10.1016/j.neuropharm.2018.04.007.

Okano, Hideyuki, Tomoo Hirano, and Evan Balaban. 2000. "Learning and Memory." *Proceedings of the National Academy of Sciences* 97 (23): 12403–4. https://doi.org/10.1073/pnas.210381897.

Ouyang, Y., A. Rosenstein, G. Kreiman, E. M. Schuman, and M. B. Kennedy. 1999. "Tetanic Stimulation Leads to Increased Accumulation of Ca(2+)/Calmodulin-Dependent Protein Kinase II via Dendritic Protein Synthesis in Hippocampal Neurons." *The Journal of Neuroscience: The Official Journal of the Society for Neuroscience* 19 (18): 7823–33.

Pacitti, Dario, Riccardo Privolizzi, and Bridget E. Bax. 2019. "Organs to Cells and Cells to Organoids: The Evolution of in Vitro Central Nervous System Modelling." *Frontiers in Cellular Neuroscience* 13: 129. https://doi.org/10.3389/fncel.2019.00129.

Paridaen, Judith TML, and Wieland B Huttner. 2014. "Neurogenesis during Development of the Vertebrate Central Nervous System." *EMBO Reports* 15 (4): 351–64. https://doi.org/10.1002/embr.201438447.

Patil, Deepak P., Chun-Kan Chen, Brian F. Pickering, Amy Chow, Constanza Jackson, Mitchell Guttman, and Samie R. Jaffrey. 2016. "M(6)A RNA Methylation Promotes XIST-Mediated Transcriptional Repression." *Nature* 537 (7620): 369–73. https://doi.org/10.1038/nature19342.

Pessoa, Luiz, and Patrick R. Hof. 2015. "From Paul Broca's Great Limbic Lobe to the Limbic System." *Journal of Comparative Neurology* 523 (17): 2495–2500. https://doi.org/10.1002/cne.23840.

Pielot, Rainer, Karl-Heinz Smalla, Anke Müller, Peter Landgraf, Anne-Christin Lehmann, Elke Eisenschmidt, Utz-Uwe Haus, Robert Weismantel, Eckart D. Gundelfinger, and Daniela C. Dieterich. 2012. "SynProt: A Database for Proteins of Detergent-Resistant Synaptic Protein Preparations." *Frontiers in Synaptic Neuroscience* 4: 1. https://doi.org/10.3389/fnsyn.2012.00001.

Pin, J. -P., and R. Duvoisin. 1995. "The Metabotropic Glutamate Receptors: Structure and Functions." *Neuropharmacology* 34 (1): 1–26. https://doi.org/10.1016/0028-3908(94)00129-G.

Ping, Xiao-Li, Bao-Fa Sun, Lu Wang, Wen Xiao, Xin Yang, Wen-Jia Wang, Samir Adhikari, et al. 2014. "Mammalian WTAP Is a Regulatory Subunit of the RNA N6-Methyladenosine Methyltransferase." *Cell Research* 24 (2): 177–89. https://doi.org/10.1038/cr.2014.3.

Rando, Thomas A. 2006. "Stem Cells, Ageing and the Quest for Immortality." *Nature* 441 (7097): 1080–86. https://doi.org/10.1038/nature04958.

Renner, Marianne, Pascale N. Lacor, Pauline T. Velasco, Jian Xu, Anis Contractor, William L. Klein, and Antoine Triller. 2010. "Deleterious Effects of Amyloid β Oligomers Acting as an Extracellular Scaffold for MGluR5." *Neuron* 66 (5): 739–54. https://doi.org/10.1016/j.neuron.2010.04.029.

Ries, Ryan J., Sara Zaccara, Pierre Klein, Anthony Olarerin-George, Sim Namkoong, Brian F. Pickering, Deepak P. Patil, Hojoong Kwak, Jun Hee Lee, and Samie R. Jaffrey. 2019. "M6A Enhances the Phase Separation Potential of MRNA." *Nature* 571 (7765): 424–28. https://doi.org/10.1038/s41586-019-1374-1.

Ris, Laurence, Brigitte Capron, Coralie Sclavons, Jean-François Liégeois, Vincent Seutin, and Emile Godaux. 2007. "Metaplastic Effect of Apamin on LTP and Paired-Pulse Facilitation." *Learning & Memory* 14 (6): 390–99. https://doi.org/10.1101/lm.571007.

Rolls, Edmund T. 2015. "Limbic Systems for Emotion and for Memory, but No Single Limbic System." *Cortex; a Journal Devoted to the Study of the Nervous System and Behavior* 62 (January): 119–57. https://doi.org/10.1016/j.cortex.2013.12.005.

Rolls, Edmund. 2016. *Cerebral Cortex: Principles of Operation*. Oxford University Press.

Rolls, Edmund. 2019. "The Orbitofrontal Cortex and Emotion in Health and Disease, Including Depression." *Neuropsychologia* 128 (May): 14–43. https://doi.org/10.1016/j.neuropsychologia.2017.09.021.

Sacktor, Todd Charlton, and André Antonio Fenton. 2018. "What Does LTP Tell Us about the Roles of CaMKII and PKMζ in Memory?" *Molecular Brain* 11 (1): 77. https://doi.org/10.1186/s13041-018-0420-5.

Sakamoto, Kensuke, Kate Karelina, and Karl Obrietan. 2011. "CREB: A Multifaceted Regulator of Neuronal Plasticity and Protection." *Journal of Neurochemistry* 116 (1): 1–9. https://doi.org/10.1111/j.1471-4159.2010.07080.x.

Saletore, Yogesh, Kate Meyer, Jonas Korlach, Igor D. Vilfan, Samie Jaffrey, and Christopher E. Mason. 2012. "The Birth of the Epitranscriptome: Deciphering the Function of RNA Modifications." *Genome Biology* 13 (10): 175. https://doi.org/10.1186/gb-2012-13-10-175.

Sanhueza, Magdalena, and John Lisman. 2013. "The CaMKII/NMDAR Complex as a Molecular Memory." *Molecular Brain* 6 (1): 10. https://doi.org/10.1186/1756-6606-6-10.

Santos, Magda S., Haiyan Li, and Susan M. Voglmaier. 2009. "SYNAPTIC VESICLE PROTEIN TRAFFICKING AT THE GLUTAMATE SYNAPSE." *Neuroscience* 158 (1): 189–203. https://doi.org/10.1016/j.neuroscience.2008.03.029.

Saunders, Richard C., Douglas L. Rosene, and Gary W. Van Hoesen. 1988. "Comparison of the Efferents of the Amygdala and the Hippocampal Formation in the Rhesus Monkey: II. Reciprocal and Non-Reciprocal Connections." *Journal of Comparative Neurology* 271 (2): 185–207. https://doi.org/10.1002/cne.902710203.

Sboner, Andrea, Xinmeng Jasmine Mu, Dov Greenbaum, Raymond K. Auerbach, and Mark B. Gerstein. 2011. "The Real Cost of Sequencing: Higher than You Think!" *Genome Biology* 12 (8): 125. https://doi.org/10.1186/gb-2011-12-8-125.

Schwartz, Schraga, Maxwell R. Mumbach, Marko Jovanovic, Tim Wang, Karolina Maciag, G. Guy Bushkin, Philipp Mertins, et al. 2014. "Perturbation of M6A Writers Reveals Two Distinct Classes of MRNA Methylation at Internal and 5' Sites." *Cell Reports* 8 (1): 284–96. https://doi.org/10.1016/j.celrep.2014.05.048.

Scoville, William Beecher, and Brenda Milner. 1957. "LOSS OF RECENT MEMORY AFTER BILATERAL HIPPOCAMPAL LESIONS." *Journal of Neurology, Neurosurgery, and Psychiatry* 20 (1): 11–21.

Scutenaire, Jérémy, Jean-Marc Deragon, Viviane Jean, Moussa Benhamed, Cécile Raynaud, Jean-Jacques Favory, Rémy Merret, and Cécile Bousquet-Antonelli. 2018. "The YTH Domain Protein ECT2 Is an M6A Reader Required for Normal Trichome Branching in Arabidopsis." *The Plant Cell* 30 (5): 986–1005. https://doi.org/10.1105/tpc.17.00854.

Sendinc, Erdem, David Valle-Garcia, Abhinav Dhall, Hao Chen, Telmo Henriques, Jose Navarrete-Perea, Wanqiang Sheng, Steven P. Gygi, Karen Adelman, and Yang Shi. 2019. "PCIF1 Catalyzes M6Am MRNA Methylation to Regulate Gene Expression." *Molecular Cell* 75 (3): 620-630.e9. https://doi.org/10.1016/j.molcel.2019.05.030.

Shafik, Andrew M., Feiran Zhang, Zhenxing Guo, Qing Dai, Kinga Pajdzik, Yangping Li, Yunhee Kang, et al. 2021. "N6-Methyladenosine Dynamics in Neurodevelopment and Aging, and Its Potential Role in Alzheimer's Disease." *Genome Biology* 22 (1): 17. https://doi.org/10.1186/s13059-020-02249-z.

Sheng, Morgan, and Eunjoon Kim. 2011. "The Postsynaptic Organization of Synapses." *Cold Spring Harbor Perspectives in Biology* 3 (12): a005678. https://doi.org/10.1101/cshperspect.a005678.

Shi, Hailing, Xiao Wang, Zhike Lu, Boxuan S. Zhao, Honghui Ma, Phillip J. Hsu, Chang Liu, and Chuan He. 2017. "YTHDF3 Facilitates Translation and Decay of N6-Methyladenosine-Modified RNA." *Cell Research* 27 (3): 315–28. https://doi.org/10.1038/cr.2017.15.

Shi, Hailing, Xuliang Zhang, Yi-Lan Weng, Zongyang Lu, Yajing Liu, Zhike Lu, Jianan Li, et al. 2018. "M6A Facilitates Hippocampus-Dependent Learning and Memory through YTHDF1." *Nature* 563 (7730): 249–53. https://doi.org/10.1038/s41586-018-0666-1.

Sidorov, Michael S., Benjamin D. Auerbach, and Mark F. Bear. 2013. "Fragile X Mental Retardation Protein and Synaptic Plasticity." *Molecular Brain* 6 (1): 15. https://doi.org/10.1186/1756-6606-6-15.

Simone, Laura E., and Jack D. Keene. 2013. "Mechanisms Coordinating ELAV/Hu MRNA Regulons." *Current Opinion in Genetics & Development* 23 (1): 35–43. https://doi.org/10.1016/j.gde.2012.12.006.

Smith, David E., Peter R. Rapp, Heather M. McKay, Jeffrey A. Roberts, and Mark H. Tuszynski. 2004. "Memory Impairment in Aged Primates Is Associated with Focal Death of Cortical Neurons and Atrophy of Subcortical Neurons." *Journal of Neuroscience* 24 (18): 4373–81. https://doi.org/10.1523/JNEUROSCI.4289-03.2004.

Sommer, S., U. Lavi, and J. E. Darnell. 1978. "The Absolute Frequency of Labeled N-6-Methyladenosine in HeLa Cell Messenger RNA Decreases with Label Time." *Journal of Molecular Biology* 124 (3): 487–99. https://doi.org/10.1016/0022-2836(78)90183-3.

Song, Jinghui, and Chengqi Yi. 2020. "Reading Chemical Modifications in the Transcriptome." Journal of Molecular Biology, Reading DNA Modifications, 432 (6): 1824–39. https://doi.org/10.1016/j.jmb.2019.10.006.

Spires, Tara L., and Bradley T. Hyman. 2005. "Transgenic Models of Alzheimer's Disease: Learning from Animals." *NeuroRX*, Animal Models of Neurological Disorders, 2 (3): 423–37. https://doi.org/10.1602/neurorx.2.3.423.

Spires-Jones, Tara L., and Bradley T. Hyman. 2014. "The Intersection of Amyloid Beta and Tau at Synapses in Alzheimer's Disease." *Neuron* 82 (4): 756–71. https://doi.org/10.1016/j.neuron.2014.05.004.

Squires, Jeffrey E., Hardip R. Patel, Marco Nousch, Tennille Sibbritt, David T. Humphreys, Brian J. Parker, Catherine M. Suter, and Thomas Preiss. 2012. "Widespread Occurrence of 5-Methylcytosine in Human Coding and Non-Coding RNA." *Nucleic Acids Research* 40 (11): 5023–33. https://doi.org/10.1093/nar/gks144.

Sultan, Faraz A, and Jeremy J Day. 2011. "Epigenetic Mechanisms in Memory and Synaptic Function." *Epigenomics* 3 (2): 157–81.

Sun, Ting, Ruiyan Wu, and Liang Ming. 2019. "The Role of M6A RNA Methylation in Cancer." *Biomedicine & Pharmacotherapy = Biomedecine & Pharmacotherapie* 112 (April): 108613. https://doi.org/10.1016/j.biopha.2019.108613.

Taliaferro, J. Matthew, Marina Vidaki, Ruan Oliveira, Sara Olson, Lijun Zhan, Tanvi Saxena, Eric T. Wang, et al. 2016. "Distal Alternative Last Exons Localize MRNAs to Neural Projections." *Molecular Cell* 61 (6): 821–33. https://doi.org/10.1016/j.molcel.2016.01.020.

Tang, Chong, Rachel Klukovich, Hongying Peng, Zhuqing Wang, Tian Yu, Ying Zhang, Huili Zheng, Arne Klungland, and Wei Yan. 2018. "ALKBH5-Dependent M6A Demethylation Controls Splicing and Stability of Long 3′-UTR MRNAs in Male Germ Cells." *Proceedings of the National Academy of Sciences* 115 (2): E325–33. https://doi.org/10.1073/pnas.1717794115.

Tanzi, Rudolph E. 2012. "The Genetics of Alzheimer Disease." *Cold Spring Harbor Perspectives in Medicine* 2 (10): a006296. https://doi.org/10.1101/cshperspect.a006296.

Thomas, Gareth M., and Richard L. Huganir. 2004. "MAPK Cascade Signalling and Synaptic Plasticity." *Nature Reviews Neuroscience* 5 (3): 173–83. https://doi.org/10.1038/nrn1346.

Turner-Bridger, Benita, Maximillian Jakobs, Leila Muresan, Hovy Ho-Wai Wong, Kristian Franze, William A. Harris, and Christine E. Holt. 2018. "Single-Molecule Analysis of Endogenous β-Actin MRNA Trafficking Reveals a Mechanism for Compartmentalized MRNA Localization in Axons." *Proceedings of the National Academy of Sciences of the United States of America* 115 (41): E9697–9706. https://doi.org/10.1073/pnas.1806189115.

Valero, Jorge, Judit España, Arnaldo Parra-Damas, Elsa Martín, José Rodríguez-Álvarez, and Carlos A. Saura. 2011. "Short-Term Environmental Enrichment Rescues Adult Neurogenesis and Memory Deficits in APPSw,Ind Transgenic Mice." *PLOS ONE* 6 (2): e16832. https://doi.org/10.1371/journal.pone.0016832.

Vickers, Catherine A., Kirsten S. Dickson, and David J A. Wyllie. 2005. "Induction and Maintenance of Late-Phase Long-Term Potentiation in Isolated Dendrites of Rat Hippocampal CA1 Pyramidal Neurones." *The Journal of Physiology* 568 (3): 803–13. https://doi.org/10.1113/jphysiol.2005.092924.

Vousden, Dulcie A., Alexander Friesen, Xianglan Wen, Lily R. Qiu, Nicholas O'Toole, Benjamin C. Darwin, Leigh Spencer Noakes, et al. 2018. "Genetic and Behavioural Requirements for Structural Brain Plasticity." https://doi.org/10.1101/431999.

Walters, Brandon J., Valentina Mercaldo, Colleen J. Gillon, Matthew Yip, Rachael L. Neve, Frederick M. Boyce, Paul W. Frankland, and Sheena A. Josselyn. 2017. "The Role of The RNA Demethylase FTO (Fat Mass and Obesity-Associated) and MRNA Methylation in Hippocampal Memory Formation." *Neuropsychopharmacology: Official Publication of the American College of Neuropsychopharmacology* 42 (7): 1502–10. https://doi.org/10.1038/npp.2017.31.

Wang, Chen-Xin, Guan-Shen Cui, Xiuying Liu, Kai Xu, Meng Wang, Xin-Xin Zhang, Li-Yuan Jiang, et al. 2018. "METTL3-Mediated M6A Modification Is Required for Cerebellar Development." *PLoS Biology* 16 (6): e2004880. https://doi.org/10.1371/journal.pbio.2004880.

Wang, Xiao, Zhike Lu, Adrian Gomez, Gary C. Hon, Yanan Yue, Dali Han, Ye Fu, et al. 2014. "N6-Methyladenosine-Dependent Regulation of Messenger RNA Stability." *Nature* 505 (7481): 117–20. https://doi.org/10.1038/nature12730.

Wang, Xiao, Boxuan Simen Zhao, Ian A. Roundtree, Zhike Lu, Dali Han, Honghui Ma, Xiaocheng Weng, Kai Chen, Hailing Shi, and Chuan He. 2015. "N6-Methyladenosine Modulates Messenger RNA Translation Efficiency." *Cell* 161 (6): 1388–99. https://doi.org/10.1016/j.cell.2015.05.014.

Wang, Yang, Yue Li, Julia I. Toth, Matthew D. Petroski, Zhaolei Zhang, and Jing Crystal Zhao. 2014. "N6-Methyladenosine Modification Destabilizes Developmental Regulators in Embryonic Stem Cells." *Nature Cell Biology* 16 (2): 191–98. https://doi.org/10.1038/ncb2902.

Wei, Jiangbo, Fange Liu, Zhike Lu, Qili Fei, Yuxi Ai, P. Cody He, Hailing Shi, et al. 2018. "Differential M6A, M6Am, and M1A Demethylation Mediated by FTO in the Cell Nucleus and Cytoplasm." *Molecular Cell* 71 (6): 973-985.e5. https://doi.org/10.1016/j.molcel.2018.08.011.

Weinberger, Leehee, Muneef Ayyash, Noa Novershtern, and Jacob H. Hanna. 2016. "Dynamic Stem Cell States: Naive to Primed Pluripotency in Rodents and Humans." *Nature Reviews. Molecular Cell Biology* 17 (3): 155–69. https://doi.org/10.1038/nrm.2015.28.

Wen, Jing, Ruitu Lv, Honghui Ma, Hongjie Shen, Chenxi He, Jiahua Wang, Fangfang Jiao, et al. 2018. "Zc3h13 Regulates Nuclear RNA M6A Methylation and Mouse Embryonic Stem Cell Self-Renewal." *Molecular Cell* 69 (6): 1028-1038.e6. https://doi.org/10.1016/j.molcel.2018.02.015.

Weng, Yi-Lan, Xu Wang, Ran An, Jessica Cassin, Caroline Vissers, Yuanyuan Liu, Yajing Liu, et al. 2018. "Epitranscriptomic M6A Regulation of Axon Regeneration in the Adult Mammalian Nervous System." *Neuron* 97 (2): 313-325.e6. https://doi.org/10.1016/j.neuron.2017.12.036.

Widagdo, Jocelyn, and Victor Anggono. 2018. "The M6A-Epitranscriptomic Signature in Neurobiology: From Neurodevelopment to Brain Plasticity." *Journal of Neurochemistry* 147 (2): 137–52. https://doi.org/10.1111/jnc.14481.

Widagdo, Jocelyn, Justin J. -L. Wong, and Victor Anggono. 2021. "The M6A-Epitranscriptome in Brain Plasticity, Learning and Memory." *Seminars in Cell & Developmental Biology*, May. https://doi.org/10.1016/j.semcdb.2021.05.023.

Widagdo, Jocelyn, Qiong-Yi Zhao, Marie-Jeanne Kempen, Men Chee Tan, Vikram S. Ratnu, Wei Wei, Laura Leighton, et al. 2016. "Experience-Dependent Accumulation of N6-Methyladenosine in the Prefrontal Cortex Is Associated with Memory Processes in Mice." *The Journal of Neuroscience: The Official Journal of the Society for Neuroscience* 36 (25): 6771–77. https://doi.org/10.1523/JNEUROSCI.4053-15.2016.

Wilson, R.S., S.E. Leurgans, P.A. Boyle, J.A. Schneider, and D.A. Bennett. 2010. "Neurodegenerative Basis of Age-Related Cognitive Decline (e–Pub Ahead of Print)(CME)." *Neurology* 75 (12): 1070–78. https://doi.org/10.1212/WNL.0b013e3181f39adc.

Wu, Baixing, Shichen Su, Deepak P. Patil, Hehua Liu, Jianhua Gan, Samie R. Jaffrey, and Jinbiao Ma. 2018. "Molecular Basis for the Specific and Multivariant Recognitions of RNA Substrates by Human HnRNP A2/B1." *Nature Communications* 9 (1): 420. https://doi.org/10.1038/s41467-017-02770-z.

Wu, Hai-Yan, Eloise Hudry, Tadafumi Hashimoto, Kengo Uemura, Zhan-Yun Fan, Oksana Berezovska, Cynthia L. Grosskreutz, Brian J. Bacskai, and Bradley T. Hyman. 2012. "Distinct Dendritic Spine and Nuclear Phases of Calcineurin Activation after Exposure to Amyloid-β Revealed by a Novel Fluorescence Resonance Energy Transfer Assay." *Journal of Neuroscience* 32 (15): 5298–5309. https://doi.org/10.1523/JNEUROSCI.0227-12.2012.

Wu, Rong, Ang Li, Baofa Sun, Jian-Guang Sun, Jinhua Zhang, Ting Zhang, Yusheng Chen, et al. 2019. "A Novel M6A Reader Prrc2a Controls Oligodendroglial Specification and Myelination." *Cell Research* 29 (1): 23–41. https://doi.org/10.1038/s41422-018-0113-8.

Xiao, Wen, Samir Adhikari, Ujwal Dahal, Yu-Sheng Chen, Ya-Juan Hao, Bao-Fa Sun, Hui-Ying Sun, et al. 2016. "Nuclear M6A Reader YTHDC1 Regulates MRNA Splicing." *Molecular Cell* 61 (4): 507–19. https://doi.org/10.1016/j.molcel.2016.01.012.

Xie, Guoyou, Xu-Nian Wu, Yuyi Ling, Yalan Rui, Deyan Wu, Jiawang Zhou, Jiexin Li, et al. 2021. "A Novel Inhibitor of N6-Methyladenosine Demethylase FTO Induces MRNA Methylation and Shows Anti-Cancer Activities." *Acta Pharmaceutica Sinica B*, August. https://doi.org/10.1016/j.apsb.2021.08.028.

Xie, Yuanbin, Ricardo Castro-Hernández, Godwin Sokpor, Linh Pham, Ramanathan Narayanan, Joachim Rosenbusch, Jochen F. Staiger, and Tran Tuoc. 2019. "RBM15 Modulates the

Function of Chromatin Remodeling Factor BAF155 Through RNA Methylation in Developing Cortex." *Molecular Neurobiology* 56 (11): 7305–20. https://doi.org/10.1007/s12035-019-1595-1.

Xue, Chen, Yalei Zhao, and Lanjuan Li. 2020. "Advances in RNA Cytosine-5 Methylation: Detection, Regulatory Mechanisms, Biological Functions and Links to Cancer." *Biomarker Research* 8 (1): 43. https://doi.org/10.1186/s40364-020-00225-0.

Yang, Chuan, Yiyang Hu, Bo Zhou, Yulu Bao, Zhibin Li, Chunli Gong, Huan Yang, Sumin Wang, and Yufeng Xiao. 2020. "The Role of M6A Modification in Physiology and Disease." *Cell Death & Disease* 11 (11): 1–16. https://doi.org/10.1038/s41419-020-03143-z.

Yang, Ying, Phillip J. Hsu, Yu-Sheng Chen, and Yun-Gui Yang. 2018. "Dynamic Transcriptomic M6A Decoration: Writers, Erasers, Readers and Functions in RNA Metabolism." *Cell Research* 28 (6): 616–24. https://doi.org/10.1038/s41422-018-0040-8.

Yankova, Eliza, Wesley Blackaby, Mark Albertella, Justyna Rak, Etienne De Braekeleer, Georgia Tsagkogeorga, Ewa S. Pilka, et al. 2021. "Small-Molecule Inhibition of METTL3 as a Strategy against Myeloid Leukaemia." *Nature* 593 (7860): 597–601. https://doi.org/10.1038/s41586-021-03536-w.

Yassa, Michael A., L. Tugan Muftuler, and Craig E. L. Stark. 2010. "Ultrahigh-Resolution Microstructural Diffusion Tensor Imaging Reveals Perforant Path Degradation in Aged Humans in Vivo." *Proceedings of the National Academy of Sciences* 107 (28): 12687–91. https://doi.org/10.1073/pnas.1002113107.

Yen, Ya-Ping, and Jun-An Chen. 2021. "The M6A Epitranscriptome on Neural Development and Degeneration." *Journal of Biomedical Science* 28 (1): 40. https://doi.org/10.1186/s12929-021-00734-6.

Yoon, Ki-Jun, Francisca Rojas Ringeling, Caroline Vissers, Fadi Jacob, Michael Pokrass, Dennisse Jimenez-Cyrus, Yijing Su, et al. 2017. "Temporal Control of Mammalian Cortical Neurogenesis by M6A Methylation." *Cell* 171 (4): 877-889.e17. https://doi.org/10.1016/j.cell.2017.09.003.

Yu, Danfang, Huanhuan Yan, Jun Zhou, Xiaodan Yang, Youming Lu, and Yunyun Han. 2019. "A Circuit View of Deep Brain Stimulation in Alzheimer's Disease and the Possible Mechanisms." Molecular Neurodegeneration 14 (1): 33. https://doi.org/10.1186/s13024-019-0334-4.

Yu, Jun, Mengxian Chen, Haijiao Huang, Junda Zhu, Huixue Song, Jian Zhu, Jaewon Park, and Sheng-Jian Ji. 2018. "Dynamic M6A Modification Regulates Local Translation of MRNA in Axons." *Nucleic Acids Research* 46 (3): 1412–23. https://doi.org/10.1093/nar/gkx1182.

Yu, Jun, Yuanchu She, and Sheng-Jian Ji. 2021. "M6A Modification in Mammalian Nervous System Development, Functions, Disorders, and Injuries." *Frontiers in Cell and Developmental Biology* 9: 1343. https://doi.org/10.3389/fcell.2021.679662.

Yu, Wilson, and Esther Krook-Magnuson. 2015. "Cognitive Collaborations: Bidirectional Functional Connectivity Between the Cerebellum and the Hippocampus." *Frontiers in Systems Neuroscience* 9: 177. https://doi.org/10.3389/fnsys.2015.00177.

Yue, Yanan, Jun Liu, Xiaolong Cui, Jie Cao, Guanzheng Luo, Zezhou Zhang, Tao Cheng, et al. 2018. "VIRMA Mediates Preferential M6A MRNA Methylation in 3′UTR and near Stop Codon and Associates with Alternative Polyadenylation." *Cell Discovery* 4 (1): 1–17. https://doi.org/10.1038/s41421-018-0019-0.

Zalcman, Gisela, Noel Federman, and Arturo Romano. 2018. "CaMKII Isoforms in Learning and Memory: Localization and Function." *Frontiers in Molecular Neuroscience* 11 (December): 445. https://doi.org/10.3389/fnmol.2018.00445.

Zeng, Yong, Shiyan Wang, Shanshan Gao, Fraser Soares, Musadeqque Ahmed, Haiyang Guo, Miranda Wang, et al. 2018. "Refined RIP-Seq Protocol for Epitranscriptome Analysis with Low Input Materials." *PLOS Biology* 16 (9): e2006092. https://doi.org/10.1371/journal.pbio.2006092.

Zhang, Feiran, Yunhee Kang, Mengli Wang, Yujing Li, Tianlei Xu, Wei Yang, Hongjun Song, Hao Wu, Qiang Shu, and Peng Jin. 2018. "Fragile X Mental Retardation Protein Modulates the Stability of Its M6A-Marked Messenger RNA Targets." *Human Molecular Genetics* 27 (22): 3936–50. https://doi.org/10.1093/hmg/ddy292.

Zhang, Sicong, Boxuan Simen Zhao, Aidong Zhou, Kangyu Lin, Shaoping Zheng, Zhike Lu, Yaohui Chen, et al. 2017. "M6A Demethylase ALKBH5 Maintains Tumorigenicity of Glioblastoma Stem-like Cells by Sustaining FOXM1 Expression and Cell Proliferation Program." *Cancer Cell* 31 (4): 591-606.e6. https://doi.org/10.1016/j.ccell.2017.02.013.

Zhang, Tie-Yuan, Christopher L. Keown, Xianglan Wen, Junhao Li, Dulcie A. Vousden, Christoph Anacker, Urvashi Bhattacharyya, et al. 2018. "Environmental Enrichment Increases Transcriptional and Epigenetic Differentiation between Mouse Dorsal and Ventral Dentate Gyrus." *Nature Communications* 9 (1): 298. https://doi.org/10.1038/s41467-017-02748-x.

Zhang, Yuhao, Xiuchao Geng, Qiang Li, Jianglong Xu, Yanli Tan, Menglin Xiao, Jia Song, Fulin Liu, Chuan Fang, and Hong Wang. 2020. "M6A Modification in RNA: Biogenesis, Functions and Roles in Gliomas." Journal of Experimental & Clinical Cancer Research 39 (1): 192. https://doi.org/10.1186/s13046-020-01706-8.

Zhang, Zeyu, Meng Wang, Dongfang Xie, Zenghui Huang, Lisha Zhang, Ying Yang, Dongxue Ma, et al. 2018. "METTL3-Mediated N6-Methyladenosine MRNA Modification Enhances Long-Term Memory Consolidation." *Cell Research* 28 (11): 1050–61. https://doi.org/10.1038/s41422-018-0092-9.

Zhao, Boxuan Simen, Ian A. Roundtree, and Chuan He. 2017. "Post-Transcriptional Gene Regulation by MRNA Modifications." *Nature Reviews. Molecular Cell Biology* 18 (1): 31–42. https://doi.org/10.1038/nrm.2016.132.

Zhao, Fanpeng, Ying Xu, Shichao Gao, Lixia Qin, Quillan Austria, Sandra L. Siedlak, Kinga Pajdzik, et al. 2021. "METTL3-Dependent RNA M6A Dysregulation Contributes to Neurodegeneration in Alzheimer's Disease through Aberrant Cell Cycle Events." *Molecular Neurodegeneration* 16 (1): 70. https://doi.org/10.1186/s13024-021-00484-x.

Zhao, Xu, Ying Yang, Bao-Fa Sun, Yue Shi, Xin Yang, Wen Xiao, Ya-Juan Hao, et al. 2014. "FTO-Dependent Demethylation of N6-Methyladenosine Regulates MRNA Splicing and Is Required for Adipogenesis." *Cell Research* 24 (12): 1403–19. https://doi.org/10.1038/cr.2014.151.

Zheng, Guanqun, John Arne Dahl, Yamei Niu, Peter Fedorcsak, Chun-Min Huang, Charles J. Li, Cathrine B. Vågbø, et al. 2013. "ALKBH5 Is a Mammalian RNA Demethylase That Impacts RNA Metabolism and Mouse Fertility." *Molecular Cell* 49 (1): 18–29. https://doi.org/10.1016/j.molcel.2012.10.015.

Zhou, Lujia, Joseph McInnes, Keimpe Wierda, Matthew Holt, Abigail G. Herrmann, Rosemary J. Jackson, Yu-Chun Wang, et al. 2017. "Tau Association with Synaptic Vesicles Causes Presynaptic Dysfunction." *Nature Communications* 8 (1): 15295. https://doi.org/10.1038/ncomms15295.

List of Figures

List of Tables

Acknowledgements

First of all, I would like to thank Prof. Dr. André Fischer for taking me in as a student almost four years ago. Since then, his supervision, valuable mentoring and support have made it possible for me to develop my knowledge and skills in an environment of freedom and encouragement.

I also want to express my gratitude to the members of my Thesis Committee, Prof. Dr. Tiago Outeiro and Prof. Dr. Markus Zweckstetter. Their comments, feedback and insights during the duration of my PhD were of great value to improve my work and explore other avenues for research. In addition, I want to thank the members of my extended examination board: Prof Dr. Thomas Dresbach, Dr Camin Dean and Dr. Brett Carter, for agreeing to be present during my defense. I can already thank you all in advance for the great questions and comments.

Next, a giant thank you to Tea. She was the greatest source of help and support, especially as I was starting in the lab and had no idea of anything, always happy to help and discuss to overcome all the obstacles that came up in this work. Tea started the project of m6A in aging and AD preparing some of the samples used in this work and her analysis were very valuable in the preparation of this manuscript.

Also, a huge thanks to Susi, not only for being the greatest sequencing machine but also for her friendship and support. Always there for a chat and willing to lend a hand when the work got too much, even when her plate was already full.

My appreciation too to all my students. Particularly to Kristin and Masha, whose work helped me advance in my projects and is included in this thesis. But not only them, I also thank Buket and Steffi for being great students and awesome people. To all of you, thank you for always being interested and willing to learn, you've thought me how to be a supervisor and I hope you have fond memories of your time with me.

To Tona, thank you so much for all the help and support in doing a bunch of analyses. I knew nothing about bioinformatics and now I kind of know a bit, and that's in good part thanks to you.

To other members of the Fischerlab, past and present, thank you for your friendship, your willingness to help, support each other and discuss, or just have a chat or beer to distract ourselves. Thank you, Henning, Robert, Sasha, Sakib, Masha, Gaurav, Anna-Lena, Lalit, and everyone who's had an influence in me during the last four years. To Uli and Daniel, thank you for all your support and for always being there for us, despite always having too much to do.

And finally, to my family. To Janna, thanks for being the best life partner I could ever ask. A mis padres, Carmen y Ricardo. He tenido todas las oportunidades que haya podido desear en la vida y se lo debo a ustedes. Gracias por todo su amor y apoyo, durante los últimos treinta años.